WIND TURBINE ENGINEERING DESIGN

David M. Eggleston • Forrest S. Stoddard

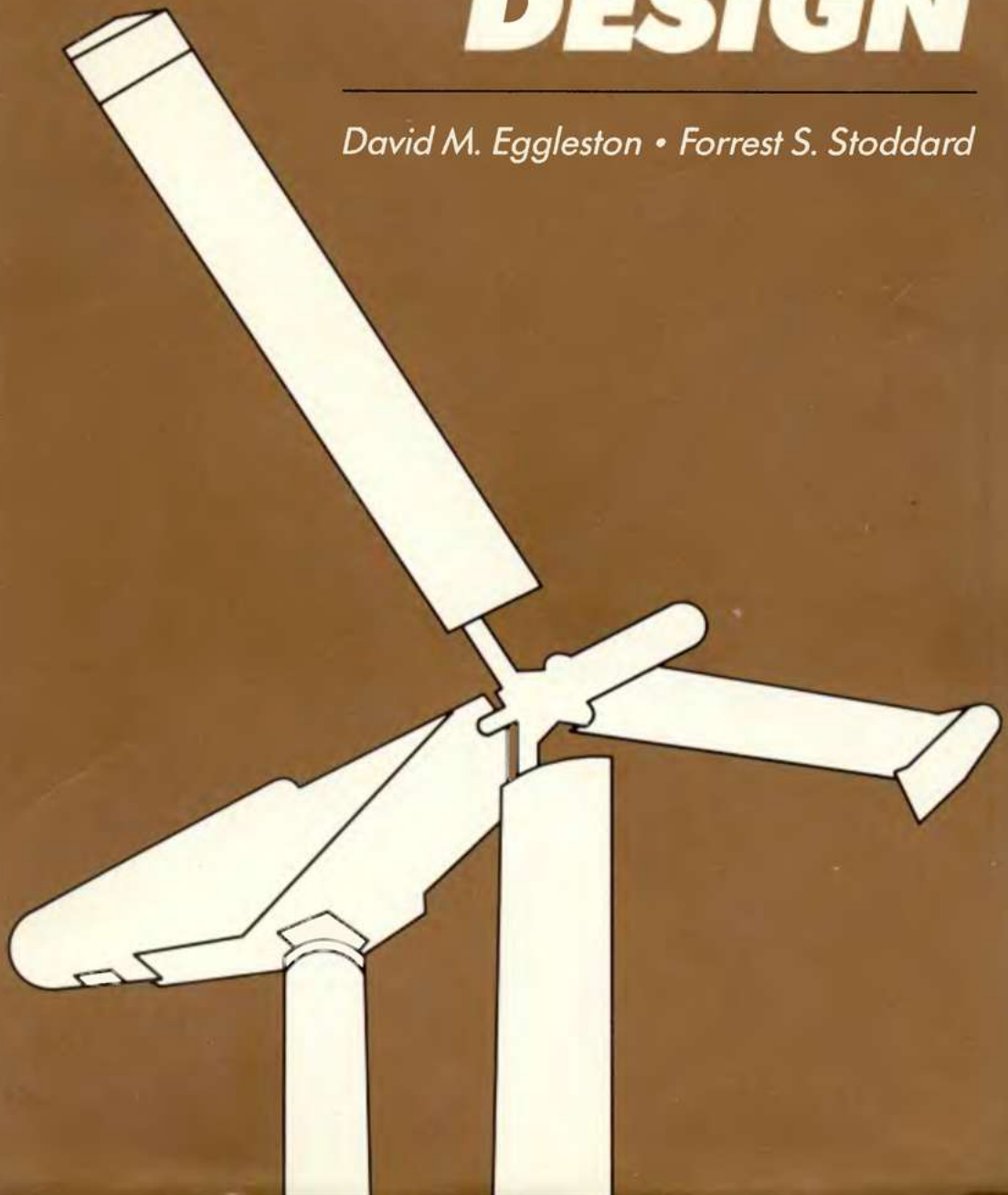

WIND TURBINE ENGINEERING DESIGN

David M. Eggleston
University of Texas at Permian Basin

Forrest S. Stoddard
Pioneer Wind Power

VAN NOSTRAND REINHOLD COMPANY
New York

Library of Congress Catalog Card Number 86-23331

ISBN 0-442-22195-9

Printed in the United States of America

Van Nostrand Reinhold Company Inc.
115 Fifth Avenue
New York, New York 10003

Van Nostrand Reinhold Company Limited
Molly Millars Lane
Wokingham, Berkshire RG11 2PY, England

Van Nostrand Reinhold
480 La Trobe Street
Melbourne, Victoria 3000, Australia

Macmillan of Canada
Division of Canada Publishing Corporation
164 Commander Boulevard
Agincourt, Ontario M1S 3C7, Canada

16 15 14 13 12 11 10 9 8 7 6 5 4 3 2 1

Library of Congress Cataloging-in-Publication Data

Eggleston, David M., 1935–
Wind turbine engineering design.

Includes bibliographies and index.
1. Air-turbines—Design and construction.
I. Stoddard, Forrest S., 1944– . II. Title.
TJ828.E34 1987 621.4'5 86-23331
ISBN 0-442-22195-9

In all the world, few indeed are those who have a clear insight into both mathematical analysis and how it does, and does not, fit physical phenomena.

PREFACE

It is some sort of tragedy that many get caught up in the idea of generating power from the wind and attempt to build machines before they have mastered the discipines required. On the other hand, those who have mastered the disciplines often have no particular interest in wind turbines or committment to their design. It is, then, to the engineers who strive for both goals that this book is dedicated, for only they have both the capability and the spirit to design, build, and test machines in the proper manner.

This book provides an overview of the engineering design of wind turbines. Since the field is so broad, we have not attempted to cover every aspect in detail. There are a number of excellent manuals for mechanical design, electrical machinery design, airfoil design, and so on, that may be used as references by a competent designer. We have concentrated on those areas of most direct relevance to wind-turbine design. We have also attempted to guide the reader to some of the most relevant reference materials known to the authors.

A fairly high level of quantitative skill is required to master the various disciplines required for design. For this reason, a background equivalent to a B.S. degree in engineering is assumed. Nevertheless, we hope that designers who do not meet these requirements will be encouraged to study and be guided to the proper subject areas by browsing through this book. We also urge that builders who do not possess the necessary background in a particular area important to their design seek expert assistance. We have seen a number of machines that have not succeeded simply because the designer devoted most of his effort to one pet aspect of the design and neglected other vital areas.

Competent engineering design requires a sound understanding of the mathematical models used and of the various assumptions upon which basic theory rests. In many cases, derivations from first principles are given to help provide the necessary insight. True mastery is obtained only through an intense curiosity and years of experience in both design and testing.

The book is divided into three major sections: aerodynamics, structural dynamics, and system engineering. Although we have attempted to describe the present state of the art in these areas, research is continuously adding new information. There are also many areas where current information is

inadequate and research is needed. In such cases the designer is subjected to the necessity for extensive testing to verify a design.

Our experience had led us to believe that the design and development of a successful wind turbine is not as easy as might be supposed. Plenty of opportunity for creative design exists, and the perfect wind turbine has yet to appear.

In Part I—Aerodynamics—the first chapter gives a brief introduction to the history of wind-turbine design. In Chap. 2, the basic methods for modelling rotor aerodynamics are presented. Chapter 3 treats the rotor sizing problem, whereas some of the details of rotor design are covered in Chap. 4. Digital programs for wind-turbine design and analysis are discussed in Chap. 5, and Part I of the book is concluded by Chap. 6, on performance, economics, and siting.

Part II treats the structural dynamics of wind turbines including system engineering model (Chap. 7), blade equations of motion (Chap. 8), blade motions (Chap. 9), blade and hub loads (Chap. 10), instabilities (Chap. 11), and load specification (Chap. 12).

Part III concludes the book with Chap. 13 on fatigue, Chap. 14 on electrical generators, and Chap. 15 on control systems.

As with any major effort, the authors owe thanks to many for whatever good qualities the work may possess. To our wives, Helen and Anne, and to many colleagues we want to express our gratitude. Clay Waldon contributed Chap. 13 and most of Chap. 15 and had other helpful suggestions. Many points in rotor aerodynamics were clarified in discussions with James Tangler, now of SERI. Lee Kilgore, formerly with Westinghouse and now a consultant, contributed the basic electrical machine treatment of Chap. 14, whereas Dan Handman of ESI enriched it in with important points gleaned from operating experience. Francis Scheda of Westinghouse also made contributions to this chapter.

A book attempting to cover such a broad area can never be said to be finished, as there is always something that has been inadequately treated or omitted or an important point brought to light after the final pages were printed. Whatever its faults, we hope that the basic purpose of the book has been achieved and that it will be found useful by many future wind-turbine designers and others who wish to have a more complete understanding of the machinery necessary to harness wind energy.

DAVID M. EGGLESTON
FORREST S. STODDARD

LIST OF SYMBOLS, PART I

A = Rotor swept area perpendicular to free stream
A_0 = Rotor streamtube cross-sectional area at station 0
AR = Aspect ratio, R/c
a = Axial interference factor, v/V_0
a' = Rotational interference factor, $w/r\Omega$
B = Number of blades
C_H = Head loss coefficient
C_P = Power coefficient, $P/\frac{1}{2}\rho A V_0^3$
C_Q = Torque coefficient, $Q/\frac{1}{2}\rho A V_0^2 R$
C_T = Thrust coefficient, $T/\frac{1}{2}\rho A V_0^2$
c = Blade chord, Weibull windspeed normalizing factor
c_1 = Blade-segment profile drag coefficient (from $c_d = c_1 + c_2\alpha^2$)
c_2 = Blade-segment coefficient of α^2 (in $c_d = c_1 + c_2\alpha^2$)
c_l = Blade-segment lift coefficient, $L/\frac{1}{2}\rho W^2 c\Delta r$
c_d = Blade-segment drag coefficient, $D/\frac{1}{2}\rho W^2 c\Delta r$
c_m = Blade-segment moment coefficient, $M/\frac{1}{2}\rho W^2 c\Delta rc$
D = Blade-segment drag force
F = Prandtl loss factor
I = Moment of inertia
k = Weibull shape factor ($k = 2$ for Rayleigh distribution)
L = Blade-segment lift force
M = Blade segment moment about 1/4 chord point
p = Pressure
Q = Rotor torque
ΔQ = Volumetric flow quantity
R = Blade tip radius
Re = Reynolds number of blade = Wc/ν
S = Cross-sectional area of control volume (Sec. 2.3)
S = Plan form area of wing (Sec. 2.5)
r = Local blade radius
T = Thrust on rotor
u = Wind speed through rotor plane
V_0 = Free-stream wind velocity
v = Change in velocity, $V_0 - u$, induced by rotor
W = Relative wind at blade segment
W = Freestream windspeed = V_t (Chap. 3)
w = Local tangential wind velocity at rotor plane
X = Tip speed ratio, $R\Omega/V_0$
x = Local speed ratio, $r\Omega/V_0$

Greek

α = Blade segment angle of attack
δ = Profile drag parameter, $\sigma c_1 X^3/8$
ϵ = Drag/lift ratio, c_d/c_l
θ = Angle of blade chord with rotor plane (twist, decalage)
ζ = Drag increase with lift parameter, $16c_2/\sigma x A^2$
ν = Kinematic viscosity of air
ρ = Air density
σ = Average solidity (of rectangular blade) = $B(cR/\pi R^2) = Bc/\pi R$
σ_l = Local solidity = $Bc\Delta r/2\pi r\Delta r = Bc/2\pi r$
σ_t = Total integrated solidity, $B \int c(r)\, dr/\pi R^2$
ϕ = Angle of relative wind from rotor plane
ψ = Rotor coning angle
Ω = Rotor angular velocity
ω = Rotational wind angular velocity

LIST OF SYMBOLS, PART II

A = Axisymmetric flow term = $(\lambda/3) + (\theta_p/4)$
A_2 = Axisymmetric flow term = $(\lambda/2) + (\theta_p/3)$
A_3 = Axisymmetric flow term = $(\lambda/2) + (2\theta_p/3)$
A_4 = Axisymmetric flow term = $(2\lambda/3) + (\theta_p/4)$
B = Gravity term = $G/2\Omega^2 = 3g/2R(1 - e)$
b = Number of blades
C_P = Power coefficient = $P/\frac{1}{2}\rho A V_0^3$
C_d = Section drag coefficient
C_l = Section lift coefficient
C_{l_α} = Lift curve slope = $dC_l/d\alpha$
c = Blade chord
dm = Differential mass element
E = Young's modulus
e = Flapping hinge offset
e_2 = Lead-lag hinge offset
G = Gravity term = $2\Omega^2 B = gM_b x_g R/I_b$
g = Acceleration due to gravity
I = Moment of inertia
$I_b = I_\beta$ = Blade flapping mass moment of inertia = $\int_0^R r^2\, dm$
$I_f = I_\theta$ = Blade feathering mass moment of inertia = $\int_0^R Y_I^2 m\, dr$
I_I = Blade elastic-axis moment of inertia = $\int_0^R Y_I^2\, dm$
I_R = Blade elastic-axis product of inertia = $\int_0^R Y_I r\, dm$

K = Nondimensional flapping frequency = $1 + \epsilon + (K_\beta/I_b\Omega^2) = (\omega_\beta/\Omega)^2$
K_2 = Nondimensional lead-lag frequency = $\epsilon_2 + (K_\zeta/I_b\Omega^2) = (\omega_\zeta/\Omega)^2$
K_3 = Nondimensional feathering frequency = $1 + [K_\theta/(I_f + I_I)\Omega^2] = (\omega_\theta/\Omega)^2$
K_β = Flapping hinge spring
K_ζ = Lead-lag hinge spring
K_θ = Feathering hinge spring
K_1 = Vertical wind shear gradient
a = Blade normal mode coefficient
l = Rotor-tower offset
$\bar{l}$ = Nondimensional rotor-tower offset = l/R
M = Bending moment
M_β = Flapping bending moment
M_ζ = Lead-lag bending moment
M_b = Mass of blade
n = Harmonic index
P = Power
p = Nondimensional flapping frequency = ω_β/Ω
Q = Hub pitching angular velocity
q = Nacelle yaw angular velocity
$\bar{q}$ = Nondimensional yaw angular velocity = q/Ω
q_L = Tower lateral deflection
R = Blade radius
r_g = Radius to center of mass
S = Shear force
S_β = Flapping shear
S_ζ = Lead-lag shear
T = Blade tension
T_b = Kinetic energy of blade
T_t = Kinetic energy of tower
TSR = Rotor tip speed ratio = $\Omega R/V_0$
U = Potential energy
U_0 = Crosswind velocity
$\bar{U}_0$ = Nondimensional crosswind velocity = $U_0/\Omega R$
$\bar{U}$ = Nondimensional crosswind plus yaw translation = $\bar{U}_0 + \bar{q}\bar{l}$
U_T = Stream velocity tangential to blade element
U_P = Stream velocity perpendicular to blade element
V_0 = Free-stream velocity
$\bar{V}_0$ = Nondimensional free-stream velocity = $V_0/\Omega R$
V_R = Resultant stream velocity at blade element
v_i = Induced velocity at blade element

x_g = Nondimensional radius to center of mass = r_g/R
$X_{\beta'}$ = Flapping velocity coefficient (see Eq. 9.41)
$Y_I = x_I$ = Chordwise distance from elastic axis to mass axis
$Y_A = x_A$ = Chordwise distance from elastic axis to aerodynamic axis

GREEK

α = Blade section angle of attack
α = Mathieu's equation solution coefficient (Chap. 8)
β = Blade flapping angle
β_0 = Blade coning angle, or collective flapping
β_{1c} = Cyclic flapping angle, foward tilt of rotorplane
β_{1s} = Cyclic flapping angle, lateral tilt of rotorplane
γ = Lock number = $\rho C_{l_\alpha} c R^4 / I_b$
Δ = Determinant of coefficients = $K[(K-1)^2 + (\gamma/8)^2]$
δ = Mathieu's equation solution coefficient (Chap. 8)
ϵ = Flapping hinge offset term = $3e/2(1-e)$
ϵ_2 = Lead-lag hinge offset term = $3e_2/2(1-e_2)$
ζ = Blade lead-lag angle
ζ_0 = Collective lead-lag angle
ζ_{1c} = Cyclic lead-lag angle, vertical blade scissoring
ζ_{1s} = Cyclic lead-lag angle, horizontal blade scissoring
η = Nondimensional span station = r/R
θ = Blade element (feathering) angle
θ_0 = Blade linear twist angle
θ_p = Blade pitch angle
λ = Nondimensional inflow = $(V_0 - v_i)/\Omega R$
λ_i = Nondimensional induced velocity = $v_i/\Omega R$
μ_0 = Rotor advance ratio, reciprocal of tip speed ratio = 1/TSR = $(V_0/\Omega R)$
ξ = Damping ratio
ρ = Density
σ = Stress
τ = Torque
ϕ = Blade element relative wind angle
ψ = Blade azimuth angle (zero is vertically down)
Ω = Rotor angular velocity
ω = Frequency of vibration
ω_{NR} = Frequency of vibration of nonrotating blade
ω_R = Frequency of vibration of rotating blade
ω_β = Frequency of vibration in flapping
ω_ζ = Frequency of vibration in lead-lag
ω_θ = Frequency of vibration in feathering

Subscripts

$_0$ = Relative to blade hinge
$_\beta$ = Relative to flapping direction
$_\zeta$ = Relative to lead-lag direction
$_\theta$ = Relative to feathering direction

Superscripts

$\dot{}$ = First derivative with respect to time (d/dt)
$\ddot{}$ = Second derivative with respect to time (d^2/dt^2)
$'$ = First derivative with respect to azimuth $(d/d\psi)$
$''$ = Second derivative with respect to azimuth $(d^2/d\psi^2)$

CONTENTS

1

INTRODUCTION

1.1 INTRODUCTION AND SCOPE

Many publications on wind energy exist, ranging from works of backyard inventors and alternative energy buffs to theoretical papers on advanced engineering. The search through all this literature to find pertinent information and methods useful for engineering design can be a frustrating and exhausting one. The objective of this volume is to present concisely the basic technical facts, recommended procedures, and a guide to the most useful handbooks and references so that a technically trained person will be able to design a sound, reliable, cost-effective wind turbine.

Deciding what to call such machines poses problems. The general public in the U.S.A. has a general concept—the windmill—that they apply universally to any device that harnesses wind power, be it a water pump, electrical generator, or device that makes the ground vibrate to keep rodents from getting a good night's sleep. Engineers are uncomfortable calling a machine a mill when it is in fact not a mill and so have developed special terms such as *wind turbine, wind energy conversion system* (WECS), *horizontal-axis wind turbine* (HAWT), *vertical-axis wind turbine* (VAWT), and others. Even the term *wind generating system* has been used but discarded because it seems to imply that the machine is generating the wind, not electricity. In this book, we will use *wind turbine* as our generic term for a machine with rotating blades that converts the kinetic energy of a flow of air (wind) into useful power.

The extraction of power from wind is an ancient endeavor beginning with wind-powered ships, grain mills, and threshing machines. That the mechanical insight and technology of sailing ships carried over into windmills is evident in the canvas "sails" of the Cretian and Dutch windmills. Only toward the beginning of this century has development of "high-speed" wind turbines for generation of electrical power been pursued. This book will be devoted primarily to the extraction of electrical power from the wind.

Windmill designers and builders of the early ages succeeded or failed in accordance with their experience of years of trial and error devoted to their craft. The triumph of the modern era is that we can now explore wind turbine

designs on paper and computer *before* physically constructing a full—or even reduced—scale model. The savings in time, effort, and money thus realized are so significant that, as in the aircraft and automotive industries, the economic viability of wind turbines may ultimately depend upon their use. It is the hope of the authors that this volume may lead to a higher level of success and a lowering of the costs of the production of power from the wind.

The design of a wind turbine is not a trivial task. Because of the variability of the power source, it is a little like designing a bridge that will be used by a succession of vehicles having random weights. The bridge can be built as strong as you like, but sooner or later a vehicle too heavy may come along and destroy it. Lest this thought make us too gloomy, however, remember that some windmills built in the early 1600s are still operational. Needless to say, a design life of 350 years isn't bad!

The typical visitor to a wind turbine site during the last 15 years has had a rather poor likelihood of finding the machine in operation. The list of reasons is interminable. The wind is too weak, the wind is too strong, the machine is down for repair or modification, and so forth and so on. A number of manufacturers have gone into business selling machines before their design was properly worked out either on paper or in the field. We suspect that much of the theory available has not been properly applied in these designs. That wind turbines are always more expensive than they should be is not surprising. It is absurdly uneconomic to engineer and install a retrofit "fix" on 300 machines that have already been built.

There are many technical and nontechnical pitfalls in wind turbine production and use. Quite a number of disciplines are involved, ranging from material fatigue to electromagnetic interference caused by metal blades, and neglect or insufficient consideration given to any one of them can result in expensive failures.

This volume will be devoted almost entirely to horizontal-axis wind turbines (HAWT). Vertical-axis wind turbines (VAWT) incorporate most of the same principles, but their design is quite specialized, and the necessary design expertise resides in but a few organizations. Many research studies have been done by the National Research Council of Canada and at Sandia National Laboratories in Albuquerque, NM. Additional studies and manufacturing work have been done by ALCOA, DAF Indal Ltd., Forecast Wind Industries, Flow-Wind, and other companies. The reader interested in vertical-axis machines should have relatively little trouble in locating VAWT papers in the literature.

It is hoped that readers of weak technical background but high interest level will be able to improve their understanding of wind turbines using this volume. Contrariwise, readers of strong technical background who lack experience with the phenomena and technology of wind turbines should find encouragement and guidance to expand their experience.

Very few mathematicians or engineers have spent time hanging on at the top of a 100-ft (30.5-m) tower in a 50-mph (22.4-m/s) wind to gain experience in the wind turbine craft. Although the authors do not recommend this experience, it is apparent that wind turbine design requires a judicious blend of analytical engineering and creative experimentation, not to mention a profound respect for the power of the wind.

1.2 HISTORY OF WIND TURBINE DESIGN

Why should we be concerned with the history of windmill design? The answer is, of course, that there is much to be learned from previous efforts.

When the NSF-NASA Mod 0 wind turbine was first operated, severe oscillations resulted in the fatigue life of the blades being rapidly used up. The project management and/or engineers that designed it had lost sight of the fact that downwind rotors do not work well with a large, effectively solid tower in front of them. The resulting analysis and redesign of the system produced useful information but at the cost of funds that could have been used for something else. It is hoped that, with all the sophisticated methods of analysis, computers, and materials now available, future designs will avoid incorporating the known mistakes of the past.

Windmills have a distinguished history that dates back many centuries. Informative pictorial surveys are contained in the books, *Windmills and Watermills* by John Reynolds[1] and *Windmills* by S. Beedell.[2] An excellent scientific history is given by E. W. Golding.[3] Eldridge's *Wind Machines* gives a beautifully illustrated survey of these machines.[7] An extensive report by R. Champly[8] gives descriptions, drawings, sizes, experimental data, and discussions of the mechanical operation of a large number of wind pumps and wind electric generators both in Europe and the U.S. in the 1900–1930 era. Notable in his work are descriptions of experiments with tip brakes, tilt-up towers, gearboxes and shafts for transmitting mechanical power down the tower from a horizontal-axis rotor, voltage regulators, and many other topics.

The kind of engineering design based on analysis in the presently understood sense could not begin, of course, until the necessary mathematics and engineering applications of it had been conceived. Such design as embodied in practice, however, is clearly shown in photographs in these and other books. The level of engineering understanding the millwrights possessed is indelibly recorded in the various design features of the early windmills.

A number of these aspects of design in the early English, Dutch, and Danish windmills are worthy of note. Many of them are discussed by Golding and also in the book, *Research Inspired by the Dutch Windmills*, by the Prinsenmolen Committee.[4] This committee, which included technically trained people, was organized to take charge of one of the large old Dutch windmills, the Prinsenmolen, in late 1935. The Prinsenmolen, built in the year 1628,

has a 92-ft (28-m) rotor. It is owned by the Schieland Catchment District, a governmental entity similar to a county in the U.S. Thus political, historical, ecological, economic, and technical problems were all of importance. The committee undertook an evaluation and modernization of the mill and research into the design and performance of other old Dutch windmills in light of modern airfoil theory. To apply their theories, they built and tested a quarter-scale model of the mill with a four-bladed airfoil-type rotor and developed and installed spar fairings on the full-size machine. Their results make quite interesting reading.

Early Design Features

A review of the old English and Dutch windmills shows the basic features of the "standard" design. This design incorporates an upwind rotor turning before a large-diameter tower. In the case of the early post mills, the entire tower rotated on a fixed post to face the wind. In later models—the "smock" or tower mill—only the cap of the tower rotated.

A perspective drawing of the Herne Mill, Kent, England is shown in Fig. 1.1. The four-bladed rotor has variable solidity that is automatically controlled by a mechanical shutter system in which the thrust force on the blade shutters is balanced by weights.

The main structural members of the rotors of most of these old mills (the stocks) very nearly pass through the quarter-chord point of the blade. This is now known to be the location of the *effective lift force*. Location of the stocks at this point minimizes the torque tending to twist the blades on the stocks. Thus what we know from wind tunnel tests, the early millwrights learned from experience.

Since the blade members, called *whips*, were bolted to the stocks, they were replaceable. Thus the machines were maintainable with local materials and didn't require a maintenance engineer to come out from the factory.

Some of these mills have survived for 400 to 600 years, and several built more than three centuries ago are still in operating condition. The English post mill at Outwood, Surrey—the oldest operating mill in Great Britain—was constructed in 1665. The Dutch Prinsenmolen mill, discussed earlier, was built in 1628. This is quite an impressive design life! The basic design philosophy inherent in these machines is that simple, easily replaceable parts are designed to fail first, protecting the major assemblies from destruction.

Power is transmitted from the main rotor shaft to a vertical shaft by means of a large wooden-toothed gear, called the *brake wheel*, that meshes with a smaller "wallower" gear. This pair constitutes a wooden obtuse-angle bevel gear set, with replaceable teeth. The early mills used greased hardwood gear teeth to transmit the power from the main windshaft to the driven members.

The automatic, spring-loaded slat system and the many flexible members in the drive train provided the compliance needed to smooth the effects of

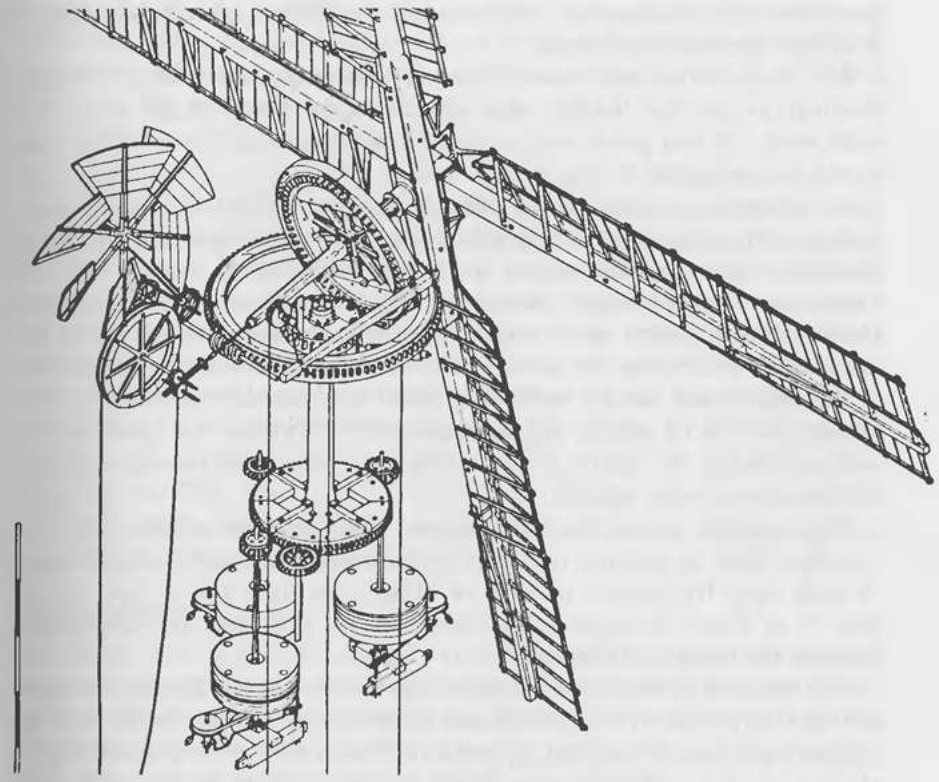

Figure 1.1. Herne Mill, Kent. (From Ref. 1.)

wind gusts. Modern builders have had to relearn the necessity of including such compliance. Flyball governors in each of the tentering systems for the grinding stones provided automatic load control, the most significant effect of which would be to help regulate speed and prevent the machine from stalling during brief periods of slack wind.

Provision for stopping the rotor incorporated a wooden (later, iron or steel) shoe or band brake that acted on the large main gear, called, appropriately, the *brake wheel*. Note that the brake was mounted directly on the rotor shaft and would be effective even if the main drive-gear teeth failed. More than one modern wind turbine has self-destructed, in part because the brake was not located on the rotor shaft.

During the classic period of windmills in Europe (1200 to 1900 A.D.), it was sometimes found to be impossible to stop a high-wind, run-away rotor using the brake. Occasionally, mills were even set on fire by sparks generated by an overheated brake. Other means of stopping windmill rotors included yawing them out of the wind and/or overloading the millstones by choking them with too much grain. Modern wind turbine operators have had to relearn,

sometimes with catastrophic consequences, the dangers of trying to stop a fixed-pitch rotor in high winds.

The stocks of the early windmills were tapered to support the maximum bending moment near the hub, thus minimizing the weight of the rotor. The main windshaft was also tapered so that the bending strength and bearing area would be appropriate for the applied loads.

In the later models, the main windshaft was tilted back to allow more blade clearance from the tower and to help center the rotor weight over the main bearing. Earlier windmills without this feature suffered from wear of the main bearing that resulted in the shaft being tipped downward, thus driving the blades into the ground or into the tower. This also put a negative load on the rotor thrust bearings so that the rotor shaft tended to fall out of the mill.

The blade width and the number of blades of these old mills accords with modern theories of solidity and tip-speed ratio. The rotational speed is also well-matched to the intended use, which may have been running a set of millstones or a water wheel.

The argument as to whether a twisted blade is more efficient than an untwisted blade is centuries old, as is apparent from the many windmill rotors of each type. The modern research of Miller et al. (see vol. 2, Sec. 3.4 of Ref. 5 in Chap. 2) supports the idea that the difference in performance between the two types is small.

John Smeaton of England was perhaps the first to *measure* the power output and tip-speed ratios of many candidate blade designs. To do so, he used an ingenious mechanical rotational apparatus and small model rotors (see Golding[3]). He won a gold medal from the Royal Society in 1759 for his work. His conclusions with regard to windmill rotors (he uses the word "sails"), some of which are given below, are reminiscent of Newton's laws (Smeaton uses the word "effect" to mean "power"):

1. Beyond a certain degree the more the area is crowded with sail the less effect is produced in proportion to the surface. . . . So that when the whole cylinder of wind is intercepted, it does not then produce the greatest effect for want of proper interstices to escape.
2. The velocity of windmill sails, whether unloaded, or loaded, so as to produce a maximum, is nearly as the velocity of the wind, their shape and position being the same.
3. The effects of the same sails at a maximum are nearly, but somewhat less than, as the cubes of the velocity of the wind.
4. In sails of a similar figure and position, the number of turns in a given time will be reciprocally as the radius of length of the sail.

Rotor Speed Control

Perhaps the most difficult problem in all wind-power machines is to limit rotor speed and protect the rotor in storm conditions, while still realizing

useful power to the maximum extent possible. The early English and Dutch windmills solved this problem by using a fixed-pitch, variable-solidity blade. The solidity was first controlled manually, by successively furling the canvas sail as in Fig. 1.2, an operation that required physically stopping the rotor and adjusting the sail cloth on each blade in turn. Doing so amounted to full-time manual control. In 1772, Andrew Meikle (see Golding[3]) introduced the "spring sail," in which the blades were spring-loaded to dump the direct pressure from the blades when the wind became too strong. This allowed steady operation of the mill over a much broader range of wind conditions. Finally, with an invention in 1789 by Captain Stephen Hooper, the control of the "patent" slats was regulated by a continuous control system utilizing a rod through the center of the main rotor shaft. The wind load on the blades was regulated by a mechanical chain and weight system and was essentially balanced by the weights. This meant that the solidity of the rotor would change automatically during operation but could still be adjusted without stopping the mill. The speed of the mill could also be manually reduced before the brake was applied to stop it. This was quite a sophisticated and reliable mechanical control system.

Load Control

Automatic load control to maintain grinding speed in a windmill was also common. A diagram of the automatic stone-clearance control is shown in Fig. 1.3. A flyball governor was arranged to increase the clearance between the millstones when the wind slackened in order to prevent the mill from stalling. The coarser grain so produced was sold at a lower price.

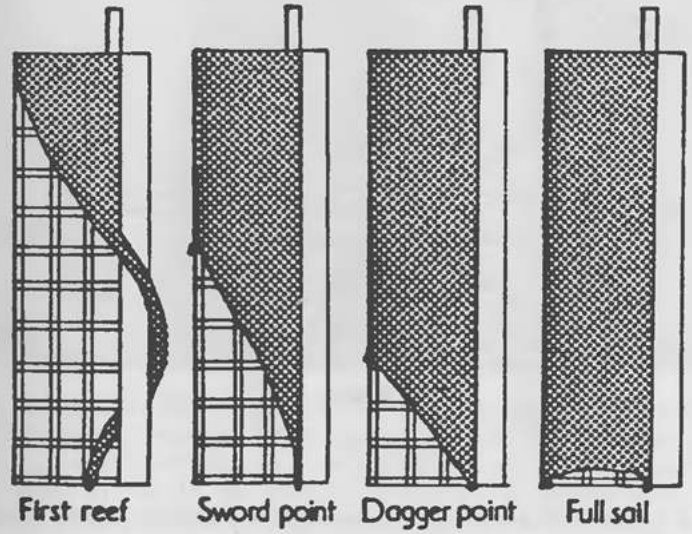

Figure 1.2. Sail reefs. (From Ref. 2.)

Yaw Control

Methods of turning the rotor into the wind were also evolved over a long period of time. Many of the early machines were cranked by hand (or "winded," pronounced with a short "i" as in "sinned") to face the wind. Later, a fantail rotor system was used, as in Figs. 1.1 and 1.4. Note that in this mill the cap was rotated by a worm gear driving a large wooden bull gear. The small side rotor was a 100-percent solidity, low tip-speed-ratio rotor arranged to respond to the cross-wind component and drive the main rotor to face the wind. This system was in essence an integrator or reset control system that would automatically force the main rotor to follow changing wind directions. Such a yaw drive can be very effective and has the advantage of responding positively, if slowly, thereby avoiding the large gyroscopic moments that would be induced as a result of fast yawing of the rotor. Recent research (see Chap. 13) has shown that this can be an effective method for avoiding large fatigue stresses in wind rotors.

A special guild of craftsmen mechanics—the millwrights—arose to build, maintain, and repair the many windmills in England and the Netherlands. These craftsmen were among the first of mankind to deal with large stationary power sources and machinery. Their expertise constituted a technology base that was extended in the industrial revolution that followed.

In more recent times, beginning in 1891, an experimental windmill test station was set up in Askov, Denmark under the direction of Professor P. La

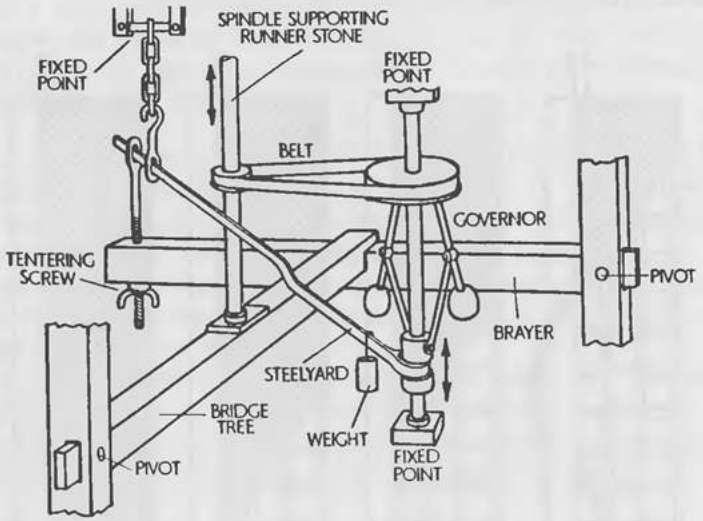

Figure 1.3. Action of governor and tentering screw (diagram not to scale). (From Ref. 2.)

Cour (discussed in more detail by Golding[3]). LaCour's objectives included economical construction, optimized performance, and the generation of electricity for use on Danish farms. His experimental wind turbine had a 22.8-m (75-ft) diameter rotor and four twisted, constant-chord blades with remotely controllable slats. An upwind machine winded by two small fantails, it drove two 9-kW generators. The use of two generators, either equal or unequal in capacity, is a design feature used on some modern Danish wind turbines.

A large (100-kW) wind turbine was constructed in Russia on the Baltic in the 1930s. A set of four designs for windmill blades was published in 1926 by Sabanin and Yuriev.[6] In the U.S., the engineer E. N. Fales published an important paper on high-speed windmills in 1928 and wrote a much-used

Figure 1.4. Pakenham Mill, Suffolk. One of the few working windmills in Britain. Note the pronounced 'weather' on the patent sails with spider striking gear, the aluminium-covered domed cap with a decorative finial, and the unusual gallery with diagonal braces. On the day the photograph was taken, the shutters were open and the mill not working, as it was being measured up for a new lightning conductor. (From Ref. 2.)

section on windmills in Marks' *Mechanical Engineers' Handbook*. A complete account of the design, construction, and testing of a large wind turbine documented in the book *Power from the Wind* by the engineer Palmer Putnam and his associates remains to this day a useful and informative work.[5] The engineering approach discussed there constitutes a basic model that any designer and project manager might follow, even though many of the technical specialties have advanced greatly since that time. The management of the "Grandpa's Knob" wind turbine project engaged the most renowned consultants of the day, and Putnam investigated all aspects of the project with a thoroughness that brings joy to the heart of an engineer. An example of his insight is that he recommended the possibility of using flaps (i.e., ailerons) to replace blade pitch control (see Ref. 5, p. 202) in future designs of large machines to reduce the size and cost of the hub and the control actuators. Studies of this option were completed in 1980 and 1984 (see Refs. 10 and 11 in Chap. 4), showing that this concept appears to remain quite viable.

Although we have concentrated on some of the most famous European work, we must note that important windmill improvements have been made in Germany, France, Denmark, Japan, and many other countries and that interest in wind power is truly international.

1.3 APPROACH TO DESIGN

In wind turbine design, many areas require attention; Table 1.1 shows some major requirements. One of the first tasks is to spell out the basic requirements for the machine to be built. Is it to be a 5-MW utility-owned machine or a small water pumper? What sort of winds will it see in operation? The design process can then proceed creatively to meet these needs in the least expensive and most efficient way. It isn't possible to satisfy all of them on the first try. As with any design, the process is iterative. A quite complete description of a wind turbine design has been given by Putnam.[5] This study documents wind measurements, economics, blade design, component procurement, and the whole iterative process by which engineering design proceeds; it is recommended reading for every wind turbine designer.

In designing, it is tempting to allow the excitement of creation to overcome reason to the extent that some pet idea or technical notion is given far more attention than is justified while other important areas are neglected. This tendency is to be avoided because any problem that does not receive proper attention is likely to return to haunt the manufacturer later. It is unwise to wait until problems have been incorporated into hardware before attempting to solve them since the costs of a fix are thus tremendously increased. The time and effort to be spent on each aspect of the design must be judged on the basis of its importance to the final product.

Design of a wind turbine is an exciting creative process. On the one hand,

Table 1.1. Design Tasks.

Rotor:	Tip-speed ratio, solidity, number of blades
	Aerodynamic optimization
	Static and dynamic operating loads
	Parked rotor loads
	Materials selection
	Manufacturing process
	Structural dynamics
	Fatigue
	Starting torque vs. friction torque
	Primary overspeed control
	Secondary overspeed control
	Blade tower clearance
	Brake system
	Yaw control
	Hub fairing (or not?)
Tower:	Height (local ordinances)
	Type: pole or truss, tilt-up?
	Structural loads
	Strength
	Structural dynamics
	Tower shadow or dam effect
	Erosion protection
Generator:	Type: ac (synchronous, 3ϕ, 1ϕ), or dc (alternator, generator)?
	Size
	Weight
	Efficiency curves
	Speed–torque characteristics
	Power conditioning
	Excitation
Gearbox:	Ratio; max. speed
	Torque capacity
	Strength and load deflections
	Noise
	Structural dynamics
	Lubrication
Control system:	Mechanical and/or electrical system
	Control algorithm
	Power supply; consequences of failure
	Startup and shutdown transients
	Wind speed and direction sensors
	Reliability
	Failure analysis
	Lightning protection
General:	Can it be simplified?
	System dynamics
	Shipping and erection
	Installation method
	Maintenance

Table 1.1. (continued)

General	Aesthetics
	Sensitivity to vandalism and UFOs
	Safety
	Corrosion protection
	Specifications and quality control
Cost:	Design life
	Development cost
	Cost per kWh of power produced
	Cost per kW installed
	Tax benefits
	Rate of return; payback period

extracting energy from wind is basically a simple conversion of energy, and many precedents and examples exist for guidance. On the other hand, mastery of all the disciplines required to build a truly efficient, reliable, and competitively priced wind turbine is an immense undertaking. Usually, one individual formulates the concept and keeps track of the development of the design. It is most convenient to have the support of technical experts in all the allied fields, such as aerodynamics, electrical machinery, structural dynamics, manufacturing processes, and the like.

Whether or not the designer has access to a staff of in-house technical experts, there is a good deal of other help available. Most of the components are conveniently purchased from suppliers, and reputable suppliers of major components have staff engineers expert in particular areas. As specifications are developed and firmed up, these experts are usually more than willing to make quotations, aid in proper choice of components, estimate costs of making modifications, and generally support the design process.

REFERENCES

1. Reynolds, John. *Windmills & Watermills*. London: Hugh Evelyn, Ltd., 1970.
2. Beedell, Suzanne. *Windmills*. Newton Abbot–London: David & Charles, 1975.
3. Golding, E. W. *The Generation of Electricity by Wind Power*. London: E. & F. Spon Ltd., 1977. (Distributed by John Wiley & Sons, Inc., New York.)
4. Prinsenmolen Committee. *Research Inspired by the Dutch Windmills*. Wageningen, The Netherlands: H. Veenman & Zonen, C. 1965 (out of print).
5. Putnam, Palmer C. *Power from the Wind*. © 1984 by S. Morgan Smith Co. (Republished by Van Nostrand Reinhold, 1974.)
6. Sabanin and Yurieff. Transactions of the Central Aero-Hydrodynamical Institute, No. 28, Moscow, 1926.
7. Eldridge, Frank R. *Wind Machines*, 2nd ed. MITRE Corp. New York: Van Nostrand Reinhold, 2nd ed., 1980.
8. Champly, R. *Théorie, construction, montage, utilisation au puisage de l'eau et á la production de l'électricité*. Paris: Dunod Publishers, 1933. (NASA Technical Translation TT F-16201. *Wind Motors: Theory, Construction, Assembly and Use in Drawing Water and Generating Electricity*, N75-19821, Apr. 1975.)

PART I

AERODYNAMICS

2

ROTOR AERODYNAMIC MODELLING

2.1 ELEMENTARY AERODYNAMIC MODELS FOR ROTORS

For wind-turbine design, it is necessary to generate mathematical models of the aerodynamic forces and moments on a rotor working in natural winds. This chapter will present several of these models after discussing the wind conditions that may be experienced by a real rotor.

Natural Winds and Their Effects on Rotors

When designing wind turbines, it is tempting to think of wind as a constant, homogeneous velocity field of fixed direction. This is the simplest wind model and offers a feasible starting point for analysis. Since such a condition doesn't exist in the real world, however, some discussion of actual conditions is relevant.

The actual wind field experienced by a given rotor may be inhomogeneous and unsteady. Upwind terrain features may reduce wind speed and generate turbulence. Since such effects will reduce the power available to a wind turbine, every reasonable effort must be made to select a suitable site and to use a tower of appropriate height to get the rotor up into relatively unobstructed wind.

To get a concept of some of the problems involved, consider a rigid tower having a set of anemometer-type axes centered at its top at hub height in such a way that the x-axis points into the wind, the y-axis is horizontal and points to the right, and the z-axis points downward. Let the direction of the local wind be represented by the angle $\phi(x, y, z, t)$ measured in a horizontal plane between the x-axis and true north, as shown in Fig. 2.1(a). We can then express a steady, homogeneous wind as $v(x, y, z, t) =$ constant, with $\phi(x, y, z, t)$ a constant. Of course, the direction, $\phi(0, y, z, t)$ in the preferred plane of the rotor, $x = 0$, may not be constant. The rotor would nominally rotate in this plane, although a rotor free to yaw usually does not do so. If the rotor is not aligned with the instantaneous wind, a yaw condition

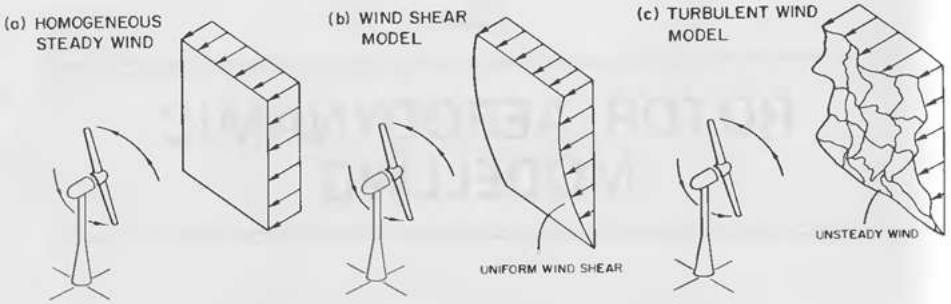

Figure 2.1 Representation of wind characteristics.

exists. A rotor yawed from the wind experiences cross-flow components whose direction changes as the blades rotate. This results in unsteady flow at the blades and dynamic (periodic) variations in the angle between the relative wind and the blade at a frequency of one cycle per revolution.

Horizontal-axis wind turbines use either passive or active yaw control in an attempt to keep the rotor plane oriented perpendicular to the wind. Passive yaw control systems sometimes allow yaw angles of 30 to 40 degrees (sometimes even 180 degrees) during operation, and even active yaw controls sometimes move so slowly that substantial yaw angles develop. Since yaw control systems can fail, moreover, no one can guarantee that a given rotor will never have to operate in a yawed condition.

For a homogeneous, constant-direction, time-varying wind, we can think of a rotor plane at $x = 0$ and a wind $v(0, y, z, t) = v(t)$, with ϕ a constant. This might be an acceptable model for, say, control system analysis if $v(t)$ consisted of an average value plus small random variations defined by a particular spectrum. Of course, it is extremely improbable that the wind velocity at every point on a rotor disk would change simultaneously, and single or multiple-point statistical correlations of measured wind data may be useful for some types of analysis.

A steady wind with vertical shear could be defined as $v(0, y, z, t) = v(z)$, with ϕ a constant, as in Fig. 2.1(b). The effect of wind shear should be smaller, the smaller the rotor diameter. Wind shear results in each section of the rotor blade (especially those sections near the tip) seeing unsteady (periodic) flow. Analysis of unsteady flow can become quite complex. If the changes in blade angle-of-attack are slow enough, steady-state analysis at equally spaced points around the rotor can give reasonably good results.

The wind field through a real rotor probably looks more like that of Fig. 2.1(c) and changes continually with time.

The problem of actually measuring the wind field of a given rotor is not an easy one. The wind may indeed have different velocities at various points in the rotor plane. Furthermore, a working rotor induces velocities that change the entire flow field in its vicinity. To measure the free stream wind field,

any anemometers must be placed well away from the rotor. Under these conditions, however, the anemometer is not measuring the windspeed actually felt by the rotor, and correlation of torque or power output with changes in measured wind velocity may fail to determine the performance of the machine. Mattson[1a] (p. 40) shows that on the basis of certain quite reasonable assumptions, the correlation of the wind velocity variations near the center of the rotor with those at other points on the rotor disc may be so poor that "it is not possible to obtain representative measurements of (the wind velocity) using an anemometer." This problem has profound implications for wind turbine testing and performance evaluation.

In general, then, the operational environment of a wind-turbine rotor may be quite complex. We attempt in analysis to formulate conditions representative of certain modes of operation and wind regimes. In design, we try to build mathematical models of the most critical conditions for the machine and gain as much insight from these models as we can.

We note that when a wind-turbine rotor is tested, there are conditions under which well-defined flow is experienced, and other conditions under which the flow breaks away, becomes turbulent, or may even reverse. Aerodynamic modelling of states where well-defined flow exists and turbulence is very small is fairly well-established, and quite fast computer codes for it exist. Modelling of unsteady flow processes for wind turbine rotors, however, is in its infancy. Further information and commentary on windspeed models for various purposes is given in Chaps. 3 and 5, in the introduction to Part II, and in Chaps. 7, 13, and 15.

Aero Technology

One must enter into wind-turbine aerodynamics analysis with a proper feeling for the complexity of the subject. The real flows of interest are governed by the Navier-Stokes equations.[4] These equations are quite complex, and over all the years only about 70 analytical solutions have been found. Although solutions may be found by numerical analysis on a computer, even these require careful choice of dimensionless variables and coordinate systems, judgment, and experience. If a reasonable approach to such a numerical analysis of a problem is found, the solutions obtained usually cannot be trusted until they are checked by wind-tunnel or water-tunnel testing under carefully controlled conditions. After doing this sort of thing full-time for 30 or 40 years with many different flow problems, you begin to have a decent understanding of how fluid is likely to flow.

Over the years, a number of useful generalizations have been found. For steady-flow problems, the gross flow field behavior may be determined from inviscid flow theory. One then uses Prandtl's boundary-layer theory to investigate the flow near surfaces. Even for steady flow over a flat plate at zero angle of attack the resulting flow pattern turns out to be of the complexity

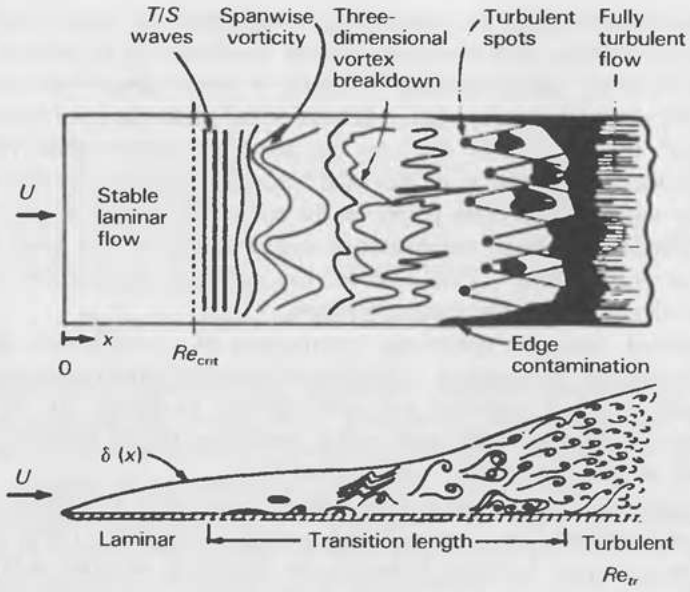

Figure 2.2. Idealized sketch of transition process on a flat plate. (From Ref. 16.)

shown in Fig. 2.2. Progressing aft from the leading edge, we start with a section having laminar flow. After the critical Reynolds number is reached, we see Tolmien-Schlichting waves, effects of spanwise vorticity due to the low aspect ratio of the plate, three-dimensional vortex breakdown, turbulent spots, edge contamination, and, finally, fully developed turbulent flow.

One can imagine how this "simple" real flow will be affected if the flat plate changes into an airfoil section of a rotor blade at an angle of attack. To this complication must be added the effects of surface imperfections from manufacturing, squashed bugs, surface-water droplets, and turbulent eddies causing unsteady motions and aggravating natural flow instabilities. Then we must consider flow separations and reattachments, as well as three-dimensional effects such as possible spanwise flow and interactions with blade hub and roots. If that weren't enough, blade flapping and torsional oscillation cause important dynamic effects in the fluid flow. This is clearly not a game for the faint-hearted.

A very large data base of information exists on the theory and testing of airfoils, wings, propellers, helicopter rotors, control surfaces, dynamic stall, etc. Some of this is directly applicable to wind-turbine design. Wind-turbine blades, however, have quite different operating requirements than aircraft wings. For example, aircraft wings do not have to operate continually in the stalled condition whereas portions of wind-turbine blades often do. Thus, although some modelling of aerodynamic forces is well grounded in previous

technology, there are other regimes of operation for which very little is known and no reliable mathematical models have ever been developed or validated. Much is yet to be learned regarding the aerodynamic forces, moments, and frequencies of oscillation of wind-turbine blades in various types of unsteady flow. Thus, full- and reduced-scale model testing remain important tools in wind-turbine development.

2.2 SEQUENCE OF AERODYNAMIC MODELS

The historical development of analytical methods of propeller design, as recounted by Glauert in Chap. 1, Sec. 4, of Durand's *Aerodynamic Theory*,[1] is also the precursor of analytic rotor aerodynamic modelling. It is interesting to follow the historical development from early gropings to sound analytical methods. Now, as then, the most reliable airfoil data is obtained from wind-tunnel tests.

Actuator Disc Model

The simplest model for propeller or wind-turbine aerodynamics is the actuator-disc model. This model requires some extremely simplifying assumptions and yet yields a number of useful approximate results, including insight into Smeaton's first postulate about blade solidity.

Glauert Annulus Momentum Vortex Theory

The next level of complexity is the Glauert strip or annulus momentum vortex theory. With this theory, each radial section of blade is analyzed independently using two-dimensional airfoil data and equations based upon continuity and conservation of momentum. Although this theory is strictly applicable only to rotors with an infinite number of blades (this assumption thereby guaranteeing that analysis can be done at one radial section independent of the others), corrections based on work by Prandtl or Goldstein have been reasonably satisfactory for extending this theory to the case of a finite number of blades. For a finite number of blades, however, the flow must become periodic when viewed in fixed coordinates, and the annulus theory is used to represent the average effects.

A number of modifications to this method have been made to improve accuracy and extend the range of applicability into regions of blade stall and nonstreamtube flow. This model provides a good approximation to the actual flow in some regimes of operation and is the most useful model for doing basic rotor design.

Prescribed-Wake Vortex Theory

Prescribed-wake vortex theory, which provides the next level of complexity, can be applied in several ways. The basic concept is that the vortices that

form a spiral trail behind the rotor-blade tips define the flow field around the rotor according to the Biot-Savart theorem. Each section of rotor blade generates a lift force that is proportional to its local bound vorticity. By integrating the effect of the trailing vortices over the blade, the induced flow, and hence the rotor forces and moments, can be determined. Again, as in the Glauert momentum vortex theory, two-dimensional airfoil data is used.

The problem with this model is that the actual path of the vortices must be defined in terms of wake equations derived from previous wake studies. The simplest approach is to assume a rigid helical wake behind the rotor. A computer program can then be written to solve for the forces and torques felt by the rotor. This method requires a good deal more computer time than the momentum vortex theory, and the effects of changes are more difficult to discern. It is useful for evaluating special effects that are not accurately described by simpler methods, such as the effect of an aileron as a control surface for rotor speed control.

Free-Wake Vortex Theory

Finally, the assumption of a rigid vortex wake can be eliminated, and one can attempt to find the exact path of the trailing vortices iteratively, as in vol. 8 of Ref. 4. Since this approach consumes a great deal of computer time, it is a research area. The results of Ref. 4 do not differ much from those of the simpler momentum theory for a simple fixed-blade rotor.

There are some regimes of operation that are very difficult to model by any known analytical method, including many types of unsteady flow. Empirical approaches may thus be necessary until satisfactory modelling methods are developed and tested.

2.3 RANKINE–FROUDE ACTUATOR DISC THEORY

To begin to understand the mechanics of rotor power absorption from winds, proposing this simple one-dimensional model provides a start. The rotor is replaced by an "actuator disc" through which the static pressure decreases discontinuously. The assumptions on which Rankine–Froude actuator disc theory are based are then as follows:

1. Steady, homogeneous wind.
2. No obstructions to wind flow either upstream or downstream
3. Uniform flow velocity at disc
4. Wind flow passing through disc separable from remaining flow by well-defined streamtube
5. Wind flow incompressible
6. No rotation of flow produced by disc

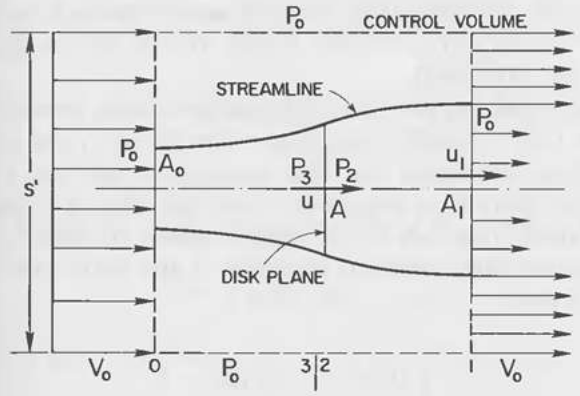

Figure 2.3. Flow pattern.

Assumption 3 requires that the disc slow the wind equally at each radius, which is equivalent to assuming uniform thrust loading on the disc.

Now consider the flow diagram of Fig. 2.3 for a cylindrical control volume of cross-sectional area S and note stations 0, 3, 2, and 1. Wind approaches the rotor at velocity V_0 far upstream at station 0 at ambient (static) pressure p_0. Energy is extracted by the rotor, and the reduced velocity causes the streamline to expand. If the velocity decrease induced by the rotor is v, then the velocity at the disc is $V_0 - v = u$, while far downstream at station 1 the wind has been slowed further to velocity u_1 and the pressure has returned to p_0. Let A be the area of the rotor disc and ρ be the air density. The momentum loss of the fluid is the result of the thrust T that the rotor exerts against the flow, combined with the net resultant of the external pressure on the control volume, as shown in Fig. 2.3. Since the ambient atmospheric pressure, p_0, acts on the entire control volume, its net resultant is zero.

Within the streamtube, continuity requires that $V_0A_0 = uA = u_1A_1$. Writing the continuity equation for flow outside the streamtube between sections 0 and 1, we find that there must be a net flow, ΔQ, out the sides of the control volume equal to the following:

$$\Delta Q = V_0[(S - A_0) - (S - A_1)] = V_0(A_1 - A_0) \tag{2.1}$$

Writing the momentum theorem for the cylindrical control volume, we obtain

$$\rho V_0^2 S - T = \rho V_0^2(S - A_1) + \rho u_1^2 A_1 + \rho \Delta Q V_0 \tag{2.2}$$

Substituting ΔQ from Eq. 2.1 and $V_0A_0 = u_1A_1$ gives the thrust as

$$T = \rho A_1 u_1 (V_0 - u_1) \tag{2.3}$$

Physically, an "actuator disc" could be approximated by a rotor with a large number of very thin, dragless blades rotating with a tip speed much higher than the wind speed.

To slow the wind, a force must be manifested as a pressure drop across the disc. The (static) pressure just ahead of the disc is p_3 and just behind the disc is p_2. Since we assume that these pressures do not vary with time, we also assume that there is no periodicity in the flow velocity at the rotor plane, a condition strictly true only for an infinite number of blades. Applying the Bernoulli theorem from section 0 to section 3 and again from section 2 to section 1, we have

$$\tfrac{1}{2}\rho V_0^2 + p_0 = \tfrac{1}{2}\rho u^2 + p_3 \tag{2.4}$$

$$\tfrac{1}{2}\rho u^2 + p_2 = \tfrac{1}{2}\rho u_1^2 + p_0 \tag{2.5}$$

The thrust on the rotor is then

$$T = A(p_3 - p_2) \tag{2.6}$$

Solving for the pressure difference using Eqs. 2.4 and 2.5 gives

$$T = \rho A(V_0^2 - u_1^2)/2 \tag{2.7}$$

Equating Eqs. 2.3 and 2.7 and using $Au = A_1 u_1$, we find that

$$u = (V_0 + u_1)/2 \tag{2.8}$$

Thus, the velocity at the disc is the average of the upstream and downstream velocities. Defining an axial interference factor, a, as the fractional decrease in wind velocity between the free stream and the rotor plane represented by

$$a = v/V_0 \tag{2.9}$$

we find that

$$u = V_0(1 - a) \tag{2.10}$$

Also

$$u_1 = V_0(1 - 2a) \tag{2.11}$$

For $a = 0$, the wind is not retarded and no power is obtained, whereas for $a = 0.5$, the wind has slowed to zero velocity behind the rotor, and,

without the presence of flow, no power is generated. The energy removed by the rotor per unit time is

$$P = \tfrac{1}{2}\rho V_0^2 Au - \tfrac{1}{2}\rho u_1^2 Au = \tfrac{1}{2}\rho Au(V_0^2 - u_1^2) = \tfrac{1}{2}\rho Au(V_0 + u_1)(V_0 - u_1) \tag{2.12}$$

Substituting u from Eq. 2.10 and u_1 from Eq. 2.11, we find that

$$P = \tfrac{1}{2}\rho AV_0^3\, 4a(1 - a)^2 \tag{2.13}$$

We define a power coefficient, $C_P = P/(\tfrac{1}{2}\rho AV_0^3)$, so that

$$C_P = 4a(1 - a)^2 \tag{2.14}$$

Obtaining a maximum C_P as a function of a gives $a = 1/3$, so that

$$C_{P_{max}} = 16/27 \cong 0.59259$$

$$u = (2/3)V_0 \tag{2.15}$$

$$u_1 = (1/3)V_0 \tag{2.16}$$

The pressure and velocity relationships in the vicinity of the rotor are shown in Fig. 2.4.

Let us examine the implications of this model. First, the wind velocity at the rotor plane is always less than the free-stream velocity when power is being absorbed. Thus, the simplistic concept of carving a rotor with pitch angle equal to arctan $(V_0/\Omega r)$ would be incorrect, giving too high a pitch.

Second, this model assumes no wake rotation, i.e., no energy wasted in kinetic energy of a twirling wake. As will be shown subsequently, slow-turning, high-solidity rotors such as the ordinary farm windmill waste a considerable amount of energy in wake rotation, thus limiting their efficiency.

Third, even with the best rotor design, it is evidently not possible to extract more than about 60 percent of the kinetic energy in the wind.

The range of the axial interference factor, a, is from 0 for no energy extraction to one-half, at which point the wind theoretically slows to zero velocity behind the rotor. Outside this range, the assumptions made in deriving this model are violated.

Additional data that can be derived from this model include the thrust loading on the rotor. The thrust on the rotor is

$$T = \tfrac{1}{2}\rho A(V_0^2 - u_1^2)$$

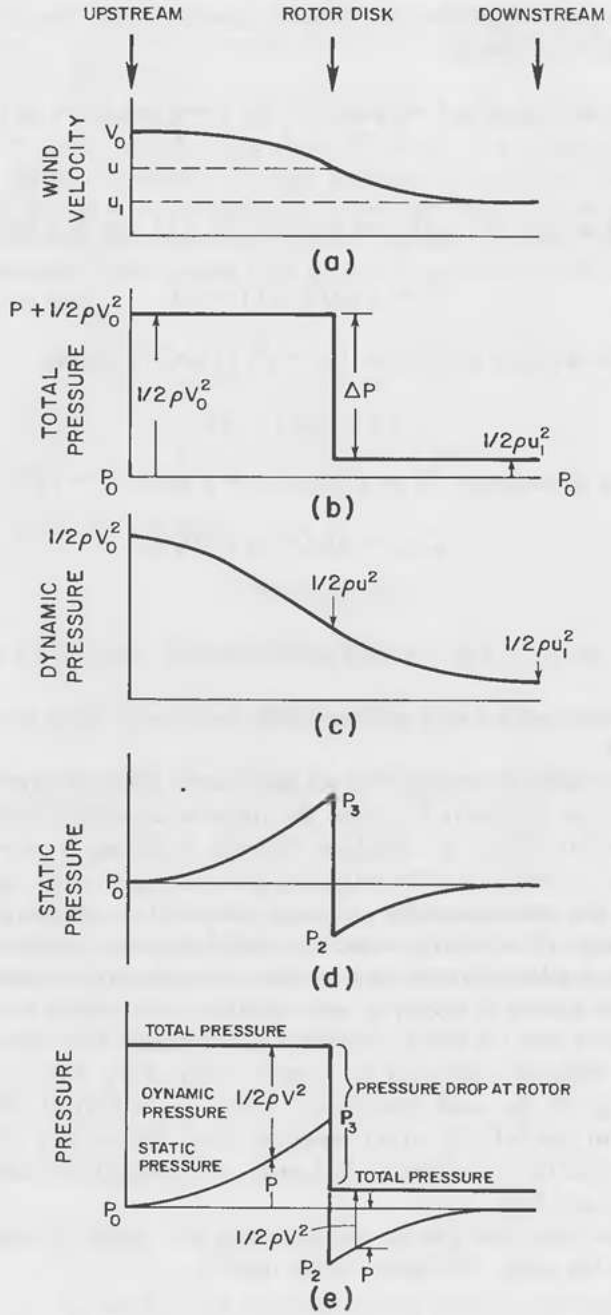

Figure 2.4. Pressure relationships.

which for $u_1 = V_0(1 - 2a)$ simplifies to

$$T = \tfrac{1}{2}\rho V_0^2 A[4a(1 - a)] = qA[4a(1 - a)] \tag{2.17}$$

where q is the dynamic pressure.

If we were thinking of the rotor as a propeller, we would define a thrust coefficient, as follows:

$$C_T = \frac{T}{qA}$$

On the other hand, if we were to think of T as a drag force on an equivalent flat plate of area equal to that of the rotor disk, we can define a drag coefficient, as follows:

$$C_d = \frac{T}{qA}$$

In either case, it is apparent from Eq. 2.14 that for these definitions

$$C_T = C_d = 4a(1 - a) \tag{2.18}$$

Since a flat plate has a drag coefficient of about 1.28, we can note that, for $a = 1/3$, we obtain an equivalent drag coefficient of $8/9$ for a rotor operating at the maximum C_P condition. Thus the rotor thrust at this condition is about 30 percent less than that of a flat plate equal in diameter to the rotor. In Sec. 2.5, we will see that in the turbulent wake state, equivalent drag coefficients as high as 2.0 are possible. It is easy to see that the thrust loads generated by continuing to operate in high winds can be very large, requiring a very strong rotor and tower.

The wind pressure on the blade becomes the following:

$$p = 4qa(1 - a)\,(2\pi r/Bc) = 4qa(1 - a)/\sigma_l \tag{2.19}$$

where B is the number of blades; σ_l is the local solidity, $BC/2\pi r$; and c is the local chord at radius r. If c is constant, this implies a triangular blade loading, i.e., one that increases linearly with r.

Another result concerns the expansion of the turbine wake. If the diameters of the wake upstream, at the rotor, and downstream are R_0, R, and R_1, respectively, continuity requires that

$$\pi R_0^2 V_0 = \pi R^2 u = \pi R_1^2 u_1 \tag{2.20}$$

Substituting $V_0(1 - a)$ for u and $V_0(1 - 2a)$ for u_1, we find the relations,

$$R = R_0/\sqrt{(1 - a)} \text{ and } R_1 = R\sqrt{(1 - a)/(1 - 2a)} \qquad (2.21)$$

Since, for the maximum power output condition, $a = 1/3$, therefore

$$R = 1.225\, R_0$$

$$R_1 = 1.414\, R \qquad (2.22)$$

Thus, at maximum power output, the rotor operates on a contracted tube of about 0.816 R in radius and produces an expanded tube of about 1.414 R in radius downstream. It is interesting to explore all these relationships numerically, a subject that will be discussed in Chap. 4.

2.4 WAKE ROTATION

To model flow near wind turbine blades more closely, the wake rotation effect must be considered.

The actuator disc concept used in the axial momentum theory enabled us to estimate the energy removed without considering that the rotor power absorbed is the product of torque Q and angular velocity Ω of the rotor and that this is directly related to the angular velocity ω of an annular section of the air. Application of the angular (moment of) momentum theorem to (assumed rigid) disc-shaped portions of the incoming and outgoing air streams shows that the torque impulse on the rotor, Qdt, requires an equal and opposite angular momentum, $Jd\omega$, in the air flow downstream of the rotor.

The resulting rotational kinetic energy is not economically recoverable and thus represents wasted energy. A rotor generating high torque at low speed will generate less power than one rotating at high speed and generating low torque (if the aerodynamic drag of the blade is small). The multibladed farm windmill is a common example of a machine whose efficiency is severely limited by wake rotation.

The complete angular momentum equations of wake rotation were presented by N. E. Joukowsky[2] in 1918 and are nicely presented by Glauert[1] as they apply to a propeller. This derivation was modified for a wind turbine rotor by Wilson and Lissaman.[2]

Derivation of the continuity, angular momentum, and radial momentum equations is simple and will be given here. The derivation of the energy equation and the algebraic reduction of these equations to a usable form are quite lengthy procedures and are given by Glauert[1] (Div. L, Chap. III, Sec. 1). Rotor airfoil drag is neglected in these equations.

The thought process required in the wake rotation equations is important

because it is necessary to consider noninteracting annular streamtubes and to assume that the local pressure, rotational velocity, and axial velocity are functions of blade radius r. The pressure drop at the disc is related to the dynamic pressure generated by the relative motion of the rotor in one direction and the wake in the other.

Even with all this analysis, the wake rotational momentum equations are not solvable in closed form without an arbitrary assumption, as will be shown. Consider the annular streamtube in Fig. 2.5. The annulus width, radius, and axial velocity are dr, r, and u at the rotor plane and dr_1, r_1, and u_1 at a section far downstream, respectively.

Continuity requires that

$$2\pi r u dr = 2\pi r_1 u_1 dr_1 \qquad (2.23)$$

No mechanism exists that could impart rotational momentum to the stream ahead of the rotor. This being true, we must assume that the wake rotation starts discontinuously (if we consider the rotor as an infinitesimally thin disk) at the rotor. Applying the angular momentum theorem to the streamtube, we find that

$$\omega r^2 = \omega_1 r_1^2 \qquad (2.24)$$

where ω and ω_1 are angular velocities of the air at the rotor and in the wake, respectively.

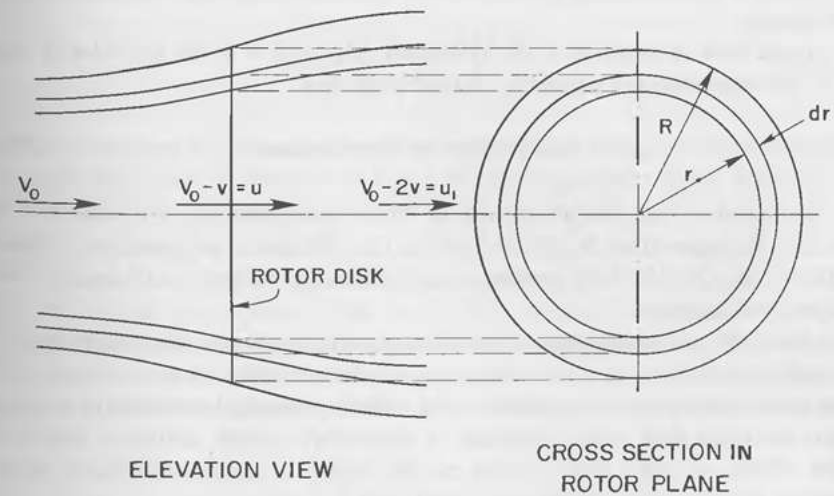

Figure 2.5. Annular streamtube.

Balancing radial forces on a segment of annular streamtube at the downstream section, we find that

$$dp_1/dr_1 = \rho r_1 \omega_1^2 \tag{2.25}$$

For derivation of the energy equation, refer to Glauert.[1] The result, as modified for wind turbines, is as follows:

$$\frac{(u_1 - V_0)^2}{2} = \left[\frac{(\omega_1/2) + \Omega}{u_1} - \frac{(\omega/2) + \Omega}{u}\right] u_1 \omega_1 r_1^2 \tag{2.26}$$

These four equations cannot be solved in closed form without additional assumptions. Insight can be obtained, however, by assuming an angular velocity distribution for the airstream and solving the remaining equations.

Following Glauert, the element of torque of the rotor is equal to the angular momentum imparted in unit time to the corresponding annular element of the slipstream:

$$dQ = \rho u \omega r^2 dA \tag{2.27}$$

From the derivation of the energy equation,

$$dT = (p_3 - p_2)\, dA = 2\pi\rho\omega r^3 [(\omega/2) + \Omega] dr \tag{2.28}$$

These expressions can be evaluated if an angular velocity distribution, $\omega(r)$, is known.

If the flow is assumed to be irrotational [curl$(\bar{v}) = 0$ for the velocity field $\bar{v}$], the circulation is constant. This implies that

$$\omega_1 r_1^2 = \omega r^2 = k = \text{constant} \tag{2.29}$$

In this case, an exact solution of these wake rotation equations can be made. Formulated by N. E. Joukowski, this solution is presented by Glauert[1] (Chap. III, Sec. 2) for propellers and modified by Wilson and Lissaman[2] for wind-turbine rotors.

Although the assumption of irrotationality is commonly used and approximately valid in many flow models, it cannot be valid near the rotation axis or at the blade tips. Nevertheless, and with experimental verification difficult, this assumed flow model provides a reasonably simple analytical model of the effects of wake rotation and can be useful in design, especially in the design of low-speed rotors.

When $\omega r^2 = k$, the wake radial velocity equation shows that u_1 cannot

vary with radius and, indeed, must be constant. If the variables a and b are defined such that

$$u_1 = V_0(1 - b) \quad \text{and} \quad u = V_0(1 - a) \tag{2.30}$$

the equation,

$$a = \frac{b}{2}\left[1 - \frac{b^2(1 - a)}{4X^2(b - a)}\right] \tag{2.31}$$

is found, where X is the tip-speed ratio, $R\Omega/V_0$. This ratio of the tip speed to the wind speed is the fundamental speed parameter for wind-turbine rotors, just as the advance ratio, J, usually defined as $J = V_0/nD$, where n = rev/sec, is fundamental for propellers. Note that the tip-speed ratio X and the advance ratio J are related by the equation, $X = \pi/J$. [Watch out for other conventions, however. Miller et al. in Ref. 5 define an advance ratio $\mu = V_0/\Omega R$; thus, their advance ratio $\mu = 1/X$ is the straight reciprocal of the tip-speed ratio, X.]

Solutions (trial and error) of the preceding equation show that, for tip-speed ratios X above 2, the axial velocity change in the wake is very nearly twice that at the disc, as was determined in the axial momentum theory.

The exact solution of the wake rotation equations permits expressions for torque, thrust, and power coefficients to be written in terms of the parameters a and b that satisfy Eq. 2.28.

The constant k needed in the thrust and torque integrals is found to be

$$k = \left[\frac{(1 - a)b^2}{2(b - a)}\right]\left[\frac{V_0^2}{\Omega}\right] \tag{2.32}$$

The assumption of constant circulation requires ω to increase without bound as r approaches zero, behavior that is not physically possible. Since the torque is calculated as the reaction to the resulting angular momentum, some modification must be made. Glauert arbitrarily stopped his integration at the point where $\omega = \Omega$ since it is unlikely that a propeller could cause the air near its hub to rotate faster than itself. The physical limitation on wake angular velocity for a wind turbine rotor is not quite so obvious. Wilson and Lissaman[2] cut out a cylinder near the axis and inserted a Rankine (rigid-disk) wake as an alternative. In their solution, if $N = \Omega/\omega_{max}$, the power coefficient becomes

$$C_P = \frac{b(1 - a)^2[2Na + (1 - N)b]}{(b - a)} \tag{2.33}$$

It is clear that the wake rotation effect greatly limits the power absorbed by a rotor designed for low tip-speed ratios.

The torque Q can best be calculated from C_P above since

$$C_P = \frac{P}{(\frac{1}{2}\rho V_0^3 A)} \tag{2.34}$$

where $P = Q\Omega$. The thrust coefficient becomes

$$C_T = \frac{T}{(\frac{1}{2}\rho V_0^2 A)} = \frac{[(1-a)b^2/(b-a)][1+2(b-2a)]\ln[b/2N(b-2a)]}{b-2Nb+4Na} \tag{2.35}$$

Since the first term inside the brackets is the result from axial momentum theory, this shows that wake rotation increases the thrust on the rotor.

2.5 WIND ROTOR STATES

We are accustomed to think of a wind-turbine rotor only in its intended state in which it removes energy from the wind and converts it to shaft power while slowing the wind accordingly. In the operation of such a rotor, however, other states of operation may occur. A wind-turbine designer should have a physical understanding of these states and their significance to rotor loads, dynamics, and speed control.

The theory and phenomenology of rotor states was presented by Glauert and was extended by Wilson and Lissaman with regard to wind-turbine rotors[2]. Further work by Stoddard[6] correlated the behavior of wind-turbine rotors with known data for helicopters. Much remains to be done before a complete understanding and methods of modelling the onset of, and the forces and moments developed during, the turbulent-wake rotor states are developed.

We will be discussing these states and attempting to correlate blade element conditions with the state of the rotor as a whole. Since other blade elements may experience different conditions, the approximate nature of this analysis should be noted.

Since horizontal-axis wind-turbine rotors almost universally use cambered airfoils, we will digress briefly to point out that the transition of a blade element from one condition to the other is more closely related to the zero-lift line for an airfoil than to the chord line. Thus, for example, the zero-slip condition occurs in Fig. 2.6 when $\alpha' = 0$, not when $\alpha = 0$. For a symmetrical

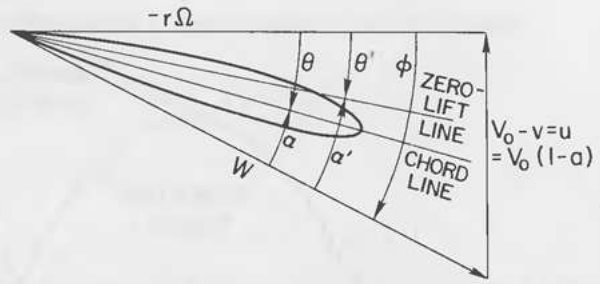

Figure 2.6. Zero-lift goemetry.

airfoil, $\alpha = \alpha'$ and $\theta = \theta'$. It is convenient to catalog these states in terms of the induced velocity, v, as represented nondimensionally in the axial interference factor, a.

From all accounts, the Glauert momentum theory provides modelling of the propeller state that is quite adequate for preliminary design, and the modified Glauert momentum theory is recommended for use in the windmill state. In the propeller and windmill states, streamlines may be traced in the fluid, whereas in the other states, streamlines are either very difficult to define or do not exist.

Consider a rotor with a free stream velocity, V_0, impinging on it. The rotor pitch may be set to any value, and the rotor rpm is maintained constant by adding or withdrawing power on the rotor shaft.* The rotor states are shown in Fig. 2.7.

Consider the blade pitch angle, θ', with respect to the relative wind angle, ϕ, as shown in Fig. 2.6. If the pitch angle θ' is greater than ϕ as in Fig. 2.7(a), the rotor is in the *propeller state*, accelerating the wind in the same direction it was originally going. Power must be supplied to the rotor to maintain rpm, and v and a are negative. If $\theta' = \phi$ as in Fig. 2.7(b), the rotor is in the *zero-slip state*, and both v and a are zero. For $\theta' < \phi$ as in Fig. 2.7(c), the *windmill state*† occurs, $0 < a < 0.5$, and the rotor develops output torque. If θ' goes negative, a point is reached where the torque goes to zero. Beyond that, the rotor acts as a brake, actively pushing the wind back from whence it came as in Fig. 2.7(d). This is the *propeller brake state*, in which v is again positive, $a > 0$, and torque must be supplied to the rotor shaft to maintain rpm. The propeller brake state can be considered to consist

*This is very similar to the actual case of a variable-pitch rotor driving an induction generator.
†The windmill state is sometimes (and with added ambiguity) called the *windmill brake state* since the rotor is braking the wind.

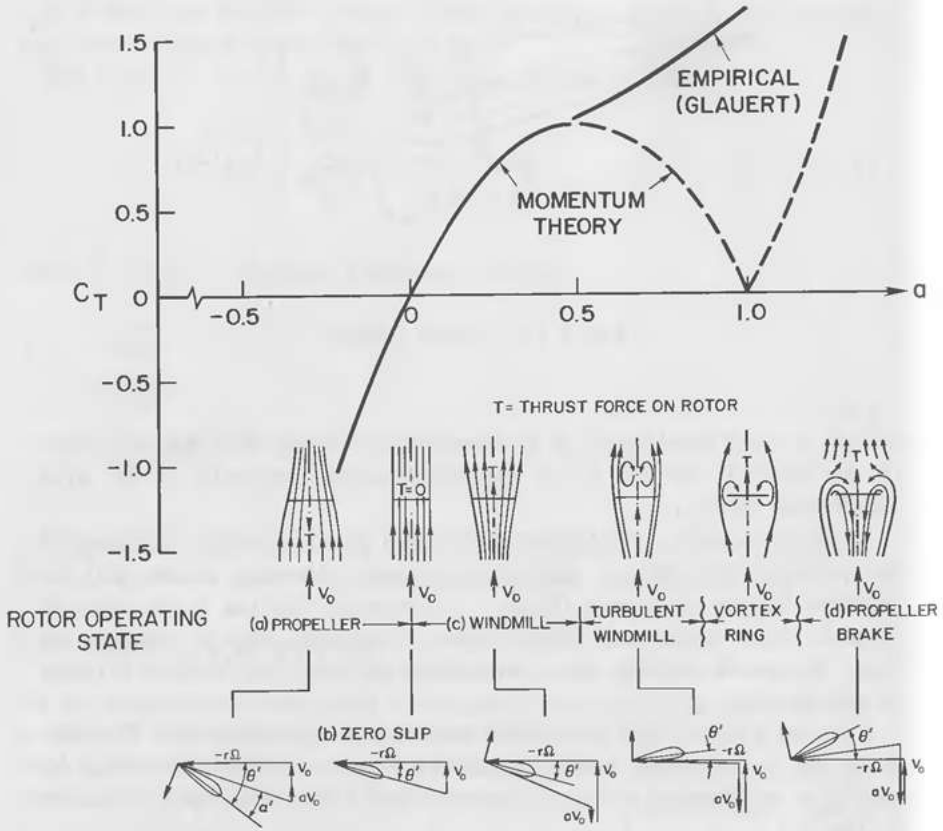

Figure 2.7. Rotor states.

of two substates: the *turbulent wake state* for $0.5 < a < 1.0$ and the *vortex ring state* for $a > 1.0$.

Each of these states has counterparts in helicopter and/or airplane aerodynamics as Wilson and Lissaman (1974) and Stoddard (1977) have pointed out. Thrust reversing for landing a fixed-wing aircraft requires going from the propeller to the propeller brake state. Helicopters go through the turbulent wake and vortex ring states during part-power descent, pilots reporting that large variations (± 30 percent) in thrust and input power are observed, with accompanying vibration and turbulence.

Although the flow streamline assumptions of actuator-disk theory are violated for $a > 0.5$, Wilson and Lissaman extended the C_T and C_P algebraic equations derived from actuator disk theory to the region, $a > 0.5$. (Consideration of the differences between momentum theory and experimental results may lead

to better understanding.) These equations are as follows:

$$C_T = 4a|1 - a| \tag{2.36}$$

and

$$C_p = 4a(1 - a)|1 - a| \tag{2.37}$$

They also showed the empirical line given by Glauert describing test data for C_T for $a > 0.5$. Figure 2.8 shows these curves with helicopter data added as given by Stoddard.[6] Thus, as might be expected, the C_T curve from actuator disk theory *fails to describe measured results* for $0.5 < a > 1.0$. This is consistent with the fact that the assumptions on which this theory is based are violated in this region.

For $a = 0.5$, momentum theory predicts zero flow downstream, in which case the rotor might behave as a large flat plate forcing the air to flow around it. As noted by Stoddard,[6] Gessow described the large slipstream expansion, turbulence, and recirculation by imagining a large circular disc's being placed

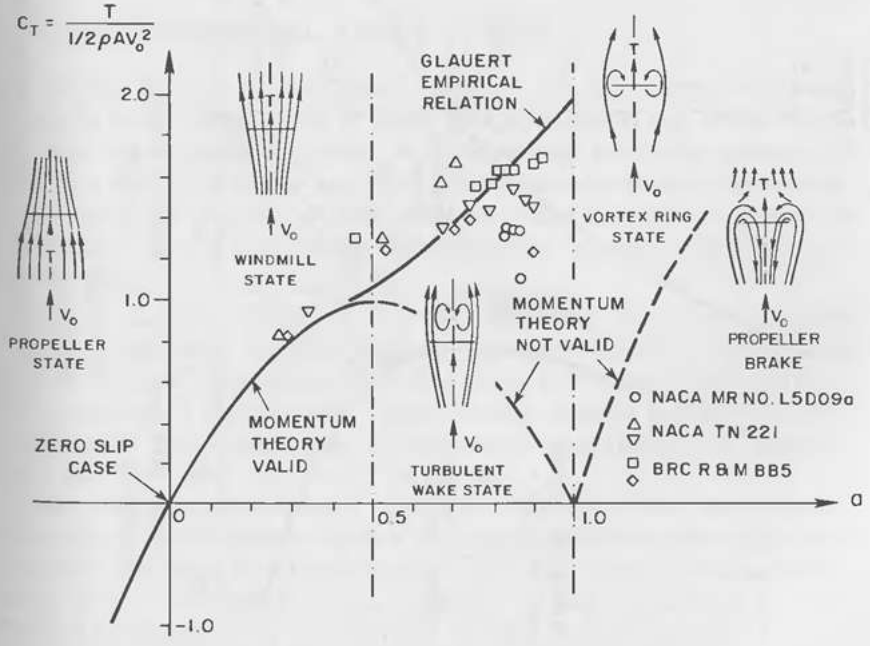

Figure 2.8. Thrust coefficient versus axial interference factor.

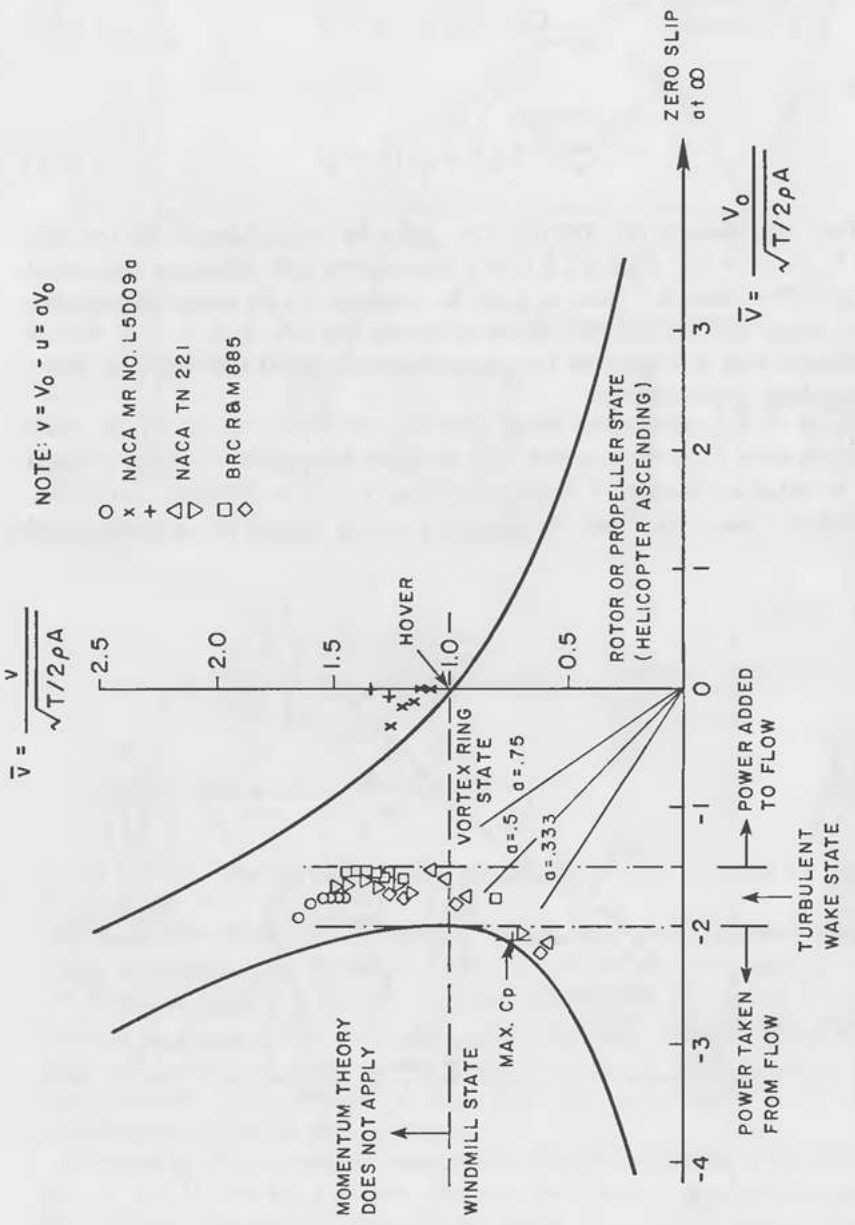

Figure 2.9. Induced velocity versus free-stream velocity.

perpendicular to the flow. Since C_T then approaches the drag coefficient of a flat plate, which ranges from 1.17 to 2.0 for $Re > 100$ (see Fig. 26 in Ref. 11), very high blade loads are possible in this state.

Another plot that portrays flow state results of dimensionless induced velocity, $\bar{v} = v/\sqrt{T/2\rho A}$, versus $\bar{V}_0 = V_0/\sqrt{T/2\rho A}$ is shown in Fig. 2.9 from Stoddard.[6]

Since Fig. 2.9 was developed for helicopter data, $\bar{V}_0 > 0$ represents the propeller state, the usual state for helicopter rotors, whereas $\bar{V}_0 < 0$ portrays the windmill state, the usual state for windmills. Note that in this plot, a is simply the ratio of ordinate to abscissa at any point.

The solid curve to the left in Fig. 2.9, which represents momentum theory, is given by $V_0 = -(1/\bar{v}) - \bar{v}$. At zero slip, $T = 0$; thus, this case occurs when $V_0 \to \pm\infty$. As a increases from zero, a windmill rotor would follow the momentum theory curve up to $a = 1/3$ for C_P max and then up to the beginning of the turbulent wake state at $\bar{v} = 1$. Again, the data *does not follow* the momentum theory curve after $a = 0.5$. A variable-pitch wind-turbine rotor that could pitch negatively past $\theta' = 0$ would in some way go through the turbulent wake and vortex ring states before reaching the propeller state.

2.6 TWO-DIMENSIONAL AIRFOIL THEORY

To use the annulus or strip theory approach to rotor design intelligently requires a basic understanding of steady-flow, two-dimensional airfoil theory, and wind tunnel testing of airfoils. Wind-tunnel tests are usually necessary to validate a new airfoil design and explore performance in off-design conditions. This section will provide the most elementary facts and some comments on use of airfoil data in wind-turbine rotor modelling, together with guidance to the literature.

A word of encouragement if due here. While the subject area is indeed vast, the basic facts are not difficult to grasp. Furthermore, the very large body of technical information on airfoils, wings, helicopters, control surfaces, etc., constitutes a resource that a clever design engineer can tap to achieve rotor designs that surpass, both in aerodynamic performance and low cost, many that have been "successful" in the past.

Many books on aerodynamics contain discussions of basic airfoil theory. McCormick[8a] and Dommasch[9] give very readable treatments with applications to aircraft. The most useful reference for small- to medium-sized wind-turbine design data is "A Catalog of Low Reynolds Number Airfoil Data for Wind Turbine Applications" by S. J. Miley.[3] Another standard reference for basic mathematical theory of airfoils and airfoil data at higher Reynolds numbers typical of large wind turbines or full-sized aircraft is by Abbott and Von

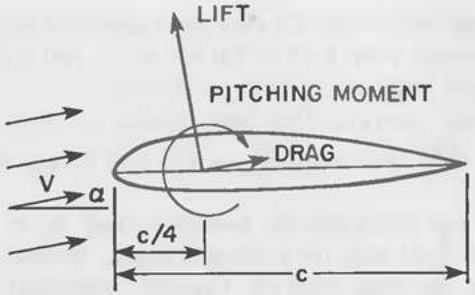

Figure 2.10. Aerodynamic forces and moment. (From Ref. 3.)

Doenhoff.[4] Two exceptionally useful books giving basic theory and a vast collection of experimental results are *Fluid-Dynamic Drag*[11] and *Fluid-Dynamic Lift*[12] by the late S. F. Hoerner.

As air flows past an airfoil, it generates both normal pressures and shear stresses at every point where the air touches the foil. The total forces on a foil can be determined by integrating these pressures and stresses over the surface of the airfoil. From statics it is known that any set of forces on a rigid body can be resolved about an arbitrary point into two perpendicular forces and one moment. For airfoils, the convention is that the drag force, D, is measured in the direction of the free-stream relative wind felt by the foil, whereas the lift force, L, is measured perpendicular to this relative wind. The aerodynamic moment is usually measured about the 25-percent chord point—i.e., one-fourth of the way back from the leading edge of the foil on a line joining the leading and trailing edges.* The length of c is called the *chord* of the foil. These conventions are shown in Fig. 2.10.

We will be dealing here with two-dimensional flow past airfoils. Thus we consider the foil to be infinitely long so that no three-dimensional flow effects can occur. By careful control and the use of suction to eliminate unwanted boundary layer effects, it is possible to approximate closely two-dimensional flow over an airfoil in a wind tunnel. Both the Glauert momentum theory to be discussed in Sec. 2.7 and the vortex prescribed-wake theory utilize this two-dimensional flow data to estimate the full three-dimensional performance of a real rotor.

In the results of experimental work in two-dimensional flow, the lift force, L, and drag force, D, together with the moment on an airfoil, M, are given

*In certain literature, a slightly different reference point, the aerodynamic center (a.c.), is used. The a.c. is the point of action of the lift and drag forces such that the aerodynamic moment (for constant V) does not change with angle of attack. Except for very thick foils, the $c/4$ point and the a.c. are usually very close together, but it is important to know which reference is being used.

in standard dimensionless ratios—c_l, c_d, and c_m—as shown below (this data is called *section data*, because it applies to a certain particular airfoil cross-section):

$$c_l = \frac{L}{\frac{1}{2}\rho V^2 S} \tag{2.38}$$

$$c_d = \frac{D}{\frac{1}{2}\rho V^2 S} \tag{2.39}$$

$$c_m = \frac{M}{\frac{1}{2}\rho V^2 S c} \tag{2.40}$$

where ρ is the air density; V, the wind velocity relative to the foil; and S, the plan form area of the foil.

The lift, drag, and moment coefficients—c_l, c_d, and c_m—are usually given as functions of the angle of attack, α, which is the angle from the direction of flow to the airfoil chord line.†

The format for graphical presentation of airfoil data is shown in Fig. 2.11. The lift and pitching moment coefficients are usually plotted versus angle of attack, whereas the drag coefficient is plotted versus the lift coefficient. A line through the origin of the latter curve tangent to the c_d vs. c_l curve gives the point of maximum lift-to-drag ratio, L/D, where $L/D = c_l/c_d$. This maximum establishes the best glide ratio for an airplane wing. In wind-turbine rotors, maximum L/D gives the best angle of the resultant aerodynamic force vector for the generation of torque, as will be seen in Fig. 2.12.

A convention in airfoil theory is that coefficients for two-dimensional flow airfoil data (i.e., section data) are given in lower-case letters, whereas coefficients for three-dimensional flow are given in capital letters. Since people freely violate this convention in much of the wind-turbine literature and use capitals to represent two-dimensional data, one should use caution and check which definition is being used.

Fluid flowing past an airfoil must split, some going above and some below. A boundary layer of slowly moving fluid begins at the leading edge and increases in thickness along the flow, on both upper and lower surfaces. As long as the pressure gradient along the flow is negative, the fluid is accelerated

†In some literature, a different reference—the *zero-lift line*—is used. This line could be scribed on the airfoil parallel to the free stream at the orientation of the foil for which no lift is generated. When the chord line is used as reference, the c_l vs. α curve generally does *not* go through the origin, whereas when the zero-lift line is used, the c_l vs. α curve *always* goes through the origin.

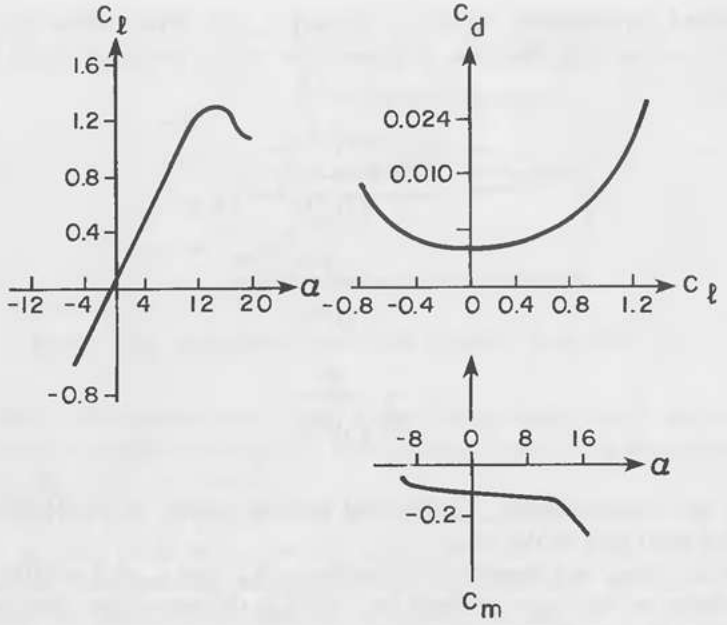

Figure 2.11. Conventional graphical presentation of airfoil characteristics. (From Ref. 3.)

and the boundary layer remains attached to the airfoil surface. If an adverse or positive pressure gradient arises, it tends to slow down the fluid and may cause the flow to break away from the surface, especially at high angles of attack. The result in this case will be increased drag and reduced lift.

Airfoil data is obtained in wind-tunnel tests because the conditions of such tests can be carefully controlled. Miley[3] gives a good short overview of wind tunnels and the relevance of their capabilities to wind-turbine rotor airfoil data. The book by Pope and Harper[13] gives a more detailed discussion of the broader aspects of low-speed wind-tunnel testing.

In wind tunnel tests, the airfoils are constructed to exact shape and polished to a very smooth surface finish, since roughness on the surface, especially near the leading edge, can materially affect the boundary layer and change the airfoil characteristics. Airfoils may differ greatly in the sensitivity of their performance to surface deposits and irregularities, and a low sensitivity is not only a desirable quality but can be designed into wind-turbine airfoils. To investigate the effects of airfoil roughness during the tests, small particles are often glued onto the foil and the tests rerun. The "standard roughness" used in many NACA tests, "consisted of 0.011 inch carborundum grains applied to the surface of the (24 inch chord) model at the leading edge over a surface

length of .08c measured from the leading edge on both (upper and lower) surfaces. The grains were thinly spread to cover 5 to 10 percent of the surface area."[4] Data for both "smooth" and "standard roughness" conditions are plotted on the same graph for comparison. Note that this standard roughness test gives some insight into the foil's sensitivity to roughness but does not simulate all the conditions, such as manufacturing imperfections, dew, squashed bugs, or other actual irregularities occurring in practice. Thus, although wind-tunnel data provides good estimates for ideal conditions, computed performance estimates always have some uncertainty associated with them.

Nevertheless, the airfoil data obtained in tests closely approximating two-dimensional flow is utilized in both the annulus momentum vortex and the prescribed-wake theory to predict forces and moments on a real wind-turbine rotor. If blade airfoils as manufactured differ in any significant particulars from the theoretically exact shape, and if it is desired that the predicted performance be as close to the real thing as possible, it would be advisable to consult an expert aerodynamicist and consider doing selected wind tunnel tests on the actual airfoil shape.

The characteristics of the flow depend upon the size of the foil and on the speed of the relative wind, W. This dependence is quantified using a dimensionless variable, the Reynolds number, Re:

$$\begin{aligned} \text{Re} &= (\text{velocity})(\text{length})(\text{density})/(\text{viscosity}) \\ &= (W)(c)(\rho)/\mu = (W)(c)/(\nu) \end{aligned} \tag{2.41}$$

where W is the relative wind at a point on the blade (see Fig. 2.12 for the definition of W) and $\nu = \rho/\mu$. Re can be interpreted as the ratio of inertial to viscous forces on the fluid.

For air at standard, sea-level conditions, Re = 69000 Wc, where W is in m/s and c is in m; where W is in ft/s and c is in ft, Re = 6350 Wc. Airfoils are usually tested at several different Reynolds numbers, and it is important either to use data taken near the correct Reynolds number (Re) or to make some corrections to account for the effect of the Reynolds number (see Sec. 4.6 of Ref. 9). If careful attention is not paid to Re effects in selecting airfoil data in rotor modelling, accurate results cannot be expected. Some modelling programs do not allow different airfoil data for each blade segment. This limits their ability to properly model the rotor.

The geometric shape of an airfoil is usually given in tabular form in which the x, y coordinates of both the upper and lower surfaces are given as measured with respect to the chord line, which is used as the reference. Both x and y coordinates are given as fractions of the chord length c.

Cambered (i.e., curved) airfoils are generated by defining a camber line and adding a thickness distribution equally above and below the camber line

at each station along the foil. The exact shape of the leading edge is determined by the leading edge radius, a circular arc centered on the camber line going through the leading edge. Cambered airfoils are capable of generating lift with a smaller drag penalty than symmetrical foils. Since the blades of a vertical-axis rotor must generate both positive and negative lift during each rotation, they cannot effectively take advantage of the low drag capabilities of cambered airfoils. This gives an aerodynamic performance advantage to horizontal-axis wind turbines over vertical-axis machines.

Airfoils differ in their lift, drag, and moment coefficients as a result of their shape. Some shapes are better structurally than others, and some shapes are more easily manufactured. It is possible to keep a favorable boundary-layer pressure gradient for a longer distance along the foil by moving the point a maximum thickness aft. This facilitates additional structure to provide bending strength to the blade. Airfoils with a thin trailing edge may have superior aerodynamics but are more sensitive to mechanical damage in handling and shipping.

An important parameter of an airfoil is its thickness. The thickness is given as a fraction of the chord length, i.e., a 12-percent thick foil has a maximum thickness that is 12 percent of the chord length. Since airfoil characteristics vary with thickness, it is important that the percent thickness of the actual rotor correspond with the data used in the design.

While we are on the subject, if a wing is tested in three-dimensional flow, standard conversion equations based on Lanchester-Prandtl wind theory are used to convert the data to equivalent two-dimensional form.[4,9] These equations are based on elliptical spanwise distributions of lift in streamline flow. Data obtained using these conversion equations tend to be less accurate than data taken in two-dimensional flow originally, and post-stall measurements cannot be converted to two-dimensional form using these conversion equations.

Further discussion of rotor aerodynamic modelling is given in Chap. 4.

2.7 GLAUERT MOMENTUM VORTEX THEORY

A more detailed momentum theory model was developed for propellers and generalized for wind turbines by Glauert.[1] This basic theory, with various modifications, is widely used for design. Presentations of this approach for wind turbines were made by Wilson and Lissaman,[2] Miller, Dugundji, et al. (vol. 2 of Ref. 5), and others.

The Glauert momentum vortex blade element theory again neglects the flow periodicity caused by a rotor with a finite number of blades. It also relies on the assumption that small radial sections of blades can be analyzed independently, a premise that is strictly true only for rotors with an infinite number of blades. Corrections for this simplification can be made by using one of

several approximate solutions for flow with a finite number of blades derived by Prandtl or Goldstein.

With these assumptions, we begin by considering an annular section of the rotor and examining a small section of length Δr of one blade. The net effect on air flowing through this annular section of the rotor results from the forces and moments on all the blades. Let B represent the number of blades.

The geometry of a blade element showing the velocities, forces, and moments is shown in Fig. 2.12. The relative wind at the rotor $W(r)$ varies with blade radius r and consists of an axial component $u(r)$ and a rotational component $r\Omega + w(r)$. The term $r\Omega$ represents the velocity caused by blade rotation, whereas $w(r)$ portrays the swirl velocity of the air. Utilizing interference factors, we represent u and w as $u = V_0(1 - a)$ and $w = r\Omega a'$. The angle of the blade chord with respect to the plane of rotation is denoted by θ. The angle of attack of the airfoil with respect to the local relative wind, W, is denoted by α, and the angle of the relative wind with respect to the rotor plane, by ϕ. The drag force, D, is aligned with the relative wind, W, while the lift force, L, is perpendicular to W. For any good airfoil. L is much larger than D.

The force component, $F_Q = L \sin \phi - D \cos \phi$, in the direction of blade

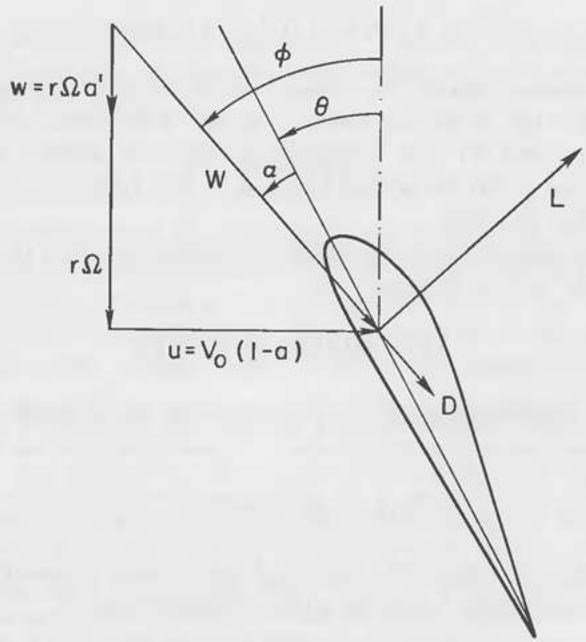

Figure 2.12. Velocity diagram.

rotation generates useful torque, whereas the component, $F_T = L \cos \phi + D \sin \phi$, in the downwind direction exerts a thrust load on the rotor.

In terms of the dimensionless coefficients, c_l and c_d of Sec. 2.6, the net force, power, and torque caused by B blades, each of local chord c, are as follows:

For torque:

$$\Delta Q = \tfrac{1}{2}\rho W^2 r[c_l \sin \phi - c_d \cos \phi]Bc\Delta r \tag{2.42}$$

For power:

$$\Delta P = \Omega \Delta Q = \tfrac{1}{2}\rho W^2 \Omega r[c_l \sin \phi - c_d \cos \phi]Bc\Delta r \tag{2.43}$$

For thrust:

$$\Delta T = \tfrac{1}{2}\rho W^2[c_l \cos \phi + c_d \sin \phi]Bc\Delta r \tag{2.44}$$

where

$$W = u/\sin \phi = (r\Omega + w)/\cos \phi. \tag{2.45}$$

In the elementary actuator disc theory, we found that the induced velocity was twice as large in the far wake as in the rotor plane, and this same behavior is assumed for each streamtube in this more detailed analysis. We also assume that the air has acquired half of its final rotational (twirl) velocity when it reaches the rotor.

With these approximations, the linear momentum loss gives the incremental thrust force ΔT on the rotor as

$$\Delta T = \rho u(2\pi r dr)2(V_0 - u) \tag{2.46}$$

and gives the incremental torque ΔQ in terms of the rate of change of rotational momentum as

$$\Delta Q = \rho u(2\pi r dr)2wr \tag{2.47}$$

Equating the expressions for thrust and torque from momentum theory to those from aerodynamic forces on a blade element leads to

$$\frac{(V_0 - u)}{u} = \left(\frac{Bc}{8\pi r}\right)\left(\frac{c_l \cos \phi + c_d \sin \phi}{\sin^2 \phi}\right) \tag{2.48}$$

and

$$\frac{w}{(w + \Omega r)} = \left(\frac{Bc}{8\pi r}\right)\left(\frac{c_l \sin \phi - c_d \cos \phi}{\sin \phi \cos \phi}\right) \tag{2.49}$$

Using dimensionless axial and radial induction factors, $a = (V_0 - u)/V_0$ and $a' = w/\Omega r$, and solidity,* $\sigma = Bc/\pi R$, we find that Eqs. 2.48 and 2.49 become

$$\frac{a}{(1 - a)} = \left(\frac{\sigma R}{8r}\right)\left(\frac{c_l \cos \phi + c_d \sin \phi}{\sin^2 \phi}\right) \tag{2.50}$$

and

$$\frac{a'}{(1 + a')} = \left(\frac{\sigma R}{8r}\right)\left(\frac{c_l \sin \phi - c_d \cos \phi}{\sin \phi \cos \phi}\right) \tag{2.51}$$

Also, from Fig. 2.12,

$$\tan \phi = \frac{u}{\Omega r + w} = \frac{V_0(1 - a)}{\Omega r(1 + a')} = \frac{(1 - a)}{x(1 + a')} \tag{2.52}$$

where $x = \Omega r/V_0$ is the local speed ratio. At the end of the blade, r becomes R, and we again find the most important parameter for wind-turbine rotors, the tip-speed ratio (TSR), or

$$X = R\Omega/V_0 \tag{2.53}$$

Thus, X is the ratio of tip speed to the free-stream wind speed, whereas x is the ratio of local (blade) tangential velocity to free-stream wind speed. Any wind-turbine rotor operating at fixed pitch exhibits a preferred tip-speed ratio, which is essentially determined by the effective pitch of the airscrew. This screw effect is often utilized together with a small unloaded rotor to form an

*"Solidity" is a dimensionless ratio of the blade area to the total swept area and a very important parameter for rotor or propeller design. A number of different solidities may be defined. The local solidity, $\sigma_l = Bc\Delta r/2\pi r\Delta r = Bc/2\pi r$, is the fraction of the annulus occupied by blades. It contains two variables, c and r, and although it diverges to infinity at the blade root, this poses no mathematical problems because it is never necessary to integrate all the way to $r = 0$ since no power is generated at the blade root. The (rectangular) solidity, σ, assumes B blades of constant chord c all the way to the axis, giving the formula, $\sigma = B(Rc)/(\pi R^2) = Bc/\pi R$, but it is used as well for nonrectangular blades where c is not constant. It is simple, having only one variable, the chord c. Miller et al.[5] call $Bc/\pi R$ a local solidity because $c = c(r)$ is the local value of c. The total integrated solidity, σ_t, is the ratio of the actual total blade area to the rotor swept area, $B\int c(r)\,dr/\pi R^2$. In all cases, the reduction of projected area resulting from blade twist is ignored in calculating solidity. When using the literature, be sure to check which definition of solidity is being used.

anemometer for measuring windspeed. A fixed-pitch rotor that is unloaded essentially "locks in" to an rpm that is proportional to the wind speed (assuming that it is unstalled). This is the reason that suddenly unloading a working rotor is so dangerous. Using X, we can then write

$$\tan \phi = \left(\frac{R}{rX}\right)\left[\frac{(1-a)}{(1+a')}\right] \tag{2.54}$$

The two-dimensional lift and drag coefficients, c_l and c_d, are both functions of the angle of attack, α, where $\alpha = \phi - \theta$. We now have a set of relations which, although not solvable in closed form, may be solved iteratively to find a and a' for any pitch angle θ (assuming convergence can be obtained).

There are many alternative forms of the Glauert momentum annulus equations and the following equations formulated by H. J. Stewart (discussed in detail in Sec. 2.8) have perhaps the most direct physical interpretation. Instead of using the average solidity as below, we will define a symbol called the *blade loading coefficient*, $\lambda = Bcc_l/8\pi r$. The parameter λ is one-fourth of the average retarding pressure the blades exert on the air flowing through the annular streamtube, normalized by the relative dynamic pressure at the blade element, $\frac{1}{2}\rho W^2$. This may be shown as follows:

From Eq. 2.44,

$$\Delta T = \tfrac{1}{2}\rho W^2[c_l \cos\phi + c_d \sin\phi]\, Bc\Delta r$$

$$= \tfrac{1}{2}\rho W^2 c_l[\cos\phi + (c_d/c_l)\sin\phi]\, Bc\Delta r$$

If $\epsilon = c_d/c_l$,

$$\Delta T = \tfrac{1}{2}\rho W^2 (Bcc_l)[\cos\phi + \epsilon \sin\phi]\,\Delta r$$

For small ϕ (true especially near the tip of a blade operating at a high-TSR) and small ϵ (true for any decent airfoil), $\cos\phi \cong 1$ and $\epsilon \sin\phi \cong 0$. Thus we have

$$\Delta T \cong \tfrac{1}{2}\rho W^2 (Bcc_l)\,\Delta r$$

as the retarding force exerted by the blades.

If this ΔT is divided by the annular area, $2\pi r\Delta r$, to get the average pressure exerted by the blades on the annulus, and normalized by $\frac{1}{2}\rho W^2$, we obtain

$$\Delta p/(2\pi r\Delta r)(\tfrac{1}{2}\rho W^2) = Bcc_l/2\pi r = 4\lambda$$

By this reasoning, the corresponding normalized average local pressure on the blade element would be

$$4\lambda(2\pi r\Delta r)/Bc\Delta r = 4\lambda/\sigma_l = c_l$$

Thus, increasing λ increases the amount of slowing of the air and the pressure on the blades, whereas when λ goes to zero the blade does not retard the wind.

Using λ and ϵ and dividing right-hand sides of Eqs. 2.50 and 2.51 by $\sin\phi$ and $\cos\phi$, respectively, we obtain

$$a/(1-a) = \lambda(\cot\phi + \epsilon)/\sin\phi \tag{2.55}$$

and

$$a'/(1+a') = \lambda(\tan\phi - \epsilon)/\sin\phi \tag{2.56}$$

These equations are in about the simplest possible form for further analysis. They are quite insensitive to the value of ϵ for high L/D airfoils. For example, using Eq. 2.55 with $\epsilon = 0$ gives values of a with less than 1-percent error for $0 < \phi < 40$ deg when compared with using the exact equation with $\epsilon = 0.01$. These relationships can be shown graphically as they are in Fig. 2.13 (plotted for $\epsilon = 0.01$). This plot is typical of the propeller design charts from Wenig's treatise on propellers and was proposed for wind turbines by U. Hütter. It is very useful for quick estimates of changes in rotor behavior, such as sudden loss of c_l, start-up when stalled, etc., but it is not accurate enough for detailed rotor analysis. For that purpose, a computer rotor analysis program is much more useful. Equations 2.55 and 2.56 will be used later in Sec. 2.8 in connection with optimal rotor design.

The iterative solution procedure, given r/R, c, $c_l(\alpha)$, $c_d(\alpha)$, θ, and V_0, is as follows:

1. Guess values of a and a'.
2. Calculate ϕ from Eq. 2.54.
3. Calculate $\alpha = \phi - \theta$ and hence c_l and c_d.
4. Update a and a' from Eqs. 2.50 and 2.51.

This computation procedure has poor convergence properties near $a = 0.5$. An improved computational procedure will be discussed later.

Although corrections of these results must be made to account for a finite number of blades, the procedure allows for the evaluation of the local forces and moments on the rotor, which can then be integrated to find the total torque and loads. This provides a method of estimating performance once a candidate blade layout is known. One can then iteratively change the blade layout and optimize the blade.

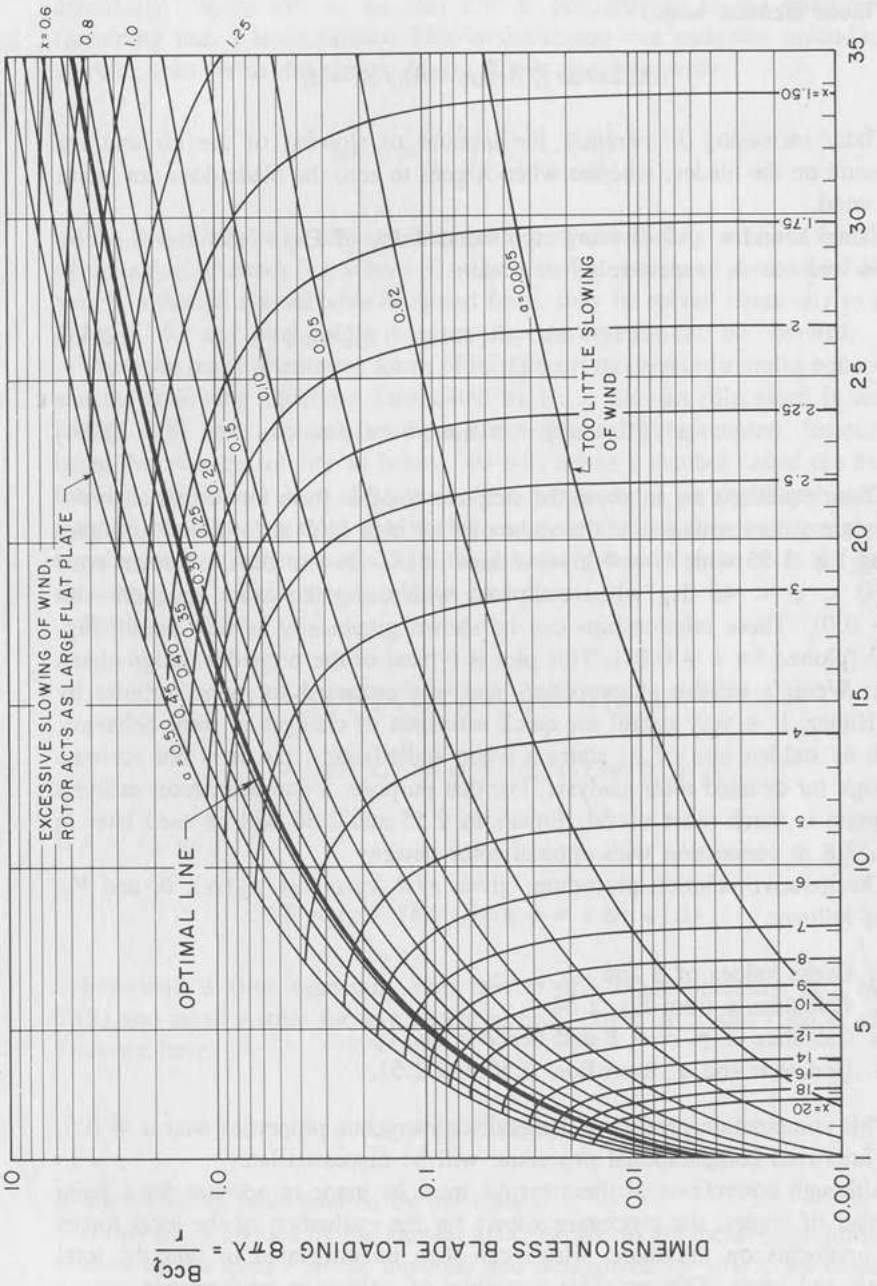

Figure 2.13. Blade element parameters.

The thrust and torque coefficients are defined as

$$C_T = T/\tfrac{1}{2}(\rho V_0^2)(\pi R^2) \quad \text{and} \quad C_Q = Q/\rho(\pi R^2)(\Omega R)^2 R \tag{2.57}$$

Following Miller et al., these equations can be reduced to the following form for integration along the blade length:

$$dC_T = 8a(1 - a)(r/R)\,d(r/R) \tag{2.58}$$

and

$$dC_Q = (4/X)\,a'(1 - a)(r/R)^3 d(r/R) \tag{2.59}$$

The Glauert momentum theory equations fail to agree with measured data when the condition $a = 0.5$ is approached, as was discussed in Sec. 2.5. A further problem is the proper treatment of the stall condition. Significant portions of a rotor may enter the stall condition, where measured c_l and c_d data is in many cases not available. Inaccurate representation of stall forces destroys the accuracy of the entire model if part of the blade is stalled. Recent research aimed at modelling both the $a \geq 0.5$ flow states and the stall conditions are reviewed in Secs. 2.9 and 2.10.

The analysis thus far has neglected the effects of having a finite number of blades. A correction can be applied that accounts for the main features of the effect of the vortex sheets behind the rotor tips. Either an approximate solution by Prandtl or a more exact solution by Goldstein can be used. Since the Prandtl solution has a simple closed form, whereas the Goldstein solution is represented by an infinite series of modified Bessel functions, but both give similar results, the Prandtl solution is most often used. For a derivation of the Prandtl solution, comparisons with the more accurate Goldstein solution, and further discussion of the application of the Prandtl solution in the case of propellers, see Part VII, Sec. 4, especially Fig. 63, and Sec. 5 of Glauert.[1] For application of the Prandtl solution as a correction factor for wind turbines, see p. 50 and the Appendix of Wilson and Lissaman.[2]

The Prandtl correction function is conveniently expressed as follows:

$$F = (2/\pi)\cos^{-1}\exp(-f) \tag{2.60}$$

where

$$f(r) = -(1/2R)(R - r)\,B\sqrt{(1 + X^2)} \tag{2.61}$$

The function, $F(r)$, approaches unity for $1 - (r/R) < 2/XB$ but goes rapidly to zero at the tips (when $r = R$).

The physical interpretation of the correction is that the maximum slowing

of the wind occurs only on the vortex sheets and that the average decrease in velocity in the wake is only a fraction, F, of this velocity.

The Prandtl correction for a finite number of blades requires that the velocity at the rotor disc be

$$u = V_0(1 - aF)$$

and that the axial and rotational interference factors a and a' must now be determined from the following equations:

$$a = \frac{p_1}{1 + p_1} \tag{2.62}$$

$$a' = \frac{p_2}{1 - p_2} \tag{2.63}$$

where

$$p_1 = \sigma(c_l \cos\phi + c_d \sin\phi)/8F \sin^2\phi \tag{2.64}$$

$$p_2 = \sigma(c_l \sin\phi - c_d \cos\phi)/8F \sin\phi \cos\phi \tag{2.65}$$

Note that when using the tip loss factor, F, the boundary of the windmill state occurs at $aF = 0.5$. Use of the tip-loss factor results in improved convergence of the iterative procedure described previously. The final forms of the most recent versions of the modified Glauert momentum equations are given in Sec. 2.9.

2.8 OPTIMAL ROTORS

The Glauert annulus momentum equations provide the essential relationships for analyzing each blade segment using two-dimensional airfoil data. What is needed in design, however, is guidance in this infinite parameter space toward those rotor aerodynamics that will be best for one particular purpose. Thus, optimal rotor theory.

There are a number of optimal rotor theories, of which the most useful will be discussed. Such theories have been advanced by Glauert, H. J. Stewart, R. Miller et al., and others.

Glauert presented a blade-element analysis to find the "ideal windmill" based on neglecting the airfoil drag but including wake rotation, or "swirl" (see Chap. XI, Sec. 2 of Ref. 1). This approach was extended by H. J. Stewart[17] to include the effects of drag so that the Glauert analysis becomes a subcase of the Stewart analysis for the case of infinite lift/drag ratio.

The Glauert analysis is simple enough and yet accurate enough to be very useful in preliminary rotor design. It can be used directly as a *synthesis* procedure, whereas almost all other approaches are really analysis procedures. Another optimal design procedure that includes drag effects was given by Miller et al. (vol. 2, pp. 29–30 of Ref. 5).

The result of the Glauert or Stewart ideal windmill theory is a preferred value of the product, cc_l, at each blade segment as a function of local speed ratio x. This yet leaves the choice of c or of c_l, the remaining parameter then following the ideal value of the product cc_l. Although this single-point optimal theory is extremely useful for first-cut design, it provides no information as to the sensitivity of the performance to off-design operation. That is, it is quite possible to come up with a design that has a very high C_P at one design tip speed ratio X but falls off quite rapidly to either side and so fails to garner the most power over a whole wind spectrum of velocities.

Another optimal design procedure that includes drag effects was given by Miller et al. (vol. 2, pp. 29–30 of Ref. 5). This theory includes drag but neglects wake rotation and proceeds from knowledge of the assumed airfoil drag polar in the form, $c_d = c_1 + c_2\alpha^2$. It is, again, a single-point optimization procedure.

In addition to modifying the Glauert optimal blade-element theory to account for drag, H. J. Stewart[17] pointed out that the design freedom in satisfying the optimal product, cc_l, can be used to find a chord c that will be optimal at *two* different speed ratios. This approach yields a design that is insensitive to performance degradations for off-design conditions.

The equations used in the Glauert ideal windmill theory are the same as those of Sec. 2.6, except that the drag coefficient c_d is assumed zero. The effect of wake rotation is included. In a well-designed rotor with a carefully shaped airfoil, the lift/drag ratio is very high, on the order of 100 or so, so that the neglect of the drag during a first-cut optimization is justified. Subsequent use of the Stewart theory usually results in small corrections to these results.

If c_d is assumed to be zero, dividing Eq. 2.51 by Eq. 2.50 gives

$$\frac{a'(1 - a)}{a(1 + a')} = \tan^2\phi \tag{2.66}$$

and combining this with Eq. 2.52 gives

$$\frac{a'(1 + a')}{a(1 - a)} = \frac{V_0^2}{\Omega^2 r^2} = \frac{1}{x^2} \tag{2.67}$$

At each radius, the right side of Eq. 2.67 is constant, and therefore the

left side must remain constant also, while the power is maximized if the quantity $a'(1 - a)$ from Eq. 2.56 is maximized. Performing these operations using Lagrange multipliers yields:

$$a' = \frac{(1 - 3a)}{(4a - 1)} \tag{2.68}$$

In the windmill state, a' must be positive for positive output torque. Thus, for small x, a approaches $1/4$ and a' becomes large, whereas for large x, a approaches $1/3$ and a' approaches zero.

Substituting a' from Eq. 2.68 into Eq. 2.67 yields the required relationship between a and the local speed ratio x as follows:

$$x = (4a - 1)\sqrt{(1 - a)/(1 - 3a)} \tag{2.69}$$

Miller et al.[5] (vol. 2, p. 27) give a power series in $1/x^2$ as an approximation for the inverse relationship:

$$a \cong \left(\frac{1}{3}\right) - \left(\frac{2}{81x^2}\right) + \left(\frac{10}{729x^4}\right) - \left(\frac{418}{59049x^6}\right) + \ldots \tag{2.70}$$

The corresponding relative wind angle, ϕ, can be found from Eq. 2.66 as given by

$$\tan\phi = (1/a)\sqrt{(1 - a)(1 - 3a)} \tag{2.71}$$

The optimum blade layout in terms of the product of chord c and lift coefficient c_l can be found from Eq. 2.49 with $c_d = 0$:

$$\frac{\sigma c_l X}{8} = \frac{\sigma_l c_l x}{4} = \left(\frac{B\Omega}{8\pi V_0}\right)(cc_l) = \left[\frac{(4a - 1)}{(1 - 2a)}\right]\sqrt{(1 - a)(1 - 3a)} \tag{2.72}$$

As mentioned previously, there is still some design freedom in that both c and c_l may be varied while their product satisfies Eq. 2.72. Thus, if chord c is held constant, c_l (and hence α and θ) will follow from Eq. 2.72. Likewise, if c_l (and hence α) is held constant, chord c must vary according to Eq. 2.72, and the twist angle θ has been specified as a function of r. Alternatively, Stewart[17] has shown that the freedom in satisfying the product relation, cc_l, can be used to define a blade that is optimal over a wider range, i.e., that is insensitive to off-design conditions. This analysis will be presented later.

Miller et al.[5] also integrate the C_P relation along the blade to give closed-form and series solutions for C_P. Thus, from Eqs. 2.56, 2.68, and 2.69,

$$dC_P = \left(\frac{12}{X^2}\right)\left[\frac{(4a - 1)(1 - a)(1 - 2a)}{(1 - 3a)}\right]^2 da \tag{2.73}$$

which must be integrated from $a = 1/4$ at $r = 0$ to the value of a at the tip, a_T, given by

$$X = (4a_T - 1)\sqrt{\frac{(1 - a_T)}{(1 - 3a_T)}} \tag{2.74}$$

The integration can be done in closed form, resulting in

$$C_P = \left(\frac{4}{729X^2}\right)\left[\left(\frac{4}{z}\right) - 12\ln\left(\frac{1}{4z}\right) - \left(\frac{4363}{160}\right) + 63z - 38z^2 - 124z^3 - 72z^4 - \left(\frac{65}{5}\right)z^5\right] \tag{2.75}$$

where $z = 1 - 3a_T$. A series expansion valid for large tip-speed ratio X is

$$C_P = \left(\frac{8}{27}\right)\left[1 - \left(\frac{2}{9X^2}\right)\ln\left[\frac{(27X^2 + 15)}{8}\right] + \frac{0.0529}{X^2} + \ldots\right] \tag{2.76}$$

For any tip-speed ratio, X, the local speed ratio is $x = Xr/R$. The parameter a is determined from Eq. 2.70, and thence ϕ from Eq. 2.71, the product cc_l from Eq. 2.72, and C_P from one of the equations 2.73 through 2.76.

To obtain a single-point optimum including the effects of drag, Stewart begins by deriving a local power coefficient:

$$C_{P'} = \frac{\Delta P}{(\frac{1}{2}\rho V_0^3 \Delta A)} = \frac{\frac{1}{2}\rho W^2 r\Omega Bc(c_l \sin\phi - c_d \cos\phi)\Delta r}{[\frac{1}{2}\rho V_0^3(2\pi\Delta r)]} \tag{2.77}$$

which, by using $W^2 = V_0^2(1 - a)^2 + r^2\Omega^2(1 + a')^2$ and Eq. 2.52 to eliminate x^2, reduces to

$$C_{P'} = (1 - a)^2(1 + \cot^2\phi)4x\lambda(\sin\phi - \epsilon\cos\phi)$$

Then, eliminating λ using Eq. 2.55 and expanding $1/(\cot\phi + \epsilon)$ in a Taylor's series of two terms, there results

$$C_{P'} = 4xa(1 - a)(\tan\phi - \epsilon)(1 + \epsilon\tan\phi) \tag{2.78}$$

The last term, $1 + \epsilon \tan \phi$ is quite small, improving the accuracy less than 1 percent for $\epsilon = 0.01$ and $\phi = 40$ deg. Thus, in most cases, it may be neglected, leaving

$$C_{P'} = 4xa(1 - a)(\tan \phi - \epsilon) \tag{2.79}$$

Since the optimum value of a is found to be quite insensitive to changes in ϵ, this implies that $C_{P'}$ decreases monotonically as ϵ increases.

By defining a local Froude efficiency, $\eta_{F'} = (27/16)C_{P'}$, we can relate the performance of each blade element to the ideal value of unity.

By dividing Eq. 2.56 into Eq. 2.55 and using Eq. 2.52 to eliminate a', there results

$$x \tan \phi = 1 - a\left[1 + \left(\frac{\tan \phi - \epsilon}{\cot \phi + \epsilon}\right)\right] \tag{2.80}$$

For small ϵ, this is closely given by

$$x \tan \phi = 1 - a \sec^2 \phi \tag{2.81}$$

If the function, $F = a(1 - a)(\tan \phi - \epsilon)$, is then maximized using $dF/d\phi = 0$, with the relation between a and ϕ given implicitly by Eq. 2.80, there results a quadratic equation, as follows:

$$\left[\frac{-a \tan^2 \phi}{(1 - a)}\right] + \left[\frac{(1 - a)}{a}\right] = 2 + \left[\frac{\epsilon \sec^2 \phi}{(\tan \phi - \epsilon)}\right] \tag{2.82}$$

Solving this quadratic, the optimal value of a including the effect of drag is given by

$$\left(\frac{1}{a}\right) = 2 + \sec \phi\,(G + \sqrt{G + H^2}) \tag{2.83}$$

where $G = \epsilon \sec \phi/2(\tan \phi - \epsilon)$ and $H = \tan \phi/(\tan \phi - \epsilon)$.

Thus, a complete single-point optimization of a rotor-blade element, given ϕ and ϵ, proceeds as follows:

1. Find a from Eq. 2.83
2. Calculate λ from $\lambda = a \sin \phi/(1 - a)(\cot \phi + \epsilon)$.
3. Find a' from $a' = a(\tan \phi - \epsilon)/[(1 - a)(\cot \phi + \epsilon) - a(\tan \phi - \epsilon)]$.
4. Then, $x = (1 - a)/[(1 + a') \tan \phi]$.

5. $C_{P'} = 4xa(1 - a)(\tan \phi - \epsilon)(1 - \epsilon \tan \phi)$.
6. $\eta_{F'} = (27/16)\,C_{P'}$.

Since $\eta_{F'}$ is the local Froude efficiency of the blade element, the optimization of the power output from this one blade element is then complete. A plot of $\eta_{F'}$ versus x for various drag/lift ratios, ϵ, is given in Fig. 2.14.

For the case in which ϵ approaches zero in Eqs. 2.77 through 2.82 one obtains the original Glauert optimal relationships parametrically in terms of ϕ.

Miller et al.[5] (vol. 1, p. 29) give an analysis for the optimal rotor including the drag effect but neglecting wake rotation. The results of this analysis would be applicable to rotors in a high TSR mode since in this regime of operation very little wake rotation occurs and blade drag begins to dissipate large amounts of power. In their analysis, a drag function, $c_d = c_1 + c_2\alpha^2$, is given, and the following two parameters are defined:

$$\zeta = 16c_2/\sigma X A^2 \quad \text{and} \quad \delta = \sigma c_1 X^3/8 \tag{2.84}$$

The results of the optimization give

$$a_{\text{opt}} = 2/(3 + \zeta + \sqrt{(3 + \zeta)^2 - 8\zeta}) \tag{2.85}$$

$$\theta_{\text{opt}} = (R/Xr)(1 - a_{\text{opt}})[1 - a_{\text{opt}}(8/\sigma XA)] \tag{2.86}$$

$$\phi_{\text{opt}} = (R/Xr)(1 - a_{\text{opt}}) \tag{2.87}$$

$$C_{P_{\max}} = 4a_{\text{opt}}(1 - a_{\text{opt}})(1 - \tfrac{1}{2}\zeta a_{\text{opt}}) - 2\delta \tag{2.88}$$

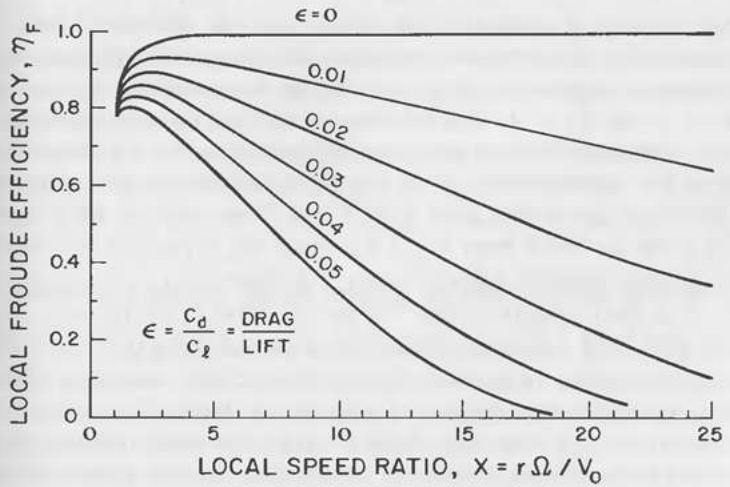

Figure 2.14. Local Froude efficiency versus local speed ratio.

Of particular interest is the result that C_P is reduced by 2δ, a correction to C_P dependent directly upon c_1 and which increases as the *cube* of the tip-speed ratio X.

Dual Optimum

Stewart[17] has pointed out that the freedom in choosing c_l to maintain cc_l at the ideal value can be used to make a blade element optimal at two different speed ratios, x_1 and x_2. This will have the effect of reducing the sensitivity of the rotor to off-design conditions.

Suppose we wish to find a blade chord c such that a blade element will satisfy the optimal conditions at two speed ratios, x_1 and x_2, where $x_1 > x_2$ (to eliminate some minus signs). Then, if $\Delta\lambda = \lambda_2 - \lambda_1$ and $\Delta\phi = \phi_2 - \phi_1$,

$$\Delta\lambda = (Bc/8\pi r)(c_{l2} - c_{l1}) = (Bc/8\pi r)a_0(\Delta\phi + \tau) \qquad (2.89)$$

where a_0 is the lift-curve slope of the airfoil in appropriate units, τ is a possible change in pitch angle of the entire blade between the two conditions, and a value of $\tau > 0$ implies that $\lambda_2 > \lambda_1$.

Since we can calculate the ideal λ and ϕ for each speed ratio x, we can calculate $\Delta\lambda$ and $\Delta\phi$. This permits determination of an optimal value of $Bc/8\pi r$, and hence the dual optimum c and the desired lift coefficients at x_1 and x_2 may be found.

For initial design purposes and assuming that good airfoils will be used (ϵ will be small), we can neglect drag and use the simpler Glauert relations. After the initial dual-optimum blade shape has been determined, we can go back and find the exact optimal conditions and refine the blade shape slightly.

For example, suppose at the tip we wish to have a blade chord optimal at both $X_1 = 6$ and $X_2 = 4$. The calculations are best done in tabular form as shown in Table 2.1. Here all angles are in degrees so that the lift-curve slope is taken to be, approximately, $a_0 \cong 0.1$. For convenience, the values of r/R along the blade are in the ratio $4/5 = 0.8$. The angle ϕ for a particular value of x can be found from Eq. 2.81. Since the inverse of this relation is needed, a programmable calculator and a printout of $x = x(\phi)$ would be helpful, or a short program using Newton's method might be used. The last two rows of Table 2.1 give the differences, $\Delta\lambda$ and $\Delta\phi$, for the two conditions.

Once these values have been found, blade chords satisfying the dual-optimum conditions are easily calculated, as in Table 2.2 for $\tau = 0$ and Table 2.3 for $\tau = 2$ deg. The $Bc/8\pi R$ row shows the variation of chord with blade radius. The dual-optimum condition for $\tau = 0$ (fixed-pitch blade) results in a blade with a slight negative taper, which is quite undesirable from

Table 2.1 Optimum parameters for $X_1 = 6$, $X_2 = 4$, $\varepsilon = 0$.

r/R	1	0.8	0.64	0.512	0.4096	0.32768
x_1	6	4.8	3.84	3.0720	2.4576	1.9661
λ_1	0.006055	0.009360	0.014388	0.021928	0.033003	0.048796
ϕ_1	6.3082	7.8455	9.7311	12.0207	14.7610	17.9727
x_2	4	3.2	2.56	2.048	1.6384	1.3107
λ_2	0.013307	0.020317	0.030660	0.045500	0.065994	0.092914
ϕ_2	9.3574	11.5693	14.2245	17.3502	20.9319	24.8943
$\Delta\lambda$	0.007252	0.010957	0.016272	0.023572	0.032991	0.044118
$\Delta\phi$	3.0492	3.7238	4.4934	5.3295	6.1709	6.9216

Table 2.2 Optimum blading for $X_1 = 6$, $X_2 = 4$, $\varepsilon = 0$, $\tau = 0$.

r/R	1	0.8	0.64	0.512	0.4096	0.32768
$Bc/8\pi r$	0.02378	0.02942	0.03621	0.04423	0.05346	0.06374
$Bc/8\pi R$	0.02378	0.02354	0.02317	0.02265	0.02190	0.02089
C_{l1}	0.255	0.318	0.397	0.496	0.617	0.766
C_{l2}	0.560	0.788	0.847	1.029	1.234	1.458

Table 2.3 Optimum blading for $X_1 = 6$, $X_2 = 4$, $\varepsilon = 0$, $\tau = 2$ deg.

r/R	1	0.8	0.64	0.512	0.4096	0.32768
$Bc/8\pi r$	0.01436	0.01914	0.02506	0.03216	0.04038	0.04945
$Bc/8\pi R$	0.01436	0.01531	0.01604	0.01647	0.01654	0.01620
c_{l1}	0.422	0.489	0.574	0.682	0.817	0.987
c_{l2}	0.927	1.061	1.223	1.415	1.634	1.879

a structural viewpoint. By allowing a pitch change, a blade with a smaller chord and a desirable taper can be found, as in Table 2.3. The design lift coefficients of this blade are higher in proportion to the reduction of chord from those of Table 2.2.

These optimal rotor theories can be used together with other design constraints from strength, structural dynamics, control, manufacture, cost, shipping, etc., to gain insight into practical rotor designs, as will be discussed in Chap. 4.

2.9 MODIFICATIONS TO GLAUERT MOMENTUM THEORY

The Glauert momentum annulus theory, first presented in 1927, was published in Durand's book in 1935. It has been widely used for propeller design. Ever since Wilson and Lissaman modified its expression for use with wind turbines and incorporated it into the PROP digital program, it has been widely used for wind-turbine design as well. Efforts to verify its accuracy will be discussed in Sec. 2.10.

In recent years, a number of modifications to the original theory have been suggested to improve agreement between theory and experiment. A review of some of these will be given here. Additions and modifications have been in the areas of modelling the turbulent wake state, modelling the stall regime, making provision for the effects of rotor pre-coning, vertical wind shear, and rotor axis tilt, and operating with the rotor yawed off the wind direction.

Revised Momentum Equations

We will begin with a presentation of the momentum equations as revised by Hibbs and Radkey of AeroVironment in Tangier et al.[8] and then discuss some of the other suggested modifications.

One of the major differences between propellers and wind-turbine rotors is that cantilevered-blade wind-turbine rotors are often pre-coned at 5 to 10 degrees so as to balance thrust and centrifugal effects and thus reduce blade root stresses, whereas propellers usually have much smaller cone angles, if any. Since the cone angle enters into momentum-theory equations in a fundamental way, the extra complexity of these equations for rotors with more than a 5-deg cone angle is justified. Coning (or blade deflection under heavy thrust loading, for that matter) would be expected to have some effect on radial flow, but although some work on radial flow has been done, any conclusions reached have not yet been verified. The 1983 Hibbs and Radkey update of the PROP program includes a number of other modifications, simplifications, and improvements over the original code (1974).

Although the rotor blades now sweep out a cone instead of a plane, the blade length and Δr dimensions project into a plane perpendicular to the rotor axis as cos Ψ, which then appears throughout the analysis. The equations, derived in Ref. 8, follow easily from Fig. 2.15 and can be summarized as follows:

Tip-speed ratio

$$X = R \cos \Psi \left[\frac{\Omega}{V_0}\right] \tag{2.90}$$

Relative wind

$$W = V_0 \sqrt{(1 - a)^2 \cos^2 \Psi + (1 - a')^2 X^2 (r/R)^2} \tag{2.91}$$

or,

$$W = V_0 (1 - a) \left(\frac{\cos \Psi}{\sin \phi}\right) \tag{2.92}$$

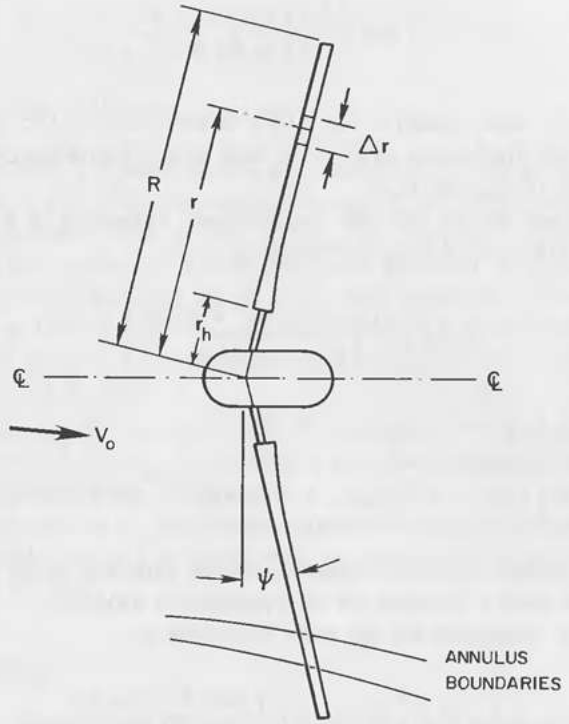

Figure 2.15. Rotor geometry.

Incoming flow angle

$$\phi = a \tan \left(\frac{R}{r}\right)\left(\frac{(1 - a) \cos \Psi}{(1 + a')X}\right) \tag{2.93}$$

Tip loss factor

$$F = \left(\frac{2}{\pi}\right)(\arccos e^{-f}) \tag{2.94}$$

where f at tip is

$$f = \left(\frac{B}{2}\right)\left(\frac{R - r}{r \sin \phi}\right) \tag{2.95}$$

and f at hub is

$$f = \left(\frac{B}{2}\right)\left(\frac{r - r_h}{r_h \sin \phi}\right) \tag{2.96}$$

Note that the same equation for $F(f)$ is used both at the tip and at the hub and that the final value of F to be used in the following equations is to be the product of F_{tip} and F_{hub}.

To incorporate the tip and hub loss relations embodied in F to find a in the windmill state, we define the following:

$$S_w = \left(\frac{\sigma}{8}\right)\left(\frac{c_l \cos^2 \Psi \cos \phi}{\sin^2 \phi}\right) \tag{2.97}$$

so that

$$a = \left[\tfrac{1}{2}(S_w + F^2)\right]\left[2S_w + F - \sqrt{F^2 + 4S_w F(1 - F)}\right] \tag{2.98}$$

Using the Glauert empirical equation for the turbulent wake state we find the variable a from a different set of equations as follows:

A head loss coefficient for the rotor is defined as

$$C_H = \left(\frac{\sigma}{2}\right)(1 - a)^2\left(\frac{\cos^2 \Psi c_l \cos \phi}{\sin^2 \phi}\right) \tag{2.99}$$

where, for C_H less than 0.96,

$$a = \left(\frac{1}{2f}\right)(1 - \sqrt{1 - C_H^2}) \tag{2.100}$$

whereas for C_H greater that 0.96,

$$a = (1/F)\left(0.143 + \sqrt{0.0203 - 0.6427(0.889 - C_H)}\right) \tag{2.101}$$

The equation for a' is

$$\frac{a'}{(1 + a')} = \frac{\sigma c_l}{8F \cos \phi} \tag{2.102}$$

The torque, thrust, and power coefficients then become

$$C_Q = \left(\frac{B}{2\pi \cos^2 \Psi}\right)\left(\frac{c}{R}\right) W^2(c_l \sin \phi - c_d \cos \phi) \tag{2.103}$$

$$C_T = \left(\frac{B}{2\pi \cos \Psi}\right)\left(\frac{c}{r}\right) W^2(c_l \cos \phi + c_d \sin \phi) \tag{2.104}$$

$$C_P = XC_Q \tag{2.105}$$

These equations are implemented in a modernized form of the PROP code given in Ref. 8. PROPSH, yet another version of the PROP code, has evolved from test evaluation work at the Rocky Flats test site, reported by J. L. Tangler.[10] This version of PROP has been modified to give output in a dimensional format, provides for up to 20 blade segments, models cross-flow effects such as yaw or axis tilt, and incorporates a 3-D post-stall airfoil data synthesization routine. A personal computer interactive version of this program will be discussed in Chap. 5.

Yet another set of versions of PROP has been developed by W. Wentz, D. Staples, and M. Snyder in connection with the wind-turbine aerodynamics research at Wichita State University.[18]

Yet another version of the Glauert momentum theory equations tracing its lineage to Miller et al.[5] is given with computed results by M. Martinez-Sanchez and R. Noll.[8]

Stall Modelling

Significant progress has occurred over the last few years in modelling the stall condition. Wind tunnel section data at large angles of attack beyond stall has almost never been measured for airfoils, since this is not an operating regime of interest to aircraft designers. About all the data that existed in 1974 was for a flat plate and also section data for the NACA 0012 and 0015, so that stall modelling in the original PROP program was, as Hibbs and Radkey have started, "somewhat arbitrary."

If reliable stall data for a given airfoil existed, it could presumably be used in the Glauert momentum theory equations and give useful results. As has been noted by Miley,[3] however, even in a 2-D tunnel stall generates a 3-D flow, so obtaining post-stall data in a wind tunnel is difficult. Force sensors respond to average effects, and since most of the post-stall data has been taken using force measurements, it may be considered suspect. Another problem is that, although conversion relationships between 2-D and 3-D data are well-established at low angles of attack, this is not the case for post-stall data, and aspect ratio effects seem to be strong.

Hibbs and Radkey have proposed a new post-stall model for the PROP program.[8] Concurrently, Viterna and Corrigan[14] and Viterna and Janetzke[7] have provided insight into post-stall rotor behavior by carefully analyzing data taken on the Mod-0 wind turbine. They observed that blade sections that should have been stalled were in fact generating substantial amounts of power

and then asked what behavior of two-dimensional c_l and c_d vs α values would have to occur in order to give constant power *for a zero-twist blade* after stall. By thus "backing into" post-stall lift and drag coefficients, they were able to obtain post-stall data synthesis equations and to show that the equations derived gave better prediction of performance of both the Mod-0 and other wind turbines than the original procedures of the PROP code.

The Viterna approach was just an empirical method that showed that there could be defined a set of two-dimensional post-stall lift and drag coefficients that would yield constant power output. Although this was a useful way of thinking about a difficult problem, it sheds no light on the causes of this behavior. If the observed effect is indeed due to three-dimensional effects of spanwise flow, then new theory should be developed to correlate the actual phoenomena.

J. L. Tangler and C. Ostowari have since made new wind-tunnel studies in the NACA 44XX series.[15] Using thicknesses of 9, 12, 15, and 18 percent; aspect ratios of 6, 9, 12, and ∞; and Re's of 250,000, 500,000, 750,000, and 1,000,000 they obtained post-stall lift and drag data. The results were correlated, in some cases using equations identical to the Viterna—Corrigan equations, and in others, somewhat different. In comparison with measured data using the new correlation equations, however, the Viterna–Corrigan equations still gave better prediction of actual results, whereas the Tangler–Ostowari equations persistently gave power coefficients 3 to 15 percent lower than measured values.

The Viterna-Corrigan post-stall equations are given below. Please note that they were derived for a section of rotor with twist angle $\theta = 0$ and will result in constant power after stall for that case only. If the rotor twist angle θ is not zero, these equations must be modified.

In the Viterna equations, AR = aspect ratio, α_s is the stall angle of attack, usually 15 degrees, and the other notation is that used previously.

In the Viterna formulation, the maximum drag coefficient is assumed to correlate with aspect ratio according to the relation, at $\alpha = 90$ degrees

$$c_{d\max} = 1.11 + 0.018AR \tag{2.106}$$

The post-stall drag coefficient is synthesized according to the equation,

$$c_d = B_1 \sin^2 \alpha + B_2 \cos \alpha \tag{2.107}$$

where $B_1 = c_{d\max}$, $B_2 = (1/\cos \alpha_s)(c_{ds} - c_{d\max} \sin^2 \alpha_s)$, and $15 \leq \alpha \leq 90$ deg.

The corresponding lift coefficient is generated from the relation

$$c_l = A_1 \sin^2 \alpha + A_2(\cos^2 \alpha / \sin \alpha) \tag{2.108}$$

where $A_1 = B_1/2$, $A_2 = (c_{ls} - c_{d\max} \sin \alpha_s \cos \alpha_s)(\sin \alpha_s / \cos^2 \alpha_s)$, and $15 \leq \alpha \leq 90$ deg.

In preliminary design, if reliable lift-drag data is not available, then the Viterna equations might be used so long as one keeps in mind the qualifications and assumptions given above. For more exact work, good post-stall airfoil data would be preferred, and model or full-scale testing of the actual rotor geometry would be necessary.

2.10 EXPERIMENTAL VERIFICATION OF ROTOR AERODYNAMIC MODELS

Although the Glauert momentum theory is well-established and widely used, it is important to have experimental verification of it for wind-turbine rotor analysis. This verification turns out to be quite difficult, for a number of reasons. First, medium and large wind turbines can be tested only in natural winds at their installation site. Such testing requires careful measurement of windspeeds, as was discussed in Sec. 2.1. Then the power gathered by the rotor should be measured, since the theory gives rotor power, not generator output power. Although direct rotor torque-speed measurements can be made, they usually require special instrumentation that may be difficult to mount on production units. Deducing rotor power using generator efficiency curves may be quite inaccurate at low power levels. The instrumentation used must be frequently checked and recalibrated and the results cross-checked. Finally, data-reduction procedures must reduce the results to standard conditions if they are to be compared on an absolute basis with data from other machines. If this is not the objective, the theory can be used to calculate the rotor power for the measured conditions at the site during the tests.

Data has been gathered on a number of wind turbines in recent years, including, in the public domain, on the Mod 0, the Mod 0A, the Enertech 1500, the UTRC 1/3 scale prototype, the Danish Gedser machine, and the Mod 2,[8,14] for which basic parameters are given in Table 4.1. A theory verification program was carried out for small wind turbines by Rockwell International at the Rocky Flats test site. This program, which was coordinated by J. L. Tangler, tested the Enertech 1500 and the UTRC 1/3 scale machines. Performance predictions, as shown in Fig. 2.16, were obtained prior to running the tests from the four contractors listed in Table 2.4.

The basic Glauert momentum theory as implemented in the PROP program and used with multiple Reynolds number data—i.e., using different two-dimensional airfoil data at each station along the blade—gave good results (Contractor B curve) for the Enertech machine and for tip-speed ratios below 5 for the UTRC 1/3-scale machine. The lack of agreement for the UTRC machine has not been entirely explained, although the discovery of bending-pitch coupling may account for some of the discrepancy. Although these

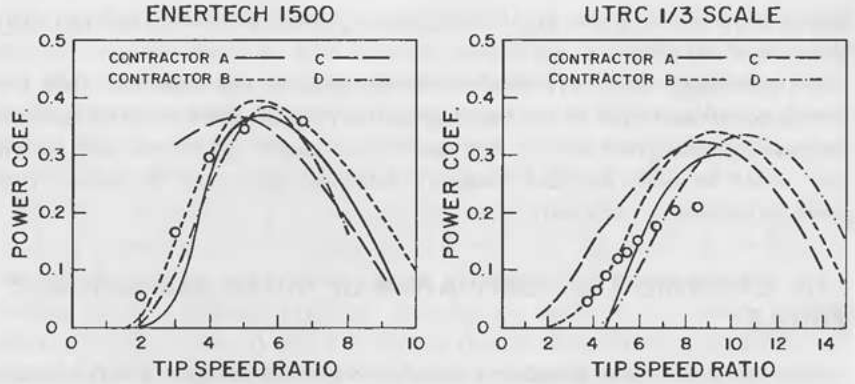

Figure 2.16. Comparison of measured and predicted performance for the Enertech 1500 and the 1/3-scale UTRC. (From Ref. 8.)

results are not definitive, with other data they certainly indicate that the Glauert momentum theory is adequate for preliminary blade design. To temper enthusiasm for it, we will quote Mr. Tangler's conclusions:

1. The correlation study between predicted and measured performance in the peak power coefficient region resulted in good agreement for the Enertech 1500 and poor agreement for the 1/3-scale UTRC rotor.
2. At low tip speed ratios, blade-element/momentum analysis substantially underpredicts performance when two-dimensional airfoil data are utilized. Good agreement can be achieved in this region utilizing synthesized three-dimensional airfoil data.
3. At high tip speed ratios, the Glauert [empirical turbulent wake state] approximation has little influence on predicted performance for optimum blade pitch. However, at pitch angles toward stall the Glauert approximation predicts higher power coefficients. Correlation studies with measured test data are necessary to provide better verification of this approximation.
4. Further studies are needed to better define the relationship between yaw angle and power output for comparing predicted and measured power of machines that operate yawed off the wind axis. [This problem has since been solved, giving the result that power varies as the cube of the cosine of the yaw angle.]
5. In order to determine wind turbine power from measured generator power at high tip-speed ratios, elimination of hysteresis effects in the measured power and the accurate determination of the generator efficiency are essential.
6. Based on this limited study, no definitive statement can be made on the

Table 2.4 Contractor List.

CONTRACTOR	*ANALYSIS*	*GLAUERT APPROXIMATION*	*TIP LOSS*	*AIRFOIL DATA*
(A) OREGON STATE	Blade-element momentum	Yes	Effective radius	Single Reynolds number
(B) AEROVIRONMENT	Blade-element momentum	Yes	Prandtl	Multiple Reynolds number
(C) ASI	Blade-element momentum	Yes	Prandtl	Single Reynolds number
(D) UTRC	Lifting line/ prescribed wake	Not required	Not required	Multiple Reynolds number

relative accuracy of blade-element/momentum analysis versus analyses using discrete vortex-type wakes. Further study is needed to systematically compare differences in their respective blade element data.

In understanding conclusion 4, we need to note that the Enertech machine, free to yaw, experienced yaw angles from −30 deg to +40 deg during the CVT tests. Conclusion 2 refers to the Viterna–Corrigan–Janetzke papers discussed in Section 2.9.

We note that, in Table 2.4, the predictions of contractor D are based on a lifting-line, prescribed-wake vortex model. One such model was presented by Miller et al.[5] For the Enertech 1500, the theory used by UTRC appears to underpredict C_P at low tip-speed ratios but gives results basically quite comparable with those of the Glauert momentum theory. Since this lifting-line, prescribed-wake analysis is apparently no more accurate than momentum theory for ordinary blades numbering two or more and requires large amounts of computer time, it is not recommended here for design of ordinary blades. It might possibly be useful for special rotors with two-section blades, surface effects, dynamic tip inducers, etc.

A competent designer must keep abreast of new work as it is published, and better insight into rotor aerodynamics will, we hope, gradually be established.

REFERENCES

1. Glauert, H. "Airplane Propellers." From Div. L, *Aerodynamic Theory*, ed. W. F. Durand. Berlin: Springer Verlag, 1935. (Reprinted by Peter Smith, Glouster, Mass., 1976.)

1a. Mattsson, Sven Erik. Modelling and control of large horizontal axis wind turbines. Doctoral dissertation, Lund Institute of Technology, Lund, Sweden, 1984.

2. Wilson, R. E., and Lissaman, P. B. S. *Applied Aerodynamics of Wind Power Machines.* Oregon State University, 1974.

3. Miley, S. J. A catalog of low Reynolds number airfoil data for wind turbine applications. Prepared for Rockwell International Corp., Energy Systems Group, Rocky Flats Plant, Feb. 1982.

4. Abbott, I. H., and von Doenhoff, A. E. *Theory of wing sections, Including a summary of airfoil data.* New York: Dover Publications, Inc., 1959.

5. Miller, Rene H.; Dugundji, J.; et al. Wind energy conversion. MIT Aeroelastic and Structures Research Lab TR-184-7 through TR-184-16. DOE Contract No. C00-4131-T1, distribution category UC-60, Sept., 1978:
   Vol. 1: Methods for design analysis of horizontal axis wind turbines.
   Vol. 2: Aerodynamics of horizontal axis wind turbines.
   Vol. 3: Dynamics of horizontal axis wind turbines.
   Vol. 4: Drive system dynamics.
   Vol. 5: Experimental Investigation of a horizontal axis wind turbine.
   Vol. 6: Nonlinear response of a wind turbine rotor.
   Vol. 7: Effects of tower motion on the dynamic response of a wind machine rotor.

   Vol. 8: Free wake analysis of horizontal axis wind turbines.
   Vol. 9: (Not available)
   Vol. 10: Aeroelastic stability of wind turbine rotor blades.

6. Stoddard, F. S. Momentum theory and flow states for windmills. *Wind Technology Journal* **1,** No. 1 (Spring, 1977).

7. Viterna, L. A., and Janetzke, D. C. Theoretical and experimental power from large horizontal axis wind turbines. Proceedings of the Fifth Biennial Wind Energy Conference and Workshop, October 5-7, 1981, vol. 2, pp. 265–280.

8. Tangler, J. L., et al. Horizontal-axis wind system rotor performance model comparison. Report RFP-3508, UC 60, Rockwell International, Rocky Flats Plant, Feb. 1983.

8a. McCormick, B. W. *Aerodynamics, Aeronautics,* and *Flight Mechanics.* New York: John Wiley and Sons, 1979.

9. Dommasch, D. O.; Sherby, S. S.; and Connolly, T. F. *Airplane Aerodynamics.* New York: Pitman Publishing Co., 1967.

10. Tangler, J. L. Assessment of blade-element/momentum analysis for horizontal-axis wind turbines. Sixth Biennial Wind Workshop, Minneapolis, Minn., June, 1983.

11. Hoerner, S. F. *Fluid-Dynamic Drag.* Hoerner Fluid Dynamics, P.O. Box 342, Brick Town, N.J. 08723, 1965.

12. Hoerner, S. F. *Fluid-Dynamic Lift.* Hoerner Fluid Dynamics, P. O. Box 342, Brick Town, N. J. 08723, 1975.

13. Pope, A., and Harper. J. J. *Low-Speed Wind Tunnel Testing.* New York: John Wiley & Sons, Inc., 1966.

14. Viterna, L. A., and Corrigan, R. D. Fixed pitch rotor performance of large horizontal axis wind turbines. DOE/NASA Workshop on Large Horizontal Axis Wind Turbines, Cleveland, Ohio, July 28–30, 1981.

15. Tangler, J. L., and Ostowari, C. Horizontal axis and wind turbine post stall airfoil characteristics synthesization. DOE report on contract No. DE-AC04-76DP03533, Rocky Flats Test Site, 1984.

16. White, Frank M. *Viscous Fluid Flow.* New York: McGraw-Hill, 1974.

17. Stewart, H. J. Dual optimum aerodynamic design for a conventional windmill. *AIAA Journal* **14,** No. 11: 1524–1527 (Nov. 1976).

18. Wentz, W. H.; Stewart, H. J.; and Staples, D. L. Optimal design techniques for horizontal-axis wind turbines. Report WER-17, Wichita State University, Center for Energy Studies, Feb. 1984.

19. Staples, D. L. Optimum aerodynamic design of a 400 KW wind turbine. WER-33, Center for Energy Studies, Wichita State University, Mar. 1985.

3

WIND MODELS AND ROTOR SIZING

3.1 INTRODUCTION

To design a wind turbine properly, it is necessary to characterize the winds in which it will operate. The wind data needed depends upon the problem being addressed, and various models must be resorted to for performance evaluation, gust analysis, fatigue studies, vibration analysis, and control system design.

For performance analysis, windspeeds are characterized by their velocity distributions over time. Rotor structural analysis requires that recorded worst-case winds, frequency spectra in fixed or rotating coordinates, and discrete gust models be known. Because certain conditions of unsteady flow are not well understood, particular difficulty is encountered in characterizing the amplitudes and frequencies of aerodynamic forces whenever the flow is not well defined, such as in the stall regime. Control system design is therefore facilitated by estimates of both frequency and time-domain data on wind velocity and direction. It thus becomes obvious that many different models of wind behavior can be of service in design.

Wind characteristics are perhaps best visualized in fixed coordinates (see Sec. 2.1). In structural analysis, however, the aerodynamic forces and moments must be viewed in blade-fixed coordinates. As a result, wind velocities undergo an additional transformation that depends upon blade velocity, and both their time- and frequency-domain characteristics are changed in the process, as will be discussed subsequently.

Just as a boundary layer exists on an airfoil, so does it on the surface of the earth. This layer varies in thickness and behavior depending upon the surface roughness in the same way that it does on an airfoil. On the latter, the boundary layer may be a fraction of an inch (or a few millimeters) thick, whereas on the earth the boundary layer may be 1500 feet (or 450 m) thick. The study of the variation of windspeed with tower height is no more than the characterization of the local boundary-layer velocity gradient. While on this subject, it should be noted that at some sites, observations have shown

that windspeeds do not increase above hub height and may even decrease; due caution must thus be observed.

A good overview of wind descriptions from an older point of view was given by Golding.[1] His coverage includes chapters on estimation of the energy obtainable from the wind, wind characteristics and distribution, wind power sites, wind surveys, wind flow over hills, measurement of wind velocity, wind structure and its determination, and wind data and energy estimation. Putnam gives a good discussion of the problems involved in coming up with engineering estimates of winds in New England in the 1945 era.[2] Improved instrumentation and automatic data recording and processing by computer have greatly reduced the effort required to obtain engineering wind-energy estimates. Yet some of the problems Putnam faced must be handled again at any new site. These include making on-site measurements, correlating them with weather-station measurements made a number of miles away but accumulated over longer periods of time, determining the local terrain and possible interference effects, and judging the validity and reliability of the resulting wind-energy estimates and correlations. A good example of this is the paper by Holets[3] on the windspeed variability of the California Altamont Pass area. Some special computer programs developed to aid in assessing wind sites using large-area flow modelling are treated in Chap. 5.

3.2 WIND DATA FOR PERFORMANCE ESTIMATION

There are many ways to approach the wind-data requirements for the design of a wind-turbine rotor. If a rotor is to be designed for a particular site, detailed measurements sufficient to calculate the energy content of the winds at the proposed site, and at the proposed elevation of the hub above ground for a number of years, will be needed. With such data, it will be possible to optimize a rotor to develop the required power from these winds.

More usually, a manufacturer prefers to have a design that will give satisfactory performance for a whole class of wind sites. In either case, it is desirable to set up a master design series of windspeed distributions. This can then be used in the design process both for performance evaluation and economic analysis.

Justus et al. have analyzed wind-speed data at 138 sites within the United States. These data are given in full in Reference 4 and have been fit to a Weibull statistical distribution. For windspeeds above 3 m/s, this distribution can often be made to fit actual data at a given site rather well. In other cases, the fit is poor and would give incorrect estimates of available power. Accurate estimates for a specific site must be based on windspeed measurements at that site, since small changes in wind spectrum can make large changes in power output.

Design for a wind-turbine manufacturer could begin with the choice of three or four windspeed distributions. These could range from sites with the lowest practical average windspeed up to one with high winds that would provide substantially more power than the proposed machine could safely absorb. The basic relationships for both the Weibull and Rayleigh distributions, the latter being a special case of the former, are given in the equations that follow.

Weibull Windspeed Probability Distributions (For the Rayleigh distribution, $k = 2$)

Wind Speed Probability Distribution:

$$p(V \geq V_P) = \exp\left[-(V_P/c)^k\right]$$
$$= \text{probability of windspeed being} \geq V_P \qquad (3.1)$$

Windspeed Duration Curve in Hours per Year:

$$H(V \geq V_P) = 8760 \exp\left[-(V_P/c)^k\right]$$
$$= \text{hours of windspeed} \geq V_P \text{ in a year} \qquad (3.2)$$

Windspeed Distribution Density:

$$p(V)\,dV = (k/c)\,(V/c)^{k-1} \exp\left[-(V/c)^k\right] dV$$
$$= \text{probability of windspeed between } V \text{ and } V + dV \qquad (3.3)$$

Windspeed Distribution in Hours per Year:

$$H(V < V_P < V + dV) = 8760(k/c)\,(V/c)^{k-1} \exp\left[-(V/c)^k\right] dV$$
$$= \text{hours per year of wind between } V \text{ and } V + dV \qquad (3.4)$$

Relationship to Annual Average Windspeed, $\overline{V}$:

$$\overline{V} = c\Gamma\left[1 + (1/k)\right]$$
$$\Gamma\left[1 + (1/k)\right] = \text{gamma function of arg}\left[1 + (1/k)\right] \qquad (3.5)$$

where

V = wind speed, mph or m/sec
V_P = particular wind speed
$\overline{V}$ = annual average windspeed
k = shape factor
c = windspeed normalizing factor, of same units as V

Values of the Weibull parameters fitted for some typical locations in the U.S. at a height of 30 ft (9.1 m) are given in Fig. 3.1. Since windspeed varies with height, Weibull parameters c, k, and n must be corrected for height at the wind-turbine hub. Since variation of windspeed spectrum with height is very site-specific and varies even between day and night, corrections such as these must be used with caution. For the designer, however, they do provide a rational way of accounting for small variations in height.

The variations of the Weibull parameters with height given in Reference 4 are as follows:

$$k = k_{\text{ref}}\left[1 - 0.088 \ln (h_{\text{ref}}/10)\right]/\left[1 - 0.088 \ln (h/10)\right] \qquad (3.6)$$

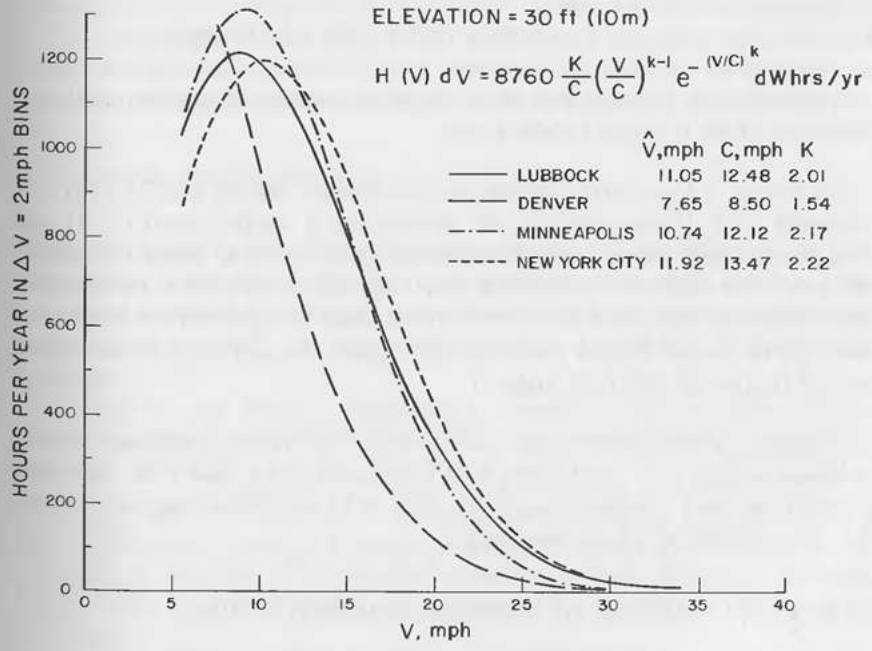

Figure 3.1. Weibull-fitted windspeed frequency distribution.

$$n = [0.37 - 0.088 \ln (c_{ref})]/[1 - 0.088 \ln (h_{ref}/10)] \quad (3.7)$$

$$c = c_{ref}(h/h_{ref})^n \quad (3.8)$$

EXAMPLE 3.1: Determine the expected number of hours per year of wind speeds between 18 and 20 mph at the Lubbock, Texas site in Fig. 3.1 at an elevation of 60 ft.

Solution: For Lubbock at 30 ft, $c = 12.48$ mph, $k = 2.01$, and $\bar{V} = 11.05$ mph. Correcting for $h = 60$ ft, we have

$$k = 2.01[1 - 0.088 \ln (3)]/[1 - 0.088 \ln (6)] = 2.156$$

$$n = [0.37 - 0.088 \ln (12.48)]/[1 - 0.088 \ln (3)] = 0.164$$

$$c = 12.48(60/30)^n = 12.48(2)^{0.164} = 13.98 \text{ mph}$$

Then,

$$H(18 < V < 20) = 8760(k/c)[(V/c)^{k-1}] \exp[-(V/c)^k]\, dV$$
$$= 8760(2.156/13.98)[(19/13.98)^{1.156}]$$
$$\cdot \exp[-(19/13.98)^{2.156}] (2 \text{ mph})$$

which yields the estimate that $H = 554.9$ hr between 18 and 20 mph at an elevation of 60 ft at the Lubbock site.

EXAMPLE 3.2: A wind turbine at the Denver site in Fig. 3.1 will be mounted on a 100-ft tower. If the turbine has a cut-out speed of 30 mph (13.4 m/s), how many hours of windspeed greater than 30 mph will probably be lost? (For want of more exact data, we will use Eqs. 3.6 through 3.8, but the change from 30 ft to 100 ft is not a small change, and these estimates may not be trusted without checking them against measurements at the Denver site at heights of 100 ft or higher.)

Solution: At the Denver site where data was taken, the fitted Weibull parameters were $c = 8.50$ mph (3.80 m/s), $k = 1.54$, and $\bar{V} = 7.65$ mph (3.42 m/s) for a reference height of 30 ft (9.14 m). Correcting these values for $h = 100$ ft (30.48 m), we have

$$k = k_{ref}[1 - 0.088 \ln (h_{ref}/10)]/[1 - 0.088 \ln (h/10)]$$
$$= 1.54[1 - 0.088 \ln (3)]/[1 - 0.088 \ln (10)] = 1.745$$

$$n = [0.37 - 0.088 \ln (c_{ref})]/[1 - 0.088 \ln (h_{ref}/10)]$$
$$= [0.37 - 0.088 \ln (8.50)]/[1 - 0.088 \ln (30/10)] = 0.201$$

$$c = c_{ref}(h/h_{ref})^n = 8.50(100/30)^{0.201} \text{ mph} = 10.83 \text{ mph } (4.84 \text{ m/s})$$

Then

$$H(V > 30 \text{ mph}) = 8760 \exp[-(30/10.83)^{1.745}] = 23.6 \text{ hr}$$

Thus, one full day of operation per year will probably be sacrificed if a cutoff speed of 30 mph (13.41 m/s) is used.

In preparing estimates of the power output to be expected, it is usually tacitly assumed that winds at a given site will have basically the same energy one year as the next. This may not be true. The wind energy at one particular site declined to as little as 40 percent and rose to as much as 170 percent of the value it had had the previous year.[4] Not all sites have such great yearly variation, as Golding[1] points out (p. 50). He quotes figures from 42 years of annual records for Southport, England, during which the largest variation was from 84 to 118 percent of the long-term average. Only by gathering many years of valid wind energy data at a given site can this variability be quantified.

The assessment of valid data on the wind energy at a particular site may require a more thorough study of the references. It may also be advisable to consult a meteorologist with special expertise in predicting wind energy.

3.3 OTHER WIND MODELS

Since windspeed variations are random in nature, it is natural to try to gain insight into windspeed behavior from statistical parameters derived from windspeed measurements. Etkin[5] summarizes turbulence models that are widely used in aircraft work. Of particular interest is his model of low-altitude turbulence.

Work by van der Hoven[6] incorporating a number of measurements of low-altitude turbulence has shown a frequency spectrum that has peaks at one cycle per 100 hrs and another at one cycle per minute, with a gap (very little energy content) for frequencies between 10 and 0.6 cycles per hour. Etkin's low-altitude model includes a velocity profile with height as given by Eq. 3.8 and includes estimates of component intensities in three directions, spectrum shapes, shear and cross spectra, and equations for the integral scales of the turbulence.

As discussed in Sec. 3.1, the accurate estimation of aerodynamic forces

due to windspeed variations requires using coordinates fixed in the blades. Work by Holley et al.[7] and Connell[8] has resulted in spectra of windspeed disturbances to a rotating point. Such a spectrum typically has a peak at the frequency of rotation.

Even if good information on wind disturbances in rotating coordinates were at hand, one would still have to find the response in terms of the aerodynamic forces. This process is complicated by the fact that airfoils have a nonlinear response at high angles of attack even in steady flow; with unsteady flow, phenomena such as dynamic stall may become important. A thorough experimental study of the aerodynamic forces and moments on a NACA 0012 airfoil undergoing high-speed pitch oscillations has been conducted by Carr, McAlister, and McCroskey.[8a] Further research into unsteady flow on wind turbine blades is needed to improve the modelling and permit more rational engineering design.

3.4 POWER REQUIRED

For any wind turbine, it is necessary to decide how much power it should be capable of generating. Choice of this important design parameter must be carefully based on the best available market surveys and predicted sales data. A mistake here can result in the financial failure of an otherwise good design. Many are the products that have failed for lack of an adequate market.

It is sometimes possible to increase the rating of a machine slightly by running it at higher RPM or increasing the blade radius. For a well-designed machine intended for mass production, however, there will be very little leeway.

The manufacturer will usually offer models in several capacity ranges. The prospective market will have determined the output rating. The size and cost of the machine will be closely related to the capacity chosen.

3.5 ROTOR SIZING

The rotor diameter required depends upon the power output needed, the wind regime in which it must operate, and the tip-speed ratio chosen. Allowance must be made for losses in the generating machine, the transmission system, and all other parts of the drive train. The rotor must therefore develop a good deal more power than the generator outputs.

The design windspeed is a very important parameter. In a high-windspeed area, a relatively small rotor can develop a large amount of power. In a low-windspeed area, a very large rotor would be required to generate even modest amounts of power. The power loading per unit area of the rotor in watts/square meter or watts/square foot is a useful index in comparing wind turbines (see Table 4.1).

Preliminary rotor sizing can be done with the elementary actuator disc momentum theory discussed in Chap. 2. The power output of an ideal rotor is given by

$$P = \tfrac{1}{2}\rho A C_P V_0^3 \tag{3.9}$$

where

ρ = air density
V_0 = wind velocity
A = rotor swept area
C_P = power coefficient

Air density, ρ, varies with altitude and temperature. For the ICAO standard atmosphere, the density below 20,000 ft (6,096 m) is closely approximated by the relation

$$\rho = \rho_0 \exp\left(-0.297\, h/10000\right) \tag{3.10}$$

where $\rho_0 = 0.0023769$ slugs/ft^3 and h is in feet.

In SI units, this equation becomes

$$\rho = \rho_0 \exp\left(-0.297\, h/3048\right) \tag{3.11}$$

where $\rho_0 = 1.22496$ kg/m^3 and h is in meters.

The air temperature defined for the standard atmosphere is a linearly decreasing function of altitude given by

$$T = 59 - 3.57(h/1000)\ ^\circ\text{F} \tag{3.12}$$

where h is in feet, or

$$T = 15 - 1.983(h/304.8)\ ^\circ\text{C} \tag{3.13}$$

where h is in meters.

In using this relationship for rotor sizing, allowances must be made for nonideal rotor performance and for power transmission losses. The maximum rotor power coefficient is $C_P = 16/27 \cong 0.59259$, whereas real rotors achieve considerably lower C_P's. With very precise, smooth airfoil blades and tip-speed ratios above 10, rotor C_P's as high as 0.45 have been reported. For most machines, a C_P of 0.3 to 0.35 would be possible with good design. With a drive train efficiency, η_d, and a generator efficiency, η_g, the actual

power output would be

$$P_{\text{out}} = \tfrac{1}{2}\rho A C_P \eta_d \eta_g V_0^3 \tag{3.14}$$

When this expression is solved for the rotor-swept area, A, we have

$$A = 2P_{\text{out}}/(\rho C_P \eta_d \eta_g V_0^3) \tag{3.15}$$

EXAMPLE 3.3: Find the area required for a rotor to generate 4.5 kw in a 5 m/s wind. Assume a drive train efficiency of 0.85, a generator efficiency of 0.75, and an altitude of 92 m.

Solution: The standard atmosphere air density at 92 m would be

$$\rho = 1.225 \exp\left[(-0.297)\,(92)/3048\right] = 1.214 \text{ kg/m}^3$$

and the standard atmosphere temperature would be

$$T = 15 - 1.983(92/304.8) = 14.4°\text{C}$$

The required rotor area would be

$$A = 2(4500)/(1.214)\,(0.35)\,(0.85)\,(0.75)\,(5^3) = 265 \text{ m}^2 = \pi R^2$$

Thus, the rotor diameter would be 18.4 m. Doing this same example in English units, we have

$$V = 5(3.2808) \text{ ft/s} = 16.404 \text{ ft/s}$$

$$\rho = 0.0023769 \exp\left[(-0.297)\,(301.8)/10000\right] = 0.0023557 \text{ slugs/ft}^3$$

$$P = (4500)\,(550)/746$$

$$= 17.7 \text{ ft lb/s}$$

Therefore,

$$A = (2)\,(3317.7)/(0.21743)\,(0.35)\,(0.85)\,(0.75)\,(16.404)\,(3)$$

$$= 3098.5 \text{ ft}^2$$

This gives a rotor diameter of 62.8 ft.

If the temperature is different from that of the standard atmosphere, a correction can be made based upon the perfect gas law that density is inversely proportional to absolute temperature. Thus, to generate 4500 W on a day when the temperature is 90°F would result in a density of $0.0021743(48.3 + 459)/(90 + 459)$, or 0.002009, giving a rotor area of $(3098.5)(0.0021743)/0.002009$, or 3353.2 sq ft and a diameter of 65.3 ft.

A rotor designed for such a low windspeed would result in a very expensive machine. The power developed by the rotor would be $4500/(0.85)(0.75)$, or 7059 W. The corresponding power loading is 7059/288, or 24.5 W/m^2. This is a very low power loading, again characteristic of a machine designed for low winds.

REFERENCES

1. Golding, E. W. The Generation of Electricity by Wind Power. London: E. & F. Spon Ltd., 1977.
2. Putnam, Palmer C. Power from the Wind, © 1948 by S. Morgan Smith Co. (Republished by Van Nostrand Reinhold, 1974.)
3. Holets, S. H. Wind Speed Variability in the California Altamount Pass Area. Proceedings, Wind Power '85, SERI/CP-217-2902, Aug. 27–30, 1985.
4. Frost, Walter; Long, B. H.; and Turner, R. E. *Engineering Handbook on the Atmospheric Environmental Guidelines for Use in Wind Turbine Generator Development.* NASA Technical Paper 1359, 1978.
5. Etkin, B. *Dynamics of Atmospheric Flight.* New York: John Wiley and Sons, Inc., 1972.
6. van der Hoven, I. Power spectrum of horizontal wind speed in the frequency range from 0.0007 to 900 cycles per hour. *J. Meteorol.* 14: 160–164.
7. Holley, W. E.; Thresher, R. W.; and Lin, S. R. Wind turbulence inputs for horizontal axis wind turbines. Wind Turbine Dynamics, NASA-CP-2185, DOE Conf. 810226. Workshop at Cleveland State University, Cleveland, OH, Feb. 24–26, 1981.
8. Connell, J. R. A primer of turbulence at the wind turbine rotor. Proceedings, Wind Power '85, SERI/CP-217-2902, Aug. 27–30, 1985.

8a. Carr, L. W.; McAlister, K. W.; and McCroskey, W. J. Analysis of the development of dynamic stall based on oscillating airfoil experiments. Ames Research Center and U.S. Army Air Mobility R&D Laboratory, Moffett Field, Calif. 94035; NASA TN-D-8382, National Aeronautics and Space Administration, Washington, D.C. Jan. 1977.

9. Swift-Hook, D. T. Describing wind data. *Wind Engineering* **3,** No. 3: 167–186. Central Electricity Generating Board, Applied Physics Division, Leatherhead, Surrey, England, 1979.
10. Baker, R. W.; Whitney, R. L.; and Hewson, E. W. A low-level wind measurement technique of wind turbine generator siting. *Wind Engineering* **3,** No. 2: 107–114 (1979).
11. Petersen, E. L. Wind atlas for Denmark, a rational method for wind turbine siting. RISØ Laboratories Report 428, Denmark, March, 1981.
12. Stevens, M. J. M., and Smulders, P. T. The estimation of the parameters of the Weibull wind speed distribution for wind energy utilization purposes. *Wind Engineering* **3,** No. 2: 132–146 (1979).
13. Hiester, T. R., and Pennell, W. T. The meteorological aspects of siting large wind turbines. DOE Report PNL-2522, Pacific Northwest Laboratories, Richland, Washington, Jan. 1981.
14. Panofsky, H.; Shirer, H. N.; Lipshutz, R.; and Larko, D. A model for wind spectra over uniform and complex terrain. AIAA/SERI Wind Energy Conference, Boulder, CO, p. 194, April, 1980.
15. Frost, W., and Shieh, C. F. Wind characteristics over complex terrain relative to WECS siting. AIAA/SERI Wind Energy Conference, Boulder, CO, p. 185, April, 1980.

4

DETAILED ROTOR DESIGN

4.1 ROTOR AERODYNAMIC GOALS AND SPECIFICATIONS

We will here focus on the details of rotor design, using for the most part theory discussed in Chap. 2. Wind-turbine rotors must satisfy static and dynamic structural criteria as well (see Chaps. 8 through 12), and at the beginning one must be aware of structural strength and vibration requirements and guess how the rotor can be built while concentrating on aerodynamics. The rotor speed-torque characteristic must match that of the generator and gearbox combination discussed in Chap. 14. Rotor-blade fatigue considerations discussed in Chap. 13 and the control problems associated with all modes of operation discussed in Chap. 15 must also be taken into account. It is assumed that design wind spectra have been chosen as discussed in Chap. 3 and that the blade length (radius), R, has been chosen. In wind-turbine design, the rotor influences every other subsystem.

To facilitate the design process, the designer must decide on the *type* of rotor needed. This and several other preliminary decisions and constraints can be summarized with numbers to constitute a set of design goals.

The design goals for a wind-turbine rotor should include the following:

1. Aerodynamic performance
2. Power rating
3. Weight, mass balancing, and weight tolerance requirements
4. Allowable blade deflections and tower clearances
5. Rotor axis tilt requirement
6. Material to be used and preferred manufacturing methods
7. Description of maximum load conditions
8. Hub mounting method
9. Type of rotor speed regulation
10. Method of starting
11. Primary and secondary overspeed control
12. Design life specifications, including fatigue allowables
13. Environmental conditions such as temperature, high humidity/salt spray, sunlight, fungus, and lightning strikes
14. Acceptance testing requirements

4.2 ROTOR AERO DESIGN

Once the design goals are established, actual aerodynamic design can begin. Much of this discussion will be directed toward design of constant-speed wind turbines, since the great preponderance of existing machines are of this type because of their simplicity and low cost. Many of the points discussed are general and will apply (perhaps at different tip-speed ratios) to rotors designed for other operating modes.

To design a rotor requires insight into how various airfoil characteristics affect rotor performance. We will examine a series of sensitivity curves to facilitate this insight. One must learn to compare characteristics of different rotors in terms of the relevant dimensionless parameters, including tip-speed ratio, X; Reynolds number, Re; lift coefficient, c_l; drag coefficient, c_d; thrust coefficient, C_T; torque coefficient, C_Q; and power coefficient, C_p. These parameters constitute the bridge between complex real-world flows and the engineering modelling thereof.

Since the rotor is the critical element of a wind-turbine design, it deserves especially careful thought. The reader may wish to browse through Part II of this book to get some background regarding the many structural dynamics problems of rotors before proceeding with this chapter.

A rotor must, as a minimum, have satisfactory performance. One may then ask, how many of the operational problems of wind turbines can be solved by rotor design alone? That is a good question. On the one hand, the manufacturing cost of the rotor may be kept low by using the simplest, easiest possible model. Problems that might result from this decision—such as inadequate means of control for overspeed, vibrations due to poor chordwise stiffness, etc.—may then have to be solved by an exotic control system or complex rotor hub design. On the other hand, one can attempt to solve all problems as part of the rotor design alone, as in the very innovative but complex FLAIR machine concept of Wortmann.[1] Between these two extremes, many possibilities exist for either solving or dramatically reducing problems of overspeed, sensitivity to dirt deposits on the blades, and so on. Certainly the designer should be aware of all important design problems and make use of whatever freedom is available in rotor design to solve or minimize them.

For each wind turbine there will be a windspeed for which rated power of the generator or other driven member is reached. For windspeeds above this value, it will be desirable to get rid of any extra power a rotor may generate, since such power cannot be absorbed without threatening the integrity of the machine. At the lower wind speed near cut-in, on the other hand, the very best performance possible is needed to increase yearly energy capture. Tangler and Somers[2] have developed special airfoils to implement rotor design objectives for improved performance and have shown for a constant-speed rotor that by constraining the maximum c_l in the tip region of the blade, the tendency to overspeed in high winds can be very significantly reduced.

Reducing Engineering Risk

Two methods sometimes used to reduce the engineering risk of a rotor design are overdesign and following the precedent of a previous design. As regards overdesign, since the procedures for defining the loads on wind-turbine blades (see Chap. 12) have not yet reached as high a level of development as in the aircraft industry, it may be thought prudent to use large margins of safety, resulting in a very robust, but heavy and expensive, machine. This conservative approach has validity when loads are poorly known. The economics of the wind-turbine market, however, requires machines with much reduced cost per installed kilowatt. Cost reductions require better methods of predicting loads, so that, as in aircraft design practice, components can confidently be built with strength just adequate for their design life. A paper by Stoddard[3] compares wind-turbine designs presently in use in California windfarms, emphasizing the performance per unit weight.

Another method of reducing engineering risk is to follow the precedent of a previous design. There has been a strong tendency to stick with an airfoil used in a previous machine on the basis of its perceived "success" or to use a two-bladed downwind rotor or a three-bladed upwind rotor because these approaches have been used in many designs. Following past precedent has both advantages and pitfalls. It may help avoid critical problems these designs have already solved, but at the same time the designer may lose the chance to make a sorely needed advance in machine performance. Although no shame attaches to following a design precedent, one should do so only if the reasons for it have been carefully investigated and are thoroughly understood.

The *best* method of handling engineering risk is to do a rigorous design job, utilizing all the best data and techniques with full knowledge of the various critical problems and with appropriate solutions for each, followed by a thorough, well-funded, and unbiased test and development program.

Number of Blades

One of the first problems is the choice of the number of blades needed, B. Wind turbines have been built with anywhere from one to 40 or more blades, but the majority of high-TSR rotors have either two or three. Low-TSR rotors for purposes such as water pumping must have higher solidity and a larger number of blades to generate the necessary large starting torque. The major factors involved in deciding the number of blades are the design TSR, the cost, the weight, the effect on power coefficient, the structural dynamics, and the means for limiting yaw rate to reduce gyroscopic fatigue effects. The two major effects on power coefficient are the (usually small) increase that can be expected from adding another blade and reducing the magnitude of the flow periodicity, versus the decrease to be expected as a result of the profile drag of additional blades.

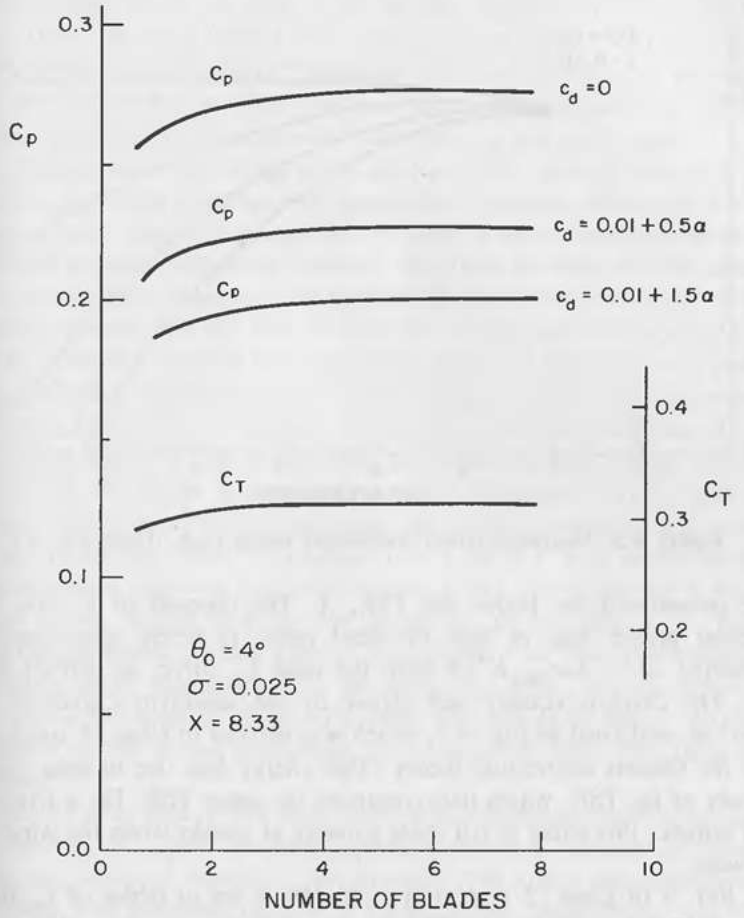

Figure 4.1. Finite number of blades—effects on power and thrust coefficients. (From Ref. 5 of Chap. 2—vol. 2, p. 192.)

Figure 4.1 shows the effect of the number of blades on the power and on the thrust coefficients for two generic blades having the drag coefficients, $c_d = 0.01 + 0.5\alpha^2$ and $c_d = 0.01 + 1.5\alpha^2$. These curves and the blade design tables given in Miller et al. (vol. 2 of Ref. 5 in Chap. 2) are based upon the more complex, rigid wake-vortex-theory model that accounts for the effects of having a finite number of blades. It is seen that there is an increase of perhaps 10 percent in going from one to two blades. There are significant advantages in using only one blade, and the FLAIR study of Wortmann[1] was aimed at developing a completely passive, compliant drive that maintains constant rotational speed.

Profile drag has a major and direct effect on power coefficient that is the

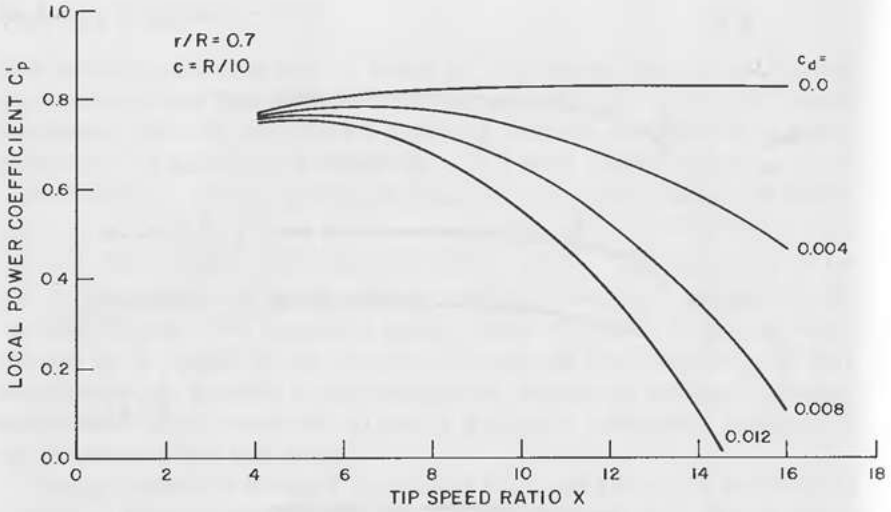

Figure 4.2. Maximum power coefficients versus drag. (From Ref. 4.)

more pronounced the higher the TSR, X. The drop-off of C_p due to the increased profile drag at high tip-speed ratios is nicely approximated by subtracting $2\delta = 2\sigma c_{d\min} X^3/8$ from the ideal C_p curve, as defined by Eq. 2.76. The effect is equally well shown by the sensitivity curves of L. S. Miller[4] as evidenced in Fig. 4.2, which was derived in Chap. 2 and is based upon the Glauert momentum theory. This energy loss due to drag varies as the *cube* of the TSR, which thus constrains the upper TSR. For a fixed-speed wind turbine, this effect is felt most strongly at startup when the wind speed is lowest.

In Ref. 5 of Chap. 2 (vol. 1, pp. 30–60), a set of tables of C_p for two different blade profile drag coefficients versus tip-speed ratio, solidity, blade pitch angle, and number of blades (B = 1, 2, 3, 4, 6, 8, and 10) is given. As an example, for only one blade and a solidity of 6 percent, a drag coefficient, $c_d = 0.01 + 0.5\alpha^2$, and a tip-speed ratio of 8.5, the C_p can be increased about 10 percent by going to two blades, about another 3 percent by going to three blades, another 1 percent by going to four blades, etc. Starting with two blades for the same case, going to 10 blades might achieve a 7.3-percent gain. Since building, mounting, balancing, and supporting the weight of all these extra blades would greatly increase the construction cost, very few designers choose more than three blades for high TSR rotors.

Blade Design

One of the most useful starting points is to use optimal blade theory to define an initial blade shape. This can be done fairly quickly with Eqs. 2.70 through 2.72 and using the c_l for max L/D at each segment to define the chord length. It can be done with a hand calculator, or better, with a computer. The PROPSH and PROPFILE programs discussed in Chap. 5 provide for their input tables for an ideal blade design to be automatically filled in, allowing rapid iterative evaluation of variations on the ideal shape.

The Glauert ideal (zero drag) blade for high TSRs tends to have very large chord and very high twist near the root. Most designers violate the ideal by making a large root cut-out and/or by using a much smaller-than-optimal chord near the root. Generally speaking, this does not have a great effect on power output since power is the product of force times velocity, and the tangential velocity near the root is quite low. Since each time a compromise is made, however, another few percentage points of the maximum possible energy gathering capability are lost, the designer makes such compromises with regret. One of the advantages of the large twist and chord near the root of the ideal blade is that it provides substantial starting torque when the remainder of the blade is hopelessly stalled. (Of course, for a fixed-pitch machine which is motored up to speed, the starting torque is not needed.) The rotor of the Jay Carter 25 machine (see Table 4.1) very much resembles the optimal rotor planform and twist and has a root cut-out of only 8 percent.

While on the subject of blade root design, let us note that R. E. Wilson[7] considered the effects of hub fairings ("spinners") on rotor performance. A hub fairing forces flow outward to the blade root area. This extra flow can have either a favorable or unfavorable effect on rotor performance, depending on whether or not it was considered in choosing the blade root pitch angle and chord.

The choice of airfoils is very important in achieving high overall performance. Recent studies of airfoils designed especially for wind turbines are given by Tangler and Somers,[2] Mueller,[5] and Althaus.[6] The airfoil data summaries of Abbott and Von Doenhoff (Ref. 4 of Chap. 2) and Miley (Ref. 3 of Chap. 2) give wind-tunnel test data on most of the existing airfoils that were designed for aircraft.

The purposes of the airfoils to be chosen for the various stations along the blade will depend on the type of rotor needed. For a fixed-pitch, constant-speed machine, Tangler and Somers[2] recommend for the .75 R region a high L/D, a low $c_{l\max}$, a mild stall, and a design insensitive to surface roughness. A very important point they bring out is that a low $c_{l\max}$ in the tip region reduces the tendency to overpower the generator in high winds. As we shall see shortly, a high $c_{l\max}$ is needed for the root.

For the purist, the airfoils can be designed as an integral part of the rotor design process. The airfoil design and analysis code of Eppler[8] is in the public domain and has been converted to run on a 256K personal computer in Fortran. Better yet is developing specifications for the airfoils needed and getting someone already expert in airfoil design and in the use of these codes

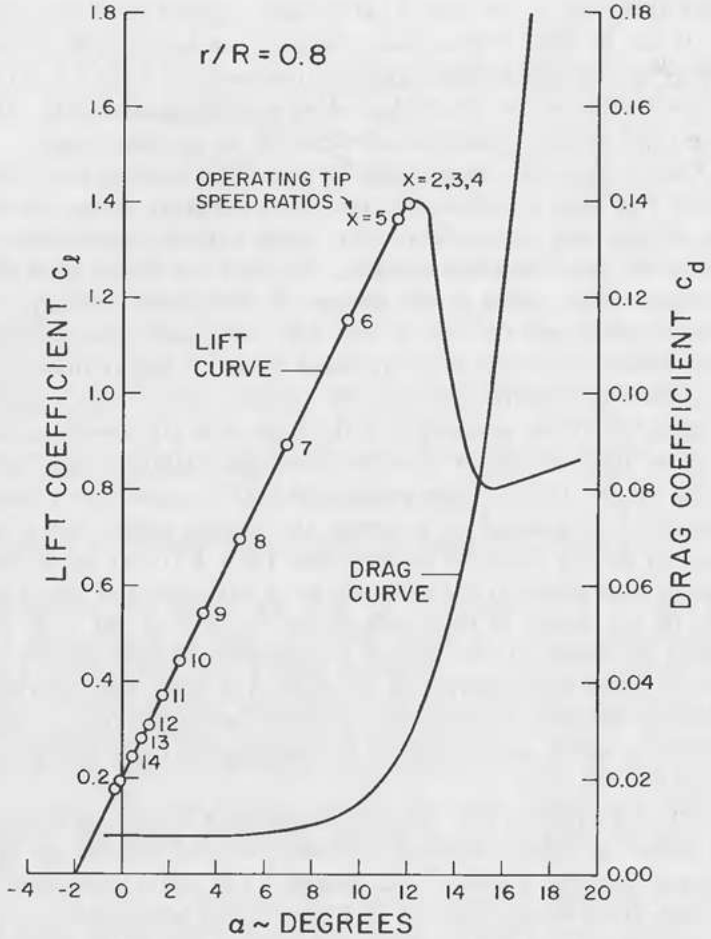

Figure 4.3. Operating conditions at various tip speed ratios. (From Ref. 4.)

to design the airfoils for you, since they can do it *much* faster and with considerably more assurance.

A number of researchers[4,5,6,9,10,11,12,20] have contributed to the understanding of the effect of various airfoil characteristics on wind-turbine rotor performance (see also Ref. 5 of Chap. 2, vols. 1 and 2). The study by L. S. Miller[4] provides a number of results useful in design that will be reviewed here. First, we must get all the relevant section variables in mind and see how they relate on the various parametric plots.

Figure 4.3 shows typical tip-speed ratios, X, superimposed upon the lift-drag curves for an airfoil section. At low TSRs, both the flow angle, ϕ, and the angle of attack, α, are large, and high values of c_l are needed to develop

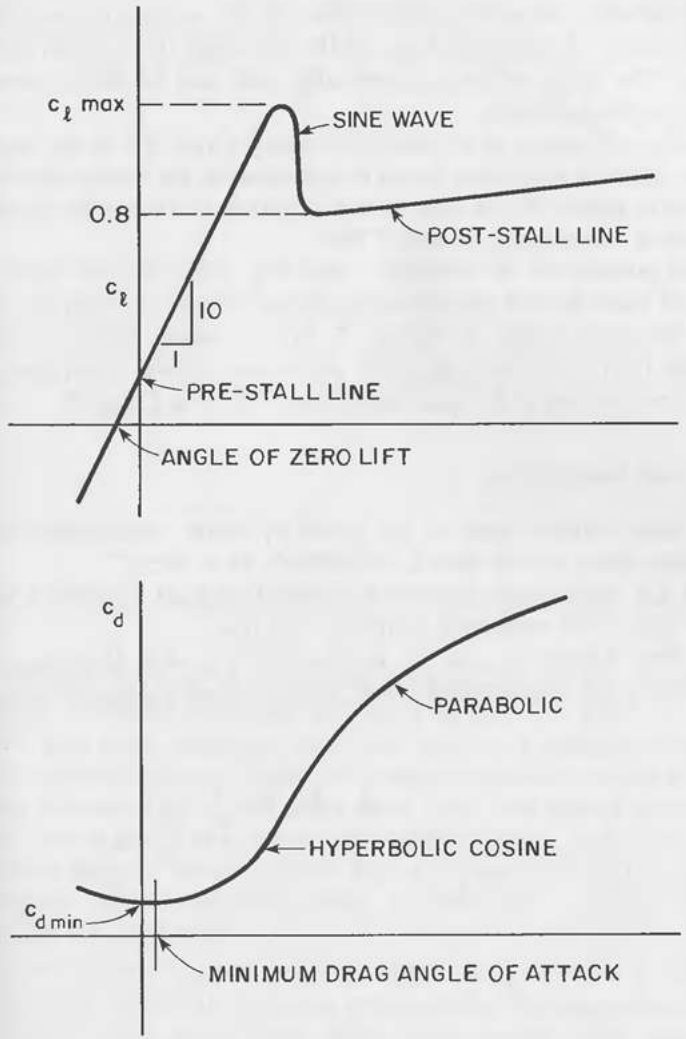

Figure 4.4. Diagram of airfoil model. (From Ref. 4.)

power. At high tip-speed ratios, ϕ and α are small, and low values of c_l are all that is needed.

A diagram of the airfoil model used in the L. S. Miller study is shown in Fig. 4.4. In this model, care was taken to use smooth, continuous curves to represent generic airfoil data to facilitate the numerical convergence of the twist optimization process. The program iteratively found the max c_p point for each condition by varying the twist, thus accounting automatically for twist effects.

Major variables for airfoil section data are the minimum drag coefficient $c_{d\min}$; the angle of minimum drag, AMD; the angle of zero lift, AZL; and the $c_{l\max}$. The shape of the c_l curve after stall and of the c_d curve as α increases is also important.

The effect of camber is to move the angle of zero lift in the negative α direction, allowing significant lift to be generated at the lowest possible drag. An extensive region of low drag in the c_d versus α curve helps to minimize losses over a whole range of high TSRs.

As was pointed out in connection with Fig. 2.12, the lift vector at any segment of blade has the greatest useful torque component when the lift/drag ratio of the airfoil section is highest. S. Miley's airfoil catalog is especially convenient for this measure of airfoil performance since it includes plots of lift/drag ratio versus α for each airfoil (see Ref. 3 in Chap. 2).

Effects and Sensitivities

We will now examine some of the effects of airfoil characteristics on rotor performance using curves from L. S. Miller's M.S. thesis.[4]

Figure 4.5 again shows the effect of airfoil drag on C_p. Rotors designed for very high TSRs must have extremely low drag.

The effect of high $c_{l\max}$ on C_p is shown in Fig. 4.6. High $c_{l\max}$ can be gotten from good airfoil design, from adding vortex generators to the upper

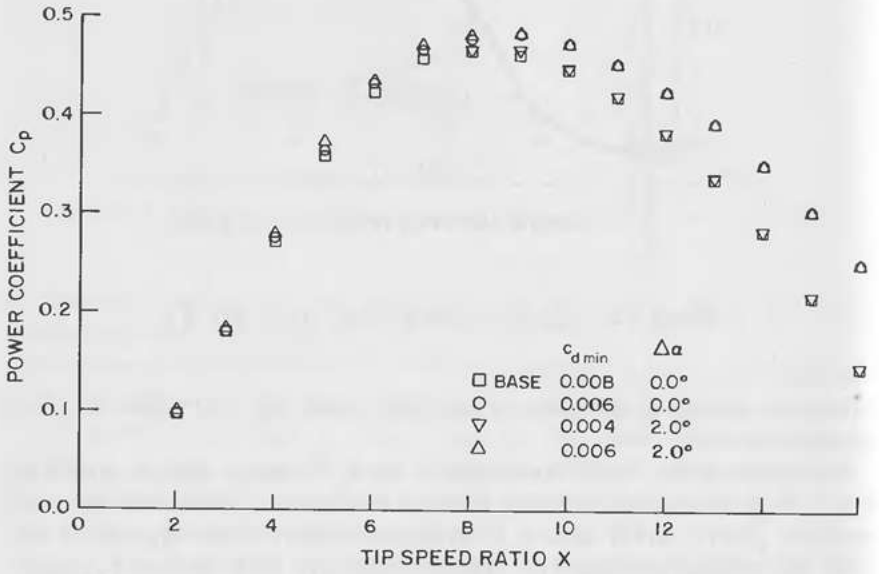

Figure 4.5. Effect of airfoil drag on turbine performance. (From Ref. 4.)

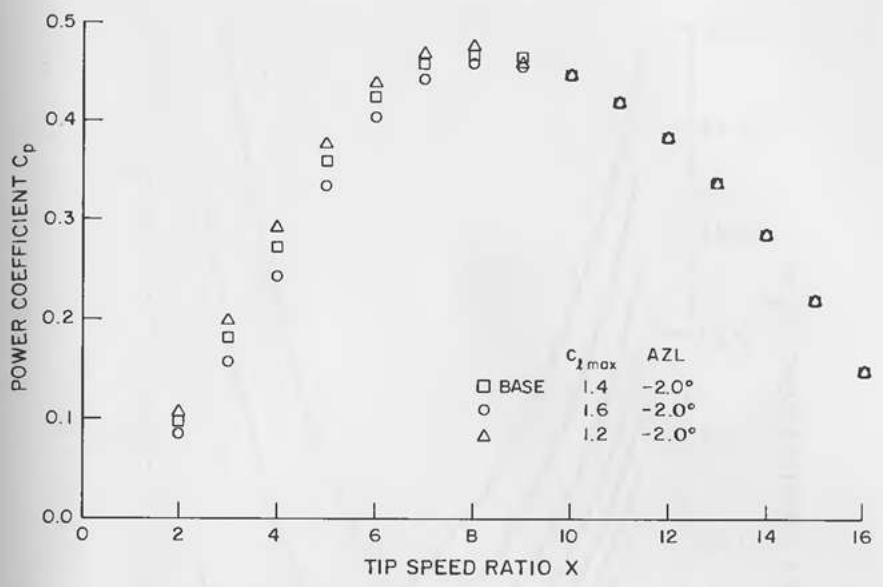

Figure 4.6. Effect of airfoil maximum lift on turbine performance. (From Ref. 4.)

airfoil surface, or from using special flaps as on aircraft wings. These matters are thoroughly discussed in Chap. 8 of Ref. 4 in Chap. 2.

Miller[4] also gives sensitivity plots that make very clear the needs of an airfoil for wind-turbine use. Figure 4.7 shows the required lift as the product of c_l and σ versus TSR X for various blade radii. The highest lift is required near the root at low TSRs. Again, this requires both a high c_l and a large chord. This effect is shown again in Fig. 4.8. Here the chord is given as a dimensionless ratio of the blade radius, R. The wider the blade, the lower the required lift coefficient.

Figure 4.9 shows the sensitivity of various blade elements to drag. Drag is critical at the blade tip, becoming progressively less important as the root is approached. Drag has a much greater effect at high TSRs than at low, again showing the 2δ effect discussed earlier. This points out clearly that it is quite easy to shut off the power production of a rotor at high TSR merely by giving the tip excess drag. This can be accomplished with a deployable end plate, a deployable spoiler, or merely by moving the tip a degree or two towards stall. The trouble with fixed surfaces is that they usually result in reduced power over a whole range of TSRs. Deployable surfaces, on the other hand, will not degrade aerodynamic performance in ordinary operating regimes but they do add complexity and must deploy reliably and simultaneously on all blades to achieve their function. Deployable surfaces must function despite ice, corrosion, mechanical binding due to load deflections, or other

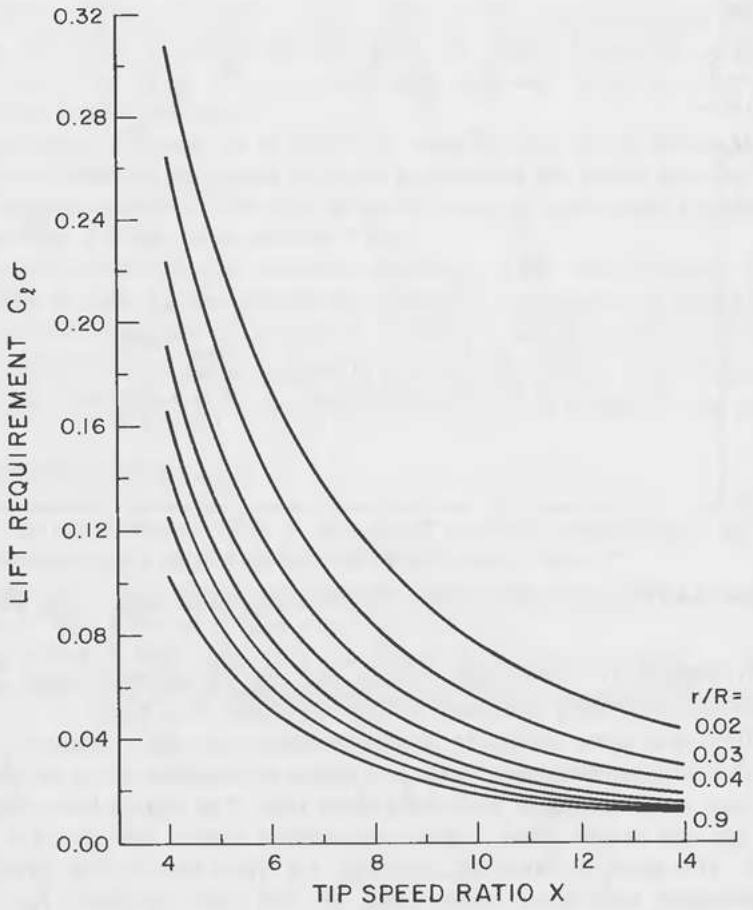

Figure 4.7. Required lift for maximum performance at a given radius. (From Ref. 4.)

phenomena. (In engineering design, a deployable mechanism that fails to work properly is soon relabeled a "deplorable mechanism.")

Finally, Fig. 4.10 shows the effect of lift sensitivity at various radii and TSRs. Lift coefficient is much more critical at the tip than at the root and at high TSRs than at low.

Although almost all of the current wind-turbine designs operate in a constant-speed mode, various researchers have inquired into the possible advantages of operating in a variable-speed, constant-TSR mode. If a machine could be controlled to operate at or near its TSR of maximum efficiency, improved energy-gathering performance should be possible. If one assumes a wind turbine could be made to operate always at maximum C_p, improvements of

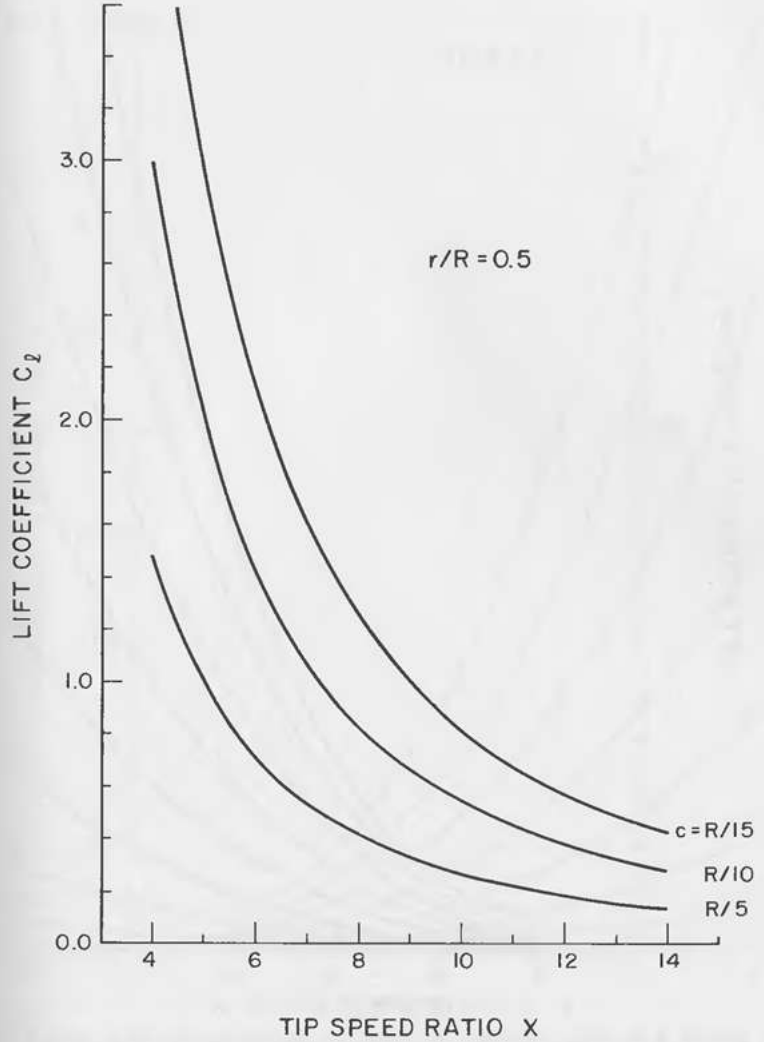

Figure 4.8. Required lift coefficient for various chord values. (From Ref. 4.)

the order of 25 percent in performance would result. In practice, not all of this gain could be realized. Work by A. H. P. Swift[18] tends to indicate that no increased performance whatever is gained by operating in a constant TSR mode. The exact conditions under which additional performance is actually achieved is an area awaiting further research.

It is apparent that there are many varied and challenging trade-offs in aerodynamic blade design.

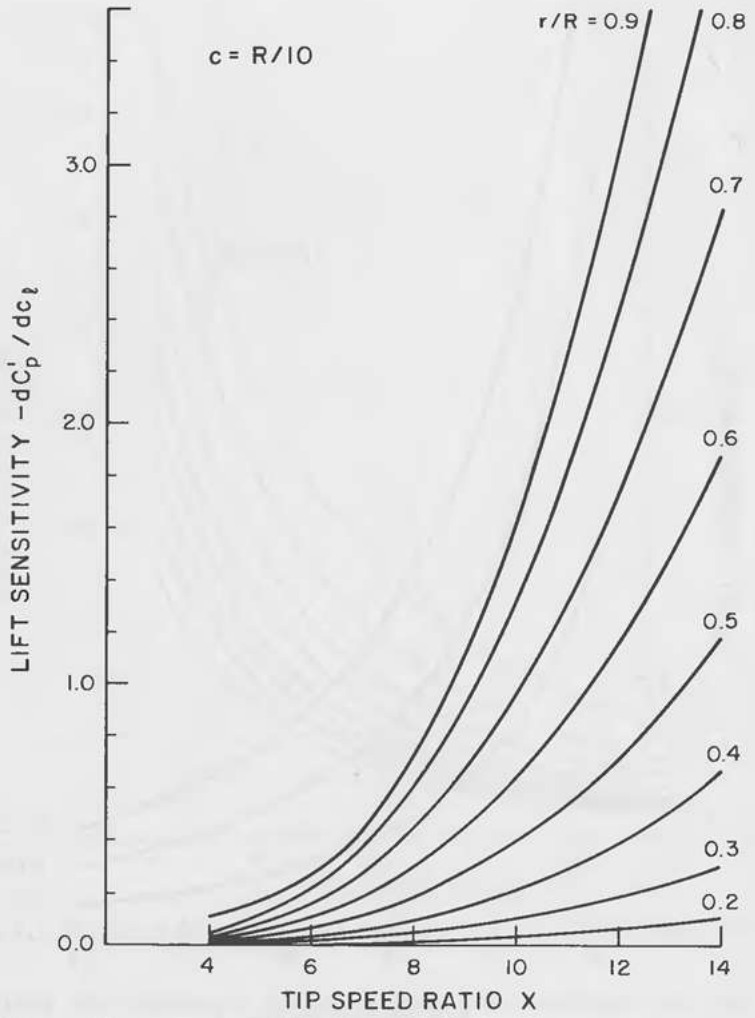

Figure 4.9. Drag sensitivity for various radius positions. (From Ref. 4.)

4.3 PREVIOUS DESIGNS

As with wind turbine history in general, much is to be learned from previous designs. Many famous machines have been discussed in Chap. 1, and reports on others are scattered throughout the literature.

It is not always easy to obtain information on existing machines. Most manufacturers regard detailed technical information on their machines as proprietary. Their attitude is, "After all the money we spent getting smart,

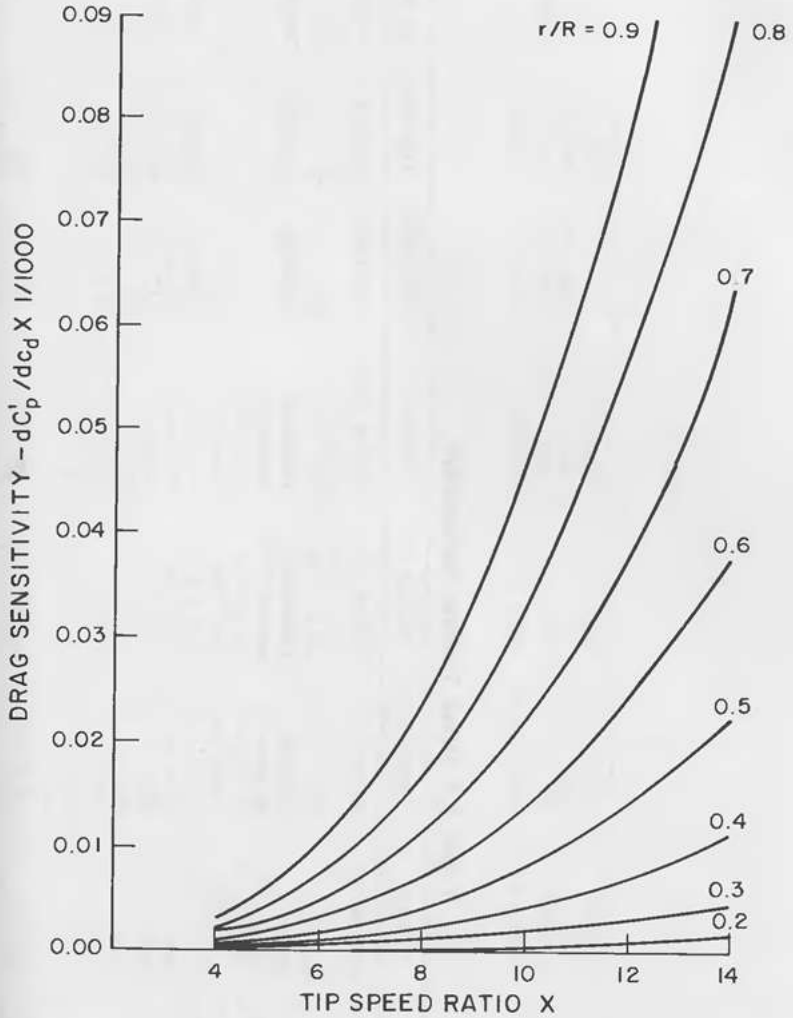

Figure 4.10. Lift sensitivity for various radius positions. (From Ref. 4.)

why should we help anyone else, who will then have the power to give us competition and cut into our profits." Even though this attitude is entirely understandable, it impedes dissemination of important technical information, with the result that large amounts of capital are wasted by other people in the industry in attempts to learn the same thing. From the point of view of the country as a whole, it is important to have a responsible technical organization that investigates technical problems and disseminates the results. It is hoped that the SERI, which has inherited this function, will be adequately

Table 4.1 Wind Turbine Parameters.

Machine	Gedser	Mod-0	Mod-2	Carter 25	Enertech 15	ESI-54	Grum WS/33	UTRC-8KW	Gav MV2E
Rotor dia., m/ft	24/78.7	39.2/128.6	91.4/300	9.8/32	13.4/44	16.5/54	10.1/33.25	9.45/31.0	2.05/6.73
No. of blades	3	2	2	2	2	2	3	2	5
Swept area, m^2	452	1207	6576	75	141	192	80	70	3.3
Type	Upwind	Downwind	Upwind	Downwind	Downwind	Downwind	Downwind	Downwind	Downwind
Hub ht, m/ft	24/78.7	30.5/100	61/200	60–120 ft	60–80 ft	24.4/80			
Ratings									
Power, kW	200	100	2500	25	15	56	15	9.5	
at V_0, m/s hub	15	12	12.5	11.6		15.6	10.7	8.9	
at V_0, mph hub	33.6	26.8	27.5	26		35	24	20	
at ang. vol., rpm	30.2	20.6	17.5	121	51.5	77.0	74.1	110	
Rotor									
Power ldg, W/m^2	442	83	380	333	106	291	188	159	
Solidity	0.088	0.033	0.033			0.033	.0615	.0568	.23
TSR cut-in/rated	7.6/2.5		13.9/4.2	18.4/5.3		18.6/4.2	7.3/5.25	4.5/8.5	
Precone, deg.	0	3	0	6		5	3.5	8	0
Axis tilt, deg.			2.5	0	0	0	0	0	0
Airfoil	SEAS	NACA 23024	NACA 23024	NACA 23XXX	NACA 23XXX	NACA 23XXX	NACA64$_4$421	NACA 23112	?FX72-MS-?
Twist, deg.	13 linear	0	0	30 parabolic	5 linear	10 linear	0	0	0
Tip 0-lift, deg.	9.2		−2.2	0	1.7				
Root 0-lift, deg.			4.34	30	6.7	9.2			
Tip pitch, deg.	0.8	0	−4.0	−1	−2.5		0	2	21
Root pitch, deg.	13.8	0	2.55	29	5	7.5	0	2	21
Root cutout	25%		20%	8%	10%	10%		18%	59%
Chord	1.5 m constant	77.3 in. to r/R = 0.234; linear taper to 26.4 in. at r/R = 1.0	136 in. to r/R = 0.297; linear taper to 56.4 in. at r/R = 1.0	50 in. at r/R = 0.08; parab. taper to 13 in. at r/R = 0.6; const. to r/R = 1.0	17.5 in. at r/R = 0.1; linear taper to 24 in. at r/R = 0.636; linear taper to 20 in. at r/R = 1.0	17.8 in. at r/R = 0.1; linear taper to 24 in. at r/R = 0.31; linear taper to 13 in. at r/R = 1.0	18 in. constant	15 in. constant	13 in. constant
Thickness	12% const.	24% inbd.; 18% outbd.	28% at r/R = 0.2; linear reduction to 12% at r/R = 1.0	21% at r/R = 0.6; linear reduction to 15% at r/R = 1.0	30% at r/R = 0.364; linear reduction to 10% at r/R = 1.0	32% at r/R = 0.15; linear reduction to 13% at r/R = 1.0	22%	12%	
Generator									
	200kW 3ϕ 8-pole	100kW 3ϕ Ind.	2500kW 3ϕ Synchn.	25kW 1 or 3ϕ Ind.	25kW 1ϕ Ind.	75HP 3ϕ Ind.	20kW 3ϕ Ind.	15kW 3ϕ Ind.	None-pump
Gen. rpm	750	1800	1800	1800	1800	1800	1800–1860	1800	
Gear ratio	1:24.83	1:87.4	1:102.8	1:14.9	1:35	1:23.4	1:25.1	1:17	1:1

funded by the government and will have the support of the industry and the public as well.

Another problem in obtaining information arises because severe problems of previous machines have never been clearly explained in public or may not have been understood even by their builders. The extreme reticence of people to admit mistakes and failures guarantees that most such problems will be supressed.

Nevertheless, a great deal of information still exists in the open literature on some machines, especially those that have benefited from the expenditure of public monies and for which the results are required to be in the public domain.

Table 4.1 is a brief compilation of some of the key parameters of wind turbines, assembled from published reports. Although strong efforts were made to make the data accurate, some information was not available, and other data may vary with the exact model, prototype, or test. Nevertheless, Table 4.1 provides a framework against which new designs may be compared and should be of help to designers.

Structural Considerations

While striving to optimize the aerodynamics, the designer must satisfy the structural static and dynamic constraints discussed in Chaps. 8, 9, and 11. The blade may be thought of structurally as a flattened tube that must have adequate bending stiffness in both flapping and lead-lag directions. This implies keeping sufficient moment of inertia I in both flapping and lead-lag. Adequate torsional stiffness is also required, which translates into sufficient polar moment of inertia J. Since both the bending stiffness in the flapping direction and the torsional stiffness vanish as the blade thickness approaches zero, adequate thickness must be maintained.

A properly constructed blade does not have uniform mass distribution, since, to avoid flutter, the chordwise mass center should preferably be at, or forward of, the axis of rotation of the blade. For this reason, the forward part of the blade should be quite a bit heavier than the trailing part. Such mass-balancing is critical on the control surfaces of aircraft, but it is also critical on blades if there is any rotational freedom about the blade's longitudinal axis. For a small turbine with a rigidly mounted blade, this chordwise mass distribution requirement can be eased, as discussed in Part II of this book.

A wealth of other lore regarding blade manufacture exists, most of it beyond the scope of this book. As a guide to such considerations, the designer should consult Refs. 13 through 15. These papers at least present fundamental ideas and thus provide a basis for further study of the problems involved.

REFERENCES

1. Wortmann, F. X. Experiences with FLAIR-8 and FLAIR-4 rotors. Proceedings, European Wind Energy Conference, Hamburg, FRG, Oct. 22–26, 1984.
2. Tangler, J. L., and Somers, D. M. Advanced airfoils for HAWTS. AWEA-U.S.DOE-SERI Windpower '85 Conference, San Francisco, CA, Aug. 27–30, 1985.
3. Stoddard, F. S. The California Experience. Presented at DANWEA '86, International Wind Technology Exhibition, Herning, Denmark, June, 1986.
4. Miller, L. S. Identification of airfoil characteristics for optimum wind turbine performance. M.S. thesis, Texas A&M University, Dec. 1983.
5. Mueller, T. L. The influence of laminar separation and transition on low Reynolds number airfoil hysteresis. AIAA Paper No. 8 1617, AIAA 17th Fluid Dynamics Plasma Dynamics and Lasers Conference, Snowmass, CO, June 25–27, 1984.
6. Althaus, D. Polar measurements of the profiles FX 8 W-097, 8 W-127, 8 W-140, 8 W-175, 8 W-218. 12th Meeting of Experts—Aerodynamic Calculational Methods for WECS, ISSN 0343-7639, Technical University of Denmark, Mar., 1985.
7. Wilson, R. E. The effect of hub fairings on wind turbine rotor performance. *ASME J. Fluids Engineering* 100:120 (Mar. 1978).
8. Eppler, R., and Somers, D. M. A computer program for the design and analysis of low speed airfoils. NASA TM-80210, 1980.
9. Habron, B. F.; Goldschmied, F. R.; and Kirschbaum, H. S. Wind turbine power improvement with modern airfoil sections and multiple-speed generators. AIAA/SERI Wind Energy Conference, Colorado, April, 1980.
10. Griffiths, R. T. The effect of airfoil characteristics on windmill performance. Aeronautical Journal Paper No. 251, July 1977.
11. Walker, S. N. Performance and optimum design analysis computation for propeller type wind turbines. Ph.D. thesis, Oregon State University, May, 1976.
12. Snyder, M. H. Airfoil data for use of wind turbine designers. Wind Energy Laboratory, Wichita State University, Wichita, KS.
13. Lark, R. F.; Gougeon, M.; Thomas, G.; and Zuteck, M. Fabrication of low-cost mod-OA wood composite wind turbine blades. DOE/NASA/20320-45, NASA TM-93323, Feb. 1983.
14. Peery, D. J., and Weingart, O. Low cost composite blades for large wind turbines. AIAA/SERI Wind Energy Conference, Boulder, CO, Apr. 1980.
15. Cheney, M. C. UTRC 8 kW wind turbine tests. AIAA/SERI Wind Energy Conference, Boulder, CO, Apr., 1980.
16. Wentz, W. H.; Snyder, M. H.; and Calhoun, J. T. Feasibility study of aileron and spoiler control systems for large horizontal axis wind turbines. NASA CR-159856, May 1980.
17. Miller, D. R., and Puthoff, R. L., Aileron controls for wind turbine applications. NASA Lewis Research Center paper presented at IECEC Conference, San Francisco, CA, Aug. 21, 1984.
18. Swift, A. H. P. Extensions to the Wilson-Lissaman prop code for steady and dynamic rotor performance prediction. U.S. Army Corps of Engineers paper, presented at the ASME ETCE, Houston, TX, Jan. 30-Feb. 3, 1983.
19. Rasmussen, Flemming. Blade and rotor loads for the Vestas 15. RISØ National Laboratory Riso-M-2402 (English translation). ISBN 87-550-094, June 1, 1983.
20. Ormsbee, A. I., and Maughmer, M. D. A class of airfoils having finite trailing-edge pressure gradients. AIAA Paper No. 85-0206, AIAA 23rd Annual Aerospace Sciences Meeting, Reno, NV, Jan. 1–17, 1985.

5

Digital Programs

5.1 INTRODUCTION

Digital programs implementing repetitive calculations are an essential part of any modern design process that can range from simple procedures or subroutines developed and proven on a programmable calculator to complex interacting algorithms running on a mainframe computer.

Some designers will have access to mainframe or minicomputers through their company; others will have to provide their own facilities.

The field of low-cost computer hardware is changing rapidly. Personal computers capable of extensive engineering number-crunching are within the financial capabilities of almost any designer. These include multimegabytes of memory, 10- to 40-megabyte hard disks, high-resolution screen graphics, printers, plotters, and communications and networking equipment.

With all the fine new hardware, demand for good software to run on it has increased. Any engineering designer should be capable of writing a program in one of the high-level languages implementing one of the sets of equations given in this book. Anyone who does so will get genuine appreciation for the time and effort involved. As is well known among programmers, if the bare bones of a program can be written in x person-hours (days, weeks, months), then, by the time convenient interactive input, complete error trapping, methods of backing out of errors, file-handling, printing, and plotting are added in, the time may have extended to $10x$ person-hours (days, weeks, months) or more. The savings in having programs already written for the more complex design tasks are quite substantial.

One approach, given this situation, is to try to adapt programs originally written for mainframes to run on smaller computers. Although some carry-over of effort to smaller computers usually exists, the problems with converting to a new language, changing all the input and output, and adapting to interactive keyboard operation are nearly equivalent to writing the program ab initio.

A problem for the designer is locating information on all the latest software. Some of it has been presented in technical papers; some programs are sold commercially and still others are available at little or no cost from researchers.

Reference 5 contains a section, "Wind Energy Models," that summarizes information on programs: their availability, cost, documentation, principal investigators, language, machine, and contact person (with address and phone number). Designers should contact SERI, 1617 Cole Blvd., Golden, CO 80401, or phone their Technical Inquiry Service at (303) 231-7303 for the latest information.

For modelling the control dynamics of wind turbines, one of the general-purpose modelling programs such as CSMP (Control System Modelling Program) may be used. CSMP is essentially a digital program set up to emulate a large analog or hybrid computer facility. It is very convenient for use with the typical control dynamics math models, incorporating various integration options, second-order pole pairs, and print-plots of transient response. Another program used by S. E. Mattsson (see Ref. 1 in Chap. 15) in his control analysis of large horizontal-axis wind turbines is SIMNON, by H. Elmqvist.[18] Mattsson includes modular SIMNON control dynamics codes for representing a turbine, synchronous generator, drive train and gearbox, pitch servo, wind, electrical bus, excitation system and voltage controller, pitch angle controller, and connecting system.

Whatever the source of the computer code, it is important that the designer understand the capabilities and limitations of the mathematical model upon which the program is based, that the program be carefully documented and checked out, and that input and output procedures be clear. Keeping track of the units is a prime method of checking engineering calculations, and this is no less important in digital programs.

The levels of effort, cost, and time required to obtain a program and get it running on your computer hardware and operating system are important factors to consider. Other considerations include computation speed, provision for obtaining help with problems from someone already expert in using the program, adequate memory to avoid slow and complex virtual memory or overlay techniques, adequate on-line storage, appropriate word size and computational precision, and provision for convenient plotting of results. The coding should also have been shown to be trustworthy by exhaustive test cases and cross-checks.

5.2 PROGRAMMABLE CALCULATORS

Many calculations such as stress analysis, load computations, and even aerodynamic performance can be done on the more capable programmable calculators. The truth of this is illustrated by the design programs given, for example, in such a book as Shigley and Mitchell's *Mechanical Design*.[1] Robert E. Wilson of Oregon State University, one of the original authors of the PROP program, has written, together with E. M. Patton, an aerodynamic

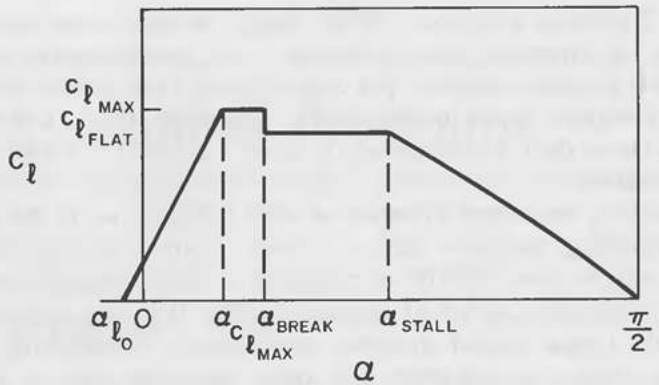

Figure 5.1. Curve fit of c_l versus α.

performance prediction program named AERO, which is in the public domain. Written in both HP-41C calculator code and in Fortran, AERO uses the simplified linear and constant-lift coefficient model represented by Fig. 5.1. It is compared with the equivalent PROP program model for the NACA 4415 airfoil in Fig. 5.2. A complete comparison of results from the AERO and PROP programs for analysis of the Enertech 1500 and the UTRC one-third

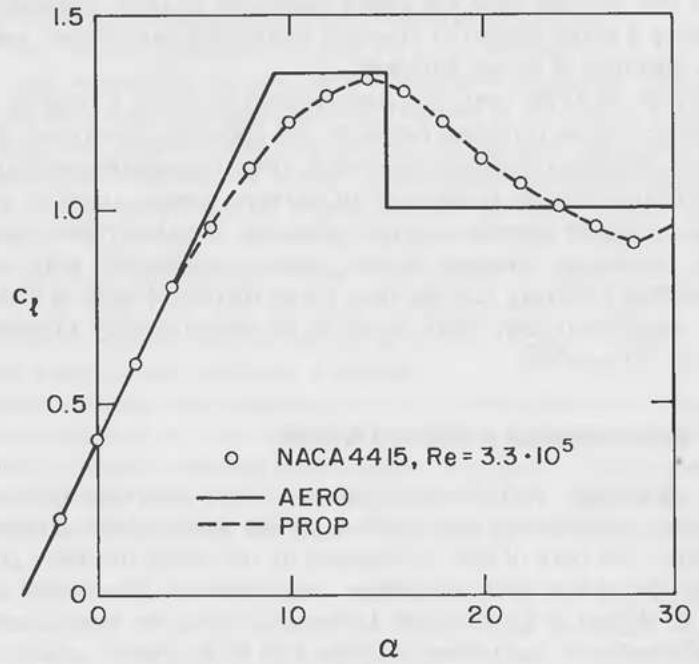

Figure 5.2. Lift coefficient models.

scale machines, together with test data, is given in Wilson and Patton.[2] The AERO program shows fair agreement with the PROP program in many particulars. It does not use the Prandtl tip-loss model but rather the simpler expedient of cutting off the torque contribution from the blade a short distance from the tip. The AERO program does not have a built-in provision for different c_l and c_d curves at each radial segment, as does the PROP program. Although we recommend the PROP program for design, the AERO program is remarkable in that it puts aero design computational power in the hands of anyone who can afford an HP-41C.

5.3 PERSONAL COMPUTERS

Most of the computations needed in wind-turbine design can be done on the more capable personal computers. Although complex prescribed-wake aerodynamic analysis and many-element, coupled structural dynamics or finite-element programs are usually too large to be considered for contemporary personal computer hardware, it is difficult to predict how long this state of affairs will continue. Inexpensive 32-bit machines with large memory banks are coming on the market, and these may soon be capable of almost all the design analysis needed. The necessary hardware will probably come a number of years before adequate software for these complex tasks is available. Running the full-fledged version of NASTRAN on your home mainframe computer may not be possible for a few years yet.

The PROP program was originally written in Fortran, which seems to be little used in personal computers. A version of PROP called *PROPSH* was developed at the Rocky Flats site for dimensional outputs and used for correlation with wind-turbine tests. Versions of the PROP program are now available in BASIC for several personal computers at reasonable prices. Reference 8 documents another interactive version of PROP called *PROPFILE*. Melvin Snyder of Wichita State University has developed a program "Wind II" for performing rotor design on the TRS-80 computer.[7] The convenience of going through the aerodynamic design process with 24-hour accessibility to one of these programs on your own personal computer is remarkable.

The drawing capabilities of personal-computer plotters and dot-matrix printers are also impressive. Given suitable software, an entire rotor design having blade profiles drawn up with full-scale cross sections showing proper twist, etc., will be possible with present hardware for up to medium-sized wind turbines.

Another capability of personal computers is the spreadsheet, or combined spreadsheet–database–word–processing program. An engineering-oriented spreadsheet program having all the usual transcendental math functions and single-variable optimization capability allows complex engineering tradeoffs to be done with great convenience. Even ordinary business spreadsheet

programs are superb for doing economic analysis studies. In the hands of a knowledgeable engineer, these programs can be a powerful adjunct to engineering design.

Airfoil Design

An airfoil design program called *PROFILE*, by R. Eppler and D. M. Somers, is available from COSMIC (Computer Software Management and Information Center), the NASA distribution organization for computer software.* PROFILE, which is written in Fortran, is a design and analysis code for low-speed airfoils. It was mentioned briefly in Chap. 4.

5.4 PRESCRIBED-WAKE ANALYSIS

Prescribed-wake analysis codes already exist in the public domain. For example, see App. D., Vol. 2, in Ref. 5 of Chap. 2, or consult the UTRC report on the WECSPER program of Egolf and Landgrebe in Ref. 8 in that chapter. Other such programs may be available soon. Although such programs may not provide higher accuracy than the simpler Glauert momentum strip theory, they are applicable to more complex designs, such as aileron control surfaces or dynamic tip inducers.

5.5 STRUCTURAL DYNAMICS PROGRAMS

A wind-turbine designer needs to have insight into all the significant structural vibrations and deflections of various parts of the machine under operational load conditions. Some of this insight can be gained by elementary simply-supported or cantilever beam theory together with superposition. Other components may be modelled by writing basic equations of motion, identifying the dominant terms, and gathering data to implement the model. Abundant examples of such models are given in Part II of this book. Some parts of a wind turbine are difficult to model simply and require use of finite-element substructure models to establish flexibilities, deflections, frequencies of vibration, and mode shapes. If wind turbines are ever mass-produced as automobiles are now, some of the techniques discussed in Kamal and Wolf[4] will be applicable.

Components that must be modelled include the rotor, the drive train, the generator and associated circuitry, the bedplate or yaw column, the tower, and the control system.

Several general-purpose structural dynamics programs can be of use in wind-turbine design. The most comprehensive program for general-purpose

*University of Georgia, 112 Barrow Hall, Athens, GA 30602; phone: (404) 542-3265.

structural modelling is the (full) NASTRAN program, which is capable of detailed finite-element structural-vibration analysis. It is quite complex—six months may be needed for an engineer to become confident in using it—and probably has limited application in wind-turbine design except for verifying substructure approximations in other, more simplified structural programs.

Other, simpler programs capable of modelling a 2-D or 3-D structure with 50 to 150 structural nodes are designed to run on personal computers. Several programs of this type are listed in Ryono.[16]

One of the most appropriate programs for coupled wind-turbine structural dynamic analysis is the MOSTAB series.[3] This series enables coupled dynamic analysis, including rotor flapping and lead-lag, tower vibration, drive-train dynamics, control-system interactions, and so on. The simplest of these programs, MOSTAB-HFW, calculates periodic solutions of blade motions. It

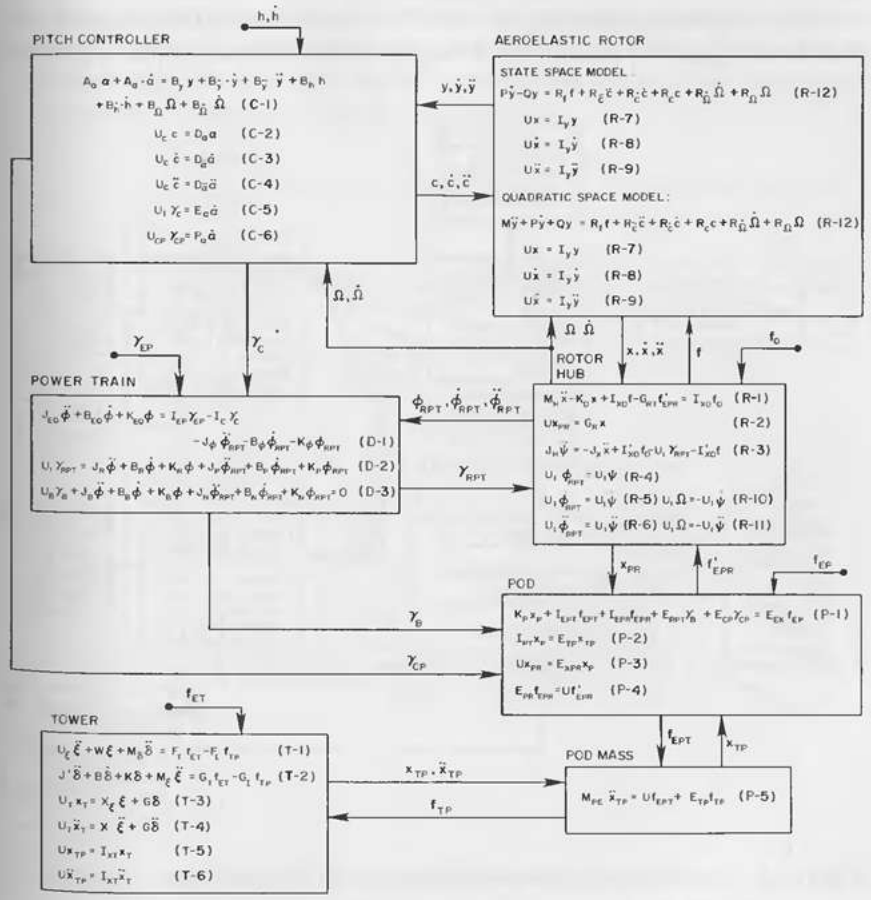

Figure 5.3. Wind-turbine-system block diagram. (From Ref. 3.)

is reported that this is the only one of the series that is small enough to get fast turnaround time on the NASA LERC computer system. (The others took overnight to run and required a good deal of expert programmer support.) Use of this program would be called for when preliminary structural analysis indicates the possibility of significant coupling between vibration modes of parts of the machine. Although application of these programs entails considerable expense in terms of mainframe run time and engineering and programmer support, this must be balanced against the costs of rebuilding and repairing large numbers of wind turbines after testing has shown design flaws. The development of a complex program such as NASTRAN is very expensive, requiring thousands of person-hours of expert programming and checkout. The MOSTAB series, developed and extended over a number of years of contract work, may be a useful adjunct in analyzing the more complex interactions encountered in wind-turbine design.

Several diagrams illustrating the MOSTAB series of coupled programs are given here. Figure 5.3 shows a block diagram of the dynamic coupled equations

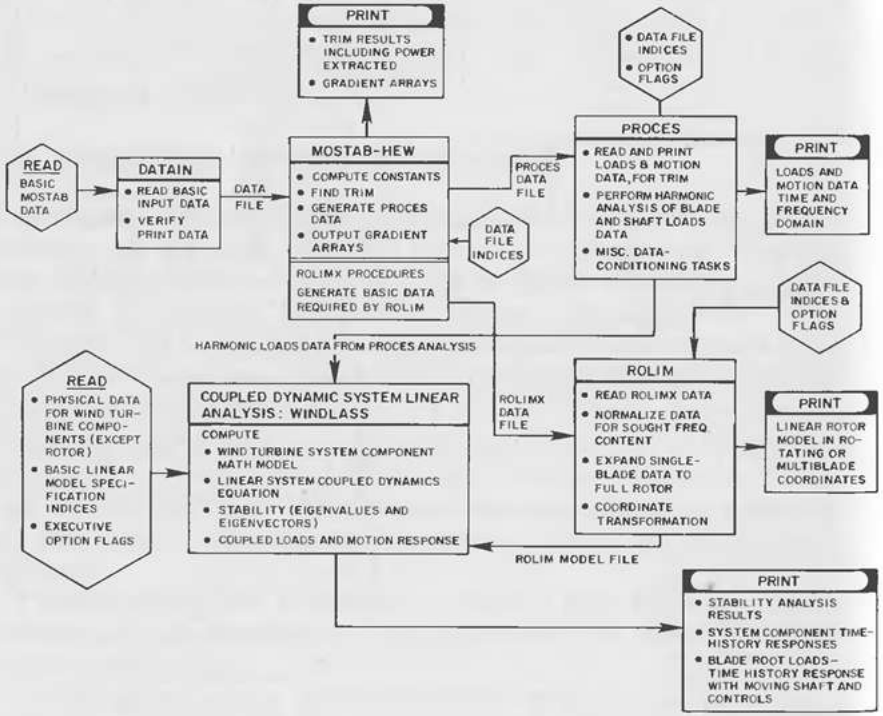

Figure 5.4. Coupled dynamic analysis (MOSTAS)—global arrangement. (From Ref. 3.)

for a wind turbine system. Many different sets of coordinates are necessary to account for tower, rotor, drive-train, and control-system motions. The MOSTAB programs allow six DOF elastic modes for each blade. Included is a provision for extracting linear coefficient models by determining trim conditions from the original nonlinear equations of motion. This capability, which is necessary for aircraft analysis, has been extended to cover wind-turbine rotors in the program shown in Fig. 5.4.

Results of analysis using MOSTAB for the blade-tip deflection of the Mod-0 rotor in response to tower shadow effects are shown in Fig. 5.5 for several design modifications, all compared with a baseline configuration.

As a comparison, consider the advances that have been made in automobile design as a result of the complete digital modelling described by Kamal and Wolf in *Modern Automotive Structural Analysis*.[4] The great expense of building and testing prototypes has been abandoned in the automotive industry in favor of detailed digital modelling. It is simply not possible to produce low-cost, efficient, and competitive automobiles using the old methods. Wind-turbine designers must likewise make use of the best tools to permit the manufacture of low-cost, efficient, and reliable wind turbines.

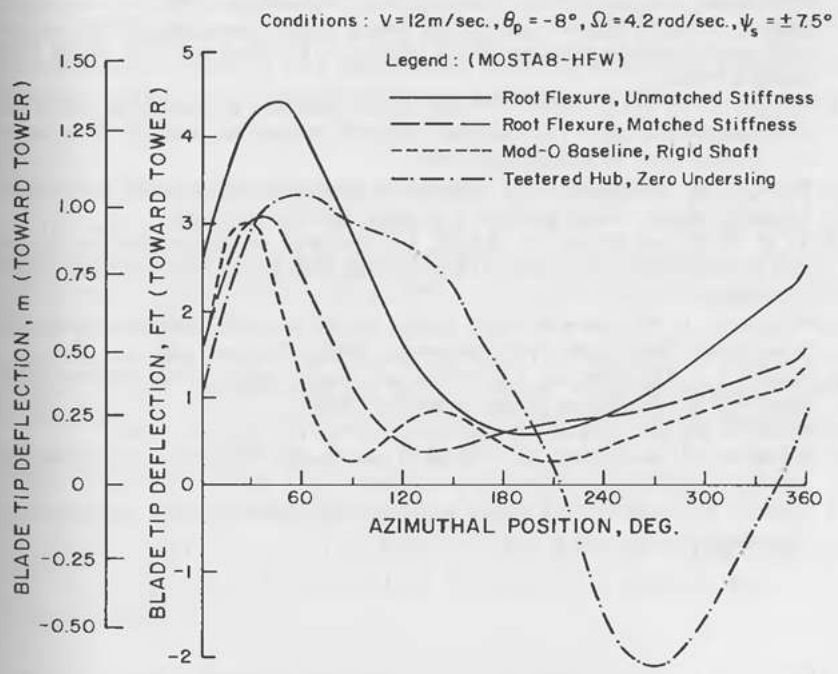

Figure 5.5. Blade tip deflection. (From Ref. 3.)

REFERENCES

1. Shigley, Joseph E., and Mitchell, L. D. *Mechanical Engineering Design*. New York: McGraw-Hill, 1983.
2. Wilson, R. E., and Patton, E. M. The AERO performance prediction method. Computer and calculator programs for predicting HAWT performance. Oregon State University. (See Ref. 8 of Chap. 2.)
3. Hoffman, J. A. Coupled dynamics analysis of wind energy systems. NASA CR-135152, Paragon Pacific, El Segundo, CA, Feb. 1977.
4. Kamal, Mounir M., and Wolf, Joseph A., Jr., eds. *Modern Automotive Structural Analysis*. New York: Van Nostrand Reinhold, 1982.
5. Grundstrom, Suzanne. Solar energy computer models directory. Wind Energy Models, Technical Information Branch, SERI, 1617 Cole Blvd., Golden, CO 80401.
6. Miller, Dean R., ed. Wind Turbine Structural Dynamics. NASA Conference Publication 2034, DOE Publication CONF-771148, workshop held at Lewis Research Center, Cleveland OH, Nov. 15–17, 1977.
7. Snyder, Melvin H. Wind-II, a computer code for predicting wind turbine performance. Presented at the 1983 Wind and Solar Energy Conference, Kansas City, MO, April 25–26, 1983.
8. Fairbank, D., and Rogers, E. PROPFILE, IBM PC version. Program manual, Jetstream, P.O. Box 27, Lake Geneva, WI.
9. Eppler, R., and Somers, D. M. A computer program for the design and analysis of low-speed airfoils. NASA TM-80210, Hampton, VA. NASA Langley, 1980.
10. Hoffman, J. A. Development report: Wind energy system time-domain (WEST) analyzers using hybrid simulation techniques. NASA CR-159737, Cleveland, OH, 1979. NASA Lewis Research Center.
11. Janetzke, D. C. Use of the WEST I wind turbine simulation to predict blade fatigue load distribution. NASA TM-83532, Cleveland, OH, 1983. NASA Lewis Research Center. Report also available under DOE/NASA/20320-56.
12. Miller, A. H. and Formica, W. J. Development and Verification of MOD-2 and MOD-0A Simulation Models. Pacific Northwest Laboratory, Richland WA, 1983.
13. Tu, P. K. C., and Kertesz, V. SEACC: The systems engineering and analysis computer code for small wind systems. RFP-3510, Rocky Flats Wind Energy Research Center, Golden, CO, 1983.
14. Waldon, C. A. Wind machine fatigue analysis and life prediction. RFP-3135, Rocky Flats Wind Systems Program, Rockwell International, Golden CO, April, 1980.
15. Tangler, J. L. Horizontal axis wind turbine performance prediction code PROPSH. Rocky Flats Wind Energy Research Center, Golden CO, 1983.
16. Ryono, B. Let your apple do the drafting. *A+* 2, No. 12: 29–47 Dec. 1984.
17. Snyder, M. H., and Staples, D. L. Wind II users manual. Wichita State University, July 1982.
18. Elmqvist, H. SIMNON-user's manual. Department of Automatic Control, Lund Institute of Technology, Sweden. Report TFRT-4091, 1975.

6

Performance, Economics, and Siting

6.1 PERFORMANCE

Once a wind turbine has been installed and passed its operational check-outs, it is put in regular operating mode. As a piece of machinery, it can then be evaluated on its performance, reliability, and maintenance costs and compared with other similar machinery on an economic basis. In performance evaluation, standard procedures are necessary for processing data so that results will be comparable and have a reliable meaning. Since performance results are often prepared by organizations under heavy pressure to "make things look good," bias will creep in, and only with standard data reduction procedures, independent laboratory testing, careful maintenance and calibration of measurement equipment, and frequent cross-checks can the validity of performance data be maintained.

Several guidelines for testing wind turbines are available to designers. One is *Performance Test Code 42*, available from the ASME.[14] This code provides standard instructions for conducting performance tests of wind turbines. Another is *Performance Standards for Wind Turbines* by the AWEA (American Wind Energy Association).[2]

Reports and data on electrical power generation in the U.S., including wind turbines, can be obtained from the Electric Power Research Institute (EPRI) of Palo Alto, CA, a research organization funded for mutual benefit and maintained by contributions from participating electric utility companies. Another source of current U.S. windfarm production and performance data is the California Energy Commission, Sacramento, CA.

Additional information on performance testing of wind turbines may be obtained from the research organizations devoted to this purpose, and a short list is included below.

- Solar Energy Research Institute, 1617 Cole Blvd., Golden, CO 80401.
- Alternative Energy Institute, Kilgore Research Center, West Texas State University, Box 248, Canyon, TX, 79016.

- RISØ National Laboratory, P.O. Box 49, Roskilde, DK-4000, Denmark
- Netherlands Energy Research Foundation, P.O. Box 1, Petten, 1755 ZG, The Netherlands.
- National Wind Turbine Centre, National Engineering Laboratory, East Kilbride, G75 OQU, United Kingdom.
- Atlantic Wind Test Site, 49 Pownal St., Charlottetown, PEI CIA 3W2, Canada.

The problems of testing to verify the performance of a wind turbine include the very real one of actually measuring the wind near the rotor, which was considered in both Chaps. 1 and 3. For recommended methods. see the reports by Akins[16] and by Hansen and Hausfeld.[17]

The parameters for evaluation of electrical-power-generation machinery were established long ago and carry over without modification into the evaluation of wind turbines. The "capacity factor" is a good example.

If an ac generator is rated at 10 MW, then in normal operation one may expect it to produce 10 MW. If it ends up in practice to produce only 8.32 MW over a fixed period of time, it is said to have operated with a capacity factor of 0.832 or 83.2 percent. The capacity factor, then, is merely the ratio of actual average power produced to rated power over a fixed period. The period can be yearly, monthly, weekly, or any other established length of time.

There is an obvious problem in applying this definition to wind turbines. If the wind doesn't blow at all during one day, the turbine cannot reasonably be expected to produce rated power that day. Nevertheless, the definition of the capacity factor is given and may not be changed. Some other measure must be defined to quantify how much wind there was during this period.

Another problem lies in assessing performance if the turbine was out of operation for any reason during the period. Since the ideal turbine would *always* be available, we may define a machine availability factor as the ratio of the time the machine was available for use divided by the total time in the period. If the machine was available at only 60-percent capacity for 15 percent of the period, it was not fully available, and even finer measures of availability may be needed. To maintain the desired meaning of machine availability, it would be necessary in this case to give the machine credit for being 60 percent available during this time. The machine availability could then be defined as the ratio of Σ (percent rating available) $\times$ Δ (time) over total time for the period. Even this definition fails when the reason the machine is out of service or operating at reduced capacity is unrelated to technical evaluation. To allow exceptions, however, is to invite manipulation and misuse of the evaluation criteria; consequently, such exceptions should probably not be permitted.

Wind turbines have cut-in and cut-out speeds. If the wind is below the cut-in speed, no power can be generated. If the wind is too strong and could damage or destroy the machine, the manufacturer may recommend shutting down the machine or have a cut-out mode built in so that the machine will automatically shut down in high winds. This being the case, another useful and easily measured piece of data is the number of hours a machine is synchronized with the grid (or the number of hours the field is energized to produce output power for a dc machine).

Vachon and Schiff have given results for test performance of large wind turbines (WT).[1] A useful set of parameters they present is as follows:

Weekly wind availability

$$= (\text{hours wind is within WT operating range})/(168 \text{ hr per wk}) \quad (6.1)$$

Weekly WT unit availability

$$= (\text{hours of WT synchronous operation})/168 \text{ hr per wk}) \quad (6.2)$$

Weekly capacity factor

$$= (\text{WT energy generated per wk})/(P_{\text{rated}})(168 \text{ hr per wk})$$

$$= \overline{P}/P_{\text{rated}} \quad (6.3)$$

where:

$\overline{P}$ = weekly average power
P_{rated} = WT rated power

These measures of wind-turbine performance are generally measurable and useful, although the weekly wind availability reflects only the number of hours the wind was within the operating range of the WT and does not therefore constitute a good measure of the wind energy available.

At the time of publication, performance data on the windfarms in California was available up to the third quarter of 1985.[18]

Although the short-term power-generation performance is of interest, many other measures may be imposed to quantify the reliability and robustness of a machine. Always foremost is its record in service. This includes design life data, maintenance costs, operational anomalies, control effectiveness, fatigue life, and many other factors. The need for high reliability and low maintenance becomes strikingly clear when one considers trying to maintain windfarms consisting of, say, 1000 separate machines. As both its power-generation performance and the engineering adequacy of its design become more and more established, a machine gradually becomes a known quantity to both its manufacturers and its users.

6.2 ECONOMICS

Of very great importance in the development of wind power is the economic evaluation of wind turbines. A number of somewhat different viewpoints exist, depending upon whom the analysis is done for—whether the designer, a supplier, a home or ranch owner, a commercial business, a windfarm developer, or a public utility.

The economics of windfarms is an important part of wind turbine economics. Although much of windfarm financing is outside the scope of this work, some of the economic aspects of wind farms are relevant. Particularly useful is the technique of working backwards from assumptions on capacity factor, site costs, and energy price per kWh to determine what can be paid for the wind turbine installation and still make a specified profit, as proposed by R. Lynette.[19] This technique yields a target cost for wind turbines as a function of energy price.

For windfarms to be profitable, not only the initial cost, but the reliability, the operation and maintenance costs, the effectiveness of siting each turbine, and the interference effects between adjacent turbines are all important factors to consider. Performance and siting effects of arrays of wind turbines were discussed by Lissaman et al.[15] Computerized monitoring systems are an indispensable tool in keeping track of large numbers of dispersed wind turbines.

The evaluation of the economy of purchase of an individual wind turbine involves the following steps:

1. Estimating the output-power characteristic of the machine to be used versus wind speed.
2. Estimating the wind spectrum at the proposed site at hub level.
3. Estimating all costs associated with the purchase, installation, and operation of the machine.
4. Determining the worth of the utilized and "exported" electrical power produced.
5. Evaluating financial implications, including all applicable Federal and state tax credits, depreciation, costs of borrowing capital, and the effect of Federal and state income taxes.
6. Applying basic principles of engineering economy to evaluate the economic performance of the investment.

Standard measures of economic performance include the effective cost of the power produced, the net present value, the payback period, and the internal rate of return.

It will be assumed that the reader is familiar with the basic concepts of engineering economy, the time value of money, and the use of interest factors,

although examples will be given to illustrate their use. See one of the many books on these subjects, such as Refs. 3 to 5, for further information.

In calculating the net effective cost of electrical power, it is common to "levelize" expenses or incomes over the life of a wind turbine into an equivalent yearly amount. This means taking an expense that occurs during a particular year and converting it to an equivalent equal amount for each year. As an example, suppose it were necessary to replace an alternator at a cost of $1000 during the eleventh year of operation for a machine having an assumed 25-year life. The result is entirely dependent on the interest rate. For illustration, let us assume our money can be invested at 15 percent. The worth of the $1000 cost at the beginning (year zero) would be

$$\begin{aligned} \$1000(\text{P/F } 0.15, 11) &= \$1000\left[1/(1+i)^n\right] = \$1000\left[1/(1.15)^{11}\right] \\ &= \$1000(0.2149) \\ &= \$214.94 \end{aligned}$$

The levelized equivalent amount over a 25-year life would be found as

$$\begin{aligned} \text{P(A/P } 0.15, 25) &= \$214.94\left[i(1+i)^n/((1+i)^n - 1)\right] \\ &= \$214.94\left[0.15(1.15)^{25}/(1.15^{25} - 1)\right] \\ &= \$214.94(0.1547) \\ &= \$33.25 \end{aligned}$$

Thus, a cost of $33.25 must be charged each year to pay for the replaced alternator. Levelizing can be applied to any expense or credit including depreciation, initial cost, etc.

There is usually some uncertainty in the input data for the economic evaluation of a wind turbine. It is usually impossible to predict exactly the windspeeds, the initial costs, or the machine performance and maintenance costs. To the extent that firm data on inputs can be used, this uncertainty can be reduced or removed.

A simplified analysis of the purchase of a single small wind turbine, neglecting depreciation effects, will illustrate some of the methods involved.

EXAMPLE 6.1: Suppose that a homeowner can purchase a wind turbine complete with tower, wiring, and controls for $4000, and that installation will cost another $1000. Maintenance and insurance is estimated at $200 per year, interest at 10 percent, and machine life at 20 years. Salvage value is estimated at $500 at the end of 20 years. The machine is estimated to produce

3000 kWh of power at the proposed site per year. What is the estimated cost of the electricity produced?

Solution: We will portray the capital costs as an equivalent yearly cost, the capital recovery with return, and add to that the yearly operating costs. This yields a total equivalent yearly cost. Dividing this cost by the kilowatt-hours produced yields the equivalent cost per kWh.

The capital recovery is

$$\mathrm{CR}(i) = (\mathrm{P} - \mathrm{F})(\mathrm{A/P}\, i, n) + \mathrm{F}i \tag{6.4}$$

where P represents the present expense; F, the future (salvage) value; i, the interest rate (in this case, $i = 0.10$); and n, the number of years of machine operating life.

The interest factor,

$$\mathrm{A/P}\, i, n = i(1 + i)^n/[(1 + i)^n - 1] \tag{6.5}$$

is called the capital recovery factor.

Substituting values, we find that

$$\begin{aligned}\mathrm{CR}(0.10) &= (5000 - 500)(\mathrm{A/P}\ 0.1, 20) + 500i \\ &= 4500(0.1175) + 50 \\ &= \$578.75\end{aligned}$$

This figure represents the equivalent yearly cost of this investment, including recovery of both the capital and the interest on it. Adding the yearly maintenance and insurance cost of \$200, we obtain a total equivalent yearly cost of \$778.75. If this is the cost of 3000 kWh of power, we have a unit cost of \$778.75/3000, or 25.96 cents per kWh.

If a tax credit is applicable, we should include its effect. Suppose that a Federal tax credit of \$2000 is applicable so that the owner's taxes are reduced by this amount one year after the purchase. The \$2000 thus saved, when discounted one year at 10 percent, is worth \$1818.18, so that P becomes \$5000 − \$1818.18, or \$3181.82. The new CR is then

$$\mathrm{CR}(0.1) = (3181.82 - 500)(0.1175) + 500(0.1) = \$365.11$$

resulting in a unit cost of \$565.11/3000, or 18.84 cents per kWh.

If a 25-percent state tax credit also applies, the worth of this tax credit discounted one year is \$1250/(1 + 0.1), or \$1136.36, and the CR then

WIND ENERGY ECONOMICS WORKSHEET

A. Preliminary Costs	per machine
1. Site analysis and site control	
wind resource assessment	\$_____
environmental impact	_____
2. Preliminary/detail engineering	
soil analysis	\$_____
electrical	_____
mechanical	_____
technical support	_____
other	_____
3. Permitting and approval costs, financing, legal, etc.	\$_____
B. Purchasing, shipping, and installation	
1. Factory price-FOB/need to determine what is included or not included	
machine cost	\$_____
tower cost	_____
special electrical equipment costs	_____
other costs	_____
2. Shipping expenses	
export packing	\$_____
factory to dock charges	_____
dock receiving charges	_____
export declaration papers/brokers' fee	_____
wharfage	_____
ocean or air freight	_____
destination handling charge, storage at the docks (should be avoided)	_____
interisland barge shipment/needed if no direct delivery is possible	_____
trucking to site	_____
other expenses	_____
3. Site preparation	
access for equipment	\$_____
fencing for security	_____
other	_____
4. Installation	
footing excavation	\$_____
reinforcement rods	_____
anchor rods and plates	_____
concrete/delivered to site	_____
erection equipment rental/leasing/purchase	_____
labor	_____
electrical hookup	_____
special electrical equipment such as a power substation, transformer, telephone poles, etc.	_____
transmission line or energy storage costs	_____
other	_____
TOTAL CAPITAL or First Costs	\$_____

Figure 6.1. Worksheet for estimating wind energy costs. (From Ref. 4.)

C. Tax Benefits (see new tax laws for 1987, etc.)
- Federal solar tax credit
  - residential benefit
    (40% of total cost up to $10,000 total solar benefit or $4,000 per individual)
  - business investment tax credit $_____
- Federal R&D tax credit (case by case) $_____
- State tax credit $_____
  - individual (10% of cost, no limit)
  - business (10% of cost, no limit)
- Federal 5 year accelerated depreciation allowance $_____
- State depreciation allowance $_____

NET CAPITAL COSTS . . . . . $_____

D. Annual Costs and Benefits

1. Revenue factors
   - a) Estimated total annual kWh $_____
   - b) Value of kWh used by owner at the utility rate _____
   - c) Value of kWh sold to the utility at the avoided cost or negotiated value _____

   GROSS REVENUE or ANNUAL VALUE $_____
   Less down time (force outage, 5 to 10%) $_____
   NET ANNUAL REVENUE . . . . . $_____

2. Operating Expenses
   - a) Debt retirement $_____
     (based on the life of the loan, interest rate, or a simplified annualization factor, etc.—see attached sample table)
   - b) Operating and maintenance costs (possibly 10 to 20% annual)
     - routine maintenance _____
       (servicing monthly or every 6 months, painting, corrosion protection, etc.)
     - extraordinary maintenance or parts replacement _____
       (estimated 5% to 10% capital cost each year)
   - c) Land rent (if required, fixed and/or percent of gross revenue) $_____
   - d) Insurance _____
   - e) Taxes-Income and general excise (on energy sold to the utility) _____

   NET ANNUAL OPERATING EXPENSES . . . . . $_____

NET ANNUAL INCOME . . . . . $_____

Figure 6.1. (*Continued*)

becomes

$$CR(0.1) = (\$3181.82 - 1136.36 - 500)(0.1175) + 500(0.1) = \$231.59$$

The equivalent unit cost is then \$431.59/3000, or 14.39 cents per kWh.

The recommended procedure in a practical case is to explore the problem with a number of different estimates and determine both the absolute numbers and the sensitivities of the calculations to changes in the variables. The owner would then have a good insight into the overall transaction and the effects of changes. In this problem, for example, a reduction of the yearly (maintenance plus insurance) cost could improve the results a good deal. Calculations such as this are conveniently done on a programmable calculator. A personal computer spreadsheet program would be even better, although it might represent overkill in such a simple problem.

A fairly complete economic analysis method for a single wind turbine is given in Suyderhoud, Neill, and Takahashi.[4] Their worksheet for estimating costs, reproduced in Fig. 6.1, is reasonably general. The results of their wind spectrum vs. machine output characteristic study are shown for some particularly attractive wind sites in Hawaii in Fig. 6.2. This figure also shows the effect of having either an especially good or especially bad wind year on the expected power produced. The results of their cash flow analysis for a \$100,000, 50-kW wind turbine installed at a Hawaiian site having 17-mph average windspeed are given in Fig. 6.3. They also give a sensitivity analysis for these results, which is reproduced in Fig. 6.4.

If the costs of a wind farm were divided and levelized on a per-machine basis, this form of analysis could evaluate the economics for the installation of an entire wind farm equally well.

As this example shows, installation of a good wind turbine at a good site can yield a quite acceptable rate of return. This is, of course, the driving force behind the rapid growth of windfarms in California and Hawaii.

	Kahuku			Honolulu
	Best Year	Mean Year	Low Year	Airport Mean
Average Wind Speed	17.4	17	16.4	11.9
Gross kWh Generated	197,500	181,600	177,400	102,600
kWh Used (Saved) (@12¢)	144,700	135,300	128,200	90,000
kWh Exported (Sold) (@5¢)	52,800	46,400	49,200	12,600
Est. Gross Value of Energy (Used and Sold, less down time)	$20,000	$18,600	$17,000	$11,400

Assumptions:
1) Uses 20 year simulated wind data at Kahuku Opana.
2) Uses 30 kW maximum, exports surplus.
3) Value of energy used is 12¢/kWh.
4) Value of energy sold is 5¢/kWh.

Figure 6.2. Computer simulations of ESI-54 WECS at Kahuku and Honolulu airport. (From Ref. 4.)

Year	1 Revenues	2 Expenditues	3 Debt Service	4 Interest	5 Depreciation	6 Tax Credit	7 Cash Flow	8 Taxable Income	9 After Tax Cash Flow	10 Net Present Value
1	$16,200	$3,500	$17,889	$15,000	$15,000	$30,000	$24,811	−$17,300	$33,461	$ 739
2	18,144	3,745	17,889	14,422	22,000	-----	−3,490	−22,023	7,521	5,190
3	20,321	4,007	17,889	13,729	21,000	-----	−1,575	−18,415	7,632	8,664
4	22,760	4,288	17,889	12,897	21,000	-----	583	−15,424	8,295	11,568
5	25,491	4,588	17,889	11,898	21,000	-----	3,014	−11,995	9,011	13,995
6	28,550	4,909	17,889	10,700	---------	-----	5,752	12,941	−719	13,846
7	31,976	5,253	17,889	9,262	---------	-----	8,834	17,461	104	13,863
8	35,813	5,620	17,889	7,537	---------	-----	12,304	22,656	976	13,982
9	40,111	6,014	17,889	5,466	---------	-----	16,208	28,631	1,892	14,161
10	44,924	6,435	17,889	2,982	---------	-----	20,600	35,508	2,846	14,367

Internal after tax rate of return (return on investment) = 72%
Financial Assumptions:
-50kW WECS
-Installed cost = $100,000
-Annual O&M = 2% of installed cost
-Annual property tax = 0.5% of installed cost
-Expense escalation rate = 7%
-Annual energy production = 180,000 kWh (18 mph equiv.)/ (allowing 10% for downtime)
-Investment tax credit = 30% (Federal 20% and Hawaii 10%)
-Discount rate for PV calculation = 30%
-Investor tax bracket = 50%
-Depreciation schedule = (15%, 22%, 21%, 21%, 21%)
-Initial energy value 9¢/kWh
-Annual energy escalation rate = 12%
-Length of loan = 10 years
-Loan interest rate = 20%
-Amount of debt = $75,000
-Amount of equity = $25,000

Relationship among columns:

(7) = (1 + 6) − (2 + 3)

(8) = 1 − (2 + 4 + 5)

(9) = 7 − 0.5(8)

$$(10)\ \mathrm{NPV} = \sum_{t=1}^{t} [\mathrm{ATCF}/(1 + 0.30)^{t}] - 25{,}000$$

Figure 6.3. Cash flow analysis. (From Ref. 4.)

Parameter	(Base Case)	Percent Change in Base Case Value −40	−20	−10	+10	+20	+40	+60	+80	+100
Annual kilowatt-hour (kWh) Output (energy value)	(180,000kWh) ($0.09/kWh)	0.49*	0.80	0.92	1.08	1.16	1.31	—	—	—
Energy Escalation	(12%)	0.93	0.97	—	—	1.03	1.06	1.09	1.12	1.15
Installed Cost	($100,000)	1.49	1.20	1.09	0.92	0.84	0.70	—	—	—
Investment Tax Credit	(30%)	0.59	0.78	0.89	1.12	1.24	1.51	—	—	—
Interest Rate	(20%)	1.15	1.08	1.04	0.95	0.90	0.79	—	—	—
Annual Operating and Maintenance (O&M) Cost Factor	(2%)	1.04	1.02	—	—	0.98	0.96	0.94	0.92	0.89
Cost Escalation	(7%)	1.007	1.004	1.002	0.998	0.996	0.992	—	—	—

Base Case IRR = 72%
*For example when annual kilowatt output decreases by 40% the IRR becomes 0.49 × 72% = 35%

Figure 6.4 Sensitivity Analysis: Effect of changes in economic parameters on WECS internal rate of return (IRR) factor. (From Ref. 4.)

Digital Programs

There are several digital programs for evaluating the economics of wind-turbine installations, including LIFECC (Life Cycle Cost Computer Code),[7] ROSEW (Representation of Solar Electric-Wind),[8] WECSAM (Wind Energy Conversion System Analysis),[9] and Windmill Performance.[10] For summary information, please consult Ref. 5 in Chap. 5.

6.3 SITING

The problem of siting a wind turbine has already been discussed in Chap. 3. Of course, the problems of siting an individual wind turbine are different than those for siting an entire wind farm. The paper by Lissaman et al.[15] also discusses siting problems for wind turbine arrays. Siting problems for particular terrain can be studied by means of wind tunnel tests. Such problems can also be studied using numerical simulation programs on a digital computer. A number of interesting possibilities arise, such as using different tower heights for different parts of the array, or even of using a mixture of high and low, small and large, horizontal and vertical axis machines, etc., to get maximum power production from a given plot of land.

There are several digital programs that may provide help in correlating historical data with expected winds at a new site, namely COMPLEX and NOABL. The COMPLEX program[11,12] aids in estimating wind resources at specific sites, using standard historical weather reports from different sites in a region. The other program, NOABL (New Objective Analysis Boundary Layer),[12] predicts wind fields when the terrain under question is not flat. Input includes at least one point where wind data has been observed, and the program attempts to predict wind speeds taking terrain into effect.

REFERENCES

1. Vachon, W. A., and Schiff, D. Test performance of large wind turbines. Presented at ASME Wind Energy Symposium, New Orleans, LA, March 7–10, 1982.
2. American Wind Energy Association. *Performance Standards for Wind Turbines*. AWEA, 1516 King St., Alexandria, VA 22314.
3. Thuesen, H. G.; Fabrycky, W. J.; and Thuesen, G. J. *Engineering Economy*, Prentice-Hall. 6th ed., 1984.
4. Suyderhoud, J.; Neill, R.; and Takahashi, P. Real world economics of wind energy. Proceedings, Wind Energy Expo '82, AWEA, Amarillo, TX, Oct. 1982.
5. Krawiec, S. Economics of selected WECS dispersed applications. AIAA/SERI Wind Energy Conference, Boulder, CO, Apr., 1980.
6. Lotker, M. Economic incentives to wind systems commercialization. AIAA/SERI Wind Energy Conference, Boulder, CO, April, 1980.
7. Sherman, J. M.; Gresham, M. S.; and Ferguson, D. L. Wind systems life cycle cost analysis. RFP-3448, Rocky Flats Wind Energy Research Center, Golden, CO, July 1982.

8. Percival, D., and Harper, J. Electric utility value determination for wind energy—Vol. I: A methodology; Vol. II: A user's guide. SERI/TR-351-604 and SERI/TR-732-604R, Golden, CO, 1981 and 1982.
9. Arthur D. Little, Inc. Wind energy conversion system analysis model (WECSAM) computer program documentation. SERI/SP-19136-4, Golden, CO, 1982.
10. Katzman, M. T. *Solar and Wind Energy: An Economic Evaluation of Current and Future Technologies*. Towota, N.J.: Littlefield, Adams, 1984.
11. Endlich, R. M., and Lee, J. D. An improved diagnostic model for estimating wind energy. PNL-4526, Pacific Northwest Laboratory, 1983.
12. Bhumralker, C. M.; Ludwig, F. L.; and Mancuso, R. L. Estimation of wind characteristics at potential wind energy conversion sites. PNL-3074, Pacific Northwest Laboratory, Richland, WA, 1979.
13. Phillips, G. T. Preliminary user's guide for the NOABL objective analysis code. DOE/ET/20280-78, Washington, DC, 1979.
14. *Performance Test Code 42*. American Society of Mechanical Engineers, United Engineering Center, 345 E. 47th St., New York, NY 10017.
15. Lissaman, P. B. S.; Zalay, A.; and Gyatt, G. W. Practical considerations for designing wind turbine arrays. Proceedings, AWEA Wind Energy Expo '82, Amarillo, TX, Oct. 24–27, 1982.
16. Akins, R. E. Performance evaluation of wind energy conversion systems using the method of bins—current status. Sandia Lab. Report. SAND77-1375, 1977.
17. Hansen, A. C., and Hausfeld, T. E. Correlation of wind turbine power output with turbulent winds. SERI Report under ASC 19296PB, Feb. 1985.
18. California Energy Commission. Reports from the wind project performance reporting system, 3rd quarter, 1985, P500-86-002, CEC Accounting Office, 1516 Ninth St., MS-2, Sacramento, CA, 95814.
19. Lynette, R. Report card on the wind turbine industry. Paper presented at the AWEA/CalWEA Seminar, Anaheim, CA, June, 1986.

PART II

STRUCTURAL DYNAMICS

Dynamics and aeroelastic studies of wind turbine systems can be discussed within the context of three interdependent forces—the aerodynamic, the structural, and the inertial, often known as the "aeroelastic triangle" (see Ref. 1 of Chap. 7).

The *aerodynamic* forces are the most difficult to visualize and to test; they are inherently unsteady and nonlinear, and, in the case of wind turbines, are further complicated by the random processes of the atmosphere. The *structural* forces are the elastic restraints that relate to deflections. And the *inertial* forces separate dynamics from statics by the introduction of mass, motion and gravity.

There are three major tools at our disposal in pursuing these studies: theoretical analysis, testing at subscale, and testing at full scale. None of them can be subordinated to another in the long run. For wind turbines, all are in their infancy, and even though mature techniques are being used in each area, much remains to be done before design engineering for wind turbines can be performed with the confidence it is for flight vehicles. The effort of this Part lies primarily in the first area, that of theoretical analysis, although test results are examined and discussed where they have been available. Unfortunately not enough data are yet available to verify *any* wind turbine theory, sophisticated or not; such verification will simply have to take the test of time, as it has in the helicopter industry.

Wind-turbine design engineers must be familiar with many aspects of mechanical, civil, and aeronautical engineering. Wind-turbine structures are complex, vulnerable, and subject to vibration. Although tethered to the ground, they must be made safe and reliable as aircraft. They are exposed to a wide range of environmental conditions, and their cost effectiveness relies ultimately on their practicality. Wind-turbine designers are less constrained by weight and more constrained by dollars than aircraft designers. Wind-turbine blades must be constructed with attention to traditional helicopter design parameters: torsional stiffness, bending stiffness, mass distribution, moment of inertia, control and mass axis placement, and hub attachment. Other parameters have additional significance as well: blade planform and twist for ease of fabrication,

low-cost materials, weathering and fatigue life, unattended operation, and long-term dynamic response.

Part II discusses the modelling and dynamic behavior of a wind-turbine rotor system that is exposed to idealized aerodynamic, elastic, and inertial conditions. The aerodynamics of wind-turbine rotors was discussed in Part I of this text. The aerodynamic study of wind turbines is more complex and more difficult than the structural study and can be argued to be more important since all major structural loads begin with aerodynamic forces. The aerodynamics is more difficult than the others because of a basic lack of physical understanding and of an inability to describe mathematically the unsteady aerodynamic behavior of the blades. Also, the range of aerodynamic conditions to which wind-turbine rotors are exposed is much greater than for most other aerodynamic devices. For these reasons, the state-of-the-art of wind-turbine aerodynamics, especially the time-varying, unsteady aerodynamics that is so important in blade-life calculation, still lags behind the state-of-the-art in structural dynamics.

The rotor response to atmospheric fluctuations is a complex problem that remains unsolved in detail. Turbulent shear flow interacts with the rotor to cause perturbations in the airflow across the airfoil in an unsteady and random way. This causes unsteady and random forces that bring about a dynamic response in the rotor in a like manner. To describe the wind fluctuations in a manner sufficient for the calculation of unsteady airloads and rotor response, the powerful tools of stochastic analysis will be necessary in the future. This text uses a deterministic approach, as does all of helicopter preliminary design development. Stochastic atmospheric studies are introduced in Chap. 12, however, and discussed further in Chap. 13 in relation to the subject of fatigue.

In this part of the text, major assumptions concerning the aerodynamics of the blades are made. These have been made in the past for the study of helicopters with great success, and it is logical and practical to apply them here as well. The dynamic solutions so derived are analytical, algebraic expressions that can be scrutinized to gain physical insight at the expense of the high accuracy that can come only from expensive computer programs and "global" solutions. The first assumption is that of *2-D linear aerodynamics*. This entails describing the airfoil lift-curve slope as a straight line that doesn't stall. Obviously, wind turbines often operate with stalled flows, and dynamic loading caused by stall does occur. A practical description of stall and stall-induced dynamic loading is given in Chap. 11. The chief dynamic response of the blades does not occur when the blade is stalled, however, and the proper operation of a wind turbine requires that some portion of the blades be in the unstalled region. The other major assumption is the *neglect of airfoil drag*. This is also a historically valid assumption and means simply that stalled behavior is not intended to be modelled. The effective result of the neglect of drag is that angle-of-attack variations are emphasized over flow speed changes at the airfoil. This approach is certainly logical to uphold since an airfoil is much more sensitive to small angle-of-attack changes than small flow-velocity changes.

These assumptions made in the modelling of the structural system are routine in the helicopter industry. The simple blade hinge-spring model, which represents only the fundamental natural frequency of a blade, has time and time again been proven a valid concept in rotary-wing preliminary design, as has the momentum theory. This assumption again allows the dynamic solutions to be analytical and algebraic. To include more bending modes in the structural calculation requires a computer program, and certainly one is needed for very accurate calculations. Also, the higher-order coupling terms in the algebraic solutions are neglected in this text, leaving only the physically dominant ones for discussion. Chapter 11 retains the major structural coupling terms that bear on dynamic instabilities. The derivation of the dynamic equations in the text allows the reader/user to modify the models and select the specific terms to be included or discarded for the mathematical development of other cases of special interest.

Part II derives and discusses the fundamental dynamics and vibration of a horizontal-axis wind-turbine rotor. It does not attempt to be the last word about wind-turbine rotors, only a first step towards understanding their behavior. It is hoped that the reader will be struck by the broadness and simplicity of the treatment and so, on the one hand, will find it a useful textbook for teaching and, on the other, a convenient reference for calculations. Furthermore, it is hoped that enough specific design criteria can be learned to allow a wind turbine designer to be confident of a preliminary design.

The reader needs a good background in mathematics to use this text fully. Algebraic manipulation and differential equations at the college sophomore level are prerequisite for the dynamics formulations and solutions. The physics follows routine statics and dynamics concepts, again at a college sophomore level. Since the author has had experience in helicopter as well as wind-turbine design, the nomenclature should be understandable to both disciplines even when the definitions are different. Effort has been made to keep the solutions and discussion as "physical" as possible to gain deeper insight into the dynamic behavior.

Chapter 7 presents an overall wind-turbine system model and develops the mathematics of the blade structural model. Chapter 8 uses the blade structural model to establish the blade equations of motion, at first with only inertial and elastic forces but later with aerodynamic forces. Chapter 9 examines blade

motions and deflections under the influence of all the effects and perturbations. In Chap. 10, the blade loads are combined to determine rotor, hub, and tower loads and to examine yawing stability; the chapter ends with a numerical example of rotor dynamic-load calculation. Blade instabilities, such as flutter, are discussed in Chap. 11, which treats very flexible blades and the coupled structural motions to which they are vulnerable, including various preset and control system inputs. A simplified but complete design-load specification is developed in Chap. 12, building on the structural dynamics solutions derived in the foregoing text.

7

SYSTEM ENGINEERING MODEL

7.1 INTRODUCTION

A wind-turbine system is a network of interconnected dynamic subsystems, each of which has its own degree of freedom and resultant natural frequencies. Additionally, coupling between the subsystems will exist when the boundary deflections are large enough to cause reaction or inertial forces, and vice versa. The subsystem "boundaries" are straightforward to visualize. The important subsystems are the *rotor*—or aerodynamic-momentum exchange device—the torsional *mechanical drive*, including the load, and the *tower*. A *control system* with suitable servomechanical capability over the system variables can also be included as a separate subsystem to provide stability and control capability and add extra freedom. A diagram of a wind-turbine system is shown in Fig. 7.1.

If the designer can correctly predict the loads and deflections in each subsystem, he will be able to design an efficient, cost-effective machine. Steady loads are straightforward; all are direct or indirect results of gravity and wind force on the blades. Performance studies are concerned with loads of this sort. The true grit of engineering design, however, lies in the structural dynamics: the determination of the motion of the system, the fatigue load spectrum, the response to external forcing functions, and possible mechanical instabilities inherent in the complex system.

The oscillatory response of a wind turbine to a given atmospheric forcing function can be thought of mathematically as the isolated response of each subsystem through its "transfer function" and the coupling functions. The most significant subsystem to this overall vibratory response is the rotor.

The rotor system is also more difficult to analyze than other subsystems since the main forcing function and the damping are due to aerodynamic loading, which is unsteady, nonlinear, and aperiodic. The dynamics of helicopter rotors and propellors have been well studied, but new assumptions concerning the aerodynamic loading are necessary for wind turbines. Also, the mass, stiffness, and geometric parameters of wind-turbine rotors are sufficiently different from those of helicopter rotors to dictate a reexamination and redevelopment of the basic system response. The balance of this section

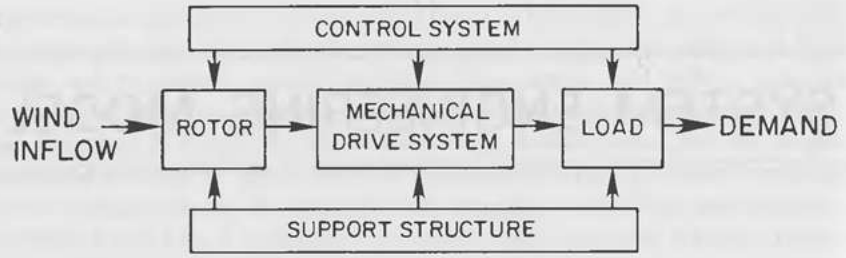

Figure 7.1. Wind-turbine system.

describes a suitable wind-turbine system model. The rest of the text will concentrate on blade and rotor analysis.

7.2 SYSTEM ENGINEERING MODEL

The system model can be simplified to a horizontal-axis wind turbine in a free stream, V_o, with rotor, hub, drive, load (in this case, an electric generator), supports, and tower, as diagrammed in Fig. 7.2.

The torsional drive subsystem, which can be treated as an elastic torsional system, consists of the horizontal rotor shaft, with moment of inertia, I_1, and angular velocity, Ω; the speedup mechanism, with I_2 and ω_2; and the generator rotor, with I_3 and ω_3. The generator torque can be applied to the bedplate in either of two perpendicular vertical planes (e.g., the fore and aft plane X′Z′ in Fig. 7.2 or the X′Y′ plane in Fig. 7.3). The applied forces and moments from the rotor are as follows:

S_H = the sum of all the hub shears (downwind, or Z′ direction)
τ_H = the applied rotor shaft torque
F_G = the resultant of all hub vertical forces
M_H = the sum of all hub moments (the Y′ component alone is shown)

The reactions at the tower bedplate attachment are as follows:

ΣF_V = the sum of all vertical forces
ΣF_H = the sum of all horizontal forces (or thrust)
ΣM_T = the sum of all tower moments

The mechanical drive system has its own torsional degrees of freedom and natural frequencies. The major inputs for this system are the applied rotor shaft torque, which contains specific periodic (sinusoidal) components, and the applied generator torque, which also contains periodic components. For systems analysis, the *bedplate* and internal supports are usually assumed to be rigid, thereby transmitting the weights and rotor reactions without deflection

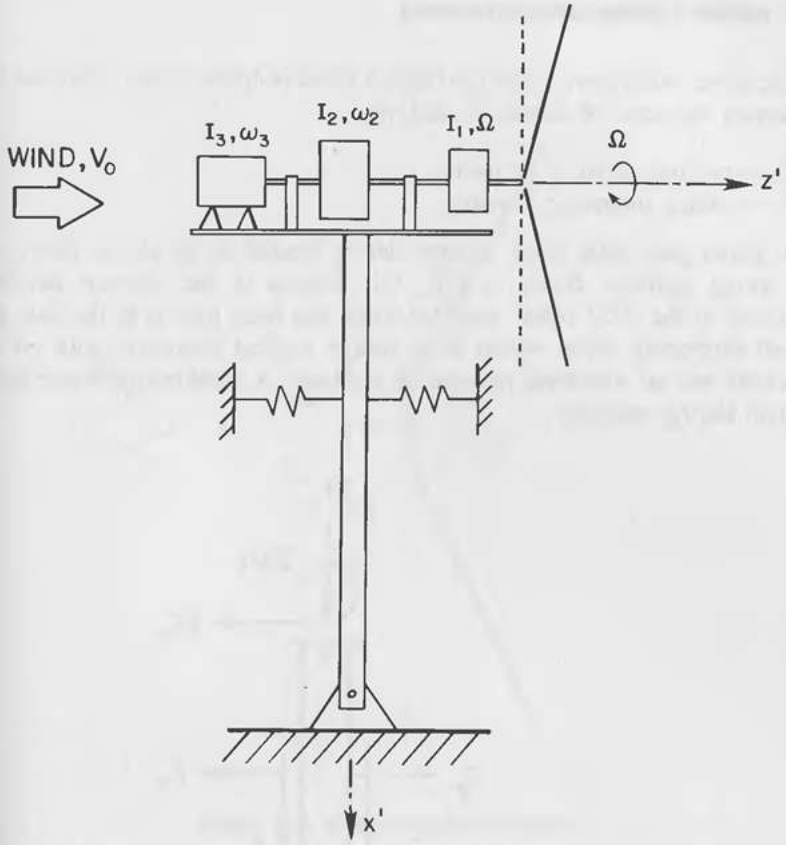

Figure 7.2. Overall coupled system.

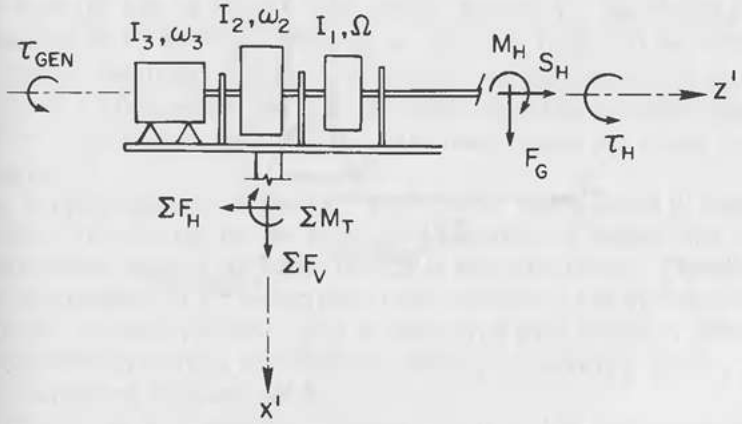

Figure 7.3. Mechanical drive system.

to the tower attachment. The mechanical drive/bedplate system also has two important moments of inertia, as follows:

$I_{y'}$ = pitching moment of inertia
$I_{z'}$ = rolling moment of inertia

A guyed pole mast tower system can be treated as an elastic beam with the spring restraint shown in Fig. 7.4. Motion in the diagram has been restricted to the X′Z′ plane, and the origin has been moved to the base pin. A self-supporting tower would be a simple vertical cantilever with no guy restraints and an additional moment at the base. A combination tower would contain all the reactions.

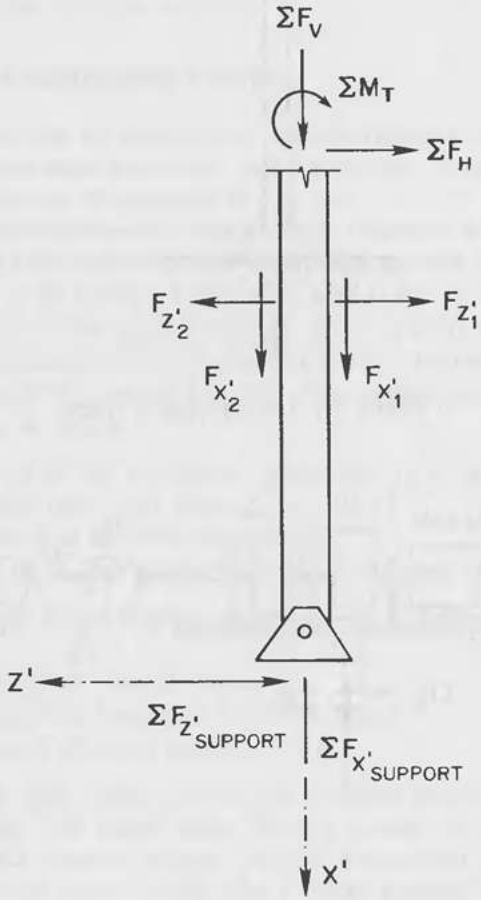

Figure 7.4. Tower system.

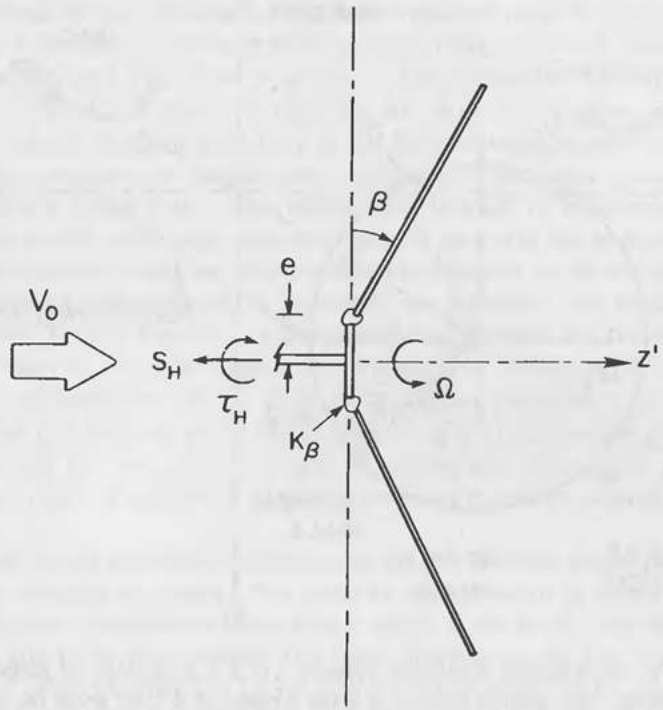

Figure 7.5. Rotor coordinate systems.

The rotor system can be simplified to a rigid hub and shaft with rotating hinged blades, as shown in Fig. 7.5. The blades are modeled as rigid members, offset from the axis of rotation, with spring restraint K_β. The flapping angle is indicated by β; the hinge offset, by e. The rotor blade can be isolated in the rotating coordinate system (xyz system) and the forces and moments determined for that system first and then transformed into the nonrotating hub and tower coordinate system. All the coordinate systems are shown together in Figure 7.6.

The coupled response of the total wind-turbine system could in theory be determined by deriving the set of coupled equations of motion that mathematically relate motions and forces in each of these subsystems. The equations could be linearized (e.g., higher-order terms discarded) and the transient and steady-state dynamic response could be determined from the set of differential equations through various computational techniques, including stability derivatives and analog computer studies.

In this text, a more pragmatic approach is taken. For preliminary design, and for a physical "feel" for the system, only the dominant, or "first-order,"

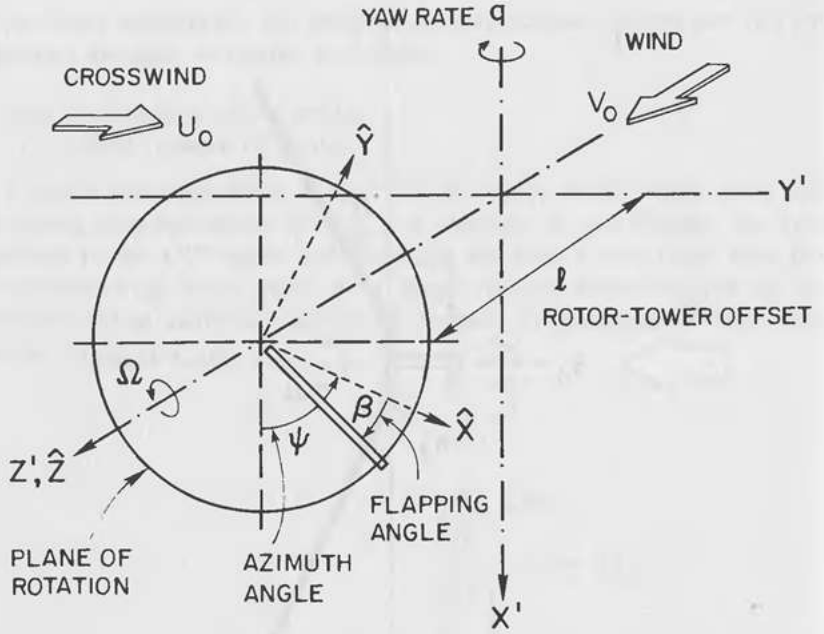

Figure 7.6. Wind-turbine coordinate systems: (1) *X'Y'Z' System*, or *Bedplate Coordinate System*—Yaw angular velocity q is the rotation of X'Y'Z' about the fixed tower axis X'; (2) $\hat{X}\hat{Y}\hat{Z}$ *System*, or *Rotor Hub Coordinate System*—$\hat{X}\hat{Y}\hat{Z}$ rotates around the Z' axis at constant speed Ω; (3) *xyz System*, or *Blade Coordinate System*—xyz is fixed to the blade and inclined to the $\hat{X}\hat{Y}\hat{Z}$ system by Euler angle, β.

forces, torques, and frequencies need to be considered. The text concentrates on the structural dynamics of the rotor. For the drive train and tower analyses, more routine methods are available, all well documented in the literature.

7.3 DYNAMIC BLADE MODEL

The vibration of a tapered and twisted wind-turbine blade is a complex phenomenon. A classic method of solution may involve a description of assumed orthogonal, uncoupled, bending- and torsional-mode shapes, a force equilibrium using the boundary conditions, and resulting combined mode shapes and frequencies. The EI (bending stiffness) and mass taper of the beam define the bending-mode shapes, and the torsional stiffness and mass distribution define the torsional-mode shapes. The elastic axis/mass axis offset yields inertial coupling between different modes, and the geometric twist produces structural, or EI, coupling between bending modes.

The usual engineering approach to this problem is to use finite element

representations of each structural element in sufficient detail to permit use of the classical elasticity equations.[1] Such a project yields combined mode shapes and frequencies to a high order of accuracy. One drawback to this method is the uncertainty of modulus and damping for most nonisotropic composite materials and the resulting sensitivity of the finite element program to errors. Thus, these programs in industry are continually refined and updated with proprietary test results from actual blades.[2] In the study of helicopter blades, it has been argued with some wisdom that such programs are unnecessary in preliminary design since the aerodynamic environment is so complex and unsteady. It is very difficult to represent the unsteady, or higher-order, aerodynamic forces; therefore, it may seem unimportant to represent the vibrating beam to any great degree of complexity, and hence a first order or first-mode representation of the blade is considered practical in preliminary design. The first bending mode is the one with the lowest natural frequency of motion and the one with the largest tip deflections. This mode provides the greatest range of possibility of transfer of energy from an external forcing function.

The blade model used here considers only the first bending mode, uncoupled from other bending or torsion. The complex tapered beam is represented by a simple hinged, cantilevered beam with a spring at the hinge. The equivalent beam is uniform in cross section and mass distribution and has a hinge of value K_β at offset eR. (See Fig. 7.7.) The equivalent beam has the same mass as the original beam, but the blade mass moment of inertia, I_b, is not the same by virtue of the mass center being more outboard on the equivalent beam.

The tapered beam has a fundamental bending frequency in a "soft" direction (i.e., flapping, flapwise, out-of-plane, etc.) and another frequency in a "hard" direction (i.e., edgewise, lead-lag, chordwise, inplane, etc.). The dynamic model thus has a hinge equivalent for flapping (K_β, eR) and another for lead-lag (K_ζ, e_2R).

The beam has a higher frequency of vibration when rotated as a blade

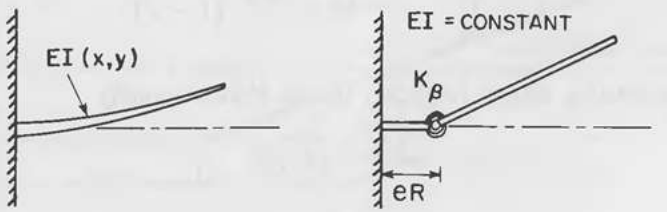

Figure 7.7. First bending mode.

because of centrifugal stiffening. The degree of stiffening depends on the mass distribution and the rotational speed, Ω. For the present, the beam may be considered to be representable by two already known bending frequencies: a nonrotating frequency, ω_{NR}, and a rotating frequency, ω_R, at a specific value of Ω. These two frequencies are important. The usual method of finding them during preliminary design is to model the blade mathematically as a series of connected lumped masses and springs and then do a Myklestad table analysis for the nonrotating case and a Myklestad-Prohl table analysis for the rotating case. Such a frequency calculation is described in Reference 3. Another, more direct, but more costly method is to build a blade and test it until one gets these frequencies. Experimentally derived frequencies are always more credible than predicted ones, even in the helicopter industry.

Once the two (rotating and nonrotating) frequencies are known, vibration analysis of the equivalent blade is straightforward. The mass moment of inertia for a uniform blade hinged at the root is

$$I_b = \int_0^R r^2\, dm = \frac{M_b R^2}{3} \tag{7.1}$$

where:

I_b = mass moment of inertia [slug-ft^2] or [ft lb-sec^2]
r = distance along radial direction
R = radius
M_b = mass of blade

Hinge-Offset Blade

For the same blade with nondimensional hinge offset, e, the integration starts at the hinge, as follows:

$$I_b = \int_0^{R(1-e)} r^2\, dm = \frac{M_b R^2}{3}[1-e]^3 \tag{7.2}$$

The nonrotating natural frequency of this blade is simply

$$\omega_{NR} = \sqrt{K_\beta / I_b} \tag{7.3}$$

Nonrotating Natural Frequency of Hinge-Offset Blade

The rotating natural frequency will be higher as a result of centrifugal force "stiffening" the blade. The frequency for the uniform blade hinged at the root is

$$\omega_R^2 = \omega_{NR}^2 + \Omega^2 \tag{7.4}$$

Rotating Natural Frequency of Hinged Blade

The hinge-offset blade has a somewhat different geometry, as shown in Fig. 7.8.

The hinge-offset blade is assumed to be vibrating at the hinge at its natural frequency. An energy balance can be done to find the frequency. The distance over which the centifugal force acts on mass element dm is AB, or

$$AB = [r - r\cos\theta] \simeq r(\theta^2/2)$$

The potential energy of mass dm is the work done, or the force times the distance, as follows:

$$\Delta PE = (\Omega^2 r'\, dm) \times r(\theta^2/2)$$

And the total potential energy is the integral over the vibrating blade, as follows:

$$\begin{aligned} u &= \int_0^{R(1-e)} \Delta PE = \int_0^{R(1-e)} r'\Omega^2(r\theta^2/2)\, dm \\ &= \tfrac{1}{4}\Omega^2\theta^2 M_b R^2 e(1-e)^2 + \tfrac{1}{2}\Omega^2\theta^2 I_b \end{aligned} \tag{7.5}$$

If the vibration is at frequency ω, the kinetic energy of mass dm is

$$\Delta KE = \tfrac{1}{2}dm \times V^2 = \tfrac{1}{2}dm(AB)^2\omega^2 = \tfrac{1}{2}dm\theta^2 r^2\omega^2$$

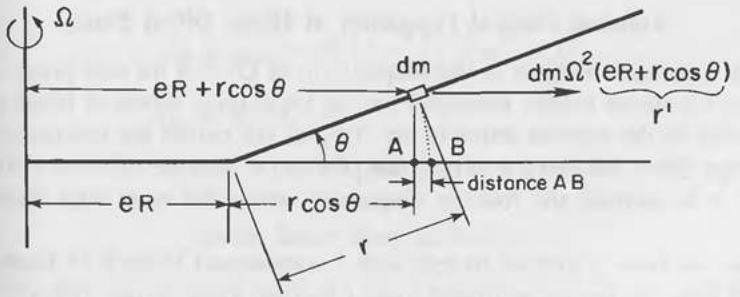

Figure 7.8. Hinge offset blade.

And:

$$KE = \int_0^{R(1-e)} \Delta KE = \tfrac{1}{2}\theta^2\omega^2 I_b \tag{7.6}$$

KE and *PE* can be equated to obtain ω, as follows:

$$\left(\frac{\omega}{\Omega}\right)^2 = 1 + \frac{1}{2}\left(\frac{M_b R^2}{I_b}\right) e(1-e)^2 \tag{7.7}$$

But for the equivalent blade,

$$I_b = \left(\frac{M_b R^2}{3}\right)(1-e)^3$$

which gives

$$\left(\frac{\omega}{\Omega}\right)^2 = 1 + \left(\frac{3}{2}\right)\left(\frac{e}{1-e}\right) \tag{7.8}$$

The rotating frequency of the simple blade is then

$$\omega_R^2 = \omega_{NR}^2 + \Omega^2$$

Thus, the complete rotating natural frequency of the hinge-offset blade is

$$\omega_R^2 = \omega_{NR}^2 + \Omega^2\left[1 + \left(\frac{3}{2}\right)\left(\frac{e}{1-e}\right)\right] \tag{7.9}$$

Rotating Natural Frequency of Hinge Offset Blade

This expression reduces to the simple form of Eq. 7.4 for zero hinge offset. Figure 7.9 shows natural frequency curves for various values of hinge offset. By virtue of the squared terms in Eq. 7.9, all the curves are quadratic. With no hinge offset, the curve is simply that of Eq. 7.4, and the effect of increasing offset is to increase the rotating frequencies more and more with increasing Ω.

Now we have a method to represent a complicated tapered EI beam by a simple hinge equivalent beam with hinge offset and hinge spring. The equivalent beam has the same nonrotating natural frequency as the original beam and the same rotating natural frequency calculated at some operational Ω. The

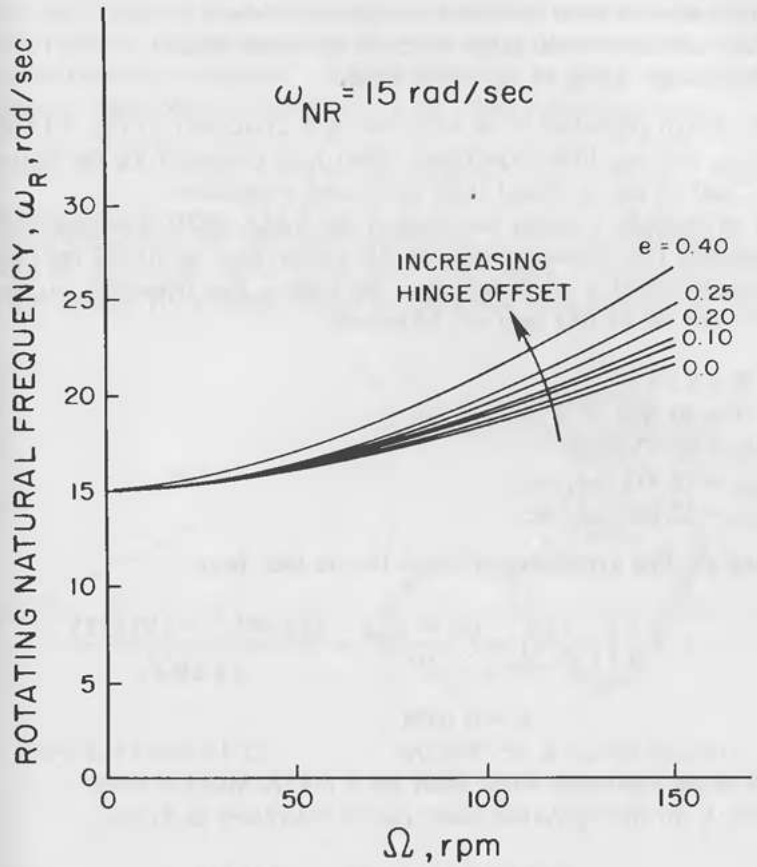

Figure 7.9. Rotating natural frequencies of various equivalent blades.

beam equivalence relations (see also Eqs. 7.2, 7.3, and 7.9) are as follows:

$$\omega_R^2 = \omega_{NR}^2 + \Omega^2\left[1 + \left(\frac{3}{2}\right)\left(\frac{e}{1-e}\right)\right]$$

$$\omega_{NR}^2 = K_\beta / I_b \tag{7.10}$$

$$I_b = (M_b R^2/3)\,[1-e]^3$$

Beam Equivalence Relations

where:

ω_R = rotating frequency of original beam
ω_{NR} = nonrotating frequency of original beam

I_b = mass moment of inertia of equivalent beam
e = nondimensional hinge offset of equivalent beam
K_β = hinge spring of equivalent beam

The design procedure is to solve the first expression in Eq. 7.10 for e, given ω_R and ω_{NR} from experiment. Then I_b is computed for the equivalent beam, and K_β can be found from the second expression.

As an example, consider the blade of the NASA MOD-O turbine.[4,5,6] The fundamental flap frequency, ω_{NR}, is 100 cycles/min, or 10.472 rad/sec. At a rotational speed Ω of 50 rev/min, the rotating flap frequency, ω_R, is 115 cycles/min, or 12.043 rad/sec. Moreover,

R = 62.5 ft
Ω = 50 rpm = 5.236 rad/sec
M_b = 61.53 slugs
ω_{NR} = 10.472 rad/sec
ω_R = 12.043 rad/sec

Solving the first expression in Eq. 7.10, we then have

$$1 + \frac{3}{2}\left(\frac{e}{1-e}\right) = \frac{\omega_R^2 - \omega_{NR}^2}{\Omega^2} = \frac{(12.043)^2 - (10.472)^2}{(5.236)^2}$$

$$e = 0.1620$$

which is the equivalent hinge offset for a NASA MOD-O blade.

Then I_b for the equivalent blade can be calculated as follows:

$$I_b = (M_b R^2/3)\,[1 - e]^3 = 47{,}142 \text{ slug-ft}^2$$

And finally, the equivalent hinge spring is

$$K_\beta = \omega_{NR}^2 I_b = 5.171 \times 10^6 \text{ ft-lb/rad}$$

And the MOD-O dynamic model is as shown in Fig. 7.10.

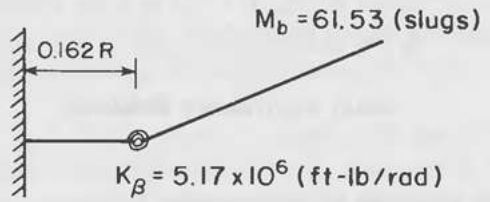

Figure 7.10. NASA MOD-O dynamic blade model.

Since the equations are solved for a specific value of Ω, the equivalence, strictly speaking, is good only for that frequency. However, other studies[7] have shown that the "stiffening" factor in Eq. 7.9, $1 + \frac{3}{2}(e/1 - e)$, represents a particular mode shape "coefficient" in the more general equation,

$$\omega_R^2 = \omega_{NR}^2 + a\Omega^2 \tag{7.11}$$

Such mode shapes are geometric orthogonal modes as illustrated in Fig. 7.11 and are the normal modes of the beam. The values of stiffening coefficient a are also shown. The example modes are calculated for a nonrotating, uniform

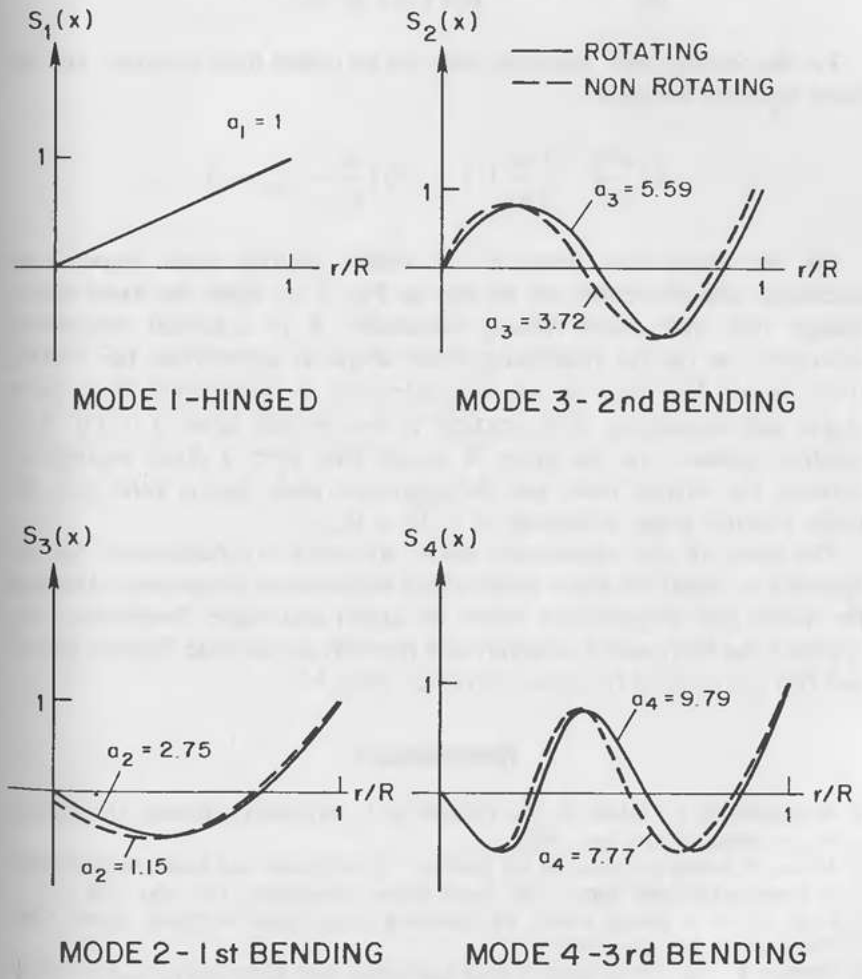

Figure 7.11. Normal modes of uniform blade, where a = the normal mode shape coefficient. (From Ref. 8.)

hinged blade with the following:

$$k^2 = \frac{EI}{m\Omega^2 R^4} = \text{constant} = 0.0055$$

where m = running mass.

The modes represent analytical solutions to the following form of Lagrange's equation and are specific for the example mass and stiffness distribution:

$$\frac{\partial^2 \phi_n}{\partial \psi^2} + a_n^2 \phi_n = \frac{1}{\Omega^2 R^2 f(n)} \int_0^1 \frac{\partial F}{\partial x} S_n(x)\, dx$$

For the rotating case, however, there are no closed form solutions, and the mode equation becomes

$$k^2 \frac{d^4 z}{dx^4} - \frac{1}{2}\frac{d}{dx}\left[(1 - x^2)\right]\frac{dz}{dx} - a_n^2 z = 0$$

For the above case, where $k^2 = 0.0055$, rotating blade shapes were calculated, and the results can be seen in Fig. 7.11. Since the mode shapes change very little under rotating conditions, it is a normal engineering assumption to use the nonrotating mode shape to approximate the rotating mode shape. And since we are only interested in fundamental (first) mode shapes and frequencies, it is practical to assume that factor a in Eq. 7.11 remains constant over the entire Ω range. This gives a direct equivalence between the original blade and the equivalent blade that is valid over the entire dynamic range of interest: $0 \leq \Omega \leq \Omega_{MAX}$.

The limits of this equivalence model are really not determined, but the approach is useful for blade motions and fundamental frequencies. Although the model gets progressively worse for higher and higher frequencies, this approach has been used extensively and routinely to calculate flapping motion and hub moments of hingeless helicopter rotors.[8,9]

REFERENCES

1. Bisplinghoff, R. L.; Ashley, H.; and Halfman, R. L. *Aeroelasticity*. Reading, MA: Addison Wesley Publishing Co., Inc., 1955.
2. Jarosch, S. Fatigue properties and test procedures of GRP plastic rotor blades. Paper presented at American Helicopter Society 25th Annual Forum, Washington, D.C., May 1969.
3. Prohl, M. A. A general method for calculating critical speeds of flexible rotors. *ASME Transaction A-142* (Sept. 1945).
4. Donham, R., et al. 100-kw hingeless metal wind turbine blade design, analysis, and fabrication. Preprint S-998, presented at American Helicopter Society 31st Annual Forum, Washington, D.C., May 1975.

5. Thomas, R., et al. Preliminary results of the large experimental wind turbine phase of the national wind energy program. NASA TM-X-71796, NASA Lewis Research Center, Cleveland, OH, October 1975.
6. Chamis, C. C., and Sullivan, T. L., Free vibrations of the ERDA-NASA 100 kw wind turbine. NASA TM-X-71879, NASA Lewis Research Center, Cleveland, OH, March 1976.
7. Den Hartog, J. *Mechanical Vibrations*. 4th ed. New York: McGraw-Hill, 1956.
8. Bramwell, A. R. S. *Helicopter Dynamics*. New York: John Wiley & Sons, 1976.
9. Yntema, R. T. Simplified procedures and charts for the rapid estimation of bending frequencies of rotating beams. NACA TN-3459, 1955.

8

BLADE EQUATIONS OF MOTION

8.1 INTRODUCTION

For preliminary design of wind turbines, it is important to look at the "uncluttered" effects of gravity, yaw rate, crossflow, etc., first when studying the dynamics. Hence, these effects are considered separately in this chapter. It is important to gain a "feel" for the physical forces and motions that are theoretically possible in order to explain the complicated phenomena that are likely to be encountered in actual wind-turbine testing.

In the interest of clarity, and to isolate the fundamental blade dynamics, the derivations here will include only the inertial effects and are kept as simple as possible. The aerodynamic terms are dealt with separately in Sec. 8.5. The blade degrees of freedom are uncoupled. A detailed dynamic analysis including the three coupled motions, deflections, and degrees of freedom (flapping, lead-lag, feathering) will be found in Reference 8.

The offset hinge-spring equivalent blade is assumed to be isolated and rotating at constant angular frequency, Ω, about the $Z'(\hat{Z})$ axis. The x, y, z axis system rides with the blades: the x axis spanwise and the y axis forward in-plane, as shown in Fig. 7.6. The blade is shown at flapping angle β. As described in Chap. 7, the rotor hub is stationary and the blade is comprised of rigid, uniform parts. The equations of motion are derived, as the simplest method for understanding the dynamics, from simple force and moment balances of the free body diagram.

8.2 SINGLE-BLADE EQUATIONS OF MOTION

Blade-flapping Equation of Motion

The nonaerodynamic forces acting on the elemental mass, dm, at radius r from the flapping hinge are due to centrifugal force (since the xyz system is rotating), gravity, and hinge spring restraint. These vectors are shown in Fig. 8.1. The angle ψ is the blade azimuth angle, where $\psi = 0$ represents vertical

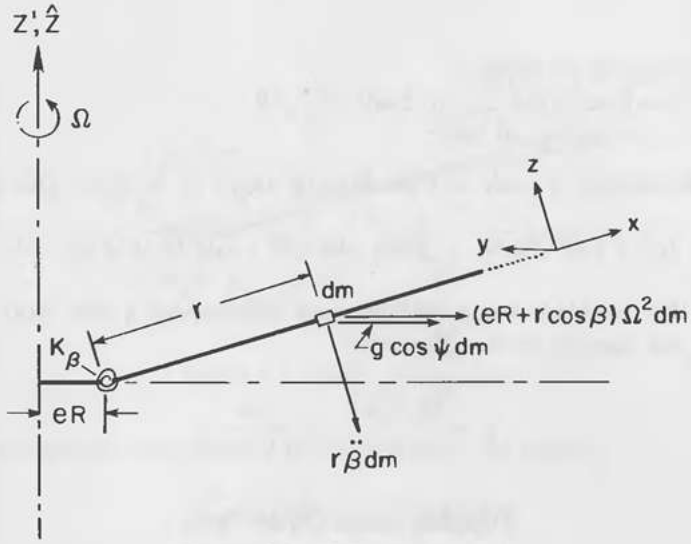

Figure 8.1. Blade flapping mode.

downward. As shown in the preceding chapter, the integration along the blade starts at the hinge.

Taking moments about the flapping hinge, we have

$$\sum M = \int_0^{R(1-e)} r^2 \ddot{\beta} dm + \int_0^{R(1-e)} (eR + r\cos\beta) r\Omega^2 \, dm \sin\beta + \int_0^{R(1-e)} r(g\cos\psi \sin\beta) dm + K_\beta \beta = 0 \tag{8.1}$$

The blade mass moment of inertia (sometimes ambiguously called "polar moment of inertia") is

$$I_b = \int_0^R r^2 \, dm$$

or, for the hinged blade,

$$= \int_0^{R(1-e)} r^2 \, dm$$

This gives

$$I_b\ddot{\beta} + eR^2\Omega^2 x_g M_b \sin\beta + I_b \cos\beta\Omega^2 \sin\beta + g\cos\psi \sin\beta M_b x_g R + K_\beta\beta = 0 \tag{8.2}$$

where

M_b = mass of the blade
x_g = nondimensional c.g. of blade = r_g/R
r_g = radius to c.g. of blade

The assumption is made that the flapping angle, β, is small, thus giving

$$I_b\ddot{\beta} + [eR^2\Omega^2 x_g M_b + g\cos\psi M_b x_g R + I_b\Omega^2]\beta + K_\beta\beta = 0 \qquad (8.3)$$

Now that the blade has a uniform mass distribution, a new term can be defined, the *flapping hinge offset term*:

$$\epsilon = \frac{M_b e x_g R^2}{I_b} = \frac{3e}{2(1-e)} \qquad (8.4)$$

Flapping Hinge-Offset Term

and a new relationship, the blade flapping equation of motion:

$$\ddot{\beta} + \Omega^2\left[1 + \epsilon + \frac{G}{\Omega^2}\cos\psi\right]\beta + \frac{K_\beta}{I_b}\beta = 0 \qquad (8.5)$$

Blade Flapping Equation of Motion

where the *gravity term*, G, is defined as

$$G = \frac{gM_b x_g R}{I_b} \qquad (8.6)$$

Gravity Term

Blade Lead-Lag Equation of Motion

The prominent in-plane force is due to rotation, that is, centrifugal force. The motion in lead-lag is first derived including only this force, since the geometry is complex. The blade is shown in Fig. 8.2, looking at the plane of rotation, with the blade at a deflected inplane angle, ζ. Again, the integration begins at the hinge, so that the radius arm, r, is measured from that point.

For small ζ, the rotation arm to dm is $(e_2R + r)$, and the centrifugal force on dm is

$$dF = (e_2R + r)\Omega^2\, dm$$

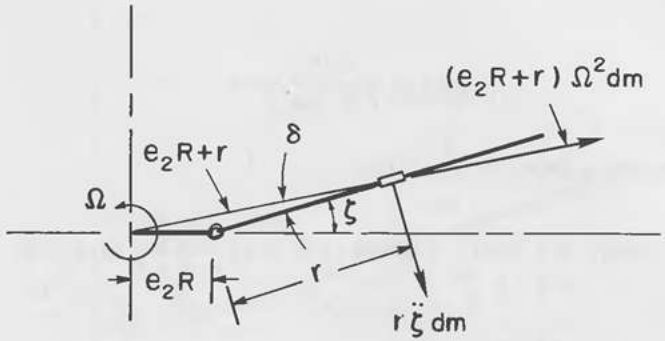

Figure 8.2. Blade lead-lag mode.

The component that produces a moment about the hinge is

$$dF_\zeta = (e_2R + r)\Omega^2 \sin\delta\, dm$$

where δ is the small angle between the blade and the centrifugal moment arm. The angle is found from the diagram shown in Fig. 8.3. From the geometry of this figure,

$$\zeta = \gamma + \delta$$
$$h = e_2R\sin\gamma = r\sin\delta$$

or

$$\sin\delta = \frac{e_2R}{r}\sin\gamma$$

For small angles,

$$\sin\delta \simeq \delta = \frac{e_2R}{r}\gamma = \frac{e_2R}{r}(\zeta - \delta)$$

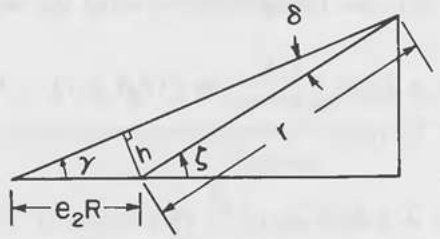

Figure 8.3. The angle, δ between the blade and centrifugal moment arm.

Thus,

$$\sin \delta = \frac{e_2 R}{r + e_2 R} \sin \zeta \tag{8.7}$$

Taking moments about the lag hinge,

$$\sum dM_\zeta = r^2 \ddot{\zeta} dm + r\,\Omega^2\, dm\,(e_2 R + r)\frac{e_2 R}{r + e_2 R} \sin \zeta = 0$$

Thus,

$$I_b \ddot{\zeta} + \Omega^2 e_2 R \sin \zeta M_b X_g R = 0$$

or,

$$I_b \ddot{\zeta} + e_2 M_b x_g \Omega^2 R^2 \sin \zeta = 0 \tag{8.8}$$

As in Fig. 8.4,

$$\epsilon_2 = \frac{M_b e_2 x_g R^2}{I_b} = \frac{3e_2}{2(1 - e_2)} \tag{8.9}$$

Lead-Lag Hinge Offset Term

$$I_b \ddot{\zeta} + \epsilon_2 I_b \Omega^2 \sin \zeta = 0 \tag{8.10}$$

Blade Lead-Lag Equation (For Centrifugal Force Only)

The final forces on the elemental mass are shown in Fig. 8.4. The lead-lag offset, e_2R, and the lead-lag spring, K_ζ, are derived from considerations of beam flexibilities, as eR and K_β were for the flapping mode. A Coriolis acceleration due to flapping motion, $\dot{\beta}$, is included. Other nonaerodynamic forces are centrifugal, gravitational, and hinge-spring.

Referring to Fig. 8.4, and taking moments about the lag hinge, we have

$$\sum dM_\zeta = \underbrace{r^2 \ddot{\zeta} dm}_{\text{Inertial}} + \underbrace{r\,\Omega^2\, dm \frac{e_2 R}{e_2 R + r} \sin \zeta\,(e_2 R + r)}_{\text{Centrifugal}} - \underbrace{2r^2\, dm\, \Omega\, \dot{\beta} \sin \beta}_{\text{Coriolis}}$$

$$+ \underbrace{r\, dm\, g \sin(\psi + \zeta)}_{\text{Gravitational}} + \underbrace{K_\zeta \zeta}_{\text{Hinge-spring}} = 0 \tag{8.11}$$

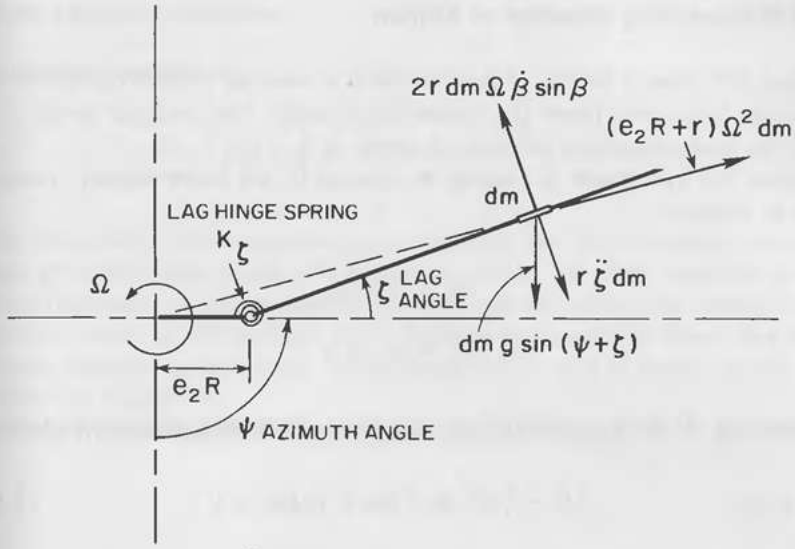

Figure 8.4. Blade lead-lag mode.

Integrating, we have

$$I_b \ddot{\zeta} + \epsilon_2 M_b x_g \Omega^2 R^2 \sin \zeta - 2 I_b \Omega \dot{\beta} \sin \beta + g \sin(\psi + \zeta) M_b x_g R + K_\zeta \zeta = 0$$

Again,

$$G = \frac{g M_b x_g R}{I_b}$$

and

$$\epsilon_2 = \frac{M_b e_2 x_g R^2}{I_b}$$

Then, $\sin(\psi + \zeta) = \sin \psi + \zeta \cos \psi$, and the blade-lagging equation including gravity, hinge offset, and flapping velocity, $\dot{\beta}$, is

$$\ddot{\zeta} + \left[\epsilon_2 \Omega^2 + G \cos \psi + \frac{K_\zeta}{I_b}\right]\zeta - 2\Omega \dot{\beta} \beta + G \sin \psi = 0 \tag{8.12}$$

Blade Lagging Equation

Blade Feathering Equation of Motion

Figure 8.5 shows a section of the blade with a torsional (feathering) deflection, θ, away from some preset or constant pitch angle. The torsional spring is K_θ and the feathering mass moment of inertia is I_f.

Since the xyz system is rotating at constant Ω, the Euler angular velocities are as follows:

$$\omega_y = \Omega \sin \theta$$

$$\omega_z = \Omega \cos \theta$$

Neglecting all other coupled effects, the simple feathering oscillator is derived:

$$I_f\ddot{\theta} + I_f \Omega^2 \sin \theta \cos \theta + K_\theta \theta = 0 \tag{8.13}$$

Or, for small θ, we have

$$\ddot{\theta} + \left[\Omega^2 + \frac{K_\theta}{I_f}\right]\theta = 0 \tag{8.14}$$

Blade Feathering Equation

8.3 ELEMENTARY DYNAMIC MOTIONS

Equations 8.5, 8.12, and 8.14 were derived for the simple hinge-equivalent blade with lead-lag, torsion, and flapping degrees of freedom. These second-order equations describe the fundamental motion of the blade in the absence of aerodynamic forces. Much can be learned from a qualitative look at the dynamic system they represent.

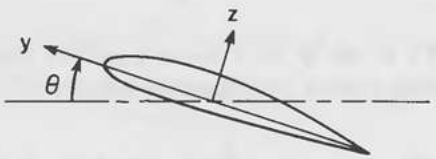

Figure 8.5. Blade section with torsional deflection.

Simple Flapping Response

The flapping equation is

$$\ddot{\beta} + \left[\Omega^2(1 + \epsilon) + G \cos \psi + \frac{K_\beta}{I_b}\right]\beta = 0 \tag{8.15}$$

From inspection of this equation, it can be seen that for no gravity, hinge-offset, or hinge-spring forces ($G = \epsilon = K_\beta = 0$), the blade oscillates at a natural frequency, Ω, to an impulsive input, with no dissipation. This is an important result, as will be seen later. Expressed in words, it means that the "natural flapping motion of the blade hinged at the hub is exactly equal to its speed of rotation."[2]

Adding first the hinge offset, ϵ, the new natural frequency is

$$\omega^2 + \Omega^2(1 + \epsilon) \tag{8.16}$$

When the natural frequency of the motion is increased, the new flapping oscillation will be out of phase with the blade azimuth, ψ. In hinged helicopter rotors, the hinge factor, ϵ, is on the order of 0.06, giving a flap frequency about 3 percent higher than shaft frequency (see Reference 8 in Chap. 7).

A cantilevered blade has higher flap frequency than a hinged blade by virtue of its root restraint, which is modeled here by a hinge spring. Adding hinge spring K_β greatly increases the natural flap frequency:

$$\omega^2 + \frac{K_\beta}{I_b} \tag{8.17}$$

This is precisely the relationship used in Chap. 7 to derive the hinge-equivalent blade. It represents the natural bending frequency of a simple beam with hinge stiffness K_β, and mass moment of inertia, I_b. In this, it models the first bending mode only of the more complex cantilevered blade that it represents.

Adding the hinge offset gives a complete equation for inertial flapping frequency that was also derived in Chap. 7:

$$\omega_\beta^2 = \Omega^2(1 + \epsilon) + \frac{K_\beta}{I_b} \tag{8.18}$$

Inertial Flapping Frequency

The problem of choosing flapping frequency reduces to this equation if the designer has a blade material that gives him the latitude of vary K_β and ϵ. Neglecting for the moment the other structural blade considerations (ultimate strength, fatigue, endurance, etc.), the dynamic response of the blade in flapping is largely determined by this equation. For example, by varying the root stiffness and offset, the flapping frequency can be located, for a given Ω, at any desired percentage of rotational speed. Thus, a blade can be designed, if necessary, to have a flapping frequency well separated from all other periodic inputs (inertial, gravitational, aerodynamic, and generator excitation). The gravity-excited system will be covered in Section 8.4.

Simple Lead-Lag Response

The lead-lag equation is

$$\ddot{\zeta} + \left[\epsilon_2\Omega^2 + G\cos\psi + \frac{K_\zeta}{I_b}\right] - 2\Omega\,\dot{\beta}\beta + G\sin\psi = 0 \qquad (8.19)$$

The last two terms give a "steady" baseline value of ζ caused by flapping velocity (Coriolis) and gravity. They will both be periodic, one at a frequency Ω and the other at the natural frequency of flapping motion, but usually both these terms are very small.

Looking, then, at the natural-frequency terms, the lead-lag frequency of a blade hinged in lead-lag, in the absence of gravity and hinge spring, is

$$\omega_\zeta^2 = \Omega^2\epsilon_2 \qquad (8.20)$$

The lead-lag frequency is much lower than the rotational frequency, typically 25-percent Ω. (Note that for zero hinge offset, the hinge/spring blade dynamic model derived here is not applicable since it is no longer an oscillator and the next in-plane cantilever mode must be included.) Including the lag spring restraint gives the inertial lead-lag frequency:

$$\omega_\zeta^2 = \Omega^2\epsilon_2 + \frac{K_\zeta}{I_b} \qquad (8.21)$$

Inertial Lead-Lag Frequency

The lead-lag spring increases lag frequency. The "softer" dependency of lag stiffness with increasing Ω is seen here. In the flapping case, "centrifugal stiffening" appears as $(1 + \epsilon)$, but, in the lag case, stiffening is greatly attenuated by geometry and appears as the much smaller amount, ϵ_2. The significance of the gravity effect is covered in Section 8.4.

Simple Feathering Response

For simplicity, the axis of feathering is assumed to be the c.g. axis of the blade given in this section. Feathering motion is usually more complex, as can be seen in Chap. 11. The feathering equation of motion is

$$\ddot{\theta} + \left[\Omega^2 + \frac{K_\theta}{I_f}\right]\theta = 0 \qquad (8.22)$$

In the absence of torsional stiffness at the hinge (i.e., $K_\theta = 0$), the blade oscillates at frequency Ω. This simply means that the feathering motion is exactly one cycle per revolution, which gives a feathering moment that must be resisted by the pitch mechanism. This feathering moment is called the "tennis racket moment" in the helicopter literature, and can be explained by looking at the centrifugal force couple on a blade section, as shown in Fig. 8.6.

When the blade is pitched through θ, the couple caused by centrifugal force tends to reduce pitch. As with flapping, the centrifugal force thus provides a spring with natural frequency exactly equal to Ω.

When the torsional spring, K_θ, is added, the natural frequency in feathering is greatly increased. For wind turbines, K_θ is usually very high, and I_f is on

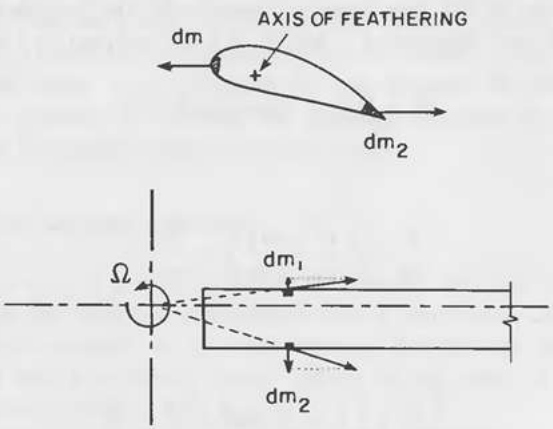

Figure 8.6. Blade feathering moment.

the order of only 1 percent of I_b so that the elastic frequency of torsional oscillation is usually orders of magnitude higher than either flapping or lead-lag motion. However, in the event of a loss of K_θ, which might occur as a failure in the pitch actuation or pitch link system, the equation would describe the dynamics of the blade motion, and the aerodynamic terms, including blade pitching moment, will become very significant.

8.4 GRAVITY AND YAW INDUCED EFFECTS

The gravity forces were included in the foregoing derivations. They are significant in the flapping equation of motion (see Eq. 8.5), as follows:

$$\ddot{\beta} + \Omega^2 \left[1 + \epsilon + \frac{K_\beta}{I_b \Omega^2} + \frac{G}{\Omega^2} \cos \psi \right] \beta = 0$$

Flapping Equation of Motion

and also in the lead-lag equation of motion (see Eq. 8.12), as follows:

$$\ddot{\zeta} + \left[\epsilon_2 \Omega^2 + G \cos \psi + \frac{K_\zeta}{I_b} \right] \zeta - 2\Omega \dot{\beta} \beta + G \sin \psi = 0$$

Lead-Lag Equation of Motion

Effects of Gravity

The gravity term in the flap equation complicates the response by adding a periodic coefficient. Neglecting ϵ and K_β for the moment, we have

$$\ddot{\beta} + [\Omega^2 + G \cos \psi] \beta = 0 \tag{8.23}$$

Substituting,

$$\frac{d}{dt} = \left(\frac{d}{d\psi} \right) \left(\frac{d\psi}{dt} \right) = \frac{d}{d\psi} \Omega$$

we have

$$\frac{d^2\beta}{d\psi^2} + \left[1 + \frac{G}{\Omega^2} \cos \psi \right] \beta = 0 \tag{8.24}$$

This is a linear differential equation, a form of the classical Mathieu's equation that describes a physical system with a periodic change of stiffness, which can lead to special stability problems.

For the blade lag equation,

$$\ddot{\zeta} + \left[\epsilon_2 \Omega^2 + \frac{K_\zeta}{I_b} G \cos \psi \right] \zeta = 0 \tag{8.25}$$

or,

$$\frac{d^2\zeta}{d\psi^2} + \left[\epsilon_2 + \frac{K_\zeta}{I_b \Omega^2} + \frac{G}{\Omega^2} \cos \psi \right] \zeta = 0 \tag{8.26}$$

Again, this is the special form of Mathieu's equation. A detailed discussion of pendular instability can be found in References 3 and 4.

These pendular instabilities cannot be considered true aeroelastic instabilities, which are discussed in Chap. 11. However, they still must be considered for wind turbines with actual lead-lag or flapping hinges and are examined in more practical detail in Chap. 9. Most wind turbine blades of interest are cantilevers, however, and they are usually reduced to the hinge-spring model for simplicity of analysis. Such blades do not experience pendular instabilities because the actual frequency ratios are very different from the ratios that would cause instability.

It should be noted here that lag instabilities in helicopter rotors are historically more numerous and destructive than flap instabilities. The reason is that aerodynamic damping in lag is on the order of only 2 to 5 percent of critical damping, whereas flap damping is usually 90 to 100 percent of critical. Physically, this is because lag damping originates with only the small changes of aerodynamic drag on a blade as the blade oscillates, whereas flap damping experiences the much larger lift changes on the blade. For a wind turbine that uses a lag hinge, it is important for the designer to identify the lag frequency and possibly to employ lag damping to avoid or attenuate the gravity-induced instabilities defined by Eq. 8.26.

Effects of Yaw Angular Velocity

The effect caused by a steady yaw angular velocity, q, about tower axis X' is considered in this section. Aerodynamic forces caused by yaw rate are also important and are derived in the next section. The present discussion will deal only with the (gyroscopic) inertial effects on the blade. The coordinate systems are shown again in Fig. 8.7.

The only forces or moments are caused by accelerations resulting from rotation. If the yaw rate, q, is constant, the translations of the blades will not contribute to the gyroscopic forces, only the rotation around tower axis

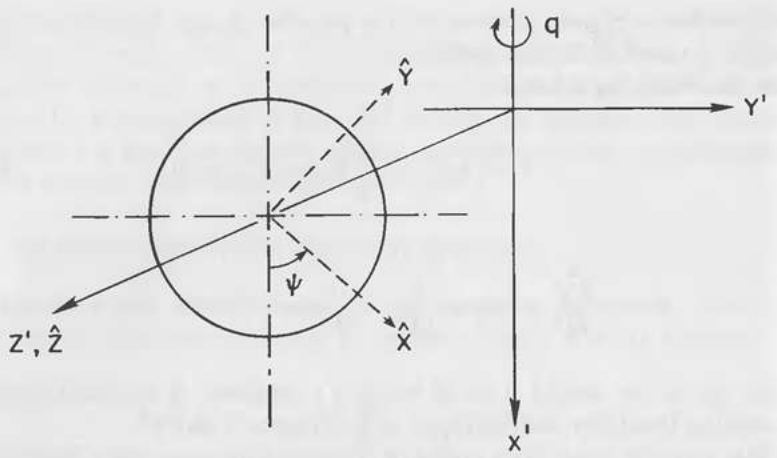

Figure 8.7. Yaw system. (NOTE: The xyz system is fixed to the blade and is inclined to the system by Euler angle $-\beta$, which is not shown.)

X'. However, the translational velocities will affect the relative wind and hence the angles of attack on the blade and will thus affect the aerodynamic forces. These effects will be shown later, but for the moment, the flapping angle will be ignored. The derivation follows the classical Euler theory as used by Halfman.[5] In the xyz (or $\hat{X}\hat{Y}\hat{Z}$) system,

$I_x = I_f$ = feathering mass moment of inertia
I_y = flapping mass moment of inertia
I_z = lead-lag mass moment of inertia

The angular velocity components of the blades are as follows:

$$\omega_x = \omega_{\hat{x}} = q \cos \psi$$

$$\omega_y = \omega_{\hat{y}} = -q \sin \psi \tag{8.27}$$

$$\omega_z = \omega_{\hat{z}} = \Omega$$

Euler's dynamical equations appear in the following form if there are no axes of symmetry of the body, and the primary (xyz) axis system therefore is fixed

to, and rotates with, the body:

$$M_{xe} = I_x \frac{d\omega_x}{dt} - [I_y - I_z]\omega_y\omega_z$$

$$M_{ye} = I_y \frac{d\omega_y}{dt} - [I_z - I_x]\omega_z\omega_x \tag{8.28}$$

$$M_{ze} = I_z \frac{d\omega_z}{dt} - [I_x - I_y]\omega_x\omega_y$$

where M_{xe}, M_{ye}, and M_{ze} are the external moments in the torsional, flapping (negative), and lead-lag directions, respectively. This gives the following:

$$M_{xe} = I_x \frac{d}{dt}[q \cos \psi] - [I_y - I_z][-q \sin \psi]\Omega$$

$$M_{ye} = I_y \frac{d}{dt}[-q \sin \psi] - [I_z - I_x][q \cos \psi]\Omega$$

$$M_{ze} = I_z \frac{d}{dt}[\Omega] - [I_x - I_y][q \cos \psi][-q \sin \psi]$$

or

$$M_{xe} = q\Omega \sin \psi[I_y - I_z - I_x]$$

$$M_{ye} = -q\Omega \cos \psi[I_y + I_z - I_x] \tag{8.29}$$

$$M_{ze} = q^2 \cos \psi \sin \psi[I_x - I_y]$$

These are the external (gyroscopic) moments on the blade caused by a constant yaw rate, q. They give rise to a vibratory input to the hub and tower. For the case of a single or a two-bladed turbine, the forcing frequency is twice the rotational speed, Ω. This is also the source of the "yawing roughness" often observed with high-speed, two-bladed rotors and with two-bladed aircraft propellers. A complete description of this is found in Section V-A of Stoddard.[3]

Equation 8.28 can be reduced to simpler form if approximations are made. The flapping and lead-lag mass moments of inertia are not strictly equal. They would be exactly so for an X-axis of symmetry but are usually close enough to be considered equal ($= I_b$). Also, the value of I_b is much greater

than that of I_f, the feathering moment of inertia. Thus,

$$\begin{aligned} I_x &\simeq I_f \\ I_y &\simeq I_b \\ I_z &\simeq I_b \end{aligned} \tag{8.30}$$

The moments can now be written as follows:

$$\begin{aligned} M_{xe} &= -M_\theta \simeq -q\Omega \sin\psi I_f \\ M_{ye} &= -M_\beta \simeq -2q\Omega \cos\psi I_b \\ M_{ze} &= M_\zeta \simeq -q^2 \cos\psi \sin\psi I_b \end{aligned} \tag{8.31}$$

The effect of flapping angle can now be added. By going back to the original angular velocity components (Eq. 8-27), a flapping deflection, β, can now be introduced, as follows:

$$\begin{aligned} \omega_x &= \omega_{\hat{x}} \cos\beta + \omega_{\hat{z}} \sin\beta = q \cos\psi \cos\beta + \Omega \sin\beta \\ \omega_y &= \omega_{\hat{y}} = -q \sin\psi \\ \omega_z &= \omega_{\hat{z}} \cos\beta - \omega_{\hat{x}} \sin\beta = \Omega \cos\beta - q \cos\psi \sin\beta \end{aligned} \tag{8.32}$$

Going back through the Euler analysis again, the final values for gyroscopic moments can be obtained. After taking the small-angle assumption on β and neglecting terms containing q^2 (see Ormiston[8]), we have

$$\begin{aligned} M_\theta &= I_f q\Omega \sin\psi \\ M_\beta &= 2I_b q\Omega \cos\psi \\ M_\zeta &= 0 \end{aligned} \tag{8.33}$$

The blade equations of motion thus affected are, first, the flapping equation of motion:

$$\ddot{\beta} + \Omega^2\left[1 + \epsilon + \frac{K_\beta}{I_b\Omega^2} + \frac{G}{\Omega^2}\cos\psi\right]\beta = -2q\Omega \cos\psi \tag{8.34}$$

Flapping Equation of Motion

and, second, the feathering equation of motion:

$$\ddot{\theta} + \Omega^2\left[1 + \frac{K_\theta}{I_f\Omega^2}\right]\theta = -q\Omega \sin\psi \tag{8.35}$$

Feathering Equation of Motion

The effect of yaw rate on the blade is thus to introduce a periodic moment proportional to the yaw rate, q, in both the flapping and the feathering degrees of freedom and with frequency Ω. Since no damping exists in these (non-aerodynamic) equations, dynamic instability would result when the natural frequency of motion is exactly Ω. Such would be the case in the flapping equation for a free hinge with no offset and no gravity and would also occur for a free hinge in feathering—a purely academic example. Theoretically, then, a rotating blade with no flapping hinge spring or offset would, in the absence of gravity and aerodynamic forces, be excited at its natural frequency in flapping with no chance of damping.

8.5 AERODYNAMIC FORCES AND MOMENTS

Derivation of Lift Function

To derive the aerodynamic forces, a classical blade-element theory approach is used. A blade element dr at radius r is isolated, and a vector diagram of the velocities perpendicular and tangential to the rotor plane is drawn as shown in Fig. 8.8. Here the effect of the hinge offset is neglected since it makes no difference in the aerodynamic force on the blade. The axis of rotation is the $\hat{z}$ axis, and the blade is inclined at flapping angle β. (See also Miller et al.,[4] Gessow and Myers,[6] and Reference 8 in Chap. 7.)

Looking at the blade element down the $\hat{x}$ axis, we have the vector relationships diagrammed in Fig. 8.9, where

U_p = velocity perpendicular to rotor plane ($\hat{z}$ direction)
U_T = velocity tangential to blade element ($-\hat{y}$ direction) and primarily due to rotation, Ωr
ϕ = blade element relative wind angle = $\tan^{-1}(U_p/U_T)$
θ = blade element feathering angle
θ_p = blade element pitch angle
α = blade element angle of attack
L = lift force on blade element per unit span

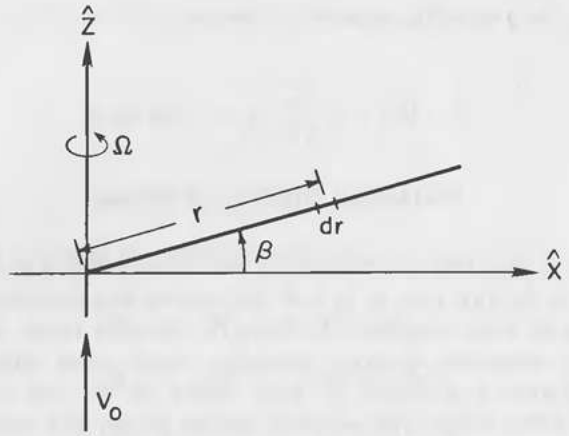

Figure 8.8. Blade element along blade.

The lift on the blade element is then

$$L = \tfrac{1}{2}\rho C_{l_\alpha} c V_R^2 \alpha \tag{8.36}$$

where

ρ = air density
C_{l_α} = slope of lift curve = $dc_l/d\alpha$
c = chord
V_R = resultant stream velocity = $\sqrt{U_T^2 + U_P^2}$
α = angle of attack

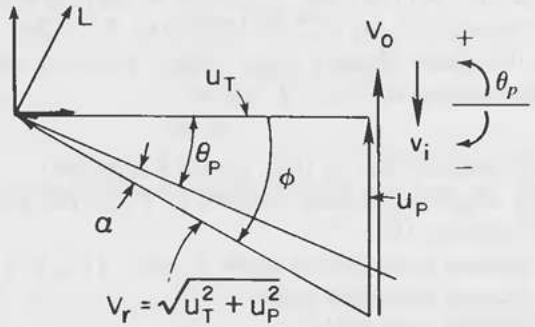

Figure 8.9. Blade element diagram. (NOTE: Increasing θ_p increases α as well as lift; this convention is exactly the same as that of the helicopter and propeller literature, which has θ_p increasing in the direction of increasing lift, or thrust.)

The drag, which would appear in the V_R direction, is neglected since it is small compared to lift. Since the significant aerodynamic perturbations will depend on changes in the angle of attack, α, V_R will also be allowed to remain constant. A further assumption is made, that the magnitude of V_R is roughly the same as that of U_T. The effect of these assumptions on the model is to decrease the sensitivity of the aerodynamic forces to magnitude changes in velocity and to increase the relative significance of angle-of-attack changes, which are retained. These assumptions are consistent with the development of helicopter preliminary design methods and the linear first-order goal of the dynamic solutions.[8]

If we assume that $U_P \ll U_T$, then $V_R^2 \simeq U_T^2$. Lift is

$$L = \tfrac{1}{2}\rho C_{l_\alpha} c V_R^2 \alpha$$

and

$$\alpha = \tan^{-1}(\phi - \theta) \simeq \phi - \theta = \frac{U_P}{U_T} - \theta$$

$$\theta \equiv -\theta_P$$

This gives the lift per unit length as

$$L = \tfrac{1}{2}\rho C_{l_\alpha} c [U_T^2 \theta_p + U_P U_T] \tag{8.37}$$

The velocities in the diagram of Fig. 8.9 can be written as follows:

$$U_T = \Omega r$$

$$U_P = [V_o - v_i]\cos\beta - r\dot{\beta}$$

where

V_o = constant free stream (axial wind) velocity
v_i = axial induced velocity (caused by lift on the blade)
$r\dot{\beta}$ = contribution of flapping velocity to U_P

Taking the nondimensional induced velocity, λ_i, as

$$\lambda_i = v_i/\Omega R$$

assumes that the momentum theory is used or that the induced velocity is constant for $0 \le r \le R$, or over the entire rotor disc. This induced velocity

is the effect of lift on the blade, but there are other velocities that are "induced" by dynamic perturbations and blade motions, i.e., wind shear. These perturbations are the source of dynamic forces and are retained to first order. Therefore, the uniform inflow restriction of momentum theory has negligible effect on the blade dynamic solutions. This gives

$$\begin{aligned} U_T &= \Omega r \\ U_P &= V_o[1 - \lambda_i] \cos \beta - r\dot{\beta} \end{aligned} \tag{8.38}$$

Effects of Crosswind and Yaw Rate on Function

If the wind has a component parallel to the rotor plane (crosswind), U_o, the component in the blade element velocity vector is shown in Fig. 8.10. The crosswind is along the Y' axis and perpendicular to the free stream, V_o, which is along the Z' axis. Also shown is the relative velocity at the blade element caused by flapping velocity $r\dot{\beta}$.

The delta in U_P caused by crosswind is $-U_o \sin \beta \sin \psi$. The velocity perpendicular to the blade is now

$$U_P = [V_o - v_i] \cos \beta - r\dot{\beta} - U_o \sin \beta \sin \psi$$

where ψ is the azimuth angle and $\psi = 0$ when vertical downward. Likewise, the tangential velocity can be represented as

$$\Delta U_T = -U_o \cos \psi$$

A yaw motion (q rad/sec) about the x' (tower) axis at the yaw moment arm,

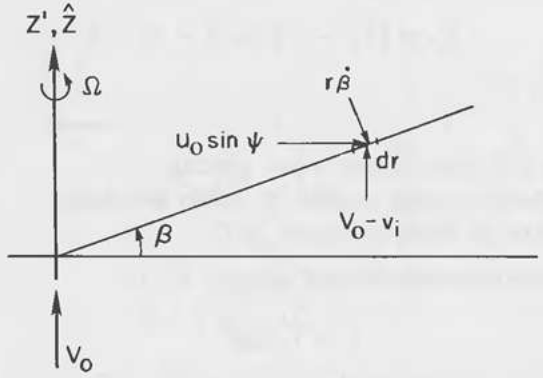

Figure 8.10. Crosswind deltas.

l, also produces harmonic velocity deltas at the blade element. These are more complex because there are effects caused by rotation, q, and translation, ql, as follows:

$$\begin{aligned} \Delta U_P &= -rq \sin \psi \cos \beta - ql \sin \psi \sin \beta \\ \Delta U_T &= -rq \cos \psi \sin \beta - ql \cos \psi \cos \beta \end{aligned} \tag{8.39}$$

Finally, the complete equations up to this point for U_P and U_T are the following:

$$\begin{aligned} U_P &= [V_o - v_i] \cos \beta - r\dot{\beta} - [U_o \sin \beta + q(l \sin \beta + r \cos \beta)] \sin \psi \\ U_T &= \Omega r - \cos \psi [U_o + q(r \sin \beta + l \cos \beta)] \end{aligned} \tag{8.40}$$

Assuming small β and retaining harmonic ψ, we have the following blade element velocities:

$$\begin{aligned} U_P &= [V_o - v_i] - r\dot{\beta} - [U_o\beta + q(l\beta + r)] \sin \psi \\ U_T &= \Omega r - [U_o + q(r\beta + l)] \cos \psi \end{aligned} \tag{8.41}$$

Blade Element Velocities

Effect of Wind Shear on Function

Wind shear is the variation, with height, of velocities U_o and V_o. Its effects are not considered important for small wind turbines, on the order of 10 meters diameter or less. Wind shear is very important for rotors larger than this, however, and for all rotors located at sites with extreme shear flow. A number of fatigue failures have been attributed to wind-shear-induced blade loads, and wind shear is now thought to be the primary cyclic moment for all teetering wind-turbine rotors.[7] For a more complete treatment of wind shear effects, see Ormiston.[8]

Assuming that U_o and V_o vary linearly with height across the rotor disc, we have

$$\begin{aligned} V_o &= V[1 - \eta K_1 \cos \beta \cos \psi] \\ U_o &= U[1 - \eta K_2 \cos \beta \cos \psi] \end{aligned} \tag{8.42}$$

where U and V are axial wind and crosswind at the rotor hub, and K_1 and K_2 are gradients of V_o and U_o across the rotor disc. To include wind shear in the aerodynamic force function, one must include the above expressions in the already derived expressions for U_P and U_T at the blade element and carry

through the analysis that follows in the text. The resulting deltas are for vertical shear, K_1, only:

$$\begin{aligned} \Delta U_P &= -\eta K_1 V_o \cos\beta \cos\psi \\ \Delta U_T &= (\text{none to first order}) = 0 \end{aligned} \tag{8.43}$$

where η is the nondimensional span station, r/R.

Blade Element Lift Function

According to Eq. 8.37, lift is given by

$$L = \tfrac{1}{2}\rho C_{l_\alpha} c[U_T^2\theta_p + U_P U_T]$$

The original assumption was that the in-plane velocity, U_T, could be used to approximate the local blade-element total velocity, V_R, at each station. This assumption allows us to retain azimuthal variation in angle of attack in both the U_P and U_T terms of the above expression. Hence,

$$\text{Angle of attack} = \alpha = \left[\frac{U_p}{U_T} - \theta\right] = \frac{1}{U_T^2}[U_T^2\theta_p + U_P U_T] \tag{8.44}$$

where $\theta \equiv -\theta_p$.

U_P and U_T consist of steady and harmonic perturbation values. These are given in Table 8.1, which summarizes the development of the last few sections.

The values of the blade-element velocities are given by the following:

$$\begin{aligned} U_P &= [(V_o - v_i) - \eta K_1 V_o \cos\psi]\cos\beta - r\dot{\beta} \\ &\quad - [U_o \sin\beta + q(l\sin\beta + r\cos\beta)]\sin\psi \\ U_T &= \Omega r - \cos\psi[U_o + q(r\sin\beta + l\cos\beta)] \end{aligned} \tag{8.45}$$

Table 8.1. Blade Element Velocity Disturbances.

Case	ΔU_P	ΔU_T
Axial flow	$[V_o - v_i]\cos\beta - r\dot{\beta}$	Ωr
Crosswind	$-U_o \sin\beta \sin\psi$	$-U_o \cos\psi$
Yaw rate	$-ql \sin\psi \sin\beta$	$-rq \cos\psi \sin\beta$
	$-rq \sin\psi \cos\beta$	$-ql \cos\psi \cos\beta$
Wind shear	$-\eta K_1 V_o \cos\beta \cos\psi$	(none to first order)

These are simplified by assuming that flapping angle β is small, and thus, $\cos\beta \simeq 1$ and $\sin\beta \simeq \beta$. We then have

$$\begin{aligned} U_P &= \lambda - r\dot{\beta} - [U_o\beta + q(l\beta + r)]\sin\psi - \eta K_1 V_o \cos\psi \\ U_T &= \Omega r - [U_o + q(r\beta + l)]\cos\psi \end{aligned}$$

Furthermore, the moment arms can be simplified by the approximations

$$\begin{aligned} l\beta + r &\simeq r \\ r\beta + l &\simeq l \end{aligned}$$

which give, in nondimensional form,

$$\begin{aligned} U_P &= \lambda - r\dot{\beta} - [\mathrm{U}_o\beta + \mathrm{qr}]\sin\psi - \eta K_1 V_o \cos\psi \\ U_T &= \Omega r - [U_o + ql]\cos\psi \end{aligned} \tag{8.46}$$

The nondimensional quantities are as follows:

λ = nondimensional inflow = $(1/\Omega R)(V_o - v_i)$
λ_i = nondimensional induced velocity = $v_i/\Omega R$
$\overline{U}_o$ = nondimensional crossflow = $U_o/\Omega R$
$\overline{V}_o$ = nondimensional free stream = $V_o/\Omega R$
$\overline{U}$ = nondimensional total crossflow = $(1/\Omega R)(U_o + ql)$
η = nondimensional span station = r/R
$\overline{q}$ = nondimensional yaw rate = q/Ω
γ = Lock number = $\rho C_{l_\alpha} cR^4/I_b$
β' = azimuthal derivative of flap angle = $(1/\Omega)\dot{\beta}$

The necessary values for the integrands in the next section are U_P^2, U_T^2, and U_P/U_T. These are found algebraically from Eq. 8.46. The resulting expressions can be further simplified by eliminating the higher order terms such as $\overline{U}_o^2$, etc.

Aerodynamic Forces and Moments

With the derived expression for lift (Eq. 8.37), the aerodynamic force in the axial (flapping) direction and the in-plane (lead-lag) direction can be found by integration. Likewise, the moments about these two hinges and the blade tension can be found.

The force component in the flapping ($\hat{z}$) direction is $L\cos\phi\cos\beta$. In the in-plane (lead-lag) direction, the force is $L\sin\phi$, which produces the shaft torque and in-plane moments at the hub.

Oscillatory components introduced in the velocities and angles of attack will result in oscillatory thrust, moments, and shaft torque. This derivation has suppressed higher order variations in the velocities in the interest of simplicity. For example, if all the higher order terms were included, the flapping moment equation would have 40 terms and the lead-lag moment equation, 60. The present approach is justifiable for practical frequency information and stability calculations but may be less suitable for detailed studies of the lift distribution and rotor performance.[9]

In parametric aerodynamic performance studies, as opposed to dynamic analysis, a more exact aerodynamic approach, one that simulates the actual velocities at each span station, should be used. Such methods are described in Part I of this text. The forces and moments derived from such a detailed computer program may also be used in these dynamic studies by employing the familiar quasi-steady force assumption.[10] However, the frequency information and overall dynamic behavior is retained by the present, more simplified, and more "physical" approach.

The aerodynamic hub shear in the flapping direction (vertical shear at the hinge) is given by the following:

$$S_\beta = \int_0^R L \cos\phi \cos\beta \, dr \simeq \int_0^1 LR \, d\eta$$

The aerodynamic hub shear in the lead-lag direction is

$$S_\zeta = \int_0^R \mathrm{L} \sin\phi \, dr \simeq \int_0^1 LR \left(\frac{U_P}{U_T}\right) d\eta$$

The flapping moment caused by aerodynamics is

$$M_\beta = \int_0^R L \cos\phi \cos\beta \, rdr \simeq \int_0^1 LR^2\eta \, d\eta$$

And the aerodynamic lead-lag moment is

$$M_\zeta = \int_0^R \mathrm{L} \sin\phi \, dr \simeq \int_0^R LR^2 \left(\frac{U_P}{U_T}\right) \eta \, d\eta$$

The lift integrands from the last section are

$$L = \tfrac{1}{2} \rho \, C_{l_\alpha} \, c[U_T^2 \, \theta_p + U_P U_T] \tag{8.47}$$

$$L \frac{U_P}{U_T} = \frac{1}{2} \rho \, C_{l_\alpha} \, c[U_P U_T \theta_p + U_P^2] \tag{8.48}$$

where

θ_p = pitch angle, usually evaluated at $r/R = 0.75$ for dynamic analysis, and measured positive downwind (i.e., direction away from feathering)

After substitution and manipulation, the final aerodynamic hinge forces and moments are as follows. The vertical hub shear caused by aerodynamics is

$$S_\beta = \frac{1}{2} \gamma I_b \frac{\Omega^2}{R} \left\{ \frac{\lambda}{2} + \frac{\theta_p}{3} - \frac{\beta'}{3} - \cos\psi \left[\bar{U} \left(\lambda - \frac{\beta'}{2} - \theta_p \right) + \frac{K_1 \bar{V}_o}{3} \right] - \sin\psi \left[\frac{\bar{U}_o \beta}{2} + \frac{\bar{q}}{3} \right] \right\} \tag{8.49}$$

Vertical Hub Shear

The aerodynamic flapping moment is

$$M_\beta = \frac{1}{2} \gamma I_b \Omega^2 \left\{ \frac{\lambda}{3} + \frac{\theta_p}{4} - \frac{\beta'}{4} - \cos\psi \left[\bar{U} \left(\frac{\lambda}{2} + \frac{\beta'}{3} + \frac{2\theta_p}{3} \right) + \frac{K_1 \bar{V}_o}{4} \right] - \sin\psi \left[\frac{\bar{U}_o \beta}{3} + \frac{\bar{q}}{4} \right] \right\} \tag{8.50}$$

Aerodynamic Flapping Moment

The inplane hub shear caused by aerodynamics is

$$S_\zeta = \frac{1}{2} \gamma I_b \frac{\Omega^2}{R} \left\{ \lambda \left[\lambda + \frac{\theta_p}{2} \right] - \beta' \left[\lambda + \frac{\theta_p}{3} \right] - \cos\psi \left[K_1 \bar{V}_o \left(\lambda + \frac{\theta_p}{3} \right) + \bar{U} \theta_p \lambda - \beta' \left(\frac{2}{3} K_1 \bar{V}_o + \frac{\bar{U}_\theta}{2} \right) \right] - \sin\psi \left[\bar{q} \left(\lambda + \frac{\theta_p}{3} \right) - \beta' \left(\frac{2}{3} \bar{q} \right) + \beta \bar{U}_o \left(2\lambda + \frac{\theta_p}{2} - \beta' \right) \right] \right\} \tag{8.51}$$

Inplane Hub Shear

The aerodynamic lead-lag moment is

$$M_\zeta = \frac{1}{2}\gamma I_B \Omega^2 \left\{ \lambda\left(\frac{\lambda}{2} + \frac{\theta_p}{3}\right) - \beta'\left(\frac{2}{3}\lambda + \frac{\theta_p}{4}\right) - \cos\psi\left[K_1\bar{V}_o\left(\frac{2}{3}\lambda + \frac{\theta_p}{4}\right) + \frac{\bar{U}\theta_p\lambda}{2} - \beta'\left(\frac{K_1\bar{V}_o}{2} + \frac{\theta_p\bar{U}}{3}\right)\right] - \sin\psi\left[\bar{q}\left(\frac{2}{3}\lambda + \frac{\theta_p}{4}\right) - \beta'\left(\frac{\bar{q}}{2}\right) + \beta\bar{U}_o\left(\lambda + \frac{\theta_p}{3} - \frac{2}{3}\beta'\right)\right]\right\} \quad (8.52)$$

Aerodynamic Lead-Lag Moment

REFERENCES

1. Miller, R. H. Wind energy conversion—Progress report to July 15, 1975, Appendix D: Notes on aeroelastic stability. NSF Grant AER 75-00826, Massachusetts Institute of Technology, Cambridge, MA, Aug. 1975.
2. Prouty, R. W. *Helicopter Aerodynamics*. Cicero, IL: *Rotor & Wing International*, PJS Publications Inc., 1984.
3. Stoddard, F. S. Structural dynamics, stability, and control of high aspect ratio wind turbines. NTIS Report RFP-3027/67925/3533/79-9, University of Massachusetts, Amherst, MA, 1979.
4. Miller, R. H.; Dugundji, J.; Chopra, I.; et al., Dynamics of horizontal axis wind turbines: Wind energy conversion. ASRL-TR-184-9, NTIS Report COO-4131-Ti (vol. 3), Massachusetts Institute of Technology, Cambridge, MA, Sept. 1978.
5. Halfman, R. L. *Dynamics: Particles, Rigid Bodies, and Systems*. Reading, MA: Addison-Wesley Publishing Company, Inc., 1962.
6. Gessow, A., and Myers, G. C., Jr. *Aerodynamics of the Helicopter*. New York: Frederick Ungar Publishing Company, 3rd printing, 1952.
7. Ham, N. D. Notes on the aerodynamics, dynamics, and aeroelasticity of wind turbines and rotorcraft. Course presented at UCLA, Sept. 1976.
8. Ormiston, R. A. Dynamic response of wind turbine rotor systems. Preprint S-993, American Helicopter Society 31st Annual Forum, Washington, D.C., May 1975.
9. Miller, R. H. Rotor blade harmonic airloading. Preprint 62-82, Institute of Aeronautical Sciences 30th Annual Meeting, New York, Jan. 1962.
10. Hoffman, J. A. Coupled dynamics analysis of wind energy systems. NASA CR-135152, Contract NAS 3-19767, NASA Lewis Research Center, Cleveland, OH, Feb. 1977.

9

BLADE MOTIONS

9.1 INTRODUCTION

In the last chapter, the isolated blade equations of motion in flapping, lead-lag, and feathering were developed. The *inertial* effects discussion did not include *aerodynamic* forces, which are complex. This chapter uses the aerodynamic forcing functions derived in Sec. 8.5 to complete the flapping and lead-lag equations and determine the blade motions. A similar, though less complete, derivation of blade motions for wind turbines can be found in Ref. 8 of Chap. 8.

In order to make use of varying flexibilities in rotors, designers must be able to predict the excursions caused by forcing functions. In the case of wind turbines, the maximum blade-tip deflections often determine the size of the supporting tower, the tilt-up of the bedplate, and the yaw arm to the rotor plane. There is a clear cost trade-off between increased yaw arm and blade stiffness to avoid blade-tower interaction. This chapter concentrates on the flapping motion of wind-turbine rotor blades.

9.2 FLAPPING AND LEAD-LAG EQUATIONS OF MOTION

The complete flapping and lead-lag equations of motion can be obtained from the inertial equations—Eqs. 8.12 and 8.34—by including the aerodynamic moments—Eqs. 8.50 and 8.52—in the summation. The flapping equation is then

$$\frac{\ddot{\beta}}{\Omega^2} + \left[1 + \epsilon + \frac{G}{\Omega^2}\cos\psi + \frac{K_\beta}{I_b\Omega^2}\right]\beta = \frac{M_{\beta_{\text{aero}}}}{I_b\Omega^2} - 2\bar{q}\cos\psi \quad (9.1)$$

and the lead-lag equation is

$$\frac{\ddot{\zeta}}{\Omega^2} + \left[\epsilon_2 + \frac{G}{\Omega^2}\cos\psi + \frac{K_\zeta}{I_b\Omega^2}\right]\zeta = \frac{M_{\zeta_{\text{aero}}}}{I_b\Omega^2} + \frac{2\dot{\beta}\beta}{\Omega} - \frac{G}{\Omega^2}\sin\psi \quad (9.2)$$

The aerodynamic hinge moments are given by Eqs. 8.50 and 8.52. It is convenient to change the coordinate system to the extent that the time coordinate is changed to the azimuthal coordinate, ψ. To do so is the same as changing from the time domain to the frequency domain, which allows straightforward visualization of the blade response in frequency and geometric terms and lends itself to a simple harmonic solution. It also simplifies the algebra and interpretation involved, as will be seen.

Using the Chain Rule, we have

$$\frac{d}{dt} = \left(\frac{d}{d\psi}\right)\left(\frac{d\psi}{dt}\right) = \Omega\left(\frac{d}{d\psi}\right)$$

or

$$\ddot{\beta} = \Omega^2\left(\frac{d^2\beta}{d\psi^2}\right) = \Omega^2\beta''$$

$$\dot{\beta} = \Omega\left(\frac{d\beta}{d\psi}\right) = \Omega\beta' \tag{9.3}$$

The flapping equation then becomes

$$\beta'' + \left[1 + \epsilon + \left(\frac{G}{\Omega^2}\right)\cos\psi + \left(\frac{K_\beta}{I_b\Omega^2}\right)\right]\beta = \left(\frac{M_{\beta_{\text{aero}}}}{I_b\Omega^2}\right) - 2\bar{q}\cos\psi$$

On collecting terms, the complete flapping equation of motion, including aerodynamic moments from Eq. 8.50, is given by Eq. 9.4.

$$\begin{aligned}
&\beta'' + \left[\frac{\gamma}{8}\left(1 - \frac{4}{3}\bar{U}_o\cos\psi\right)\right]\beta' \\
&\quad + \left[1 + \epsilon + \left(\frac{G}{\Omega^2}\right)\cos\psi + \left(\frac{\gamma\bar{U}_o}{6}\right)\sin\psi + \left(\frac{K_\beta}{I_b\Omega^2}\right)\right]\beta \\
&= -2\bar{q}\cos\psi + \frac{\gamma}{2}\left[\frac{\lambda}{3} + \frac{\theta_p}{4}\right] - \frac{\gamma}{8}\bar{q}\sin\psi \\
&\quad - \cos\psi\left[\frac{\gamma}{2}\left(\bar{U}_o\left[\frac{\lambda}{2} + \frac{2\theta_p}{3}\right] + \frac{K_1\bar{V}_o}{4}\right)\right]
\end{aligned} \tag{9.4}$$

Flapping Equation of Motion

Likewise, the lead-lag equation is

$$\zeta'' + \left[\epsilon_2 + \left(\frac{G}{\Omega^2}\right)\cos\psi + \left(\frac{K_\zeta}{I_b\Omega^2}\right)\right]\zeta = 2\beta\beta' - \left(\frac{G}{\Omega^2}\right)\sin\psi + \frac{M_{\zeta_{\text{aero}}}}{I_b\Omega^2}$$

In collecting terms, the complete lead-lag equation of motion including aerodynamic forces is

$$\begin{aligned}
&\zeta'' + \left[\epsilon_2 + \left(\frac{G}{\Omega^2}\right)\cos\psi + \left(\frac{K_\zeta}{I_b\Omega^2}\right)\right]\zeta - \beta'\left[2\beta - \gamma\left(\frac{\lambda}{3} + \frac{\theta_p}{8}\right)\right. \\
&\quad \left. + \frac{\gamma}{2}\left(\frac{K_1\bar{V}_o}{2} + \frac{\theta_p\bar{U}_o}{2}\right)\cos\psi + \frac{\gamma}{2}\left(\frac{\bar{q}}{2} + \frac{2}{3}\beta\bar{U}_o\right)\sin\psi\right] \\
&= \frac{G\sin\psi}{\Omega^2} + \frac{\gamma}{2}\left[\lambda\left(\frac{\lambda}{2} + \frac{\theta_p}{3}\right)\right] - \frac{\gamma}{2}\sin\psi\left[\bar{q}\left(\frac{2}{3}\lambda + \frac{\theta_p}{4}\right)\right. \\
&\quad \left. + \beta\bar{U}_o\left(\lambda + \frac{\theta_p}{3}\right)\right] - \frac{\gamma}{2}\cos\psi\left[\bar{U}\theta_p\frac{\lambda}{2} + K_1\bar{V}_o\left(\frac{2}{3}\lambda + \frac{\theta_p}{4}\right)\right]
\end{aligned} \tag{9.5}$$

Lead-Lag Equation of Motion

9.3 HARMONIC SERIES SOLUTION

It has been straightforward to express the differential equations in the angular domain ψ. Following the accepted practice in developing the dynamics equations in the helicopter industry, a Fourier series solution is assumed for β, ζ, and θ, as follows:

$$\beta = \beta_o + \beta_{1c}\cos\psi + \beta_{1s}\sin\psi + \beta_{2c}\cos 2\psi + \beta_{2s}\sin 2\psi + \ldots \tag{9.6}$$

In this derivation, the blade flexibilities have been reduced to single fundamental mode vibration; only the first bending mode, in flapping and in lead-lag, has been used in the dynamic model. (See Fig. 9.1.) Furthermore, the solution of the differential equations, in keeping with the attempt to include only first-order effects, is restricted to the first three terms of the Fourier series. This turns out to be a very good assumption in the preliminary design of helicopters, where the combined higher order terms, or higher harmonics, usually account for 10 percent or less of the fundamental harmonics (see Reference 7 in Chap. 8).

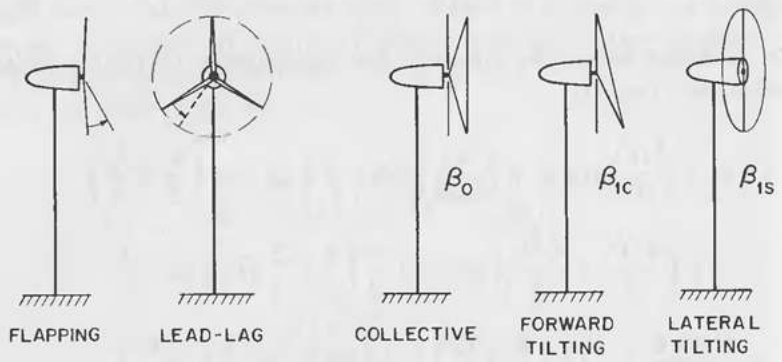

Figure 9.1. First-order blade motion.

According to this three-term Fourier model, a blade oscillating in flapping will always trace a circular tip path. This locus of points defines the tip-path plane. The terms in the Fourier series representation of β then take on a physical meaning: The first term is the constant coning angle resulting from axisymmetric equilibrium, and the next two terms represent the tilting of this tip-path plane vertically forward and yawing to the left (β_{1c} and β_{1s}, respectively).

The next higher order terms would represent the higher modes of vibration of the blades. In the case of a rigid blade hinged (articulated) at the rotor axis, the first three terms completely and uniquely describe the motion of the blade. In the case of cantilevered blades, they represent the most significant motions of the blade and constitute a good engineering approximation.[1] Hence the Fourier series can be truncated to three terms:

$$\begin{aligned} \beta &= \beta_o + \beta_{1c} \cos\psi + \beta_{1s} \sin\psi \\ \beta' &= -\beta_{1c} \sin\psi + \beta_{1s} \cos\psi \\ \beta'' &= -\beta_{1c} \cos\psi - \beta_{1s} \sin\psi \end{aligned} \tag{9.7}$$

The solution is found by substituting the above expressions into the equation of motion. The resulting equation will contain a system of three linear equations, obtained simply by equating the harmonic coefficients to zero. Thus

we have

$$f_1[\beta_o, \beta_{1c}, \beta_{1s}] \cos\psi + f_2[\beta_o, \beta_{1c}, \beta_{1s}] \sin\psi + f_3[\beta_o, \beta_{1c}, \beta_{1s}] = 0$$

Therefore

$$\begin{aligned} f_1[\beta_o, \beta_{1c}, \beta_{1s}] &= 0 \\ f_2[\beta_o, \beta_{1c}, \beta_{1s}] &= 0 \\ f_3[\beta_o, \beta_{1c}, \beta_{1s}] &= 0 \end{aligned}$$

and the Fourier coefficients can be found from the resulting system of linear equations:

$$[A_{ij}] \begin{Bmatrix} \beta_o \\ \beta_{1c} \\ \beta_{1s} \end{Bmatrix} = [B_{ij}] \tag{9.8}$$

9.4 FLAPPING BEHAVIOR

Flapping Dynamics

The flapping equation can be rewritten from Eq. 9.4 in more simplified, nondimensional form:

$$\begin{aligned} \beta'' + \frac{\gamma}{8}\left[1 - \frac{4}{3}\cos\psi\,(\bar{U}_o + \bar{q}\bar{l})\right]\beta' \\ + \left[K + 2B\cos\psi + \frac{\gamma}{6}\bar{U}_o \sin\psi\right]\beta \\ = \frac{\gamma}{2}\left[A - \frac{\bar{q}}{4}\sin\psi\right] - 2\bar{q}\cos\psi \\ - \frac{\gamma}{2}\left[(\bar{U}_o + \bar{q}\bar{l})\left(\frac{\lambda}{2} + \frac{2\theta}{3}\right) + \left(\frac{K_1 \bar{V}_o}{4}\right)\right]\cos\psi \end{aligned} \tag{9.9}$$

where

K = nondimensional flapping frequency $= [1 + \epsilon + (K_\beta / I_b \Omega^2)]$
$= (\omega_\beta / \Omega)^2$

A = aerodynamic term $= \dfrac{\lambda}{3} + \dfrac{\theta_p}{4}$

B = gravity term $= G/2\Omega^2$

This equation describes a damped oscillator (left-hand side) with a steady and periodic forcing function (right-hand side). Comparing it to the inertial results in Eq. 8.5, it can be seen that aerodynamic terms produce all the flap damping and additionally modify the natural frequency.

For a second-order equation like this one, the flapping damping ratio is simply one-half times the coefficient of the first derivative (β' term) divided by the natural frequency (ω_o/Ω in nondimensional terms), as follows:

$$\frac{\gamma}{16}\left(\frac{1}{\omega_o/\Omega}\right) \tag{9.10}$$

Flapping Damping Ratio

Here the damping ratio is always positive if the perturbations of crosswind and yaw rate are zero.

Flexible rotors and hinged rotors have natural flapping frequencies, ω_β, close to Ω; stiffer rotors can have frequencies a factor of two or three higher. Thus, the damping will range from $\gamma/16$ for a fully articulated to about $\gamma/48$ for a very stiff blade. Typical values of γ are 5 to 10, giving a range of damping of 0.5 to 0.16. These are reasonably high values, indicating that aerodynamics alone provides a large amount of flap damping. Hence, it is not necessary for the designer to add damping to the flapping degree of freedom mechanically unless a coupling effect, such as flutter, is involved (see Chap. 11).

It is interesting to note the right-hand side of the equation. The steady term,

$$\frac{\gamma}{2}\left[\frac{1}{3}\left(\frac{\bar{V}_o}{\Omega R}-\frac{v_i}{\Omega R}\right)+\frac{\theta}{4}\right]$$

gives rise to the steady-state coning angle caused by (axisymmetric) aerodynamic thrust. As shown in detail in the next section, the magnitude of the coning can be obtained simply by dividing the above term by the actual ω^2 obtained from the left-hand side of the equation.

The other terms on the right-hand side are

$$-\bar{q}\left[\frac{\gamma}{8}\sin\psi+2\cos\psi\right]-\frac{\gamma}{4}\left[(\bar{U}_o+\bar{q}l)\left(\lambda+\frac{4}{3}\theta_p\right)+\frac{1}{2}K_1\bar{V}_o\right]\cos\psi$$

The Lock number, γ, is a nondimensional parameter that is simply the ratio of aerodynamic to inertial force on the blade (see Ref 6 in Chap. 8), as follows:

$$\gamma=\frac{\rho C_{l_\alpha} cR^4}{I_b}$$

If aerodynamics are set to zero, γ is also. Therefore, the terms above that contain the Lock number are *aerodynamic terms*. The fact that the other terms missing γ do not disappear when $\gamma = 0$ indicates that they are *inertial terms*. It is easily seen that the only nonaerodynamic term is $2\bar{q}\cos\psi$; this is the *gyroscopic moment*. It is also seen that aerodynamic effects will appear in these right-hand terms only if disturbances are present. If yaw rate, crosswind, and wind shear—q, u_o, and K_1—are set to zero, the inertial effects, plus the steady aerodynamics, determine the motion of the blade.

By referring to Eq. 9.9, these disturbances can be seen as harmonic inputs to the blade flapping system. This is what is meant by a "cosine" or "sine" disturbance. Wind shear is a vertical gradient in V_o, which naturally causes a cosine disturbance relative to the blade azimuth position. This is reflected in the equation by the K_1 term. Crosswind was defined by Fig. 7.6; it is also seen on the blade as a cosine disturbance. This effect is diminished by an interesting term that includes the three blade-element section angles, V_o, v_i, and θ_p. This term, $\lambda + \frac{4}{3}\theta_p$, is a measure of the blade-section angle of attack and appears throughout the equations of motion in both flapping and lead-lag, with slight differences in the θ_p content, which are a result of approximations in the aerodynamic analysis.

The yaw rate, q, has both a sine and cosine character that is readily explained by reviewing the dual nature of this rate: One effect is a simple rotation of the rotor, which causes a sin ψ variation, and the other effect is a simple translation of the rotor caused by the hub offset, l. The latter brings about a cosine variation through angle of attack, as does crosswind. The cosine-input perturbations that are modified by angle of attack are called "advancing-retreating" blade effects in the helicopter industry. This is a useful physical picture, and can be easily thought of as the blade "advancing" into the relative wind at the top of its arc ($\psi = 180°$) and "retreating" from the relative wind at the bottom ($\psi = 0°$). See Fig. 9.2.

Flapping Motion

Now the actual motion solution for flapping dynamics can be calculated. Using, as before, the first three terms of a harmonic series, substitution is made in the flapping equation, Eq. 9.9. Equating coefficients to zero and recalling the trigonometric identities, we have

$$\sin^2 x = \tfrac{1}{2} - \tfrac{1}{2}\cos 2x$$

$$\cos^2 x = \tfrac{1}{2} + \tfrac{1}{2}\cos 2x$$

$$\sin x \cos x = \tfrac{1}{2}\sin 2x$$

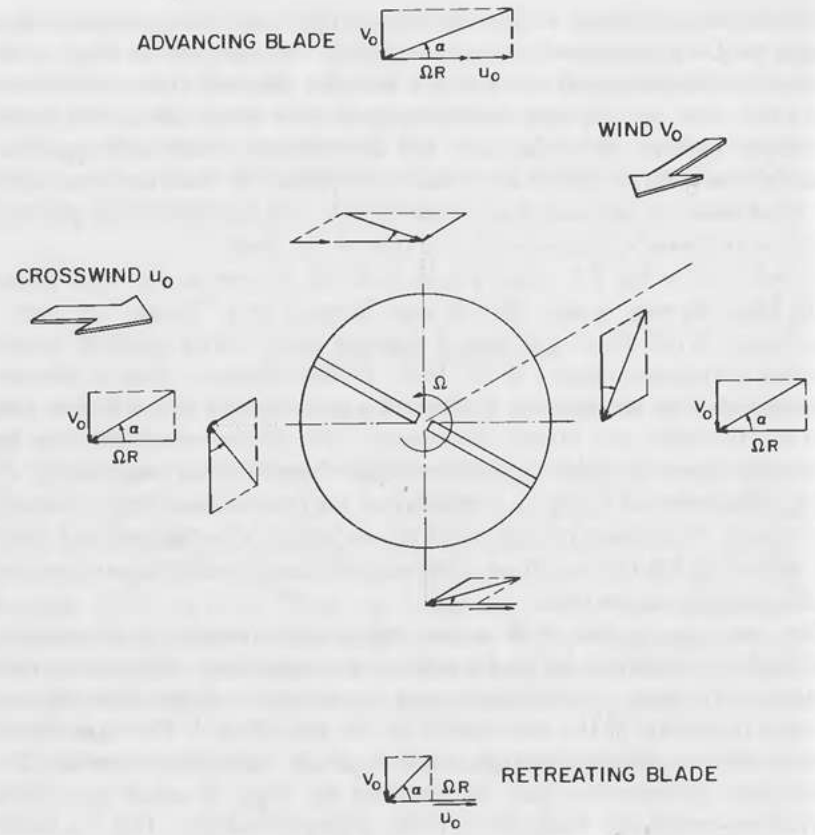

Figure 9.2. Cosine perturbation input.

We get

$$K\beta_o + B\beta_{1c} - \frac{\gamma}{12}\bar{q}\bar{l}\beta_{1s} = \frac{\gamma}{2}A$$

$$\beta_{1c}(K-1) + 2B\beta_o + \frac{\gamma}{8}\beta_{1s} = -2\bar{q} - \frac{\gamma}{2}\left[(\bar{U}_o + \bar{q}\bar{l})\left(\frac{\lambda}{2} + \frac{2\theta_p}{3}\right) + \left(\frac{K_1\bar{V}_o}{4}\right)\right]$$

$$\beta_{1s}(K-1) + \frac{\gamma}{6}\bar{U}_o\beta_o - \frac{\gamma}{8}\beta_{1c} = -\frac{\gamma}{8}\bar{q}$$

or the flapping matrix,

$$\begin{bmatrix} K & B & -\frac{\gamma}{12}\bar{q}\bar{l} \\ 2B & (K-1) & \frac{\gamma}{8} \\ \frac{\gamma}{6}\bar{U}_o & -\frac{\gamma}{8} & (K-1) \end{bmatrix} \begin{Bmatrix} \beta_o \\ \beta_{1c} \\ \beta_{1s} \end{Bmatrix} = \begin{Bmatrix} \frac{\gamma}{2}A \\ -2\bar{q} - \frac{\gamma}{2}\left[(\bar{U}_o + \bar{q}\bar{l})A_3 + \left(\frac{K_1\bar{V}_o}{4}\right)\right] \\ -\frac{\gamma}{8}\bar{q} \end{Bmatrix} \tag{9.11}$$

where

K = "inertial" natural frequency = $[1 + \epsilon + (K_\beta/I_b\Omega^2)] = (\omega_\beta/\Omega)^2$
A = axisymmetric flow term = $\lambda/3 + \theta_p/4$
B = gravity term = $G/2\Omega^2$
γ = Lock number = $\rho C_{l_\alpha} cR^4/I_b$
A_3 = axisymmetric flow term = $\lambda/2 + 2\theta_p/3$
$\bar{U}_o$ = nondimensional crossflow = $U_o/\Omega R$
$\bar{q}$ = nondimensional yaw rate = q/Ω
$\bar{l}$ = nondimensional yaw moment arm = l/R
K_1 = vertical wind shear gradient
$\bar{V}_o$ = nondimensional free stream = $V_o/\Omega R$

Since the blade has been assumed to be uniform for dynamic similitude, the gravity term can be simplified, using the hinge offset, e:

$$G = \frac{gM_b x_g R}{I_b} = \left(\frac{\epsilon}{e}\right)\frac{g}{R} = \frac{3g}{2R(1-e)} \tag{9.12}$$

A good approach to the solution of Eq. 9.11 is to assume a "design range" of values of the variables under consideration and plug in and solve the matrix for each value of q, u_o, and K_1 of interest (see Ref. 7 in Chap. 8 as well as Ref. 4 here). By computer, this process can be mechanized to give plots of flapping coefficients (β_o, β_{1c}, β_{1s}) versus abscissas of yaw rate, crosswind, etc., for every combination of blade values of interest (I_b, e, C_{l_α}, l, etc.). In preliminary design, it is much more valuable to investigate the general stability—the "physical" characteristics—of Eq. 9.11 first and then solve for the detailed behavior of the narrow variable ranges that come out. It remains a common practice in industry to evaluate stability by blindly reducing systems like that in Eq. 9.11 to the parametric graph form. It is often more rewarding

and interesting to use the present, more physical approach for which analytical complication has been simplified and approximations specifically made. Should the parametric simulation approach be taken instead, the equations could (and should) be more complicated and exact and would include more terms in the assumed harmonic series.[2,7] In the following sections, Eq. 9.11 will be examined for the effects of each input separately.

For the simplest case, where gravity, crosswind, and yaw rate are zero, and with no hinge offset or hinge spring (i.e., articulated at the root with simple axisymmetric flow), the values G, $\bar{U}_o$, $\bar{q}$, ϵ, and K_β are arbitrarily set to zero, and the matrix is consequently

$$\begin{bmatrix} 1 & 0 & 0 \\ 0 & 0 & \frac{\gamma}{8} \\ 0 & -\frac{\gamma}{8} & 0 \end{bmatrix} \begin{Bmatrix} \beta_o \\ \beta_{1c} \\ \beta_{1s} \end{Bmatrix} = \begin{Bmatrix} \frac{\gamma}{2} A \\ 0 \\ 0 \end{Bmatrix} \tag{9.13}$$

which gives the simple axisymmetric flow solution,

$$\begin{aligned} \beta_o &= \frac{\gamma}{2} A \\ \beta_{1c} &= \beta_{1s} = 0 \end{aligned} \tag{9.14}$$

In this case, β_o is the aerodynamic coning and represents the simple equilibrium between aerodynamic thrust and centrifugal force, since there is no root hinge spring.

Adding hinge spring and offset, the solution becomes

$$\begin{aligned} \beta_o &= \left(\frac{1}{K}\right) \frac{\gamma}{2} A \\ \beta_{1c} &= \beta_{1s} = 0 \end{aligned} \tag{9.15}$$

where

$$K = \left[1 + \epsilon + (K_\beta / I_b \Omega^2)\right] = \left(\frac{\omega_\beta}{\Omega}\right)^2 = p^2$$

and the determinant of the coefficients in Eq. 9.11 is

$$\Delta = K\left[(K-1)2 + \left(\frac{\gamma}{8}\right)^2\right]$$

As one would expect, the coning angle is modified by the blade root stiffness, or the ratio of "inertial" natural frequency in flapping (ω_β) to rotational speed (Ω). In the helicopter literature, the K term, called the "natural frequency," is defined as p^2 (see Ref. 8 in Chap. 8).

There is another physical meaning of the coning term, β_o. It represents the balance between the steady root moments, which are (1) lift, (2) centrifugal force, and (3) hinge spring, as follows:

$$\beta_o = \frac{\gamma A}{2K} = \frac{\textit{Flapping moments}}{\textit{Restoring moments}} = \frac{\textit{Aerodynamic moments}}{\textit{Centrifugal + Hinge spring moments}}$$

Substituting for the Lock number, we have

$$\beta_o = \left[\frac{\rho C_{l_\alpha} c R^4}{I_b}\right] \frac{A}{2K}$$

which can be reduced to

$$\beta_o = \left[\frac{\frac{1}{2}\rho C_{l_\alpha} c (\Omega R)^2 R^2}{I_b \Omega^2}\right] \frac{A}{K}$$

In this expression, the bracketed term is the "amplifier," and the other term is the "gain." The top line is the aerodynamic amplifier, and the bottom, the inertial plus elastic. It is very easily checked that A is the angle of attack, which modifies the lift equation, and that K is the hinge spring. For a hinged blade, $K = 1$, and the centrifugal moment, or $I_b\Omega^2$, is the only restoring moment. Hence these terms, A, K, and γ, have strong physical significance.

Recall that the A term is defined as follows:

$$A = \frac{\lambda}{3} + \frac{\theta_p}{4} = \frac{1}{3}\left[\frac{V_o}{\Omega R} - \frac{v_i}{\Omega R}\right] + \frac{\theta_p}{4}$$

As pitch angle θ_p is increased, blade flapping β_o increases. The first term, λ, is really the nondimensional mean flow through the rotor, and this term decreases with increasing tip-speed ratio, $\Omega R / V_o$. This indicates that high tip-speed ratio rotors are relatively more sensitive to pitch-angle changes. To a

large extent, the A term establishes the baseline operating point of the rotor around which the dynamic motions occur. As discussed in Part I of this text, the rotor induced velocity, v_i, thrust coefficient, C_T, and power coefficient, C_P, define the steady-state aerodynamic operating point of the rotor. The dynamic response is simply a linear combination of the perturbations around this operating condition.

The A term seen here is not as accurate as an aerodynamic strip theory in defining the baseline axisymmetric flow. The modeling of the aerodynamics in Chap. 8 was done by algebraic integration of the blade airfoil section values along the blade, assuming simple steady-state, 2-D aerodynamics, and using the small-angle assumption on angle of attack. Also, the induced velocity, v_i, was assumed constant over the rotor disc. The use of these assumptions has been well proven in preliminary analysis for helicopters but is not yet well proven for wind turbines, which are more susceptible to stall and unsteady aerodynamics effects.

Therefore, the induced velocity, thrust, and power coefficients can be calculated from a strip theory first and the induced velocity then used in the above expression to define the baseline steady-state rotor condition better (see Section 10.4). Another factor to keep in mind when evaluating the A term is that stall is not modeled. Use of the Lock number, γ, presupposes that the blade is always lifting in its unstalled range according to its C_{l_α}. This suggests also using various values of γ calculated in the stall and prestall regions by a strip theory to calculate the blade dynamics.[6]

Effect of Gravity on Flapping

Adding next the gravity terms, the equations become

$$\begin{bmatrix} K & B & 0 \\ 2B & (K-1) & \frac{\gamma}{8} \\ 0 & -\frac{\gamma}{8} & (K-1) \end{bmatrix} \begin{Bmatrix} \beta_o \\ \beta_{1c} \\ \beta_{1s} \end{Bmatrix} = \begin{Bmatrix} \frac{\gamma}{2}A \\ 0 \\ 0 \end{Bmatrix} \tag{9.16}$$

The determinant of the coefficients, called Δ, is defined as follows:

$$\Delta = |\text{coefficients}| = K\left[(K-1)^2 + \left(\frac{\gamma}{8}\right)^2\right] - 2B^2(K-1) \tag{9.17}$$

We then have

$$\beta_o = \frac{1}{\Delta}\begin{vmatrix} \frac{\gamma}{2}A & B & 0 \\ 0 & (K-1) & \frac{\gamma}{8} \\ 0 & -\frac{\gamma}{8} & (K-1) \end{vmatrix} = \frac{1}{\Delta}\left[\frac{\gamma}{2}A(K-1)^2 + \left(\frac{\gamma}{8}\right)^2\right]$$

$$\beta_{1c} = \frac{1}{\Delta}\begin{vmatrix} K & \frac{\gamma}{2}A & 0 \\ 2B & 0 & \frac{\gamma}{8} \\ 0 & 0 & 0 \end{vmatrix} = -\frac{1}{\Delta}\left[\gamma B(K-1)A\right]$$

$$\beta_{1s} = \frac{1}{\Delta}\begin{vmatrix} K & B & \frac{\gamma}{2}A \\ 2B & (K-1) & 0 \\ 0 & -\frac{\gamma}{8} & 0 \end{vmatrix} = -\frac{1}{\Delta}\left[\left(\frac{\gamma}{2}\right)^2\frac{B}{2}a\right]$$

The final solution is

$$\beta_o = \frac{\gamma}{2}A\left\{\frac{\left[(K-1)^2 + \left(\frac{\gamma}{8}\right)^2\right]}{K\left[(K-1)^2 + \left(\frac{\gamma}{8}\right)^2\right] - 2B^2(K-1)}\right\}$$

$$\beta_{1c} = -\left\{\frac{\gamma B(K-1)A}{K\left[(K-1)^2 + \left(\frac{\gamma}{8}\right)^2\right] - 2B^2(K-1)}\right\} \tag{9.18}$$

$$\beta_{1s} = -\left\{\frac{\left(\frac{\gamma^2}{8}\right)BA}{K\left[(K-1)^2 + \left(\frac{\gamma}{8}\right)^2\right] - 2B^2(K-1)}\right\}$$

Flapping Due to Gravity and Axisymmetric Flow

As a first check, with $B = 0$ (gravity = 0), these equations reduce to the simple coning result in Eq. 9.14. Gravity first causes a small increase in β_o by decreasing the denominator, hence slightly modifying the restoring moment. It will be seen later that this is a negligible effect. It also gives rise to a tilting of the rotor disc, both vertically backward (β_{1c}) and yawing to the right (β_{1s}).

The tilting and yawing are related by the following cyclic sharing term:

$$\beta_{1s} = \frac{\gamma}{8(K-1)}\beta_{1c} \tag{9.19}$$

Cyclic Sharing Term

This important result expresses the effect of hinge spring on the proportion of tilt between β_{1c} and β_{1s}. That is, for a very stiff cantilever, $(K - 1)$ is on the order of 10, giving $\beta_{1s} \simeq 10\%\ \beta_{1c}$. In this case, the rotor will experience mostly vertical tilting and very little yawing. If the blade is soft in flapping, $(K - 1)$ is on the order of 0.5 (or even lower for an articulated blade), giving $\beta_{1s} = 200\%\ \beta_{1c}$. This would yield mostly yawing and much less vertical tilt.

Another way to look at this "cyclic sharing" term is to examine the phase lag between input and response, a subject also discussed in Chap. 12 (see Sec. 12.5). To see this, the cyclic components must first be written in terms of the collective component, β_o:

$$\beta_o = \frac{\gamma A}{2\Delta}\left[(K-1)^2 + \left(\frac{\gamma}{8}\right)^2\right]$$

$$= \frac{\gamma A}{2\Delta}[P]$$

and

$$\beta_{1c} = -\frac{1}{\Delta}[\gamma B(K-1)A]$$

$$\beta_{1s} = -\frac{1}{\Delta}\left[\left(\frac{\gamma^2}{8}\right)BA\right]$$

Then β_{1c} and β_{1s} can be algebraically expressed as functions of β_0, as follows:

$$\beta_{1c} = -\left[\frac{2B(K-1)}{P}\right]\beta_o$$
$$\beta_{1s} = \left[-\frac{\gamma B}{4P}\right]\beta_o \tag{9.20}$$

When the ratio of β_{1s} to β_{1c} is taken as before, the same ratio results:

$$\frac{\beta_{1s}}{\beta_{1c}} = \frac{\gamma}{8(K-1)} \tag{9.21}$$

The values in Eq. 9.20 express analytically the effect of gravity on flapping. If coning angle, β_o, is zero, there is no effect, since there is no moment arm in the flapping direction. Therefore, the gravity input is maximum when the blade is vertical, or at $\psi = 0°$ and 180°. This is called a "cosine input" since the disturbance to the blade is a maximum at these positions. If the phase lag of the blade response to this input were zero, the blade would show only cosine cyclic, or β_{1c}. The preceding solution shows the blade response to be "shared" in both sine and cosine components. The familiar rule from helicopter dynamics is expressed as follows:

1. The flap response of an articulated blade lags the input by 90°.
2. The flap response of a stiff blade lags the input by less than 90° and decreases with increasing stiffness.

The truth of the rule is shown by the cyclic sharing term. The stiff blade has mostly cosine response; the soft blade, mostly sine response. A freely hinged blade would have all sine response.

This important result can also be seen directly from the solution equations (Eq. 9.18). For an articulated, or hinged, blade, $K = 1$; thus, $(K - 1)$ is zero, and the entire cyclic response is in the sine term β_{1s}, which is nonzero. This would be the case for a freely hinged blade, whose natural frequency response to any disturbance is exactly equal to its speed of rotation. Thus, the lag is 90°, as before. This describes an important "detective" tool in studying the analytical dynamics of the rotors: To discover the source of a disturbance, set $K = 1$ and examine which response is left; then look 90° earlier in the cycle. The same dynamic rule applies to the other inputs, whether sine or cosine inputs.

Another effect is the Lock number term, $\gamma/8$. If the blade has low mass

and a high design C_{l_α}, it has a high γ (10 to 15 for high-performance fiberglass). If the blade has high mass and low radius, it has a low γ (4.5 for original Jacob's blade[3]). A high γ blade will have a tendency to yaw in response to gravity excitation, whereas a low γ blade will tilt vertically in response to gravity, thus causing tower vibration through the yaw bearing. The major effect of high γ, however, is to provide flap damping, as shown in the section on flapping dynamics.

The flapping equations show the pendular instability of Mathieu's equation (see Sec. 8.3) in the denominator. The blade is unstable in flapping; that is, β_o increases without limit for

$$K\left[(K-1)^2 - \left(\frac{\gamma}{8}\right)^2\right] - 2B^2(K-1) = 0$$

or

$$K^3 - 2K^2 + K\left[1 - \left(\frac{\gamma}{8}\right)^2 - 2B^2\right] + 2B^2 = 0 \tag{9.22}$$

Taking typical values for a numerical example,

$$\gamma = 8.0$$
$$e = 0.15$$
$$R = 25 \text{ ft}$$
$$G = 2.273 = \frac{3g}{2R(1-e)}$$

Since $B = G/2\Omega^2$, the above values can be substituted in Eq. 9.22 and solved for a pair of values, K and Ω, which constitute an unstable point. Then,

$$K_{\text{Critical}} = 2.1$$
$$\Omega_{\text{Critical}} = 1.593 \text{ rad/sec} = 15.21 \text{ rpm}$$

The equation is solved, and the system is unstable in flapping. Although this is a reasonable value of blade stiffness K, it is unlikely that a 25-ft diameter rotor would be operated at a frequency of approximately 15 rpm, a more likely value being 7.5 to 12. Investigating further, for values of $K < 2.1$, the roots of Eq. 9.22 become imaginary, and the system is therefore stable.

The designer has the task of solving Eq. 9.22 for the set of structural parameters of interest in order to determine the (K, Ω) critical point.

Effect of Crosswind on Flapping

Including the crosswind terms, $\bar{U}_o$, the system of equations becomes

$$\begin{bmatrix} K & B & 0 \\ 2B & (K-1) & \frac{\gamma}{8} \\ \frac{\gamma}{6}\bar{U}_o & -\frac{\gamma}{8} & (K-1) \end{bmatrix} \begin{Bmatrix} \beta_o \\ \beta_{1c} \\ \beta_{1s} \end{Bmatrix} = \begin{Bmatrix} \frac{\gamma}{2}A \\ -\frac{\gamma}{2}\bar{U}_o\left(\frac{\lambda}{2} + \frac{2\theta}{3}\right) \\ 0 \end{Bmatrix} \tag{9.23}$$

and the determinant of the coefficients is

$$\Delta = K\underbrace{\left[(K-1)^2 + \left(\frac{\gamma}{8}\right)^2\right]}_{\text{Natural Frequency Term}} \underbrace{- 2B^2(K-1)}_{\text{Gravity Term}} + \underbrace{\left(\frac{\gamma}{8}\right)^2 \frac{4}{3}\bar{U}_o B}_{\text{Crosswind–Gravity Coupling Term}} \tag{9.24}$$

Since the same remarks of the last section concerning pendular instability still apply, including crosswind slightly changes the critical values of B, γ, and K.

Solving again for the flapping response, we have

$$\beta_o = \frac{\gamma A}{2\Delta}\left[(K-1)^2 + \left(\frac{\gamma}{8}\right)^2\right] + \frac{\gamma A_3}{2\Delta}\left[B\bar{U}_o(K-1)\right]$$

$$\beta_{1c} = -\frac{1}{\Delta}\left\{\frac{\gamma A}{2}\left[2B(K-1)\right] + \frac{\gamma \bar{U}_o}{2}\left[A_3 K(K-1) - \left(\frac{\gamma}{8}\right)^2 \frac{4}{3}A\right]\right\} \tag{9.25}$$

$$\beta_{1s} = -\frac{1}{\Delta}\left\{\left(\frac{\gamma}{8}\right)^2 8AB + 4\left(\frac{\gamma}{8}\right)^2 \bar{U}_o\left[\frac{4}{3}A(K-1) + A_3 K\right] + \frac{16}{3}\left(\frac{\gamma}{8}\right)^2 \bar{U}_o^2 A_3 B\right\}$$

Flapping Due to Gravity and Crosswind

where

$$A_3 = \frac{\gamma}{2} + \frac{2\theta_p}{3}$$

In this expression, another angle-of-attack aerodynamic term, A_3, is defined. This value is very close to the previous "gain" value, A, as shown by the following:

$$\begin{aligned} A &= \frac{\lambda}{3} + \frac{\theta_p}{4} \\ A_2 &= \frac{\lambda}{2} + \frac{\theta_p}{3} \\ A_3 &= \frac{\lambda}{2} + \frac{2}{3}\theta_p = \frac{3}{2}\left[\frac{\lambda}{3} + \frac{4}{9}\theta_p\right] \end{aligned} \tag{9.26}$$

There are two very small coupling terms—crosswind acting through gravity—in the β_o and β_{1s} terms; these will be ignored for the moment. This leaves two terms for each β_{1c} and β_{1s}, both a result of disturbance in gravity B or crosswind q. The physical interpretation of these terms will be left to the next section.

Effect of Yaw Rate on Flapping

Including only the yaw-rate perturbation term, $\bar{q}$, the system of equations is now

$$\begin{bmatrix} K & 0 & -\frac{\gamma}{12}\bar{q}\bar{l} \\ 0 & (K-1) & \frac{\gamma}{8} \\ 0 & -\frac{\gamma}{8} & (K-1) \end{bmatrix} \begin{Bmatrix} \beta_o \\ \beta_{1c} \\ \beta_{1s} \end{Bmatrix} = \begin{Bmatrix} \frac{\gamma A}{2} \\ -2\bar{q} - \frac{\gamma}{2}(\bar{q}\bar{l}A_3) \\ -\frac{\gamma}{8}\bar{q} \end{Bmatrix} \tag{9.27}$$

and the determinant of the coefficients is the simple expression, Δ, given with

Eq. 9.15:

$$\Delta = K\left[(K-1)^2 + \left(\frac{\gamma}{8}\right)^2\right]$$

If the gravity and crosswind terms are included, the complete determinant of the coefficients is

$$\begin{aligned} \Delta = \underbrace{K\left[(K-1)^2 + \left(\frac{\gamma}{8}\right)^2\right]}_{\textit{Natural Frequency Term}} - \underbrace{2B^2(K-1)}_{\textit{Gravity Term}} \\ - \underbrace{\left(\frac{\gamma}{8}\right)^2 \frac{4}{3} B(\bar{U}_o + \bar{q}\bar{l})}_{\textit{Gravity-Coupling Term}} + \underbrace{\left(\frac{\gamma}{8}\right)^2 \frac{9}{8}\bar{U}_o(K-1)}_{\textit{Crosswind Term}} \end{aligned} \tag{9.28}$$

Pendular instability should now be based on this expression, but the exercise must be considered largely academic since it is unlikely that both crosswind and yaw rate can be maintained in steady state.

Solving Eq. 9.27, the flapping solution for yaw rate is

$$\begin{aligned} \beta_o = \frac{1}{\Delta}\left\{\frac{\gamma A}{2}\left[(K-1)^2 + \left(\frac{\gamma}{8}\right)^2\right]\right. \\ \left. - \left(\frac{\gamma}{8}\right)^2 \frac{2}{3}\bar{q}^2\bar{l}\left[-2 - \frac{\gamma}{2}\bar{l}A_3 + (K-1)\right]\right\} \end{aligned} \tag{9.29}$$

$$\beta_{1c} = -\frac{K\bar{q}}{\Delta}\left\{(K-1)\left[2 + \frac{\gamma}{2}\bar{l}A_3\right] - \left(\frac{\gamma}{8}\right)^2\right\} \tag{9.30}$$

$$\beta_{1s} = -\frac{K\bar{q}}{\Delta}\left(\frac{\gamma}{8}\right)\left\{(K-1) + \left[2 + \frac{\gamma}{2}\bar{l}A_3\right]\right\} \tag{9.31}$$

and

$$A_3 = \frac{\lambda}{2} + \frac{2\theta_p}{3}$$

The coning, or β_o, is affected only by a negligible term, which represents coupling between the pure yaw effect, $\bar{q}$, and pure translation effect, $\bar{q}\bar{l}$. The other response, the tilting of the tip path plane, is complicated at first glance, containing, as it does, inertial, aerodynamic, and disturbance variables. Working

Table 9.1. Yaw Disturbances.

Disturbance	*Type*	*Phase of input*	*Affects*
Gyroscopic	Inertial	Cosine ψ	Blade inertia
Pure rotation, $\bar{q}$	Aerodynamic	Sine ψ	Angle of attack at 90° and 270°
Pure translation, $\overline{ql}$	Aerodynamic	Cosine ψ	Angle of attack at 0 and 180°

on a physical level, however, allows these to be understood. It is reasonable to identify the physical disturbance at work and then assume that the blade response consists of an independent response to each disturbance, which is no more than stating that the solutions are uncoupled. In this case, the rotor disturbances caused by yaw are given in Table 9.1.

The β_{1c} and β_{1s} solutions can be rewritten as follows:

$$\beta_{1c} = -\frac{K}{\Delta}\left\{\underbrace{2\bar{q}(K-1)}_{1} + \underbrace{\frac{\gamma}{2}\overline{ql}A_3(K-1)}_{2} - \underbrace{\frac{\gamma}{8}^2\bar{q}}_{3}\right\}$$

$$\beta_{1s} = -\frac{K}{\Delta}\left\{\underbrace{2\bar{q}\ \frac{\gamma}{8}}_{1} + \underbrace{\frac{\gamma}{8}\ \frac{\gamma}{2}\ \overline{ql}A_3}_{2} + \underbrace{\frac{\gamma}{8}\bar{q}(K-1)}_{3}\right\} \tag{9.32}$$

Next, the physical motion can be solved by finding the cyclic sharing between terms, the phase of the output, and the resulting phase of the input which caused it, as shown by Table 9.2, where the numbers indicate the appropriate terms from Eq. 9.32. Thus the blade response can be rewritten

Table 9.2. Cyclic Sharing Caused by Yaw.

Cyclic sharing, $\frac{\Delta\beta_{ic}}{\Delta\beta_{is}}$	*Output when* $K = 1$	*Input, 90° earlier*	*Disturbance*
1. $\frac{2\bar{q}(K-1)}{2\bar{q}(\gamma/8)} = \frac{K-1}{(\gamma/8)}$	β_{1s}	+ cosine ψ	Gyroscopic
2. $\frac{(\gamma/2)\,\overline{ql}\,A_3\,(K-1)}{(\gamma/8)\,(\gamma/2)\,\overline{ql}\,A_3} = \frac{K-1}{(\gamma/8)}$	β_{1s}	+ cosine ψ	Pure translation, + $\overline{ql}$
3. $\frac{-(\gamma/8)^2\,\bar{q}}{(\gamma/8)\,\bar{q}\,(K-1)} = \frac{-(\gamma/8)}{(K-1)}$	$-\beta_{1c}$	− sine ψ	Pure rotation, + $\bar{q}$

as follows:

$$\beta_{1c} = \underbrace{-\frac{2\bar{q}K(K-1)}{\Delta}}_{\text{Gyroscopic}} \underbrace{-\frac{\left(\frac{\gamma}{2}\right)\overline{ql}\,A_3K(K-1)}{\Delta}}_{\text{Yaw translation}} + \underbrace{\frac{\left(\frac{\gamma}{8}\right)^2\bar{q}K}{\Delta}}_{\text{Yaw rotation}} \tag{9.33}$$

$$\beta_{1s} = \underbrace{-\frac{2\bar{q}\left(\frac{\gamma}{8}\right)K}{\Delta}}_{\text{Gyroscopic}} \underbrace{-\frac{\left(\frac{\gamma}{2}\right)\left(\frac{\gamma}{8}\right)\overline{ql}A_3K}{\Delta}}_{\text{Yaw translation}} \underbrace{-\frac{\left(\frac{\gamma}{8}\right)\bar{q}K(K-1)}{\Delta}}_{\text{Yaw rotation}} \tag{9.34}$$

Other coupling terms exist, but they are much smaller than these three, which dominate the response.

Looking back at the previous section, the physical interpretation of the crosswind response will now be discussed. Equations 9.25 express the blade response caused by gravity and pure crosswind. Eliminating the gravity effect, the response is

$$\Delta\beta_{1c} = -\frac{1}{\Delta}\left\{\frac{\gamma\overline{U}_o}{2}\left[A_3K(K-1) - \left(\frac{\gamma}{8}\right)^2\frac{4}{3}A\right]\right\}$$

$$\Delta\beta_{1s} = -\frac{1}{\Delta}\left\{\left(\frac{\gamma}{8}\right)^2\overline{U}_o\left[4A_3K + \frac{16}{3}A(K-1)\right]\right\} \tag{9.35}$$

The first term in each is identical to the yaw response terms in Eq. 9.33 and 9.34, with $\overline{ql} = \overline{U}_o$, as would be expected. This is a cosine input; physically, it is the response to the "advancing" blade at $\psi = 180°$ and "retreating" blade at $\psi = 0°$. The other term is a $-\sin\psi$ input [since the cyclic sharing is $(-\gamma/8)/(K-1)$], which is also aerodynamic. These terms represent the small cyclic response to a crosswind when the blade has a steady coning angle, β_o, as shown in Fig. 9.3. Then, since $\beta_o = \gamma A/2K$, these small cyclic deltas can be rewritten as follows:

$$\Delta\beta_{1c} = \left[\left(\frac{\gamma}{8}\right)^2\frac{4}{3}\overline{U}_o\left(\frac{K}{\Delta}\right)\right]\beta_o$$

$$\Delta\beta_{1s} = -\left\{\left(\frac{\gamma}{8}\right)\frac{4}{3}\overline{U}_o\left[\frac{K(K-1)}{\Delta}\right]\right\}\beta_o \tag{9.36}$$

An engineering approximation can be made for preconed turbines using these

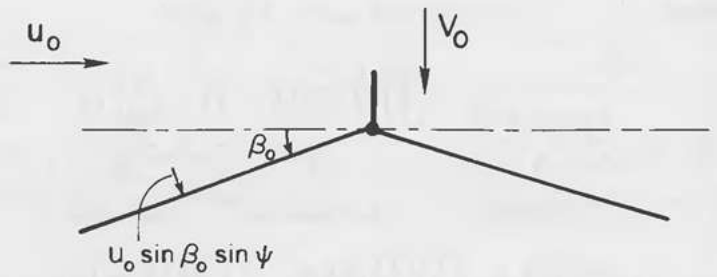

Figure 9.3. Crosswind component due to coning angle.

equations to predict yaw stability. The steady coning β_o is algebraically equivalent to steady precone β_{pc}, which can simply be substituted in Eq. 9.36 to estimate yaw moment caused by preconing.

Effect of Wind Shear on Flapping

Including only the wind shear gradient, K_1, the system of equations is

$$\begin{bmatrix} K & 0 & 0 \\ 0 & (K-1) & \frac{\gamma}{8} \\ 0 & -\frac{\gamma}{8} & (K-1) \end{bmatrix} \begin{Bmatrix} \beta_o \\ \beta_{1c} \\ \beta_{1s} \end{Bmatrix} = \begin{Bmatrix} \frac{\gamma}{2} A \\ -\frac{\gamma}{8} K_1 \bar{V}_o \\ 0 \end{Bmatrix} \tag{9.37}$$

and the blade response is

$$\begin{aligned} \beta_o &= \frac{\gamma A}{2K} \\ \beta_{1c} &= -\frac{1}{\Delta}\left\{\left(\frac{\gamma}{8}\right) K_1 \bar{V}_o K(K-1)\right\} \\ \beta_{1s} &= -\frac{1}{\Delta}\left\{\left(\frac{\gamma}{8}\right)^2 K_1 \bar{V}_o K\right\} \end{aligned} \tag{9.38}$$

The steady term is unaffected. The wind shear is a cosine ψ input, which is reflected in the cyclic terms as before. For a hinged or teetering rotor, $K =$ 1, and the entire response is $\sin \psi$. Therefore, a "soft" rotor will not track the wind if the wind shear is large (see Ref. 7 in Chap. 8).

Transient Flapping Behavior

These solutions are the approximate blade trajectories for equilibrium. That is, these equations represent the blade motion when transients have died out and the long term particular motion solution takes over. This is why the motions are conveniently expressed in terms of ψ, since the dominant forcing functions are occurring at the frequency, $\Omega = d\psi/dt$. Therefore, the stable equilibrium condition is also at frequency Ω even though the blade natural frequency may be quite different from Ω.

The true transient response in flapping can be determined from the homogeneous equations, or more precisely, from the characteristic equation derived by setting the coefficient matrix equal to zero. When solving in this way for transient motion, it is usually necessary to include more terms in the harmonic series of Eq. 9.6. Transient blade motion can be solved by substituting structural and operating parameters in the matrix and solving for the eigenvectors, which determine the damped, transient response. For this development, it has been sufficient to explore the frequency characteristics in general and to seek possible instabilities of the system as a whole. For detailed design, however, maximum transient blade excursions should be found in order to avoid unwanted interactions.

9.5 LEAD-LAG BEHAVIOR

Lead-Lag Dynamics

The lead-lag equation is

$$\begin{aligned} &\zeta'' + [2B\cos\psi + K_2]\zeta - X_{\beta'}\beta' + X_\beta \beta \\ &\quad = -2B\sin\psi + \frac{\gamma}{2}\lambda A_2 - \frac{\gamma}{2}\sin\psi\left[\bar{q}\left(\frac{2}{3}\lambda + \frac{\theta_p}{4}\right)\right] \\ &\quad\quad - \frac{\gamma}{2}\cos\psi\left[K_1\bar{V}_o\left(\frac{2}{3}\lambda + \frac{\theta_p}{4} + \frac{\bar{U}\theta_p\lambda}{2}\right)\right] \end{aligned} \tag{9.39}$$

where

$$A_2 = \frac{\lambda}{2} + \frac{\theta_p}{3}$$

$$A_4 = \frac{2}{3}\lambda + \frac{\theta_p}{4}$$

$$K_2 = \epsilon_2 + \frac{K_\zeta}{I_b\Omega^2} = \left(\frac{\omega_\zeta}{\Omega}\right)^2$$

$$X_\beta = \frac{\gamma}{2}\bar{U}_o\left(\lambda + \frac{\theta_p}{3}\right)\sin\psi \tag{9.40}$$

$$X_{\beta'} = 2\beta - \frac{\gamma}{2}A_4 + \frac{\gamma}{2}\cos\psi\left[\frac{K_1\bar{V}_o}{2} + \frac{\theta_p}{3}(\bar{U}_o + \bar{q}\bar{l})\right] + \frac{\gamma}{2}\sin\psi\left[\frac{\bar{q}}{2} + \frac{2}{3}\beta\,\bar{U}_o\right] \tag{9.41}$$

If the β' and β coupling terms are ignored for the moment, the equation has the form of a simple undamped oscillator. In actuality, some damping caused by aerodynamic drag changes does occur[4] (see also Ref. 8 in Chap. 7), but it is extremely small, and drag has thus been neglected in this treatment. Damping caused by in-plane motion has also been neglected; this term can be thought of as the "induced" part of the drag. In some helicopter systems, and in the wind turbine system studied analytically by Hirschbein,[4] this in-plane damping term can become negative, thus leading to lead-lag instability. Pure in-plane instability is rare in helicopter rotors, since flapping and torsion motions are usually involved. In helicopter systems, damping is usually added to the lag hinge to minimize the danger of lead-lag instability. How lead-lag can combine with flapping and feathering motions is more fully described in Chap. 11.

Again, the natural frequency in lead-lag is given as follows:

$$K_2 = \left(\frac{\omega_\zeta}{\Omega}\right)^2 \tag{9.42}$$

The Mathieu instabilities in lead-lag from Chap. 8 are unchanged since aerodynamic terms do not affect the oscillator. Thus, pendular instability will exist for certain values of K_2 and B.

For equilibrium motion, the right-hand side of Eq. 9.39 gives the "steady" lead-lag angles. These values are changed from those in Chap. 8 by the addition of aerodynamic forces. This forcing function contains both periodic and steady terms at frequency Ω. The higher frequency terms have been neglected but are important for two-bladed rotors, which have substantial two-per-rev excitation.

When the flap coupling terms, X_β and $X_{\beta'}$, are added, lag angle becomes dependent on flapping angle, motion through their relative geometries, and Coriolis forces. The existence of a lag hinge or in-plane flexibility offers a means for accommodating this potentially large in-plane moment but also opens the door for very serious instabilities (see Chap. 11). Vibrations in the lead-lag direction are always potentially more dangerous than flapping since there is almost no damping in lead-lag. Also, for very large turbines, the in-plane gravity load usually dominates the fatigue design of the blades since cycles are built up very fast in the in-plane degree of freedom.

For blade-motion solutions, the coupled motion can be solved by first solving for the flapping coefficients—β_0, β_{1c}, β_{1s}—and then substituting them into the lag equation.

Lead-Lag Motion

Again using the first three terms of a harmonic series solution for ζ and equating coefficients to zero, the following system for lead-lag motion is obtained (the flap coupling terms have been omitted for the moment for simplicity):

$$\zeta = \zeta_o + \zeta_{1c}\cos\psi + \zeta_{1s}\sin\psi \tag{9.43}$$

and

$$2B\,\zeta_o + (K_2 - 1)\zeta_{1c} = -\frac{\gamma}{2}\left[K_1\bar{V}_oA_4 + \frac{\theta_p\lambda}{2}(\bar{U}_o + \bar{q}\bar{l})\right]$$

$$(K_2 - 1)\zeta_{1s} = -2B - \frac{\gamma}{2}[\bar{q}A_4]$$

$$K_2\zeta_o + B\zeta_{1c} = \frac{\gamma}{2}\lambda A_2 \tag{9.44}$$

or

$$\begin{bmatrix} 2B & (K_2-1) & 0 \\ 0 & 0 & (K_2-1) \\ K_2 & B & 0 \end{bmatrix}\begin{Bmatrix} \zeta_o \\ \zeta_{1c} \\ \zeta_{1s} \end{Bmatrix} = \begin{Bmatrix} \frac{\gamma}{2}\left[K_1\bar{V}_oA_4 + \frac{\theta\lambda}{2}(\bar{U}_o + \bar{q}\bar{l})\right] \\ -2B - \frac{\gamma}{2}\bar{q}A_4 \\ \frac{\gamma}{2}\lambda A_2 \end{Bmatrix} \tag{9.45}$$

The motion solution is then

$$\zeta_o = \frac{1}{K_2(K_2 - 1) - 2B^2}\left\{\frac{\gamma}{2}\lambda A_2(K_2 - 1) + \frac{\gamma}{2}B\left[K_1\bar{V}_o A_4 + \frac{\lambda}{2}(\bar{U}_o + \bar{q}\bar{l})\theta_p\right]\right\} \tag{9.46}$$

$$\zeta_{1c} = \frac{1}{K_2(K_2 - 1) - 2B^2}\left\{-\frac{\gamma}{2}\lambda A_2 B - \frac{\gamma}{2}K_2\left[K_1\bar{V}_o A_4 + \frac{\theta_p\lambda}{2}(\bar{U}_o + \bar{q}\bar{l})\right]\right\} \tag{9.47}$$

$$\zeta_{1s} = -\frac{1}{(K_2 - 1)}\left\{2B + \frac{\gamma}{2}A_4\bar{q}\right\} \tag{9.48}$$

Lead-Lag Due to Gravity, Crosswind, Yaw Rate, and Wind Shear

Looking first at the steady lag angle, ζ_o, the pendular instability in lead-lag is given by

$$K_2(1 - K_2) + 2B^2 = 0$$

or, equivalently,

$$K_2 = \tfrac{1}{2} + \tfrac{1}{2}\sqrt{8B^2 + 1} \tag{9.49}$$

This equation constitutes the critical stiffness-frequency combination that yields lead-lag pendular instability (see Chap. 8).

The lead-lag equation (Eq. 9.39) also shows the natural frequency in the absence of gravity to be $K_2\Omega^2$. This is reiterated in Eq. 9.49 and cautions the designer to avoid values of K_2 around 1.0, where the system would be forced at its natural frequency in lead-lag. With gravity added, the range of unallowable values of K_2 is increased.

Ignoring the gravity term, the steady lead-lag angle, ζ_o, is positive, thus indicating a "leading" amount that is due to a positive torque: Power is coming out of the system.

The term ζ_o comprises all the steady "power aerodynamics" in this dynamic model. The values of λA_2 are dependent on pitch angle, θ_p; wind speed, V_o; and induced velocity, v_i. These are analytically related by momentum theory as described in Part I of this text, and the values can be substituted here to

estimate ζ_o (see Sec. 10.4). This term is unnecessary in the study of blade dynamics, however, and may be ignored for the present. For more detailed solutions, it should be calculated by using strip theory.

Recall that K_2, the in-plane frequency ratio, is $(\omega_\zeta/\Omega)^2$. In most wind turbine blades, this ratio is very high compared to flap ratio K, or $(\omega_\beta/\Omega)^2$. Looking at the values of lead-lag response a number of conclusions can be drawn.

Steady and cosine response, ζ_o and ζ_{1c}, are closely related. The steady ζ_o "power angle" discussed above has a small counterpart in the cosine term caused by gravity, and with the following cyclic sharing ratio:

$$\left.\frac{\Delta\zeta_{1c}}{\Delta\zeta_o}\right| \cong -\frac{B}{K_2} \tag{9.50}$$

due to steady power

The disturbance terms—$\bar{U}_o$, $\bar{q}$, and K,—act in reverse to this, dominating the cosine term, ζ_{1c}, and reflecting only a small portion of the steady ζ_0 term, as follows:

$$\left.\frac{\Delta\zeta_{1c}}{\Delta\zeta_o}\right| \cong -\frac{K_2}{B}$$

due to disturbances

The sine response, ζ_{1s}, contains the dominant response of the system to gravity and yaw rate. The other terms above result from gravity coupling.

9.6 FEATHERING BEHAVIOR

The dynamic torsional motion of interest to rotor designers centers on flutter. A rotor blade can experience divergence or flutter as a classical slender wing[5] that is a result of coupled torsional and flapping motion $\dot{\beta}$. These instabilities are briefly addressed in Chap. 11. For present purposes, a simplified equation of motion in feathering will be derived, with no attempt to solve for the aerodynamically induced instabilities, which are complex. The present equation of motion will be sufficient to calculate steady values of blade torsional moment and to point the way for preliminary structural design considerations.

Looking more closely at the blade, there are, in general, four noncoincident

axes: the mass axis, elastic axis, control axis, and aerodynamic axis, as follows:

1. The *mass axis* is the spanwise locus of section mass centers.
2. The *elastic axis* is the spanwise locus of points about which no section torsional deflection is incurred with bending deflection.
3. The *control axis* is simply the axis of mechanical feathering; it is completely determined by the blade retention and pitching mechanism.
4. The *aerodynamic axis* for a conventional airfoil shape within the linear performance limits (C_{l_α} assumed constant) is at the blade section quarterchord (25 percent chord).

Thus, the idealized, uniform blade would be that shown in Fig. 9.4. A blade section indicating the elemental forces and moments involved is shown in Fig. 9.5. In the latter figure,

dM_a = aerodynamic pitching moment about aerodynamic center (tending to increase angle of attack)
dM_e = blade elastic moment
dL = elemental lift
dM_c = control system elastic moment
Y_I = distance from elastic axis (shear center of blade) to center of mass
Y_A = distance from elastic axis to aerodynamic center

For the idealized blade, in which all torsional elasticity is concentrated at the root, the elastic axis and control axis are coincident, and the restoring blade elastic moment is combined with the control-system elastic moment; these are shown in Fig. 9.6.

The moments on the element are dM_a, the aerodynamic pitching moment about the aerodynamic center (moment independent of C_l) and dM_c, the elastic spring moment. The lift force is dL, acting at distance Y_A from the elastic axis. The centrifugal force is taken in two parts. First, the familiar $r\Omega^2$ spanwise term has a vertical component that is perpendicular to the plane of

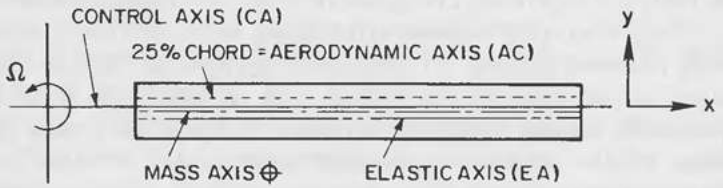

Figure 9.4. Blade spanwise axes.

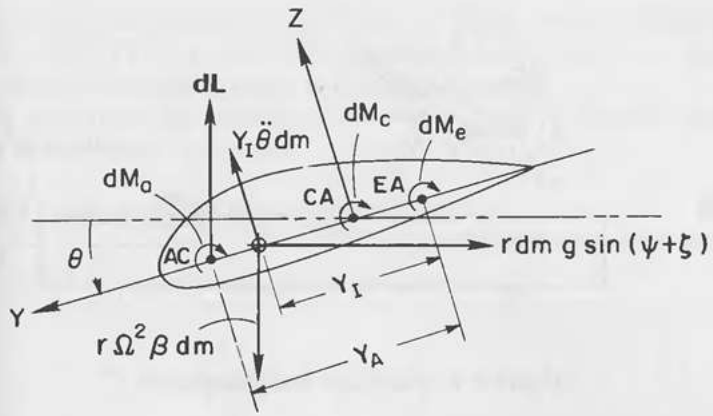

Figure 9.5. Blade flutter section.

rotation and acts at the center of mass. Also, there is a horizontal term caused by the vertical distribution of mass around the elastic axis, which is shown in Fig. 9.7.

This horizontal component perpendicular to the elastic axis is defined as follows:

$$dF_c \sin\phi \simeq dF_c\phi = r\Omega^2\, dm \left(\frac{Y_I}{r}\right) = Y_I\,\Omega^2\, dm$$

The elemental moment is then

$$dM_c = Y_I^2\theta\Omega^2 dm \tag{9.51}$$

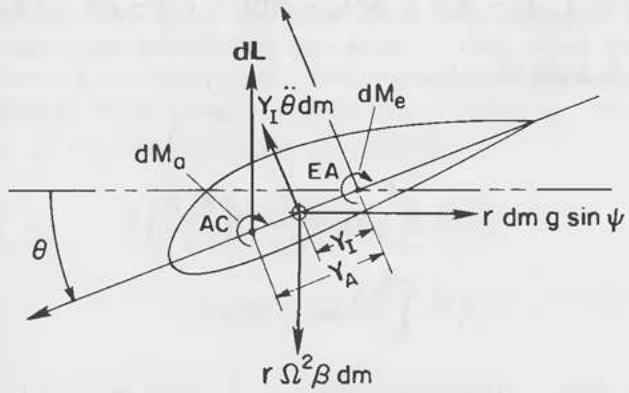

Figure 9.6. Idealized blade section (control axis not shown).

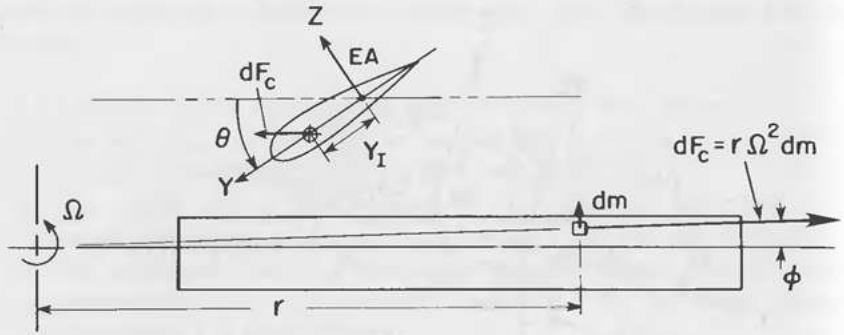

Figure 9.7. Centrifugal force components.

To this must be added the standard $I_f\Omega^2\theta$ moment about the center of mass (see the "tennis racket moment" in Sec. 8.2). Now, moments are taken about the elastic axis as follows:

$$dM_{\text{aero}} + dM_{\text{elastic}} + dM_{\text{centrifugal}} + dM_{\text{inertial}} + dM_{\text{gravity}} = 0 \quad (9.52)$$

or

$$-dM_a - dLY_a - d(K_\theta)\theta + r\Omega^2\beta\, dmY_I - Y_I^2\theta\Omega^2\, dm - d(I_f)\,\Omega^2\,\theta + r\, dmg \sin\psi Y_I \sin\theta - Y_I^2\,\ddot{\theta}\, dm - d(I_f)\ddot{\theta} = 0 \quad (9.53)$$

Integration along the blade gives

$$-M_a - Y_A\int_0^R dL - K_\theta\theta + \beta\Omega^2 I_R - \theta\Omega^2 I_I - I_I\,\ddot{\theta} - I_f\ddot{\theta} - \theta\Omega^2 I_f + I_R\, g \sin\psi\theta = 0 \quad (9.54)$$

where

$$I_R = \int_0^R Y_I r\, dm = Y_I\left(\frac{M_b R}{2}\right)$$

$$I_I = \int_0^R Y_I^2\, dm = Y_I^2 M_b$$

$$I_R g = GI_b\left(\frac{Y_I}{R}\right)$$

The aerodynamic integral, $-Y_A\int_0^R dL$, is simply the root flapping shear times the offset Y_A. In a more sophisticated analysis, Y_A could vary along the blade, and the integration would have to be performed.

After performing the integration, the single degree of freedom feathering system would appear as follows:

$$(I_f + I_I)\ddot{\theta} + (I_f + I_I)\Omega^2\theta + K_\theta\theta - I_R\beta\Omega^2 + GI_b\left(\frac{Y_I}{R}\right)\sin\psi\theta + \bar{q}\,(I_f + I_I)\Omega^2\sin\psi = -M_a - \left(\frac{Y_A}{R}\right)\left\{\frac{\gamma}{2}I_b\,\Omega^2\left[A_2 - \frac{\beta'}{3} - \sin\psi\left(\frac{\bar{U}_o}{2}\beta + \frac{\bar{q}}{3}\right) - \cos\psi\left\{\frac{K_1\bar{V}_o}{3} + (\bar{U}_o + \bar{q}l)\left(\lambda - \frac{\beta'}{2} + \theta\right)\right\}\right]\right\} \quad (9.55)$$

Single Degree of Freedom Feathering System

As a first check, the equation reduces, when aerodynamic forces, yaw rate, and mass offset are zero, to the simple oscillator of Sec. 8.3:

$$\ddot{\theta} + \left[\Omega^2 + \frac{K_\theta}{I_f}\right]\theta = 0$$

The added integral in Eq. 9.55, I_I, is simply a manifestation of the parallel axis theorem, and the aerodynamic forcing function appears as a constant moment (which is caused by airfoil pitching moment, C_m) and a lift offset component (which is dependent on Y_A/R).

The torsional behavior is dependent on flapping behavior. This simple derivation has included β coupling only in the lift term, which is very small, mainly because Y_A is usually small. When the equation of motion retains the forces caused by flapping, the free body diagram picks up a $\ddot{\beta}Y_I\, dm$ term, which gives a new coupled equation in feathering:

$$(I_f + I_I)\ddot{\theta} + \left[(I_f + I_I)\Omega^2 + GI_b\left(\frac{Y_I}{R}\right)\sin\psi + K_\theta\right]\theta - I_R\ddot{\beta} - I_R\,\Omega^2\beta = \text{Aerodynamic terms} \quad (9.56)$$

Flutter analysis in Chap. 11 combines this equation with the flapping equation of motion, which must now likewise include the coupling terms in

order to derive solutions to coupled β, θ motion and to search for instabilities. Harmonic content in the aerodynamic terms comes from all the input disturbances and from flapping angle and velocity. Other important, unsteady aerodynamic harmonic terms on the right-hand side that occur because of viscous wake effects are not modeled here. Also, the harmonics higher than order 1Ω have been neglected. All of these effects are germaine to a discussion of flutter and pitch-flap coupling instability. Usually in industry, investigation of these coupled instabilities is not undertaken until the instability has been observed; this simple analysis can then be used to describe it analytically.

To proceed, the simple feathering equation including aerodynamics then becomes

$$\theta'' + \left[K_3 + 2B\left(\frac{I_b}{I_f + I_l}\right)\left(\frac{Y_l}{R}\right)\sin\psi\right]\theta$$
$$= -\frac{M_a}{(I_f + I_l)\Omega^2} + \left(\frac{I_R}{I_f + I_l}\right)\beta - \bar{q}\sin\psi$$
$$+ \left(\frac{I_b}{I_f + I_l}\right)\left(\frac{Y_A}{R}\right)\left\{\frac{\gamma}{2}\left[A_2 - \frac{\beta'}{3} - \sin\psi\left(\frac{\bar{U}_o\beta}{2} + \frac{\bar{q}}{3}\right)\right.\right.$$
$$\left.\left. - \cos\psi\left\{\frac{K_1\bar{V}_o}{3} + (\bar{U}_o + \bar{q}\bar{l})\left(\lambda - \frac{\beta'}{2} + \theta\right)\right\}\right]\right\} \qquad (9.57)$$

where

$$K_3 = 1 + \frac{K_\theta}{(I_f + I_l)\Omega^2} = \left(\frac{\omega_\theta}{\Omega}\right)^2$$

$$B = \frac{G}{2\Omega^2}$$

$$A_2 = \frac{\lambda}{2} + \frac{\theta_p}{3}$$

Looking at the left-hand side and the stability solution, a few observations can be made. The gravity term is very small compared to the torsional frequency, $K_\theta/I\Omega^2$; hence, the torsional pendular stability is not a problem. The natural frequency of the oscillator is affected by the parallel axis theorem through I_l, but this is also a small effect.

The right-hand side contains the forcing function. The major term is the pitching moment caused by aerodynamic center offset, Y_A. The steady aerodynamic pitching moment, M_a, is very small and nose down; its tendency

to reduce torsional deflection makes it stabilizing. A mass coupling term due to coning (flapping) is an appreciable destabilizing moment that is dependent exclusively on mass axis offset and flapping angle β. Periodic terms that appear in the aerodynamic lift are caused by the applied disturbances of yaw rate, crosswind, and wind shear. Again, the effects of these are greatly attenuated by reduction of Y_A or the judicious placement of the control axis versus the aerodynamic center axis.

The designer's task is to assess the effects of mass axis offset, Y_I, and aerodynamic axis offset, Y_A, on the cyclic terms in this equation. The major design criteria are high enough torsional stiffness, K_θ, to withstand flutter and high enough torsional strength to withstand steady and cyclic pitching moments.

REFERENCES

1. Johnson, W. *Helicopter Theory*. Princeton, NJ: Princeton University Press, 1980.
2. Chopra, I. Nonlinear response of wind turbine rotor. Vol. VI, *Wind Energy Conversion*, ASRL TR-184-12, Massachusetts Institute of Technology, Cambridge, MA, Sept. 1978.
3. Shuler, S. A., et al., Wind systems technical notes: 1981. RFP-3383, DOE Contract No. DE-ACO4-76DP03533, Rocky Flats Wind Systems Program, Golden, CO, Mar. 1982.
4. Hirschbein, M. S. Dynamics and control of large horizontal axis axisymmetric wind turbines. Ph.D. dissertation, University of Delaware, University Microfilms 8006484, June 1979.
5. Saunders, G. H. *Dynamics of Helicopter Flight*. New York: John Wiley & Sons, 1974.
6. Hansen, A. C., and Wright, A. D. A simple teetering-rotor hub design model. Paper presented at American Wind Energy Association Conference and Exhibition, Pasadena, CA, Sept. 1984.
7. Wendell, J. H. Simplified aeroelastic modeling of horizontal axis wind turbines. NASA CR-168109, MIT ASRL TR-197-4, Massachusetts Institute of Technology, Cambridge, MA, Sept. 1982.

10

BLADE AND HUB LOADS

10.1 INTRODUCTION

To the designer, a companion problem to the calculation of blade motions is the estimation of loading on the blade. In general, the structural designer of the blade has two tasks:

1. To provide appropriate stiffness to avoid instabilities
2. To provide sufficient strength to withstand loads, including fatigue

The "strength design" parameters consist of the following:

1. Large loads expected rarely, called "proof loads," such as during hurricanes, which must be a "factor of safety" within the blade structural limits
2. Continuous loads resulting from normal operation, which may have different "factors of safety"
3. Periodic, or vibratory, loads, which must lie within the endurance (fatigue) limits of the blade materials.

These are described more fully in Chap. 12, which develops a complete blade loading specification for each category. Specific operating conditions are strongly site-dependent, as is the expected output during the life of a wind turbine. This chapter develops the practical expressions that can be used to calculate the blade loading using the simple blade model assumed in this text. These results are used in the calculations of Sec. 10.5 and Chap. 12.

10.2 GOVERNING EQUATIONS

The first-order blade motion is represented by a harmonic series, as follows:

$$\beta = \beta_o + \beta_{1c} \cos \psi + \beta_{1s} \sin \psi \qquad (10.1)$$

where the three angles—β_o, β_{1c}, and β_{1s}—are components that fully describe

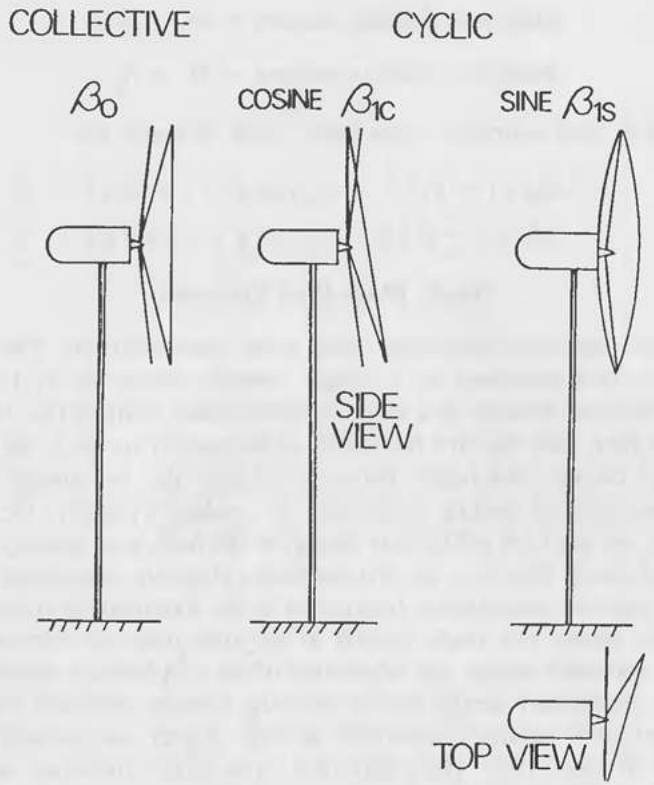

Figure 10.1. Rotor tip path plane components.

the orientation of the rotor-tip path plane behind the nacelle, as shown in Fig. 10.1. β_o is the collective, or uniform, coning; β_{1c} is the forward tilt of the rotor plane; and β_{1s} is the sideward tilt (positive to the left). Likewise, the in-plane, or lead-lag motions are represented by the harmonic series:

$$\zeta = \zeta_o + \zeta_{1c} \cos \psi + \zeta_{1s} \sin \psi \qquad (10.2)$$

where ζ_o is the steady lead-lag value; ζ_{1c} is the vertical scissoring; and ζ_{1s} is the horizontal scissoring of the blade. These equations represent the blade motion of each single blade.

The physical blade model is a rigid blade with a hinge and spring near the root analytically developed in Chap. 7. The angles represent the angular deflections of the hinge-spring model, hence the motion of the tip. The blade-root bending moments are simply the elastic restraining moments of the hinge spring, as follows:

$$\text{Blade-root flapping moment} = M_\beta = K_\beta \beta$$

$$\text{Blade-root lead-lag moment} = M_\zeta = K_\zeta \zeta$$

Expressed in their harmonic components, these moments are

$$\begin{aligned} M_\beta(\psi) &= K_\beta[\beta_o + \beta_{1c}\cos\psi + \beta_{1s}\sin\psi] \\ M_\zeta(\psi) &= K_\zeta[\zeta_o + \zeta_{1c}\cos\psi + \zeta_{1s}\sin\psi] \end{aligned} \tag{10.3}$$

Single Blade-Root Moments

Thus, each blade-root attachment must resist these moments. The torsional moment is best expressed as a steady moment caused by θ, leaving the periodic torsional motions to a more complete flutter analysis (see Chap. 11). As shown here, only the first harmonics of the motion are used. As discussed in the last chapter, the higher harmonics should also be brought into play when more detailed loading information is needed. Typically, the first five harmonics are used for preliminary design in the helicopter industry (i.e., sin 5ψ, cos 5ψ, etc.). However, the first harmonics alone are surprisingly sufficient for most practical calculations. In addition to the root-moment equations (Eq. 10.3), hub shears and blade tension at the root must be calculated for a complete structural design, but calculation of the root-bending moments alone is a good preliminary design tool in choosing between structural tradeoffs.

The first-order solutions described in this chapter are summarized and illustrated in Figs. 10.2, 10.3, and 10.4. Yaw rate, crosswind, and wind-shear disturbances are included.

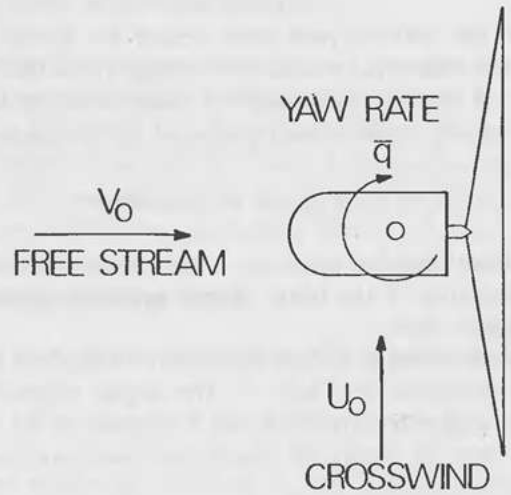

Figure 10.2. Rotor disturbances.

	Axial Flow + Hinge Spring + Gravity	Crosswind	Yaw Rate	Wind Shear
$\beta_o =$	$\frac{1}{\Delta}\left\{\frac{\gamma A}{2}\left[(K-1)^2 + \left(\frac{\gamma}{8}\right)^2\right]\right\}$	—	—	—
$\beta_{1c} =$	$\frac{1}{\Delta}\left\{\begin{array}{l} -\gamma BA(K-1) \\ \end{array}\right.$	$+\left(\frac{\gamma}{8}\right)^2\left(\frac{\gamma}{2}\right)\frac{4}{3}A\bar{U}_o$ $-\frac{\gamma A_1}{2}K(K-1)\bar{U}_o$	$-2\bar{q}K(K-1)$ $-\frac{\gamma A_1}{2}K(K-1)\,\bar{q}l$ $+K\bar{q}\left(\frac{\gamma}{8}\right)^2$	$-\frac{\gamma}{2}\left(\frac{K_1\bar{V}_o}{4}\right)K(K-1)$
$\beta_{1s} =$	$\frac{1}{\Delta}\left\{-\frac{\gamma^2}{8}BA\right.$	$-\left(\frac{\gamma}{8}\right)^2\frac{16}{3}A(K-1)\bar{U}_o$ $-\left(\frac{\gamma}{8}\right)^2 4A_1K\bar{U}_o$	$-\left(\frac{\gamma}{8}\right)^3 4A_1K\bar{q}l$ $-\frac{\gamma}{8}\bar{q}K(K-1)$ $-2\bar{q}K\left(\frac{\gamma}{8}\right)$	$-\left(\frac{\gamma}{8}\right)^2 K_1\bar{V}_oK$

where

$$\Delta = K\left[(K-1)^2 + \left(\frac{\gamma}{8}\right)^2\right]$$

Figure 10.3. Flapping equations (dominant terms only).

$$\zeta_o = \frac{1}{K_2(K_2-1)-2B^2}\left\{\frac{\gamma}{2}\lambda A_2(K_2-1)+\frac{\gamma}{2}B\left[K_1\bar{V}_oA_4+\frac{\lambda}{2}(\bar{U}_o+\bar{q}l)\theta_p\right]\right\}$$

$$\zeta_{1c} = \frac{1}{K_2(K_2-1)-2B^2}\left\{-\frac{\gamma}{2}\lambda A_2B-\frac{\gamma}{2}K_2\left[K_1\bar{V}_oA_4+\frac{\theta_p\lambda}{2}(\bar{U}_o+\bar{q}l)\right]\right\}$$

$$\zeta_{1s} = -\frac{1}{K_2-1}\left\{2B+\frac{\gamma}{2}A_4\bar{q}\right\}$$

Figure 10.4. Lead-lag equations.

10.3 HUB LOADING

The moments and forces transmitted from the blades to the hub and tower depend on the type of hub being considered. An *articulated hub* has free hinges in flapping and lead-lag, and the blade receives no mechanical restraint moment in either flapping or lead-lag. The feathering moment in the case of helicopters is transmitted to the rotor swash plate and control system through a mechanical-arm linkage called a *pitch link*, which implements pitch change commanded by the swash plate and restrains the blade in feathering (see Ref. 7 in Chap. 8). Few wind turbines have been built with articulation since the complexity of the hinges is costly.

A *teetering rotor* has two rigidly connected blades that are gimballed to the rotating shaft. Only in-plane moments are transmitted to the hub, as the flapping moments cannot be transferred through the gimbal or teeter-pin joint.

The third and most usual type of configuration for wind turbines is simple *cantilevered* blades, or a *hingeless hub*. All moments and forces are transmitted to the hub and, in turn, to the tower, as shown in Fig. 10.5.

The most direct engineering approach for the blade-root moments is to solve for the blade angular deflections and write the elastic restraining moment as we did in the previous section. This gives the following blade root moments:

$$\begin{aligned} M_\beta &= K_\beta[\beta_o + \beta_{1c}\cos\psi + \beta_{1s}\sin\psi] \\ M_\zeta &= K_\zeta[\zeta_o + \zeta_{1c}\cos\psi + \zeta_{1s}\sin\psi] \\ M_\theta &= K_\theta[\theta_o + \theta_{1c}\cos\psi + \theta_{1s}\sin\psi] \end{aligned} \tag{10.4}$$

Blade-Root Moments

These root moments contain only the collective and cyclic angles for rotor-plane equilibrium. That is, the forcing functions allowed are at frequency 1Ω, since the equilibrium motion solution simply involves a tilt of the rotor plane. Since the forcing functions considered (crosswind, gravity, etc.) are all at frequency 1Ω, the steady-state solution is at 1Ω also. All the transients, which

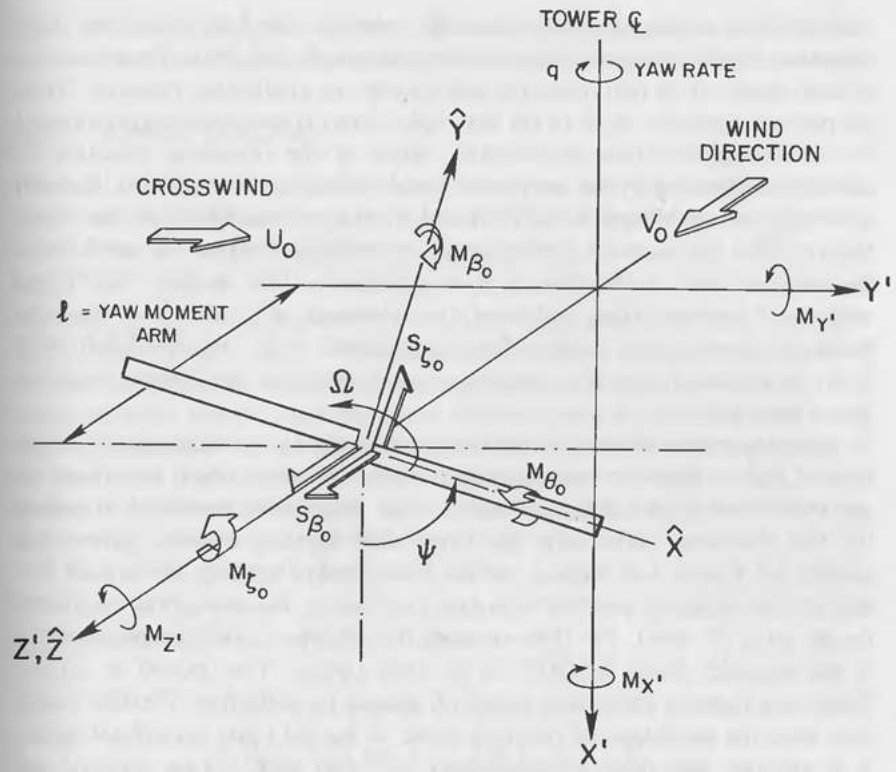

Figure 10.5. Hub forces and moments.

occur at natural frequencies of the blades and other vibrating rotor elements, will have died out. Hence, these moments are the *equilibrium* hub and tower moments that result from crosswind, U_o; yaw rate, q; gravity, B; wind shear, K_1; mean inflow, λ; and pitch and twist angle in the same way that the blade motions did in Chap. 9. For instance, the flapping moment on the blade consists of delta angles resulting from the forcing functions and can be expressed in the following way:

$$\frac{M_\beta}{K_\beta} = \underbrace{\left[\frac{\gamma A}{2\Delta}\ (K-1)^2 + \left(\frac{\gamma}{8}\right)^2\right]}_{\text{due to } \bar{q}} + \underbrace{\Delta\beta_o|}_{\text{yaw rate}} + \Delta\beta_o| + \cdots$$

$$+ \{\underbrace{\Delta\beta_{1c}|}_{\text{gravity}} + \underbrace{\Delta\beta_{1c}|}_{\text{crosswind}} + \underbrace{\Delta\beta_{1c}|}_{\text{wind shear}} + \cdots\}\cos\psi$$

$$+ \{\underbrace{\Delta\beta_{1s}|}_{\text{gravity}} + \underbrace{\Delta\beta_{1s}|}_{\text{crosswind}} + \underbrace{\Delta\beta_{1s}|}_{\text{wind shear}} + \cdots\}\sin\psi$$

In addition to the blade-root bending moments, the hub connection must withstand blade shear and tension. Shear is simply the thrust-force reaction of each blade on its hub mounting and tension the centrifugal reaction. These are present, naturally, in all of the hub types. Shear is most easily approximated by calculating the rotor aerodynamic thrust at the operating condition of interest and dividing by the number of blades (which carry the thrust). Tension is simply the centrifugal force produced by the rotating blade. If the wind-turbine rotor has a preset coning angle, centrifugal tension also produces a flapping moment at the hub, $I_b\Omega \times$ (precone). This is the "centrifugal stiffening" moment term and must be calculated and subtracted from the blade-root aerodynamic flapping bending moment. In an articulated hub, with its freely flapping hinge, this restoring moment offsets the aerodynamic moment (see Chap. 12).

These blade-root forces and moments act on the blade independently of the type of hub or retention, but the type of hub determines which root moments are transmitted to the hub. Obviously, it is structurally beneficial to reduce the hub reactions, particularly the large blade-flapping moment. Since it is usually not practical to hinge a turbine blade freely, teetering is the next best step from a structural point of view (not necessarily, however, from an overall design point of view). For three-or-more bladed rotors, since simple teetering is not possible, blade flexibility is the only option. The tradeoff is simple: Blade-root flapping moment is traded off against tip deflection. Flexible blades thus have the advantage of relieving some of the load into centrifugal terms. It is obvious that other considerations will also apply: Yaw stability and fatigue life, for example, are significantly affected by blade flexibility.

Hub reactions for the various types of hub retention are summarized in Table 10.1. For all types of hubs, the main shaft reactions are simply the summation of the blade contributions, which are discussed in the next section.

Table 10.1 Hub Reactions.

Hub reaction at blade root	Fully articulated	Teetering	Cantilevered
Flapping moment	No moment	No moment	Full moment present
Flapping shear	Thrust of one blade	Total rotor thrust acts on teeter hinge	Thrust of one blade
Lead-Lag moment	No moment	Total rotor "power torque" on main shaft	"Power torque" of one blade
Lead-Lag shear	Inplane force that produces "power torque"	Inplane force that produces "power torque"	Inplane force that produces "power torque"
Tension	Centrifugal force	Centrifugal force	Centrifugal force
Torsion	Pitching moment of one blade	Pitching moment	Pitching moment of one blade

10.4 TOWER LOADING

The hub loads developed in the last section can now be transferred to the fixed, or tower coordinate, system and the individual blades summed over the rotor. From a design standpoint, magnitudes and frequencies of the rotor forces and moments are the chief dynamic considerations for the tower and supports. Steady tower loads arise from rotor thrust and torque and the weight of the aloft system. Also, the strength of the tower and supports must be sufficient to resist the maximum expected transient loading (proof load) with adequate safety margin, and the tower stiffness must be determined to avoid tower resonance at the rotor frequencies. The frequencies and magnitudes of the operating rotor loads of interest are developed in this section. Some obscure but potentially harmful instabilities in coupled rotor-tower flapping and lead-lag are possible (see Ref. 4 in Chap. 8).

A vector, $\bar{R}$, rotating with the rotor at frequency, $\Omega = d\psi/dt$, is said to be rotating at one-per-rev or one/rev frequency. This vector can be transferred to the nonrotating tower system as follows:

$$\begin{Bmatrix} R_{X'} \\ R_{Y'} \\ R_{Z'} \end{Bmatrix} = \begin{bmatrix} \cos\psi & -\sin\psi & 0 \\ \sin\psi & \cos\psi & 0 \\ 0 & 0 & 1 \end{bmatrix} \begin{Bmatrix} R_{\hat{x}} \\ R_{\hat{y}} \\ R_{\hat{z}} \end{Bmatrix} \tag{10.5}$$

$X'Y'Z'$ Nonrotating system — $\hat{X}\hat{Y}\hat{Z}$ Rotating system

The blade-root moments consist of the flapping moment, M_β; the lead-lag moment M_ζ; and the torsional moment, M_θ, as shown in Fig. 10.5. In the rotating frame,

$$\begin{Bmatrix} M_{\hat{x}} \\ M_{\hat{y}} \\ M_{\hat{z}} \end{Bmatrix} = \begin{Bmatrix} M_\theta \\ -M_\beta \\ M_\zeta \end{Bmatrix}$$

and as follows for the nonrotating frame:

$$\begin{Bmatrix} M_{X'} \\ M_{Y'} \\ M_{Z'} \end{Bmatrix} = \begin{bmatrix} \cos\psi & -\sin\psi & 0 \\ \sin\psi & \cos\psi & 0 \\ 0 & 0 & 1 \end{bmatrix} \begin{Bmatrix} M_\theta \\ -M_\beta \\ M_\zeta \end{Bmatrix}$$

Then, the fixed tower moments are seen to be

$$M_{X'} = M_\theta \cos\psi + M_\beta \sin\psi$$
$$M_{Y'} = M_\theta \sin\psi - M_\beta \cos\psi \qquad (10.6)$$
$$M_{Z'} = M_\zeta$$

Fixed Tower Moments

The X' moment causes yaw of the nacelle. It is clockwise along the X' axis, i.e., in the same direction as the positive yaw rate, q. It is reacted by torsion on the tower if the wind turbine is fixed or restrained in yaw. The Y' moment is a "pitching moment" on the tower, positive nacelle nose up (for a downwind rotor), and is reacted on the tower top supports. The Z' moment is the nacelle "rolling moment"; it is the rotor main-shaft torque reaction on the nacelle and tower.

Combining Eqs. 10.6 and 10.4, we have the tower yawing moment caused by a single blade:

$$M_{X'} = \tfrac{1}{2}[K_\beta\beta_{1s} + K_\theta\theta_{1c}] + K_\beta\beta_o \sin\psi + K_\theta\theta_o \cos\psi$$
$$+ \tfrac{1}{2}[K_\beta\beta_{1c} + K_\theta\theta_{1s}] \sin 2\psi + \tfrac{1}{2}[K_\theta\theta_{1c} - K_\beta\beta_{1s}] \cos 2\psi \qquad (10.7)$$

Tower Yawing Moment

the tower pitching moment caused by a single blade:

$$M_{Y'} = \tfrac{1}{2}[K_\theta\theta_{1s} - K_\beta\beta_{1c}] + K_\theta\theta_o \sin\psi - K_\beta\beta_o \cos\psi$$
$$+ \tfrac{1}{2}[K_\theta\theta_{1c} - K_\beta\beta_{1s}] \sin 2\psi - \tfrac{1}{2}[K_\theta\theta_{1s} + K_\beta\beta_{1c}] \cos 2\psi \qquad (10.8)$$

Tower Pitching Moment

and the tower antitorque moment caused by a single blade:

$$M_{Z'} = K_\zeta\zeta_o + K_\zeta\zeta_{1c} \cos\psi + K_\zeta\zeta_{1s} \sin\psi \qquad (10.9)$$

Tower Antitorque Moment

An important observation here is that the single-blade one-per-rev frequency appears at one-per-rev *and* two-per-rev frequencies on the tower. Also, there are constant tower moments resulting from rotor cyclic motions.

The moments from all the blades must be added to obtain the actual tower moments; the preceding are only for the single-blade tower reactions. In addition, the tower reaction includes the weight, and the thrust, which is simply the resultant of all the hub shears. Blade tension caused by centrifugal force is realistically important in the tower reaction only for a loss of blade accident. For the case of blade imbalance (e.g., due to icing), the centrifugal force term would appear at frequency Ω and an amplitude equal to the centrifugal force of the unbalanced mass.

Equations 10.7 and 10.8—the tower moments due to a single blade—can be simplified further by noticing that the flapping motions (and moments) are much greater than the feathering moments. For a single blade, then, the tower yaw is

$$M_{X'} \simeq \tfrac{1}{2} K_\beta\beta_{1s} + K_\beta\beta_o \sin\psi + \tfrac{1}{2} K_\beta\beta_{1c} \sin 2\psi - \tfrac{1}{2} K_\beta\beta_{1s} \cos 2\psi \qquad (10.10a)$$

and the tower pitch is

$$M_{Y'} \simeq -\tfrac{1}{2} K_\beta\beta_{1c} - K_\beta\beta_o \cos\psi - \tfrac{1}{2} K_\beta\beta_{1s} \sin 2\psi - \tfrac{1}{2} K_\beta\beta_{1c} \cos 2\psi \qquad (10.10b)$$

For a two-bladed system, the total moment is the sum of the individual blades, phase π apart:

$$M_{x'} = \sum_{K=1}^{b} M_{X'_K} = M_{X'}(\psi) + M_{X'}(\psi - \pi)$$
$$= K_\beta\beta_{1s} + K_\beta\beta_o [\sin\psi + \sin(\psi - \pi)]$$
$$+ \frac{1}{2} K_\beta\beta_{1c} [\sin 2\psi + \sin(2\psi - 2\pi)]$$
$$- \frac{1}{2} K_\beta\beta_{1s} [\cos 2\psi + \cos(2\psi - 2\pi)]$$

The third and forth terms add. Thus, for two blades, the tower yaw is

$$M_{X'} = K_\beta\beta_{1s} + K_\beta\beta_{1c} \sin 2\psi - K_\beta\beta_{1s} \cos 2\psi \qquad (10.11a)$$

and the tower pitch is

$$M_{Y'} = -K_\beta \beta_{1c} - K_\beta \beta_{1s} \sin 2\psi - K_\beta \beta_{1c} \cos 2\psi \qquad (10.11b)$$

The rotor plane tilt—β_{1c} and β_{1s}—appears as a steady tower moment and as a periodic input at two-per-rev frequency. Thus, there will be two-per-rev tower forcing frequencies in a two-bladed system whether or not the blades are exactly balanced. The steady yaw moment is caused by the yaw tilt of the rotor plane and is exactly equal to the sine cyclic of one blade. The tower pitching moment is caused by the fore-and-aft tilt of the rotor plane and likewise is equal to the single-blade cosine angle. Also, both directions have the combination two-per-rev moments.

For a three-bladed rotor, the total moment is

$$\begin{aligned} M_{X'} &= M_{X'}(\psi) + M_{X'}\left(\psi - \frac{2\pi}{3}\right) + M_{X'}\left(\psi - \frac{4\pi}{3}\right) \\ &= \frac{3}{2} K_\beta \beta_{1s} + K_\beta \beta_o [\sin (\mathrm{I}) + \sin \mathrm{II} + \sin (\mathrm{III})] \\ &\quad + \frac{1}{2} K_\beta \beta_{1c} [\sin 2(\mathrm{I}) + \sin 2(\mathrm{II}) + \sin 2(\mathrm{III})] \\ &\quad - \frac{1}{2} K_\beta \beta_{1s} [\cos 2(\mathrm{I}) + \cos 2(\mathrm{II}) + \cos 2(\mathrm{III})] \end{aligned}$$

In this case, the second, third, and fourth terms all cancel, so that, for three blades, the tower moments are

$$\begin{aligned} M_{X'} &= \tfrac{3}{2} K_\beta \beta_{1s} \\ M_{Y'} &= -\tfrac{3}{2} K_\beta \beta_{1c} \end{aligned} \qquad (10.12)$$

In all other cases with three or more blades ($b \geq 3$) the second, third, and fourth terms also cancel, so that, for b blades, the tower moments are

$$\begin{aligned} M_{X'} &= \frac{b}{2} K_\beta \beta_{1s} \\ M_{Y'} &= -\frac{b}{2} K_\beta \beta_{1c} \end{aligned} \qquad (10.13)$$

Tower Moments, b Blades

The method of multiblade coordinates (see Ref. 6 in Chap. 8) makes use of this result, which can be generalized to give the following harmonic identities.

$$\begin{aligned} \sum_{i=1}^{b} \sin n\psi_i &= 0 \qquad n \neq \text{multiple of } b \\ &= b \sin n\psi \qquad n = Sb,\ S = 1, 2, \ldots \end{aligned} \qquad (10.14a)$$

$$\begin{aligned} \sum_{i=1}^{b} \cos n\psi_i &= 0 \qquad n \neq \text{multiple of } b \\ &= b \cos n\psi \qquad n = Sb,\ S = 1, 2, \ldots \end{aligned} \qquad (10.14b)$$

where

b = number of blades
ψ_i = azimuth phase angle
n = n'th harmonic of rotor speed = $\Omega = d\psi/dt$

Other periodic forces than the one-per-rev cyclic moments discussed here will exist in the rotating system. The most significant ones are the transient moments caused by oscillations of the blades at a blade natural frequency. A source of such disturbance is wind gusting, which can cause blade vibration. It has been shown that flapping transients are highly damped by aerodynamics, but lead-lag transients have very little damping. Also, coupled structural modes may be important if forced at their natural frequencies. Concerning the rotor-tower interaction, the designer's primary task is to investigate which rotor frequencies will penetrate the rotating coordinate transformation to tower coordinates and thus excite a tower resonance. The most obvious one to consider is a resonance between a rotor operating frequency and tower natural frequency.

10.5 YAW STABILITY

No reliable theory yet exists for the accurate prediction of rotor yaw stability. As seen here, rotor aerodynamics plays the major role. Some qualitative observations can be made, however, based on field observations:

1. In the absence of any yaw restraint, both upwind and downwind rotors show positive yaw stability to some degree.
2. Downwind rotors have higher yaw stability than upwind rotors.
3. Upwind rotors are yaw stable up to some yaw angle, and unstable past that angle; the critical angle depends on blade pitch.
4. Both upwind and downwind rotors show different strength yaw stability

for positive or negative yaw angles depending on the direction of rotation of the rotor (See Ref. 21 in Chap. 11).

5. Rotors with flexible blades show a higher range of angles for which they have positive yaw stability, but the strength of the restoring moment is less than for rotors with stiff blades.
6. All free-yawing rotors show occasions where they are stable both upwind and downwind.
7. Transient yaw excursions are caused by wind direction gusts, upwind wakes of other turbines, and disconnection (unloading) of the rotor from the drive train.
8. Positive coning angle improves yaw stability for both upwind and downwind rotors.
9. A teetering rotor is less yaw stable, that is, slower to respond to direction gusts.

Some light can be shed on the subject of yaw stability by studying the present equations. Looking at the multiblade results in Eq. 10.13, the tower moments for three or more blades are simpler than for two blades. The fore and aft rotor plane tilt, β_{1c}, causes a steady tower pitching moment, $M_{Y'}$. The yaw tilt of the rotor plane is β_{1s}; this gives a steady yawing moment, $M_{X'}$. In the absence of any other restoring moment, the rotor would yaw around the tower. A restoring moment is produced, however. As the rotor plane yaws, it rotates slightly out of the direct wind direction. This causes a crosswind component, $\bar{U}_o$, to be produced; thus, the rotor will yaw until the aerodynamic $\Delta\beta_{1s}$ due to crosswind balances the β_{1s} from other sources. The following sine cyclic equation is from the complete flapping equations in Fig. 10.3.

$$\beta_{1s} = \frac{1}{\Delta}\left\{\underbrace{-\frac{\gamma^2}{8}BA}_{\text{Gravity}} \underbrace{-4\left(\frac{\gamma}{8}\right)^2\bar{U}_o\left[\frac{4}{3}A\ (K-1)+A_3K\right]}_{\text{Crosswind}}\right.$$
$$\underbrace{-\frac{16}{3}\left(\frac{\gamma}{8}\right)^2\bar{U}_o^2A_3B}_{\text{Gravity-Crosswind Coupling}} \underbrace{-\left(\frac{\gamma}{8}\right)^2K_1\bar{V}_oK}_{\text{Wind shear}} \left.\underbrace{-\Delta\beta_{1s}}_{\text{Yaw rate}}\right\} \qquad (10.15)$$

where:

$$B = \frac{G}{2\Omega^2}$$

$$A = \frac{\lambda}{3} + \frac{\theta_p}{4}$$

$$A_3 = \frac{\lambda}{2} + \frac{2\theta_p}{3}$$

$$K = 1 + \epsilon + \frac{K_\beta}{I_b\Omega^2} = \left(\frac{\omega_\beta}{\Omega}\right)^2$$

$$\bar{U}_o = \frac{U_o}{\Omega R}$$

$$\bar{q} = \frac{q}{\Omega}$$

This expression, when equated to zero, gives the equilibrium yaw position of a freely yawing wind turbine. Gravity and wind shear, which are both cosine inputs to flapping (see Sec. 9.4), cause the turbine to yaw to the right, or clockwise looking up the tower. The gravity component is simple gyroscopic precession caused by the orthogonal axes of rotation, and the wind shear component is purely aerodynamic. (Recall that the rotor of the present analytical model is downwind and rotates counterclockwise.) The aerodynamic crosswind moment counteracts the destabilizing yawing moments.

This can be seen by the following example. The sine cyclic due to crosswind is

$$\underset{\text{crosswind}}{\Delta\beta_{1s}} = -\frac{4}{\Delta}\left(\frac{\gamma}{8}\right)^2\bar{U}_o\left[\frac{4}{3}A(K-1)+A_3K\right] \qquad (10.16)$$

Referring to the coordinate system in Fig. 7.6, it can be seen that a positive crosswind U_o, is equivalent to positive yaw angle, Θ, which would be counterclockwise looking up the tower. If a positive crosswind is superimposed on the rotor, a negative $\Delta\beta_{1s}$ results from Eq. 10.16. This causes a negative $M_{X'}$ tower moment, from Eq. 10.13, that acts to counteract the initial crosswind and to decrease the yaw angle, Θ, and is therefore stabilizing.

The alternating components for the two-blader in Eq. 10.11 do not affect this stability but only add alternating loads to the rotor shaft during this yaw motion. Since the three- and b-bladed rotors do not have this alternating load, they are thought of as being more "dynamically stable" than the two-bladed rotor. More properly, the two-blader is neither more nor less stable, it simply has an added two-per-rev vibration during yaw.

Going on, it can be shown that a steady yaw-tracking error will exist for most wind turbines. The turbine, if no yaw restraint is present, will by definition have its tower yaw moment, $M_{X'}$, equal to zero. This gives a β_{1s} of 0, and thus the terms in brackets in Eq. 10.15 give the equilibrium yaw-tracking error of the turbine. Taking the gravity and crosswind terms first,

the crosswind to balance gravity is

$$\bar{U}_o = -\frac{6AB}{3A_3K + 4A(K-1)} \tag{10.17}$$

In terms of angle Θ to wind direction V_o, we have the first-order yaw tracking error of a wind turbine due to gravity:

$$\tan\Theta = \frac{\bar{U}_o}{\bar{V}_o} = \frac{\Omega R}{V_o}\left[\frac{6AB}{3A_3K + 4A(K-1)}\right] \tag{10.18}$$

Tracking Error Due to Gravity

Recalling that the ratio, A/A_3, is about $2/3$ (if θ_p is small), Eq. 10.18 reduces to the following:

$$\Theta \simeq \frac{\Omega R}{V_o}\left[\frac{3B}{2(2K-1)}\right] \tag{10.19}$$

This simple result yields some important physical conclusions, as follows:

1. A soft, or teetering, rotor with $K = 1$ has a large free-tracking yaw error.
2. The yaw error increases with tip-speed ratio.
3. The tracking error term, $\frac{3}{2}B$, is proportional to gravity and can be written as $3/2\ (gM_bx_gR/2I_b\Omega^2)$, which is the ratio of the static gravity bending moment to the centrifugal force moment of the blade.
4. When the wind dies, the aerodynamic crosswind restoring moment dies out, leaving only the gyroscopic gravity destabilizing moment. The result is a yaw out of the wind (to the left in this model, downwind with counterclockwise rotation). This yaw is particularly noticeable with heavy rotors with large M_b and hence large precession acceleration.

Referring back to Eq. 10.15, it can be seen that wind shear has the same tracking error effect. Expressing the yaw balance this time for wind shear gives

$$\tan\Theta = -\frac{3K_1}{16A\left(\dfrac{K-1}{K}\right) + 12A_3} \tag{10.20}$$

When $K = 1$, the yaw tracking error due to wind shear is

$$\Theta = -\frac{K_1}{4A_3} \tag{10.21}$$

Tracking Error Due to Wind Shear

The tracking error in this case is not dependent, to first order, on tip-speed ratio or wind speed, and only weakly on pitch angle, θ_p, through the A term. This Θ is potentially large, however, since A_3 is a very small quantity.

Going on, some more light can be shed on the physical mechanism for yaw stability by examining the crosswind response more closely. The cosine cyclic component in response to crosswind is

$$\begin{aligned}\Delta\beta_{1c}\Big|_{\text{crosswind}} &= \frac{1}{\Delta}\left\{\left(\frac{\gamma}{8}\right)^2\left(\frac{\gamma}{2}\right)\frac{4}{3}A\bar{U}_o - \frac{\gamma A_3}{2}K(K-1)\bar{U}_o\right\} \\ &= \frac{\gamma\bar{U}_o}{2\Delta}\left\{\left(\frac{\gamma}{8}\right)^2\frac{4}{3}A - A_3K(K-1)\right\}\end{aligned} \tag{10.22}$$

Observing that there are terms that depend on both disc angle-of-attack terms, A and A_3, in the cosine response (Eq. 10.22) and in the sine response (Eq. 10.16), the "cyclic sharing" or ratio of cosine cyclic to sine cyclic can be found, as follows:

For the A term:

$$\frac{\Delta\beta_{1c}}{\Delta\beta_{1s}} = -\frac{\gamma}{8(K-1)} \tag{10.23a}$$

For the A_3 term:

$$\frac{\Delta\beta_{1c}}{\Delta\beta_{1s}} = \frac{8(K-1)}{\gamma} \tag{10.23b}$$

These show that there are two competing aerodynamic portions to the crosswind perturbation—one depending on the A term and other on the A_3 term—that have different phase inputs: The A term is all $(-)$ sine input, and the A_3 term all cosine input (see Sec. 9.4). As before, A/A_3 is about $\frac{2}{3}$ if the pitch angle is small. As a result, these two aerodynamic portions are nearly the same in magnitude insofar as their effect on causing rotor cyclic response.

It can be seen that the A_3 term effect, being a cosine input, is physically

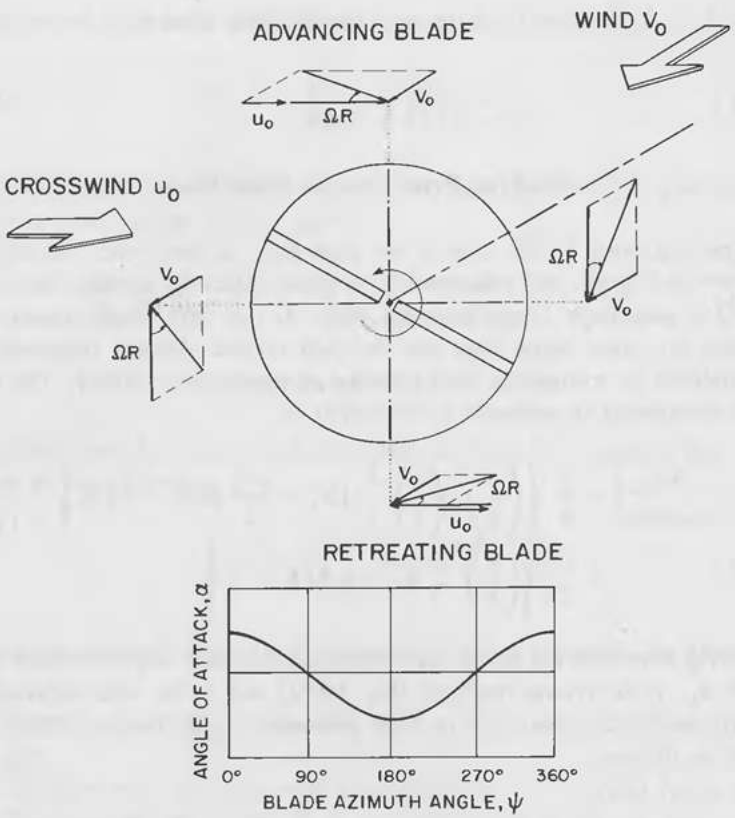

Figure 10.6. Advancing/retreating blade effect of crosswind.

the "advancing/retreating" blade effect caused by the crosswind at $\psi = 0°$ and 180° (see Fig. 10.6). The A term effect, on the other hand, is a $(-)$ sine input, which is caused by the geometry of steady coning angle β_o (see Fig. 10.7).

Both of these effects are stabilizing in yaw, as can be seen from Eq. 10.15,

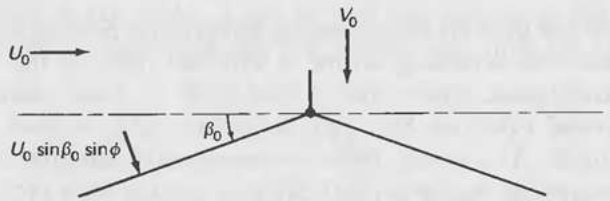

Figure 10.7. Sine input due to crosswind and coning angle β_o.

since they both produce negative $\Delta\beta_{1s}$. It is interesting to examine which stabilizing effects dominate for rotors of various stiffnesses, K. Returning to the cyclic sharing for these effects (Eq. 10.23), the advancing/retreating aerodynamic effect (A_3 term effect) is the only yaw stability effect that exists for a rotor with $K = 1$ (teetering). Likewise, the "coning" effect (A term effect) is the dominant yaw stabilizing term for rotors with $K > 1$ (cantilevered). This explains why a teetering rotor is sluggish in yaw and why a positive coning angle is effective in increasing the yaw stability of hingeless rotors.

The subject of the yaw stability of wind turbines is not yet well understood, as these simple first-order results might lead one to believe. One has only to refer to the field observations at the beginning of this section to verify this. The yawing of a turbine causes large cyclic variation of the angle of attack on the blade, leading to airfoil stall and unsteady aerodynamic effects. These effects can also be caused by turbulence in the wind, leading to observed yawing behavior of turbines that is difficult to predict. It is clear from the development given here that rotor aerodynamics provides the only stabilizing yaw moments and that in order to predict yawing stability properly one must treat the rotor aerodynamics in a more accurate manner than assumed in this first-order development.[1,2,3,8]

10.6 NUMERICAL EXAMPLE

General Description

A calculation of dynamic loading for a representative wind turbine will be presented in this section. Further calculations can be found in Ref. 8 of Chap. 8 and Refs. 4, 5, and 6 of this chapter.

The representative turbine is shown in Fig. 10.8. It is a utility-interconnected machine, with a standard gearbox speed increaser/induction motor drive train. The 40-ft diameter rotor uses a downwind, three-bladed, cantilevered, pitch-controlled hub.

Blade Structural Model

The first step is to reduce the actual rotor blade to the simple hinge-spring structural model that offers the same frequencies of vibration. This representative blade is constructed of fiberglass of a complex geometry (twist and taper) and structure. The blade mass and stiffness distributions in the flapping direction are shown in Figs. 10.9 and 10.10.

Since the principal bending modes are assumed to be uncoupled, the flapping (EI_X) and lead-lag (EI_Y) bending stiffnesses can be considered separately when deriving the hinge-spring models for each one. In this example, the

Figure 10.8. Example wind turbine.

calculation involves only the flapping degree of freedom; that for lead-lag is done in exactly the same way.

The nonrotating natural frequency of vibration for this blade is 2.98 cycles/sec from a bench test.[4] The rotating frequency, which will be higher as a result of centrifugal stiffening, is normally derived from a Myklestad-Prohl computer program (see Ref. 7 in Chap. 7) or from strain-gage test data on the actual operating turbine (e.g., see Ref. 16 in Chap. 11).

Another approximate method, being simple, practical, and available, is used here. The chart estimation method devised by Yntema (Ref. 9 in Chap. 7) allows for linear taper in mass and stiffness distribution. This method is quite accurate for uniform blades or for blades containing isotropic materials.

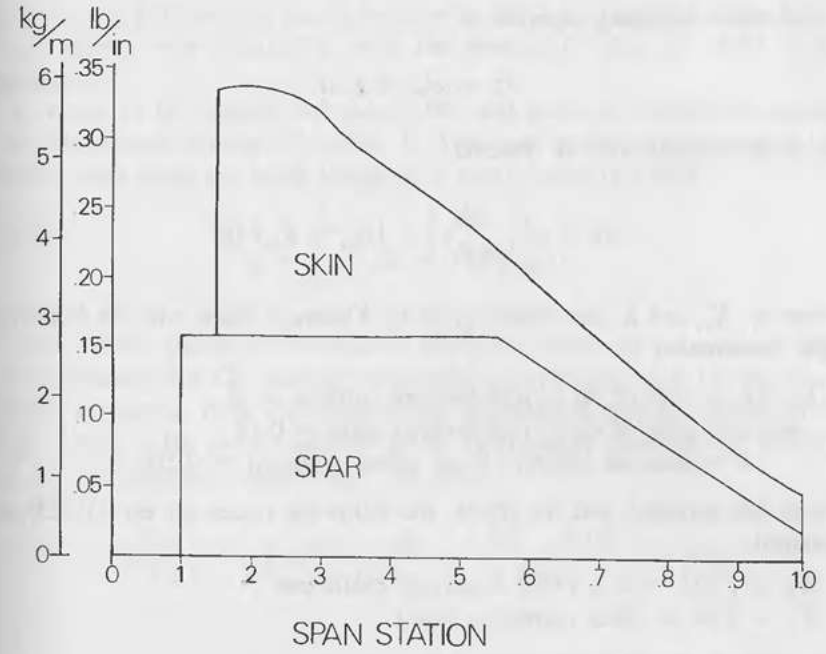

Figure 10.9. Blade mass distribution.

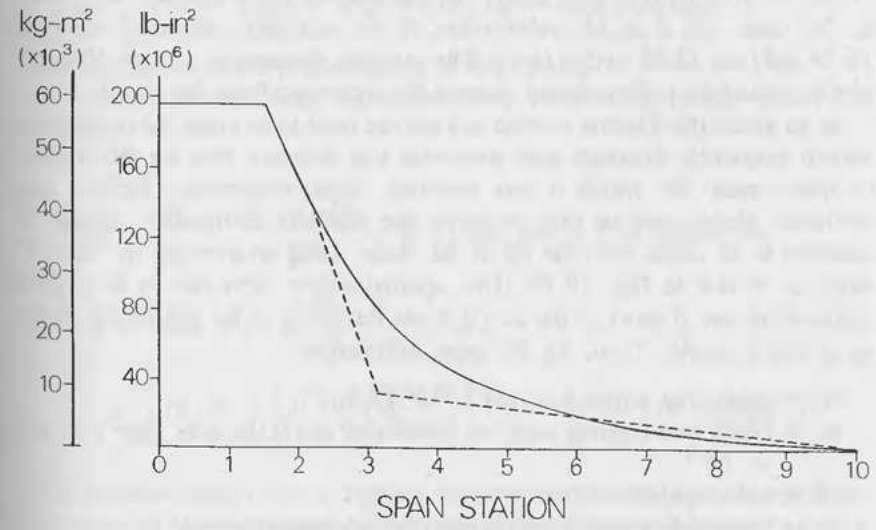

Figure 10.10. Blade stiffness distribution (flapping direction).

The basic frequency equation is

$$\omega_R^2 = \omega_{NR}^2 + K_1\Omega^2 \tag{10.24}$$

or, in the nomenclature of Yntema,

$$\omega_R^2 = a_1^2\left[\frac{EI_o}{m_oL^4}\right] + [K_{o_1} + \overline{K}_{1_1}\bar{e}]\Omega^2 \tag{10.25}$$

where a_1, K_{o_1} and $\overline{K}_{1_1}$ are values given by Yntema's charts with the following input information:

EI_t/EI_o = ratio of tip to root bending stiffness $\simeq$ 0
m_t/m_o = ratio of tip to root running mass = 0.14
$\bar{e}$ = assumed effective hinge offset (Yntema) = 0.250

Using this approach and the charts, the following values for Eq. (10.25) are obtained:

K_{0_1} = 1.235 = zero offset Southwell coefficient
$\overline{K}_{1_1}$ = 1.80 = offset correction factor

The rotating natural frequency is then

$$\omega_R^2 = 352 + 1.685\,\Omega^2 \tag{10.26}$$

Where the first term is the (square of) the nonrotating frequency, ω_{NR}, and, in this case, just a simple substitution of the accurately measured value of 18.73 rad/sec (2.98 cycles/sec). The rotating frequency, ω_R, at 100 rpm (1.67 cycles/sec) is then found to be 3.69 cycles/sec from Eq. 10.26.

As an aside, the Yntema method can also be used to estimate the nonrotating natural frequency, although with somewhat less accuracy than for the uniform or linear beam for which it was intended. From experience, for the very nonlinear blade used in this example, the stiffness distribution should be assumed to be linear from the tip of the blade, using an average, or "faired" slope as shown in Fig. 10.10. This approximation turns out to be a good engineering one if most of the actual blade flexibility is far out on the blade, as in this example. Then, for the input information:

EI_o = blade root stiffness $\simeq 40 \times 10^6$ (lb-in.^{2})
m_o = blade root running mass = 0.340 (lb/in.)/(386.4 in./sec^2) = 8.8×10^{-4}
L = blade radius = 20 ft
a_1 = first mode bending coefficient (from Yntema) = 5.6

the nonrotating frequency, ω_{NR} is found to be 20.72 rad/sec (3.3 cycles/sec), which agrees only reasonably with the measured value of 18.73 (2.98 cycles/sec).

To return to the original discussion, the next piece of information needed is the blade mass moment of inertia, I_b. The usual method for integrating the running mass along the blade length is to apply Simpson's Rule:

$$I_b = \int_0^R r^2\,dm = 134 \text{ slug-ft}^2$$

Three crucial pieces of information about the blade are now known: (1) the nonrotating and (2) rotating frequencies of vibration, and (3) the mass moment of inertia. Now the hinge-spring equivalence relations developed in Chap. 7 (Eq. 7.10) can be used to derive the dynamic blade model. Solving first for the equivalent hinge offset, we have

$$1 + \frac{3}{2}\left(\frac{e}{1-e}\right) = \frac{\omega_R^2 - \omega_{NR}^2}{\Omega^2} = \frac{3.69^2 - 2.98^2}{1.67^2} = 1.698$$

or

$$e = 0.3176$$

and, finally, the flapping hinge equivalent spring is

$$K_\beta = \omega_{NR}^2 I_b = 47{,}000 \text{ ft-lb/rad} = 826 \text{ ft-lb/deg}$$

The equivalent blade model shown in Fig. 10.11.

As a check, the rotating and nonrotating frequencies of the model are calculated:

$$\omega_{NR} = \sqrt{\frac{K}{I_b}} = \sqrt{\frac{47 \times 10^3}{134}} = 18.73 \text{ rad/sec} = 2.98 \text{ cycles/sec}$$

$$\omega_R = \left\{\omega_{NR}^2 + \left[1 + \frac{3}{2}\left(\frac{e}{1-e}\right)\right]\Omega^2\right\}^{1/2}$$

$$= \left\{18.73^2 + \left[1 + \frac{3}{2}\left(\frac{0.3176}{0.6824}\right)\right]10.5^2\right\}^{1/2} = 3.69 \text{ cycles/sec}$$

The nondimensional natural flapping frequency, p, is often used. It represents the number of cycles the blade will vibrate at its own natural frequency during

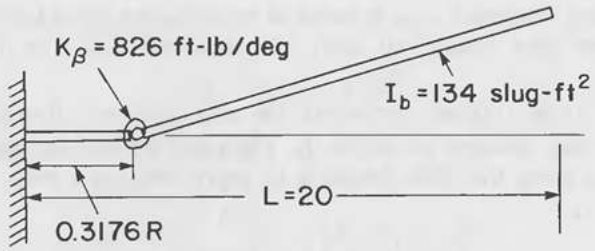

Figure 10.11. Equivalent blade hinge-spring model.

one complete rotation around the hub, or

$$p = \omega_R/\Omega = 2.213\ (1/\text{rev})$$

This parameter has great physical significance. For a fully articulated blade (flap hinge with no spring), $p = 1$; for a very stiff blade, $p = 3$ or higher. The flapping response of the blade to any disturbance is determined by p. That is, the cyclic components of the rotor-tip path plane are determined by the nondimensional flapping frequency. The flap response of an articulated blade ($p = 1$) lags the input by 90°; the flap response of a very stiff blade is much less, on the order of 20° or less of azimuth (see Sec. 9.4).

Rotor Aerodynamics

Some of the dynamic forces on the rotor are caused by aerodynamics (wind gusts, crosswind, wind shear) and some simply by mass and motion (gyroscopic effects, gravity). A convenient way of examining and comparing rotors is to look at the Lock number, the ratio of aerodynamic forces to inertial forces on the rotor:

$$\gamma = \text{Lock number} = \frac{\rho C_{l_\alpha} c R^4}{I_b} = 14.07$$

where ρ is the density, C_{l_α} is the slope of the lift curve (2π for most airfoils), and c is the blade chord (taken at 75-percent span). This representative blade has a γ of 14.07, a high value that indicates the blade is light and will be very active aerodynamically. Short or heavy blades have low γ (of 4 to 8). Composite blades and highly tapered, long blades usually have high γ (of 10 to 15).

The axisymmetric airflow on the rotor and the resulting blade angle of attack (hence lift) distribution are described by the A term from Chap. 9:

$$A = \frac{\lambda}{3} + \frac{\theta_p}{4} = \frac{1}{3}\left[\bar{V}_o - \lambda_i\right] + \frac{\theta_p}{4} \tag{10.27}$$

where:

λ = nondimensional inflow $= \dfrac{1}{\Omega R}(V_o - v_i)$

$\bar{V}_o$ = nondimensional free stream $= V_o/\Omega R$

λ_i = nondimensional induced velocity $= v_i/\Omega R$

θ_p = blade pitch at 3/4 span (NOTE: The pitch angle is measured positive nose up, or away from feather, which is the same as the convention in helicopter analysis.)

In order to use the A term, a way to relate wind speed, tip-speed ratio, induced velocity, and pitch and twist on the rotor must be found. Changing blade twist or pitch will produce a certain induced velocity, v_i, over the disc of the rotor that will depend on the tip-speed ratio. The induced velocity then determines the thrust and power produced by the windmill rotor. To calculate the induced velocity, thrust, and power, a computer strip theory is by far the most accurate method (see Chap. 2 of Part I of this text). The values from the strip theory are simply plugged into Eq. 10.27 and solved for A, for the various operating conditions of interest where dynamic loads and motions must be calculated.

Momentum theory can also be used to relate V_o, tip-speed ratio, pitch, and induced velocity for approximate calculations. Approximate results from momentum theory (derived in Ref. 8 of Chap. 8) are as follows:

Induced velocity:

$$\lambda_i \simeq \frac{C_{l_\alpha}\sigma}{8}\left[1 + \frac{2}{3}\frac{\theta_p}{\bar{V}_o}\right] \tag{10.28}$$

Thrust:

$$C_T \simeq \frac{T}{\frac{1}{2}\rho A V_o^2} \simeq 4\frac{\lambda_i}{\bar{V}_o}\left[1 - \frac{\lambda_i}{\bar{V}_o}\right] \tag{10.29}$$

Power:

$$C_P \simeq \frac{P}{\frac{1}{2}\rho A V_o^3} \simeq 4\frac{\lambda_i}{\bar{V}_o}\left[1 - \frac{\lambda_i}{\bar{V}_o}\right]^2 \qquad (10.30)$$

For this example, a tip-speed ratio of 7.0 and a tip pitch of 2° are chosen:

$C_{l_\alpha} = 2\pi$
$\sigma = 0.031$ = solidity = blade area/disc area
$\theta_p = 2°$
$\bar{V}_o = 0.143$
$\lambda_i = 0.0283$
$C_T = 0.635$
$C_p = 0.509$
Output power = 20650/737.3 = 27.8 kW

Now the A term can be evaluated. Use of the momentum theory to calculate v_i, C_T, and C_p is practical within the normal operating range of the rotor, that is, in the region, $0 \le v_i \le V_o/2$ and $0 \le C_p \le 0.5$. When v_i reaches $V_o/2$, the assumptions governing momentum theory break down. Viscous and turbulent effects take over, and the flow field is no longer represented by smooth streamlines. Once the "turbulent wake state" has been reached, other analysis methods must be used.[7] For this example, $v_i = (0.0283) \times (7) = 0.198\ V_o$.

The input values to the rotor dynamics equations are now complete:

γ = Lock number = 14.07

K = nondimensional flapping frequency = $p^2 = 4.897$

$$B = \text{gravity term} = \frac{gM_b x_g R}{2I_b\Omega^2} = 0.015$$

where, for B:

M_b = 1.38 slugs (from Fig. 10.9)
x_g = nondimensional c.g. of equivalent blade = $r_{cg}/R = 0.5$

The operating "flight" condition chosen for the example case is

$V_o = \Omega R/\text{TSR} = 30$ ft/sec = 20.5 mph
$\Omega = 100$ rpm = 10.47 rad/sec
$\theta_p = 2°$
TSR = 7.0

$$A = \frac{1}{3}[\bar{V}_o - \lambda_i] + \frac{\theta_p}{4} = \frac{1}{3}(0.1429 - 0.0283) + \frac{0.035}{4} = 0.0469$$

$$A_3 = \frac{\lambda}{2} + \frac{2}{3}\theta_p = 0.0807$$

Computed Results

The dynamic solution is given by the harmonic series,

$$\beta = \beta_o + \beta_{1c}\cos\psi + \beta_{1s}\sin\psi$$

The three angles, β_o, β_{1s}, and β_{1c}, are components that fully describe the first-order dynamic response of the rotor to the operating conditions. The angles represent the angular deflection of the hinge-spring model, and hence the tip motion. The blade-root bending moments are simply the elastic restraining force, $K_\beta\beta$. The equations of the blade flapping response—retaining only the terms affected by gravity (B), yaw rate (q), wind shear (K_1), the crosswind (U_o)—are given in Fig. 10.3.

For the example being considered here, the disturbance conditions are a 45° shift in wind direction, a wind shear of 0.25 (corresponding to a severe shear), and a yaw rate of 1/3 rad/sec (19°/sec, corresponding to a "fast yaw drive" condition). Then,

$\bar{U}_o$ = crosswind = $U_o/\Omega R$ = 21.2 fps/209.4 fps = 0.1012
$\bar{q}$ = yaw rate = q/Ω = 0.0318
$\bar{l}$ = nondimensional yaw moment arm = l/R = 0.20
$K_1\bar{V}_o$ = wind shear value = 0.25 (0.1429) = 0.0357

The dynamic response, flapping angles and moments are given in Table 10.2. A quick check can be made on the steady collective term to verify the "reasonableness" of the answer. Using simple momentum theory, the thrust force on one blade is

$$T_{\text{one blade}} = \tfrac{1}{3}\left[C_T\left(\tfrac{1}{2}\rho A V_o^2\right)\right] = 285 \text{ lb}$$

From experience, the steady aerodynamic force is known to act, owing to its triangular spanwise distribution, at about 2/3 radius. Thus, the aerodynamic bending moment is about

$$M_{\text{aero}} \simeq \tfrac{2}{3}R(285) = 3800 \text{ ft-lb}$$

Table 10.2 Rotor Response and Bending Moments.

	COLLECTIVE β_o	CYCLIC TILT FORWARD β_{1c}	CYCLIC TILT LATERAL β_{1s}
AXISYMMETRIC FLOW	3.86° 3220 ft-lb	0	0
GRAVITY	0	−0.025° −21 ft-lb	−0.011° −10 ft-lb
CROSSWIND	0	−0.6136° −513 ft-lb	−0.512° −428 ft-lb
YAW RATE	0	−0.513° −430 ft-lb	−1.054° −880 ft-lb
WIND SHEAR	0	−0.767° −640 ft-lb	−0.346° −290 ft-lb

Balancing part of this moment is the moment resulting from centrifugal force:

$$M_{\text{centrifugal}} = I_b\Omega^2 \sin 3.86° = 980 \text{ ft-lb}$$

The total amount is then roughly

$$M_{\text{total}} \simeq 2820 \text{ ft-lb}$$

This figure compares very favorably with the calculated 3220 ft-lb. Note that the steady moment can be reduced by adding pre-coning to the blade. This produces an additional centrifugal relieving moment, $I_b\Omega^2 \sin \beta_{\text{PRECONE}}$.

To proceed, the flap bending moments vs. rotor azimuth angle are plotted in Fig. 10.12. A very small gravity moment is produced in the flap direction. The major dynamic loads are due to crosswind, wind shear, and yaw rate.

The yaw rate response is primarily a large lateral tilting of the tip-path plane to the right ($-\beta_{1s}$) and a simultaneous, but smaller, backward tilting ($-\beta_{1c}$). Both gyroscopic and aerodynamic terms are at work here. The crosswind response is an almost equal lateral tilting to the right ($-\beta_{1s}$) and backward tilting ($-\beta_{1c}$). The β_{1s} term is the familiar aerodynamic yaw stability term. It works whether the windmill is upwind or downwind of the tower. The wind shear response is primarily backward cyclic. (Table 10.2 reflects the relative importance.)

The "cyclic sharing" for the individual aerodynamic portions of these disturbances (Sec. 10.5) is the same, that is,

$$\frac{\Delta\beta_{1c}}{\Delta\beta_{1s}} = -\frac{\gamma}{8}\left(\frac{1}{K-1}\right) \tag{10.32}$$

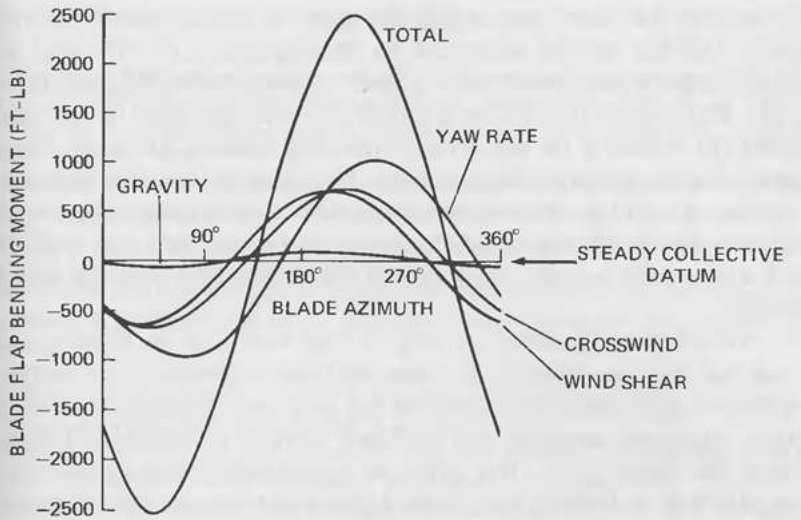

Figure 10.12. Blade dynamic bending moments vs. azimuth angle.

This result reflects that of Sec. 9.4 and relates the fore-and-aft to the lateral tilting of the rotor through the Lock number, γ, and blade stiffness, K, which is simply the square of the nondimensional flapping frequency, p. This says that a stiff rotor (K large) will have predominately lateral tilting to wind gusts and a soft rotor (K small) will have fore-and-aft tilting. The stiff rotor is much more stable in gusty winds, whereas the soft rotor, via its β_{1c} cyclic, produces higher tower moments.

The in-plane moments can be found in a similar manner. They are usually less severe and less interesting than the flapping moments. One exception is the coupled in-plane moment due to flapping motion, as follows:

$$M_{\beta'} = I_b\Omega^2 \frac{d\beta}{d\psi}\Bigg\{\underbrace{2\beta}_{\text{I}} - \underbrace{\frac{\gamma}{2}A_4}_{\text{II}} + \underbrace{\frac{\gamma}{2}\cos\psi\left[\frac{K_1\bar{V}_o}{2} + \frac{\theta_p}{3}(\bar{U}_o + \bar{q}\bar{l})\right] + \frac{\gamma}{2}\sin\left[\frac{\bar{q}}{2} + \frac{2}{3}\beta\,\bar{U}_o\right]}_{\text{III}}\Bigg\} \tag{10.33}$$

where:

$$A_4 = \frac{2}{3}\lambda + \frac{\theta_p}{4}$$

This moment has three parts. The first term (I) is the inertial (Coriolis-induced) lead-lag moment dependent on flapping angle, β. This large term produces large in-plane moments as a direct response to the flapping velocity, $d\beta/d\psi$. Fortunately, this inertial moment is mostly balanced by the second moment (II), which is the aerodynamic relieving moment due to the flapping velocity, the aerodynamic damping term. The effect of these two moments is to produce a lead-lag vibration whenever there is a flapping vibration. The third term (II) is the asymmetric contribution of yaw rate and crosswind, which adds a large periodic component to the aerodynamic relieving term just described.

To evaluate these moments correctly, a time history of the flapping angle, β, and the flapping velocity, $\dot{\beta}$, must be known. However, an "order of magnitude" approximation of the effect can be gained by using the maximum flapping angle and assuming that the blade vibrates at its natural frequency between the limits, $\pm\beta_o$. This gives an approximate vibratory moment of about 500 ft-lb in lead-lag due to the flapping disturbance. This is a sizable vibration to be superimposed on the power component of the steady in-plane moment of 2890 ft-lb. Since the aerodynamic damping is high, one would not expect this coupling moment to occur more than once for each disturbance, and then be quickly dissipated.

The tip-path plane of the equivalent blade is completely determined by angles β_o, β_{1c}, and β_{1s}. The tip motion of an articulated, gimballed, or hinged blade would be exactly this tip-path plane. The flexible cantilevered blade of this example has higher tip deflections, however, since the blade has much more curvature. For comparative studies, the β's previously calculated can be used for deflections, but for tower clearance and other problems a more accurate method is necessary.

Actual tip deflections of the complex blade cannot be predicted by this simple theory since many blade-bending modes and the actual distribution of loading along the blade need to be considered. However, an experimental approach can be used with some success. Knowing that the aerodynamic forces usually resolve around the 2/3-radius of the blade, a static tip deflection can be measured for a known test moment produced by a weight at the 2/3 radius. The equivalent hinge-spring-blade β deflection can be easily calculated. A correction factor can then be computed, relating the actual blade tip deflection from the bench test to the equivalent blade tip deflection from the equations. For the composite blade in this example, this correction factor is

$$\frac{\delta_{\text{measured}}}{\delta_{\text{calculated}}} = \frac{19 \text{ in.}}{10.6 \text{ in.}} = 1.80$$

REFERENCES

1. De Vries, O. Comment on the yaw stability of a horizontal-axis wind turbine at small angles of yaw. *Wind Engineering* 9:1, National Aerospace Laboratory, The Netherlands, 1985.
2. Miller, R. H. On the weathervaning of wind turbines. *Journal of Energy* 3:5, AIAA, New York, Sept–Oct. 1979.
3. Hansen, A. C., and Hausfeld, T. E. Correlation of wind turbine power output with turbulent wind. Paper presented at ASME Conference and Exhibition, Dallas, TX, Feb. 1985.
4. Stoddard, F. S. Dynamic rotor loads of a wind turbine via hand-held calculators. *Journal of Energy* 5:2, AIAA, New York, Mar.–Apr. 1981.
5. Stoddard, F. S. Dynamic loads of a 10-meter diameter wind turbine generator system. Paper presented at American Wind Energy Association National Conference, San Francisco, CA, Apr. 1979.
6. Stoddard, F. S. Structural dynamics considerations in wind turbine rotor design. Paper presented at International Conference on Solar & Wind Energy Applications, China Association for Science and Technology, Beijing, China, Aug. 1985.
7. Stoddard, F. S. Momentum theory and flow states for windmills. *Wind Technology Journal* 1:1, American Wind Energy Association, Washington, D.C., Spring 1977.
8. Bundas, D., and Dugundji, J. Some experiments on yaw stability of wind turbines with various coning angles. NASA CR-168108, MIT ASRL TR-197-2, Massachusetts Institute of Technology, Cambridge, MA, July 1981.
9. Perkins, F. W., and Jones, R. The effect of delta-three on a yawing HAWT blade and on yaw dynamics. Kaman Aerospace Corp. paper presented at 2nd DOE/NASA Wind Turbine Dynamics Workshop, Cleveland, OH, Feb. 1981.

11

INSTABILITIES

11.1 INTRODUCTION

Rotor blades have been viewed up to now, analytically, as having uncoupled degrees of freedom in flapping, lead-lag, and feathering. Including the coupling between the degrees of freedom yields sets of complex equations that depict the coupling "modes." The choice of particular coupling effects to study has largely depended on the observed instabilities and vibration in helicopter rotors.[1] However, the study of the *entire* coupled system with freedom in flapping, lead-lag, and torsion, as well as that obtained in hub flexibility, has received a great amount of analytical and computational effort by rotary-wing dynamicists.[2,3,4,5] Historically, only the important coupling effects have been studied; now, the whole generalized rotor model is usually written in order to search for instabilities depicted by the equations but possibly having no observed experimental occurrence. These general solutions are also quite difficult to interpret.

For wind-turbine blades, the aeroelastic terms differ in many ways from helicopter values. A significant difference is the increased planform area and twist of most wind turbines. Another is the usual aft chordwise location of the blade mass axis. The "global" solution may point out dynamic pitfalls that will have to be avoided in wind turbines, but, at present, much can be learned from test results and observations in combination with this simple linear theoretical approach. One important difference between analytical work on helicopters and wind turbines is the continually changing frequency and torque for wind turbines in operation, and in the case of variable speed turbines, the rotor speed as well.

This chapter describes the four most important aeroelastic instabilities observed and successfully explained with the linear dynamics theory for helicopter rotors: flap-lag instability, pitch-lag instability, classical flutter, and stall flutter[1] (see also Ref. 8 in Chap. 7). The results serve to provide a "feel" for similar aerodynamically induced situations on wind-turbine rotors. A few wind-turbine examples are mentioned. Few studies of the aeroelastic type have been observed and described on wind turbines, however. In each of the cases described here, only the major degrees of freedom are examined,

and only the major aerodynamic and inertial terms are retained. For in-depth analysis, the global formulation—reduced to a convenient computer plot of damping vs. parametric input or to the stability boundaries—is necessary.[13]

11.2 FLAP-LAG INSTABILITY

Flap-lag instability is an unstable oscillation of single rotor blades, consisting of a coupling of flapping motion with lead-lag motion. It is caused by the coupling of the in-plane Coriolis moment caused by flapping velocity, $\dot{\beta}$, and modification of the flapping centrifugal moment by the difference in in-plane blade velocity, $\dot{\zeta}$. No blade pitching motion is required. The instability has been observed on articulated and hingeless helicopter rotors and can be predicted from the blade-flapping and lead-lag equations of motion. This instability[15] is seen on certain hingeless helicopter rotors when operating at high thrust or high pitch levels. The stability boundary found from this analysis is then used as a critical thrust level and pitch, or coning angle, limit. The complete derivation can be found in Refs. 6, 7, 8, and 15.

This is a "mild" instability when compared to the classical flutter of blades but can still build up in a few cycles to destructive levels. Flap-lag instability is most likely to happen if the following conditions exist for the wind-turbine blade:

1. Substantial lead-lag motion, which presumes high load levels
2. Substantial, steady coning angle
3. Substantial flapping motion, which presumes high blade flexibility or high loads
4. Situations in which flap and lead-lag frequency ratios, ω/Ω, are both roughly equal to 1.15.

The additional terms in the flapping and lead-lag equations of motion already derived (Eqs. 9.4 and 9.5) are inertial or aerodynamic. The new inertial term in the flapping equation is the additional Coriolis term, $2I_b\Omega\beta\dot{\zeta}$, caused by lead-lag oscillation, $\dot{\zeta}$. It is the most significant term derived from using the new instantaneous in-plane velocity, $\Omega + \dot{\zeta}$, rather than the assumed constant, Ω, in the derivations. The lead-lag equation of motion contains the Coriolis moment, $-2I_b\Omega\beta\dot{\beta}$, already derived in Sec. 9.5. The aerodynamic moments are also coupled; the tangential velocity at the blade element is now written as

$$U_T = (\Omega + \dot{\zeta})r \tag{11.1}$$

rather than as

$$U_T = \Omega r$$

If the flapping and lead-lag mass moments of inertia are equal ($= I_b$), the coupled equations then become

$$\left(\frac{d^2\beta}{d\psi^2}\right) + \left(\frac{\gamma}{8}\right)\left(\frac{d\beta}{d\psi}\right) + \left(\frac{\omega_\beta}{\Omega}\right)^2\beta + C_{\dot{\zeta}}\left(\frac{d\zeta}{d\psi}\right) = 0 \qquad (11.2)$$

$$F_{\dot{\beta}}\left(\frac{d\beta}{d\psi}\right) + \left(\frac{d^2\zeta}{d\psi^2}\right) + F_{\dot{\zeta}}\left(\frac{d\zeta}{d\psi}\right) + \left(\frac{\omega_\zeta}{\Omega}\right)^2\zeta = 0 \qquad (11.3)$$

Flapping and Lead-lag Coupling by Coriolis Moments

where $C_{\dot{\zeta}}$ is the coupling coefficient due to coning angle; $F_{\dot{\beta}}$ is the in-plane Coriolis moment term coefficient; and $F_{\dot{\zeta}}$ is the damping term, including the artificial inplane damping, $K_{\dot{\zeta}}$—as follows:

$$\begin{aligned} C_{\dot{\zeta}} &= 2\beta_0 - \frac{\gamma}{8}\left[2\theta - \frac{4}{3}\lambda_i\right] \\ F_{\dot{\beta}} &= \frac{\gamma}{8}\left[\theta - \lambda_i\right] - 2\beta_0 \\ F_{\dot{\zeta}} &= \frac{\gamma}{8}\left[K_{\dot{\zeta}} + \frac{2C_D}{C_{l_\alpha}} + \frac{4}{3}\theta\lambda_i\right] \end{aligned} \qquad (11.4)$$

The characteristic equation of this matrix yields a quartic stability criterion, as follows:

$$\begin{vmatrix} \left[\lambda^2 + \frac{\gamma}{8}\lambda + \left(\frac{\omega_\beta}{\Omega}\right)^2\right] & C_{\dot{\zeta}}\lambda \\ F_{\dot{\beta}}\lambda & \left[\lambda^2 + F_{\dot{\zeta}}\lambda + \left(\frac{\omega_\zeta}{\Omega}\right)^2\right] \end{vmatrix} = 0$$

$$\left[\lambda^2 + \frac{\gamma}{8}\lambda + \left(\frac{\omega_\beta}{\Omega}\right)^2\right]\left[\lambda^2 + F_{\dot{\zeta}}\lambda + \left(\frac{\omega_\zeta}{\Omega}\right)^2\right] - C_{\dot{\zeta}}F_{\dot{\beta}}\lambda^2 = 0 \qquad (11.5)$$

or, using Routh's Method,

$$A\lambda^4 + B\lambda^3 + C\lambda^2 + D\lambda + E = 0 \qquad (11.6)$$

where:

$$\begin{aligned} A &= 1 \\ B &= \frac{\gamma}{8} + F_{\dot{\zeta}} \\ C &= \left(\frac{\omega_\beta}{\Omega}\right)^2 + \left(\frac{\omega_\zeta}{\Omega}\right)^2 + \frac{\gamma}{8}F_{\dot{\zeta}} - C_{\dot{\zeta}}F_{\dot{\beta}} \\ D &= \frac{\gamma}{8}\left(\frac{\omega_\zeta}{\Omega}\right)^2 + F_{\dot{\zeta}}\left(\frac{\omega_\beta}{\Omega}\right)^2 \\ E &= \left(\frac{\omega_\beta}{\Omega}\right)^2\left(\frac{\omega_\zeta}{\Omega}\right)^2 \end{aligned} \qquad (11.7)$$

The neutral stability boundary is found by equating Routh's discriminant to zero, or

$$R = BCD - D^2 - B^2E = 0$$

From Ormiston and Hodges,[6] this gives

$$\left[\theta - \frac{4}{3}\lambda_i\right]^2 = \frac{\left(\frac{\omega_\beta}{\Omega}\right)^2}{2\left[\left(\frac{\omega_\beta}{\Omega}\right)^2 - 1\right]\left[2 - \left(\frac{\omega_\beta}{\Omega}\right)^2\right]} \times \left\{\frac{2C_D}{C_{l_\alpha}} + K_{\dot{\zeta}} + \frac{64a\left[\left(\frac{\omega_\beta}{\Omega}\right)^2 - \left(\frac{\omega_\zeta}{\Omega}\right)^2\right]}{\gamma^2(1+a)\left[\left(\frac{\omega_\beta}{\Omega}\right)^2 + a\left(\frac{\omega_\zeta}{\Omega}\right)^2\right]}\right\} \qquad (11.8)$$

and

$$a = K_{\dot{\zeta}} + 2\frac{C_D}{C_{l_\alpha}} + \frac{4}{3}\theta\lambda_i$$

The instability will occur only if

$$1 \le \left(\frac{\omega_\beta}{\Omega}\right)^2 < 2 \qquad \text{and} \qquad \Omega \le \omega_\beta \le \Omega\sqrt{2} \qquad (11.9)$$

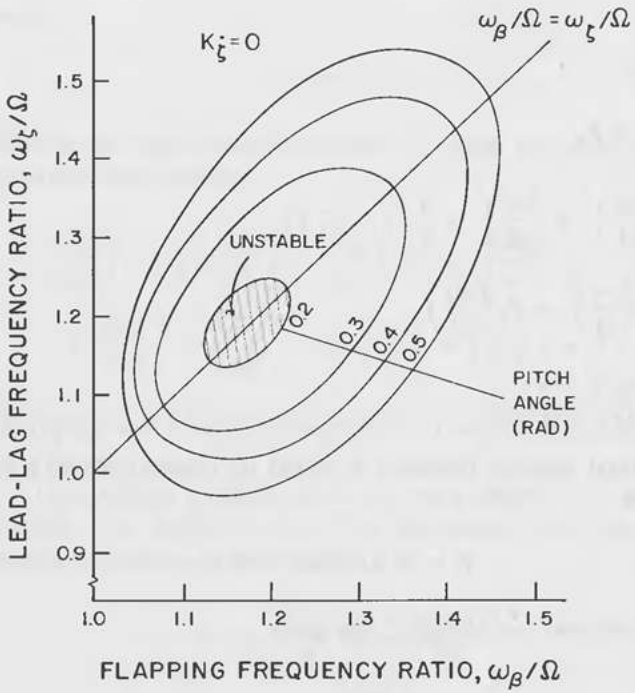

Figure 11.1. Stability boundaries for coupled flap-lag motion. (From Ref. 6.)

This range of flapping frequencies can be normal for helicopter rotors. Small wind turbines without a root hinge have much higher natural frequencies. However, large wind turbines, or turbines with flapping hinges, might fall into this range. Luckily, the instability can be easily solved by adding mechanical damping, K_ζ.

Results for $K_\zeta = 0$ (no mechanical damping) are shown in Fig. 11.1. For the instability to occur at all, flapping frequency, ω_β, must be close to lead-lag frequency, ω_ζ, and be roughly $\sqrt{4/3}\ \Omega$ in value. As pitch angle, θ, is increased, the region of instability grows in size but stays roughly centered on the $\omega_\beta = \omega_\zeta$ locus.

This instability has not been seen on helicopter main rotors, which have lower lag frequencies, but has been observed on tail rotors, where lead-lag frequencies are higher and a large range of pitch is used. The resulting lead-lag frequency of a tail rotor can be close to the flapping frequency, thus allowing the instability mechanism to appear when thrust or pitch angle is high. Wind turbines in general have "supercritical" lag frequencies, i.e., frequencies higher than the shaft speed. This instability, therefore, may be

seen more often with wind turbines, especially at high thrust levels and high pitch angles.

This condition is most likely to occur either when the windmill rotor enters the turbulent wake state and loses its flap damping or when it has been allowed to overspeed and the flap and lag frequency ratios approach $\sqrt{4/3}$. It may be a straightforward design solution to add additional structural or mechanical damping to a case of this sort, but the instability may become quite destructive if unheeded, since the existing aerodynamic in-plane damping, F_ζ, is almost nil.

11.3 PITCH-LAG INSTABILITY

Pitch-lag instability is an oscillation that can occur on an articulated blade when blade pitch angle is artificially coupled to lead-lag motion so as to reinforce a divergent motion. This is usually seen as a complication and aggravation of the flap-lag motion described in the last section. In a hingeless or cantilevered blade, structural torsional coupling, or twisting of the blade due to bending, can also cause pitch-lag instability. The instability always occurs at a frequency close to the lead-lag frequency.[1,8,9]

If structural deflection is the cause of this vibration, employing "matched stiffness" in the root structure of the blade can solve the problem. Briefly, matched stiffness can be described in this way: A blade under aerodynamic loading, especially a twisted one, will deflect in lead-lag as well as in flapping. The resulting offset of the aerodynamic axis (locus of action of all aerodynamic forces) will cause torsional moments, and hence pitch changes, at the blade root from both the flap deflection and the lead-lag deflection. The blade, by virtue of its airfoil shape, will not have equal structural stiffness in lead-lag and in flapping (i.e., $EI_x \neq EI_y$), so that the two induced moments, in general, will not cancel out. "Matched stiffness" is a design attempt to make the induced pitch moments cancel by making the two root stiffnesses equal, thereby making the induced aeroelastic torque at the root zero and the resulting pitch deflection also zero. A usual practice of the helicopter industry is to make the blade-root attachment softer than the actual blade in both flap and lead-lag by introducing a "dog bone" element (see Ref. 8 in Chap. 7). The flapping frequency is determined largely by centrifugal forces, and the lead-lag frequency by blade structure and root attachment. Thus, the induced torsional moment can be zeroed by judicious design. This approach may be useful for wind turbines if the bending deflections of blades become large enough to cause unwanted pitch changes, and if lead-lag frequencies are low. These conditions are most likely for fiberglass (glass-reinforced plastic) or wood blades that have shown high deflections in practice; they also have the potential for variable stiffness design.

In general, the torsional deflection can be written as follows[8]:

$$\Delta\theta(\psi) = \zeta(\psi)\,\beta(\psi)\left[\frac{1 - (\omega_\beta/\Omega)^2 + (\omega_\zeta/\Omega)^2}{(\omega_\theta/\Omega)^2}\right]\left[\frac{I_\beta}{I_\theta}\right] \quad (11.10)$$

From this equation, the torsional deflection can be made to be zero, no matter what the instantaneous flapping or lagging angles are, by requiring:

$$1 - \left(\frac{\omega_\beta}{\Omega}\right)^2 + \left(\frac{\omega_\zeta}{\Omega}\right)^2 = 0 \quad (11.11)$$

Thus, coupled blade twist can be largely eliminated by suitable choice of lag frequency (i.e., choice of root lag stiffness via the "dog bone" element).

Now, the torsional coupling terms of the above expression can be calculated and then added to the two coupled equations in flapping and lead-lag of the previous section, Eqs. 11.2 and 11.3. Doing so will modify the stability criterion developed before. The new approximate stability criterion for hingeless blades is then[9]:

$$F_\zeta + \left(\frac{2K_\zeta}{1 - (\beta_o/\theta_o)K_\beta}\right)\left(\frac{\beta_o^2}{\theta_o}\right)\Omega I_\zeta > 0 \quad (11.12)$$

Hingeless Blade Stability Criterion

The quantities, K_β and K_ζ are stiffness coupling coefficients derived from the torsional deflection equation, Eq. 11.10, as follows:

$$\Delta\theta = \left(\frac{1 - (\omega_\beta/\Omega)^2 + (\omega_\zeta/\Omega)^2}{(\omega_\theta/\Omega)^2}\right)\left(\frac{I_\beta}{I_\theta}\right)(\beta_o\zeta + \zeta_o\beta) \quad (11.13)$$

and

$$\Delta\theta = K_\beta\beta + K_\zeta\zeta \quad (11.14)$$

where:

F_ζ = artificial mechanical lead-lag damping
I_ζ = lead-lag moment of inertia
I_β = flapping mass moment of inertia
I_θ = feathering mass moment of inertia
β_o = coning or equilibrium flapping angle
θ_o = equilibrium pitch angle

For articulated blades, the stability criterion is

$$F_\zeta + \left[\frac{2\tan\alpha_2}{1 - (\beta_o/\theta_o)\tan\delta_3}\right]\left(\frac{\beta_o^2}{\theta_o}\right)\Omega I_\zeta > 0 \quad (11.15)$$

where

α_2 = lag hinge tilt, to cause pitch change due to lagging = $\Delta\theta/\zeta$
δ_3 = flapping hinge tilt, to cause pitch change due to flapping = $\Delta\theta/\beta$
θ_o = equilibrium pitch angle

The stability of both follows roughly the results of the previous section. For hingeless wind-turbine blades, root torsional coupling is not likely to cause pitch-lag instability unless the lag stiffness is very low, the blade is highly twisted, or the coning angle, β_o, is very high. Each case must be checked on its own.

11.4 PITCH-FLAP FLUTTER AND DIVERGENCE

The classical flutter and divergence of aircraft wings appear in a rotor blade as instabilities destructively combining torsional oscillation with flapping oscillation for flutter, or in the case of divergence, a simple twisting off of the blade. The mechanism is that, as the blade flaps, either elastically or via a hinge, the inertial forces act at the center of gravity or mass axis of the blade, and the aerodynamic forces act at the aerodynamic center of the blade (quarterchord). If these blade axes are not coincident ("mass balanced"), both inertial and aerodynamic pitching moments are introduced. Since these moments can be proportional to acceleration, velocity, or displacement, they have different phase angles and thus may lead to destructive interference. The destructive oscillation is called *flutter*.

Static divergence is a much simpler motion, which only rarely occurs in aircraft models and only then when the torsional stiffness is very small. In this instability, the blade c.g. is so far aft on the chordline and the pitch stiffness so small that the nose-up, centrifugal twisting moment in flapping causes a steady increase in angle of attack that is sufficient to drive the blade through stall on one cycle. This would be observed in a wind turbine in the event of a control-system (pitch-link) failure, which would reduce the torsional stiffness to practically zero. This, combined with an aft blade c.g. (mass axis) and flap motion, would cause the blade to "pop" to a high, nose-up pitch limit, stall out, and then return to flat, nose-down pitch when the one-per-rev gravity moment changed direction. This would be an example of a "limit cycle" vibration on the wind turbine.

Flutter on a blade might also be seen as a "limit cycle" oscillation. If flutter amplitudes are sufficient to drive the blade angle of attack through stall, the nature of the aerodynamic force will change rapidly; the simple linear, small-displacement theories used here no longer apply, and unsteady aerodynamics effects dominate the motion. These nonlinear effects are usually stabilizing, causing oscillations to become self-limiting, or "limit cycles." One example is classical "stall flutter," which will be discussed in a later section. An excellent and thorough treatment of the state of the art of dynamic stall can be found in Carr et al., [20] who discuss the applicable and observed physical processes of stall on rotor blades.

The flutter equations will not be derived here. They are found by adding the appropriate inertial and aerodynamic coupling terms to the two equations of motion already developed in Chap. 9—Eq. 9.4 for flapping and Eq. 9.57 for feathering—and also adding any other complicating geometric factors, such as steady precone angle, β_o, and pitch-flap coupling, δ_3. Flutter of rotor blades has been extensively studied in the literature; a summary follows:

Miller and Ellis[2] assumed articulated blades and have provided the most complete physical derivation

Ham assumed articulated blades and derived the general equations for unsteady aerodynamics, including steady coning, β_o (see Ref. 7 in Chap. 8)

Bramwell assumed the flexural (elastic) axis to be coincident with the aerodynamic center (see Ref. 8 in Chap. 7)

Loewy[1] has provided an excellent general discussion, defined the lift deficiency function, and described wake-induced flutter and pitch-flap kinematic coupling

Currin and Stoddard[14] have modified the equations for hingeless wind-turbine blades and included δ_3 coupling; steady coning angle, β_o; and quasi-steady aerodynamics

Miller and Chopra, et al.[13] derived the complete three-degree-of-freedom (pitch, flap, lag) equations in global generality

Johnson[15] has provided the most complete literature survey and flutter analysis history and description presently available

The simplest form of the flutter equations is derived from the simple feathering equation of motion (Eq. 9.57) and the flapping equation of motion (Eq. 9.4). Following Ref. 8 of Chap. 7 for a straight, untwisted, uniform blade with the elastic axis coincident with the aerodynamic axis ($Y_a = 0$) and all perturbations (gravity, yaw rate, etc.) equal to zero, these equations can be written as follows:

Feathering equation:

$$\theta'' + \left(\frac{\gamma}{32}\right)\left(\frac{c}{R}\right)^2\left(\frac{I_b}{I_f}\right)\theta' + \left(\frac{\omega_\theta}{\Omega}\right)^2\theta - \frac{3}{2}\left(\frac{Y_I}{R}\right)\left(\frac{I_b}{I_f}\right)(\beta'' + \beta) + \left(\frac{\gamma}{32}\right)\left(\frac{c}{R}\right)^2\left(\frac{I_b}{I_f}\right)\beta = 0 \tag{11.16}$$

Flapping equation:

$$\beta'' + \left(\frac{\gamma}{8}\right)\beta' + \left(\frac{\omega_\beta}{\Omega}\right)^2\beta - \left(\frac{\gamma}{8}\right)\theta = 0 \tag{11.17}$$

where the mass axis offset inertia term is

$$I_R = \int_o^R Y_I r\, dm = Y_I\left(\frac{M_b R}{2}\right)$$

The inertia term, β'', is included in order to account for the new degree of freedom of the flutter mechanism. In like manner, one could also include a θ'' term, but it is usually very small.

To proceed, the (approximate) torsional aerodynamic moment was evaluated by Bramwell (see Ref. 8 in Chap. 7) and appears as the θ' term in the feathering equation. Also, it has been assumed that $I_f + I_I \simeq I_f$. The simplified equations are then as follows:

Feathering equation:

$$\theta'' + \left(\frac{\gamma}{32}\right)\left(\frac{c}{R}\right)^2\left(\frac{I_b}{I_f}\right)\theta' + \left(\frac{\omega_\theta}{\Omega}\right)^2\theta - \frac{3}{2}\left(\frac{Y_I}{R}\right)\left(\frac{I_b}{I_f}\right)(\beta'' + \beta) = 0 \tag{11.18}$$

Flapping equation:

$$\beta'' + \left(\frac{\gamma}{8}\right)\beta' + \left(\frac{\omega_\beta}{\Omega}\right)^2\beta - \left(\frac{\gamma}{8}\right)\theta = 0$$

As in the previous sections, dynamic stability of these coupled equations can be studied in the classical way. Assume a complex solution, $\lambda = (\sigma/\Omega) + i(\omega/\Omega)$, where σ is the phase and ω, the frequency of the flutter. Substituting the complex form of the two variables back into the differential equations,

we have

$$\beta = \bar{\beta} e^{\lambda \Omega t}$$
$$\theta = \bar{\theta} e^{\lambda \Omega t}$$

which gives

$$\begin{bmatrix} (a_1\lambda^2 + b_1\lambda + c_1) & (d_1\lambda^2 + e_1\lambda + f_1) \\ (a_2{}^2 + b_2\lambda + c_2) & (d_2\lambda^2 + e_2\lambda + f_2) \end{bmatrix} \begin{Bmatrix} \bar{\beta} \\ \bar{\theta} \end{Bmatrix} = 0 \tag{11.19}$$

This yields the stability matrix for flutter:

$$\begin{vmatrix} \left[\lambda^2 + \left(\frac{\gamma}{32}\right)\left(\frac{c}{R}\right)^2\left(\frac{I_b}{I_f}\right)\lambda + \left(\frac{\omega_\theta}{\Omega}\right)^2\right] & \left[-\frac{3}{2}\left(\frac{Y_I}{R}\right)\left(\frac{I_b}{I_f}\right)(\lambda^2 + \lambda)\right] \\ \left[\lambda^2 + \left(\frac{\gamma}{8}\right)\lambda + \left(\frac{\omega_\beta}{\Omega}\right)^2\right] & \left[-\frac{\gamma}{8}\right] \end{vmatrix} = 0$$

which in turn gives a quartic stability equation that is the characteristic equation for the classical flutter of a uniform blade:

$$A\lambda^4 + B\lambda^3 + C\lambda^2 + D\lambda + E = 0 \tag{11.20}$$

where:

$$A = 1$$
$$B = \frac{\gamma}{8}\left[1 + \left(\frac{I_b}{4I_f}\right)\left(\frac{c}{R}\right)^2\right]$$
$$C = \left(\frac{\omega_\theta}{\Omega}\right)^2 + \left(\frac{\omega_\beta}{\Omega}\right)^2 - \left(\frac{3\gamma}{16}\right)\left(\frac{Y_I}{R}\right)\left(\frac{I_b}{I_f}\right) + \left(\frac{\gamma^2}{252}\right)\left(\frac{c}{R}\right)^2\left(\frac{I_b}{I_f}\right)$$
$$D = \frac{\gamma}{8}\left[\left(\frac{\omega_\theta}{\Omega}\right)^2 + \frac{1}{4}\left(\frac{I_b}{I_f}\right)\left(\frac{c}{R}\right)^2\right]$$
$$E = \left(\frac{\omega_\theta}{\Omega}\right)^2\left(\frac{\omega_\beta}{\Omega}\right)^2 - \left(\frac{3\gamma}{16}\right)\left(\frac{Y_I}{R}\right)\left(\frac{I_b}{I_f}\right)$$

It is interesting to compare these stability coefficients with the flap-lag coefficients of Sec. 11.2. In general, for all cases of flutter, Eq. 11.20 will have two pairs of complex conjugate roots corresponding to two different flutter frequencies. Flutter modes shapes are found by simple substitution back into the matrix of Eq. 11.19.

The coefficients of Eq. 11.20 contain the blade frequency in the form of

nondimensional frequencies in flapping, ω_β/Ω and feathering, ω_θ/Ω. The pitch change mechanism is usually the most elastic element in the torsion degree of freedom for a pitch-controlled blade. The basic structural torsional frequency is usually the most elastic element in torsion for a fixed-pitch, "stall-controlled" blade. The mass axis offset from the elastic axis (and in this simple example also the aerodynamic axis), Y_I, measured positive aft, and the blade mass moments of inertia in feathering and flapping, I_f and I_b, are important variables, as is the rotor speed, Ω. The "flutter speed" is defined as the Ω, or rpm, at which the dimensionless frequency, ω_θ/Ω, is on the stability boundary and thus flutters.

The divergence boundary for a simple blade is given simply by the last term's being equal to zero, $E = 0$, or

$$\left(\frac{\omega_\theta}{\Omega}\right)^2 = \frac{3}{16}\gamma\left(\frac{I_b}{I_f}\right)\left(\frac{Y_I}{R}\right)\left(\frac{1}{(\omega_\beta/\Omega)^2}\right) \tag{11.21}$$

Simple Blade Divergence Boundary

To solve the quartic stability equation, Eq. 11.20, for the flutter boundary, the following general procedure is used:

1. Substitute the known blade and rotor quantities in stability coefficients A through E. Normally, all quantities are known or estimated during the design process, except the feathering frequency, ω_θ. In the case of an existing prototype rotor, all the quantities can be measured.
2. Assume that $\sigma = 0$ and substitute the imaginary part of the complex solution, $i(\omega/\Omega)$, into the characteristic equations.
3. Separate the real and imaginary portions of the resulting equations.
4. Assume a value of flutter frequency, ω/Ω, and solve the equations for the feathering frequency, ω_θ/Ω.
5. A plot of the flutter boundary can then be made, with torsional stiffness, ω_θ^2, vs. mass axis offset, Y_I/c, as in Fig. 11.2.

For this simple example, the preceding procedure yields the following simple analytical flutter boundary:

$$\left(\frac{\omega_\theta}{\Omega}\right)^2 = \left(\frac{\omega}{\Omega}\right)^2 + \frac{3}{16}\left(\frac{\omega^2 - 1}{\Omega^2}\right)c^2\left(\frac{I_b}{I_f}\right)$$
$$\left(\frac{Y_I}{c}\right) = \frac{4}{3}\left(\frac{1}{\gamma}\right)\left(\frac{c}{R}\right)\left\{\left(\frac{\omega}{\Omega}\right)^2 - \left(\frac{\omega_\beta}{\Omega}\right)^2 + \left(\frac{\gamma^2}{64}\right)\left(\frac{\omega^2}{\omega^2 - 1}\right)\right\} \tag{11.22}$$

Simple Blade Flutter Boundary

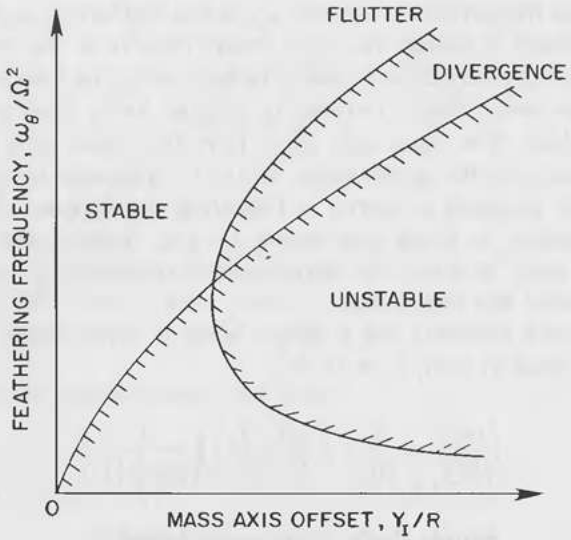

Figure 11.2. Stability boundaries: Classical flutter and divergence.

In Fig. 11.2, a particular value of mass axis offset results in a minimum acceptable torsional stiffness ω_θ/Ω. For a mass axis on, or ahead of, the aerodynamic center (negative Y_I) divergence and flutter will not occur. This is termed a "mass balanced" blade. The "flutter speed" of the blade is given by the overspeed rpm (Ω) at which dimensionless torsional frequency (ω_θ/Ω) is reduced to the flutter boundary and pitch-flap flutter can occur. As before, this instability would not occur on a mass-balanced blade.

Wind-turbine blades are usually not mass-balanced to avoid flutter because blade torsional stiffness is usually very high with fixed-pitch rotors and equilibrium overspeeds (tip speeds) are usually very low on pitch-controlled rotors. Flutter however, has been known to occur on small wind turbines.[17,19]

In the case of a fixed pitch, but torsionally soft, blade, like a uniform fiberglass pultrusion, the section torsional stiffness is low, and this can result in the tip of the blade experiencing structural flutter in overspeed when the tip speed is high. The rotor in overspeed, when a certain rpm is reached, is heard to produce a loud "buzzing" sound, which is simply the outboard blade section vibrating at the flutter frequency. This condition obviously causes rapid build-up of high-strain/high-cycle events that lead to rapid blade fatigue degradation. The solution, as achieved in the Wind Power Systems "StormMaster" turbine (see Ref. 3 in Chap. 9) is to add a tip weight forward of the leading edge, which moves the aft mass axis offset at the blade tip forward (see Fig. 11.3).

Another observed wind-turbine rotor flutter was caused by deliberate control

Figure 11.3. StormMaster anti-flutter tip.

system design, which required the working pitch-control mechanism to be very soft in blade pitch or torsion. This is the passive pitch-control strategy (U.S. Pat. No. 4,435,646) used by NorthWind Power Company on their 10-meter diameter L916 turbine and the prototype preceding it.[14] In this case, the effective ω_θ was zero, and the aerodynamic axis was offset 0.18 meters aft of the control axis. A strip chart recording of the flutter is shown in Fig. 11.4 for the small scale prototype rotor.[16] The traces are root pitch vs. time for each of the two blades in the teetering rotor system. The flutter frequency is seen to be 2.86 Hz, and the amplitude to be over 25 degrees in pitch. Both blades flutter and are 180 degrees out of phase with each other, since it is a teetering rotor. In this case, the flutter was expected and was solved by the addition of an appropriate amount of damping in pitch, which was determined from the simple linearized flutter equations. The flutter boundary can be seen in Fig. 11.5, which shows the necessary additional pitch damping required vs. blade flapping frequency for the numerical condition indicated.

It should be noted that the flutter is very sensitive to flap frequency and that a slight increase in flap stiffness results in a much smaller requirement for pitch damping. When damping was added, this rotor responded according to the theory. The effects of coning angle, β_o, pitch-flap coupling, δ_3, and mass axis offset, Y_I, where also accounted for with this simple flutter theory.

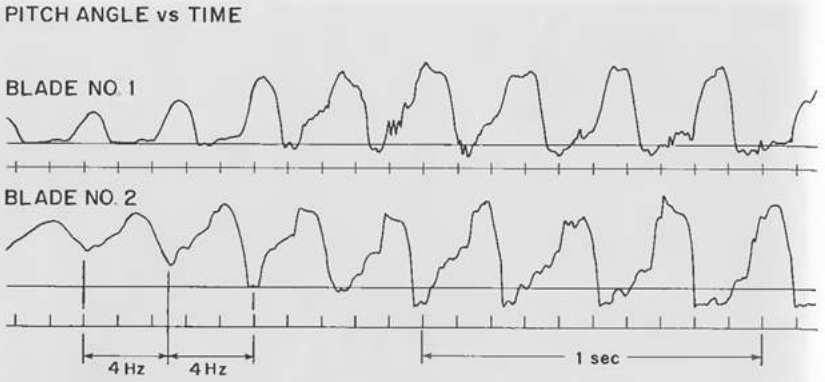

Figure 11.4. NorthWind half-scale flutter. (From Ref. 14.)

11.5 GENERAL FORMULATION OF FLUTTER

Summary of Flutter Forms

In the interest of completeness, this section lists the general flutter forms and coefficients found in the literature cited in the last section.

The equations of coupled motion are as follows:

Feathering equation:

$$M_{\ddot{\theta}/\Omega^2}\left(\frac{\ddot{\theta}}{\Omega^2}\right) + M_{\dot{\theta}/\Omega}\left(\frac{\dot{\theta}}{\Omega}\right) + M_\theta\theta + M_{\ddot{\beta}/\Omega^2}\left(\frac{\ddot{\beta}}{\Omega^2}\right) + M_{\dot{\beta}/\Omega}\left(\frac{\dot{\beta}}{\Omega}\right) + M_\beta\beta = 0 \tag{11.23}$$

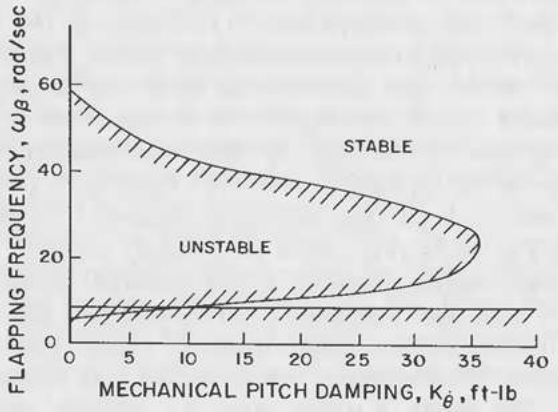

Figure 11.5. NorthWind half-scale flutter boundary. (From Ref. 14.)

Flapping equation:

$$m_{\ddot{\theta}/\Omega^2}\left(\frac{\ddot{\theta}}{\Omega^2}\right) + m_{\dot{\theta}/\Omega}\left(\frac{\dot{\theta}}{\Omega}\right) + m_\theta\theta + m_{\ddot{\beta}/\Omega^2}\left(\frac{\ddot{\beta}}{\Omega^2}\right) + m_{\dot{\beta}/\Omega}\left(\frac{\dot{\beta}}{\Omega}\right) + m_\beta\beta = 0 \tag{11.24}$$

where the basic pitching moments are as follows:

$M_{\ddot{\theta}/\Omega^2}$ = feathering moment of inertia dynamic term
$M_{\dot{\theta}/\Omega}$ = aerodynamic plus mechanical pitch damping
M_θ = pitch natural frequency, centrifugal restoring moment ("tennis racket" offset), and aerodynamic moment due to the center of pressure being off the pitching axis

The pitching moments arising from flapping are

$M_{\ddot{\beta}/\Omega^2}$ = term due to product of inertia about the pitch-flap axis I_R
$M_{\dot{\beta}/\Omega}$ = term due to lift offset from pitching axis (control axis)
M_β = term due to action of centrifugal forces acting on masses that are, on average, off both the flap and feathering axes

The flapping moments arising from feathering are as follows:

$m_{\ddot{\theta}/\Omega^2}$ = term due to product of inertia
$m_{\dot{\theta}/\Omega}$ = aerodynamic flapping moment due to blade pitch (in a quasi-steady sense, this moment is equivalent to airfoil camber)
m_θ = centrifugal flapping moment due to product of inertia and aerodynamic contribution due to lift causing a flapping moment

and the basic flapping moments are as follows:

$m_{\ddot{\beta}/\Omega^2}$ = unity
$m_{\dot{\beta}/\Omega}$ = aerodynamic and mechanical flap damping
m_β = flap natural frequency and centrifugal rotating moment; can also include the gravity excitation for the turbine, $(G/\Omega^2)\cos\psi$.

The coefficients for various complicating geometries and coupling are listed in Table 11.1.

Offsets

Usually for a wind turbine, the feathering axis, elastic axis, and control axis are all the same, as is identically true for a fixed pitch rotor and a rotor with a "soft" pitch-change mechanism. Strictly speaking, the elastic axis depends on blade-section structural properties, but when the pitch-change mechanism

Table 11.1. Coefficients of the Flutter Equations of Motion.

	Includes: X_a, X_l,$\bar{C}(k)$, K_θ, K_β	Includes: X_a, X_l, β_o	Includes: X_a, X_l, $\bar{C}(k)$, δ_3
	Flapping Equation		
m_{β/Ω^2}	1	1	1
$m_{\beta/\Omega}$	$\frac{\gamma}{8}\bar{C}(k) + \frac{\gamma}{8}k_\beta$	$\frac{\gamma}{8}$	$\frac{1}{I'}\left\{\frac{\gamma}{8}\bar{C}(k) - \left(\frac{\gamma}{6}\right)\left[\frac{3}{4}\left(\frac{c}{R}\right) - \left(\frac{X_a}{R}\right)\bar{C}(k)\tan\delta_3\right]\right\}$
m_β	$\left(\frac{\omega_\beta}{\Omega}\right)^2$	$\left(\frac{\omega_\beta}{\Omega}\right)^2 + \left(\frac{\gamma}{6}\right)\lambda\beta_o - 2\beta_o^2$	$\frac{1}{I'}\left\{\left(\frac{\omega_\beta}{\Omega}\right)^2 + (I_X - \frac{\gamma}{8})\tan\delta_3\right\}$
m_{θ/Ω^2}	$-I_X$	$-I_X(1 - \frac{1}{2}\beta_o^2)$	$-\frac{I_X}{I'}$
$m_{\theta/\Omega}$	$-\frac{\gamma}{6}\left[\frac{3}{4}\left(\frac{c}{R}\right) - \left(\frac{X_a}{R}\right)\bar{C}(k)\right]$	$-2\beta_o^2 - \frac{\gamma}{6}\left\{\left[\frac{3}{4}\left(\frac{c}{R}\right) - \frac{X_a}{R}\right]\left[1 - \frac{1}{2}\beta_o^2\right] - \lambda\beta_o\right\}$	$-\frac{1}{I'}\left(\frac{\gamma}{6}\right)\left[\frac{3}{4}\left(\frac{c}{R}\right) - \left(\frac{X_a}{R}\right)\bar{C}(k)\right]$
m_θ	$\frac{\gamma}{8}\bar{C}(k) - I_X$	$\frac{\gamma}{8} - I_X\left[1 - \frac{1}{2}\beta_o^2\right]$	$\frac{1}{I'}\left[\frac{\gamma}{8}\bar{C}(k) - I_X\right]$
	Feathering Equation		
M_{β/Ω^2}	$-I_X$	$-I_X[1 - \frac{1}{2}\beta_o^2]$	$-[I_X + I\tan\delta_3]$
$M_{\beta/\Omega}$	$-\frac{\gamma}{6}\left(\frac{X_a}{R}\right)\bar{C}(k)$	$\frac{\gamma}{2}\left\{-\frac{X_a}{3R} - \frac{2}{3}\lambda\beta_o + \frac{1}{4}\beta_o\theta_o\right\} - 2\beta_o^2$	$-\frac{\gamma}{6}\left(\frac{X_a}{R}\right)\bar{C}(k)$ $-\frac{\gamma}{8}\left\{\frac{c}{2R} - \left(\frac{X_a}{R}\right)\bar{C}(k)\right\}\left\{\frac{c}{R} - \left(\frac{2X_a}{R}\right)\bar{C}(k)\right\}\tan\delta_3$
M_β	$-I_X$	$\frac{\gamma}{2}\left[\frac{1}{4}\frac{C_{D_o}}{C_{l_\alpha}} + \lambda\left(\frac{\theta_o}{3} - \frac{\lambda}{2}\right)\right]$ $-I_X[1 - \frac{1}{2}\beta_o^2] - \frac{\gamma}{4}\left(\frac{X_a}{R}\right)\lambda\beta_o$	$\left\{\frac{\gamma}{6}\left(\frac{X_a}{R}\right) - I\left[\left(\frac{\omega_\theta}{\Omega}\right)^2 - 1\right]\right\}\tan\delta_3 - I_X$
M_{θ/Ω^2}	I	$I + \beta_o^2$	I
$M_{\theta/\Omega}$	$\frac{\gamma}{16}\left[\frac{c}{R} - 4\left(\frac{X_a}{R}\right)\bar{C}(k)\right]$ $\times\left[\frac{c}{2R} - \frac{X_a}{R}\right] + \frac{\gamma}{8}K_\theta$	$-\frac{\gamma}{2}\left\{\left[\frac{1}{8}\left(\frac{c}{R}\right) - \frac{1}{2}\left(\frac{X_a}{R}\right)\right]\left[\frac{X_a}{R} - \frac{1}{2}\left(\frac{c}{R}\right)\right]\right\}$ $-\frac{\gamma}{2}\left[\left(\frac{X_a}{R} - \frac{c}{2R}\right)\left(\frac{1}{3}\theta_o\beta_o - \lambda\beta_o\right)\right]$	$\frac{\lambda}{16}\left[\frac{c}{R} - 4\frac{X_a}{R}\bar{C}(k)\right]\left[\frac{c}{2R} - \frac{X_a}{R}\right]$
M_θ	$-\frac{\gamma}{6}\left(\frac{X_a}{R}\right)\bar{C}(k) + I\left[\left(\frac{\omega_\theta}{\Omega}\right)^2 + 1\right]$	$\frac{\gamma}{2}\left\{-\left(\frac{X_a}{3R}\right)\left(1 + \frac{C_{D_o}}{C_{l_\alpha}}\right) - \frac{2}{3}\lambda\beta_o - \frac{X_a}{R}\lambda\left(\frac{\theta_o}{2} - \lambda\right) + \frac{1}{4}\beta_o\theta_o\right\}$ $+ I\left[\left(\frac{\omega_\theta}{\Omega}\right)^2 + 1 - \beta_o^2\right]$	$-\frac{\lambda}{6}\left(\frac{X_a}{R}\right)\bar{C}(k) + I\left[\left(\frac{\omega_\theta}{\Omega}\right)^2 + 1\right]$

is more elastic than the blade, the root torsion term dominates the pitch. Parameters are as follows:

I_b = blade mass moment of inertia in flapping = $\int_o^R r^2\, dm$

I_f = blade mass moment of inertia in feathering = $\int_o^R X_I^2 m\, dr$

I_R = product of inertia = $\int_o^R mX_I r\, dr$

$I_X = I_R/I_b$

$I = I_f/I_b$

X_a = aerodynamic center offset from elastic axis (aft) $\equiv Y_a$

X_I = mass axis offset from elastic axis (aft) $\equiv Y_I$

Pitch-Flap Coupling

To determine the effect of pitch-flap coupling, δ_3, a substitution is made in the algebraic analysis (see Ref. 9 in Chap. 10), as follows:

$$\theta \rightarrow \theta - \tan \delta_3[\beta_o + \beta] \tag{11.25}$$

Thus, for δ_3 positive, pitch angle θ is replaced with the above correction factor, i.e., is configured so as to reduce the pitch with increasing β.

Unsteady Aerodynamics and Wake Vorticity

Historically, unsteady aerodynamics effects are accounted for in the $\overline{C}(k)$ term, known as *Theodorsen's Function*, which is a complex function of the reduced frequency and represents the lag and reduction in lift of the airfoil resulting from the trailing vorticities shed by the blade[2]:

$$\overline{C}(k) = F(k) + iG(k) \tag{11.26}$$

Theodorsen's Function

where the reduced frequency, k, is

$$k = \frac{\omega b}{\Omega R}$$

and

$b = c/2$ (such values for most rotors are taken at the $\frac{3}{4}$ span)

ω = airfoil pitching frequency

ΩR = tip speed

For most realistic wind-turbine cases, the blade shed vorticity is weak, and $\overline{C}(k)$ can be taken as 1.0. In helicopter rotors, the returning wake vorticity can cause wake-induced flutter if the inflow is small, and the trailing vortices build up under the rotor.[15] This is an unlikely occurrence for a wind turbine since the wake is rapidly expanding when the turbine rotor is loaded and the wake vorticity is quickly convected downwind.

The characteristic equation for Routh's method is

$$A\lambda^4 + B\lambda^3 + C\lambda^2 + D\lambda + E = 0 \tag{11.27}$$

and the stability coefficients, in general form, are as follows:

$$A = M_{\ddot{\theta}/\Omega^2} - m_{\dot{\theta}/\Omega^2} M_{\ddot{\beta}/\Omega^2}$$

$$B = M_{\dot{\theta}/\Omega} + M_{\dot{\theta}/\Omega^2} m_{\dot{\beta}/\Omega} - m_{\dot{\theta}/\Omega^2} M_{\beta/\Omega} - m_{\dot{\theta}/\Omega} M_{\ddot{\beta}/\Omega^2}$$

$$C = M_\theta + m_{\dot{\beta}/\Omega} M_{\dot{\theta}/\Omega} + M_{\ddot{\theta}/\Omega^2} m_\beta - m_{\dot{\theta}/\Omega^2} M_\beta - m_{\dot{\theta}/\Omega} M_{\dot{\beta}/\Omega} - m_\theta M_{\ddot{\beta}/\Omega^2}$$

$$D = m_{\dot{\beta}/\Omega} M_\theta + m_\beta M_{\dot{\theta}/\Omega} - m_{\dot{\theta}/\Omega} M_\beta - m_\theta M_{\dot{\beta}/\Omega}$$

$$E = m_\beta M_\theta - m_\theta M_\beta$$

For the simple case, $\beta_o = \delta_3 = 0$ and $\overline{C}(k) = 1$,

$$A = I - I_X^2$$

$$B = \frac{\gamma}{16}\left[\frac{c}{R} - 4\frac{X_a}{R}\right]\left[\frac{c}{2R} - \frac{X_a}{R}\right] + \frac{\gamma}{8} I - \frac{\gamma}{6} I_X \left(\frac{X_a}{R}\right) - \frac{\gamma}{6}\left[\frac{3}{4}\left(\frac{c}{R}\right) - \left(\frac{X_a}{R}\right)\right] I_X$$

$$C = -\frac{\gamma}{6}\left(\frac{X_a}{R}\right) + I\left[\left(\frac{\omega_\theta}{\Omega}\right)^2 + 1\right] + \frac{\gamma^2}{64}\left[\left(\frac{c}{2R}\right) - \left(\frac{2X_a}{R}\right)\right]\left[\left(\frac{c}{2R}\right) - \left(\frac{X_a}{R}\right)\right]$$
$$+ I\left(\frac{\omega_\beta}{\Omega}\right)^2 - I_X^2 - \frac{\gamma^2}{36}\left(\frac{X_a}{R}\right)\left[\frac{3}{4}\left(\frac{c}{R}\right) - \left(\frac{X_a}{R}\right)\right] + I_X\left[\left(\frac{\gamma}{8}\right) - I_X\right]$$

$$D = \frac{\gamma}{8}\left\{-\frac{\gamma}{6}\left(\frac{X_a}{R}\right) + I\left[\left(\frac{\omega_\beta}{\Omega}\right)^2 + 1\right]\right\} + \frac{\gamma}{8}\left(\frac{\omega_\beta}{\Omega}\right)^2\left[\left(\frac{c}{2R}\right) - \left(2\frac{X_a}{R}\right)\right] \times$$
$$\left[\left(\frac{c}{2R}\right) - \left(\frac{X_a}{R}\right)\right] - \frac{\gamma}{6} I_X\left[\frac{3}{4}\left(\frac{c}{R}\right) - \left(\frac{X_a}{R}\right)\right] + \frac{\gamma}{6}\left(\frac{X_a}{R}\right)\left[\left(\frac{\gamma}{8} - I_X\right)\right]$$

$$E = \left(\frac{\omega_\beta}{\Omega}\right)^2\left\{-\frac{\gamma}{6}\left(\frac{X_a}{R}\right) + I\left[\left(\frac{\omega_\theta}{\Omega}\right)^2 + 1\right]\right\} + I_X\left[\left(\frac{\gamma}{8}\right) - I_X\right] \tag{11.28}$$

11.6 STALL FLUTTER

Stall

Some discussion of stall is necessary preparatory to a discussion of stall flutter. As described in Part I of this text, stall is a nonlinear aerodynamic phenomenon that results in a catastrophic loss of flow attachment and airfoil lift when a maximum angle of attack has been reached. Typical 2-D airfoil lift and drag curves show lift dramatically decreasing and drag increasing when the stall angle is reached (see Fig. 11.6).

This stall angle, and all other useful stall criteria, are unfortunately empirical. Hence, present analytical aerodynamic formulations model only the linear unstalled region, with minor allowance for post-stall simulation. The aerodynamic-force formulations of Chap. 8 are based on the linear portion of the lift curve and make no provision for stall. The dynamic formulations in Part 2 of this text are largely based on small angles of attack so that the airfoils are unstalled.

In Chap. 8, the aerodynamic terms in the equations of motion contain the Lock number term, γ, which relates aerodynamic to inertial forces on the blade as follows:

$$\gamma = \frac{\rho c C_{l_\alpha} R^4}{I_b}$$

The C_{l_α} term, or lift-curve slope, goes to zero and then becomes negative at stall. This makes all the γ terms in the equations of motion vanish when stall is reached, thereby allowing the inertial terms to dominate the dynamics.

It is useful in a discussion of stall to define a quantity that represents the "rotor mean lift coefficient," $\bar{C}_l$. Simply stated, this is the lift coefficient that the entire blade is assumed to be working at to yield a given thrust. We derive it as follows:

The differential lift is

$$dL = \tfrac{1}{2}\rho \bar{C}_l (\Omega r)^2 c\, dr$$

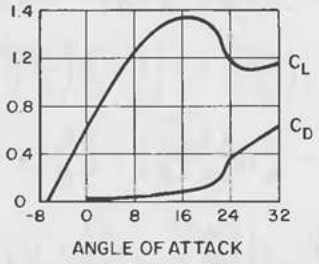

Figure 11.6. Typical 2-D lift-drag curves.

The blade lift is

$$L = \int_o^R dL = \int_o^R \tfrac{1}{2}\rho \bar{C}_l (\Omega r)^2 c\, dr$$

Now, assuming that chord c is taken to be constant and equal to the 3/4-span value,

$$L = \tfrac{1}{6}\rho \bar{C}_l c \Omega^2 R^3$$

Since thrust, T, is the sum of all b blades, or

$$T = bL = \tfrac{1}{6}\rho \bar{C}_l (\Omega R)^2 bcR$$

then

$$C_T = \frac{T}{\tfrac{1}{2}\rho A V_o^3} = \tfrac{1}{12}\bar{C}_l \left(\frac{\Omega R}{V_o}\right)\sigma$$

Where the solidity, σ, is defined as

$$\sigma = \frac{bcR}{\pi R^2}$$

Thus, the rotor mean lift coefficient is

$$\bar{C}_l = 12\frac{C_T}{\sigma}\left(\frac{1}{TSR^2}\right) \tag{11.29}$$

Rotor Mean Lift Coefficient

This is the windmill terminology form of an expression familiar to helicopter designers:

$$\bar{C}_l = 6\left(\frac{C_T}{\sigma}\right)$$

The difference is due to the definition of thrust coefficients. The reference velocity is free stream, V_o, for wind turbines, and tip speed, ΩR, for

helicopters, as follows:

$$C_T\,(\text{windmill}) = \frac{T}{\frac{1}{2}\rho A V_o^2}$$
$$C_T\,(\text{helicopter}) = \frac{T}{-\rho A(\Omega R)^2} \qquad (11.30)$$

The term, C_T/σ, can also be seen to be the nondimensional blade loading, as C_T is the nondimensional disc loading. Thus we have

$$\frac{C_T}{\sigma} = \frac{\left[\dfrac{\text{Thrust}}{\frac{1}{2}\rho\,(\text{area})\,V_o^2}\right]}{\left[\dfrac{A_{\text{blades}}}{(\text{area})}\right]} = \frac{T}{\frac{1}{2}\rho\,A_{\text{blades}}\,V_o^2}$$

Helicopters are limited in their performance by stall on the blades when thrust, or gross weight, is too high. The mean angle of attack, and hence $\bar{C}_l$, is just too high for the particular airfoil to support and not stall. For wind turbines, the event of stall is not so serious and may even be deliberate in the case of the fixed pitch "stall-control" designs. The wind-turbine mean lift coefficient is given by Eq. 11.29, indicating a tip-speed ratio dependence as well as a thrust dependence. For a wind turbine, power or torque is the key performance factor, not thrust. The wind-turbine mean lift coefficient can be approximately related to the power coefficient. From momentum theory, we have

$$C_P = C_T\,[1 - \lambda_i]$$

where λ_i is the nondimensional induced velocity. This expression is valid only up to $\lambda_i = \frac{1}{2}$, at which point momentum theory no longer holds. Recalling that another result of momentum theory is that $\lambda_i = \frac{1}{3}$ at maximum power coefficient and that $\lambda_i = 0$ for zero slip, the approximate bounds for λ_i and the resulting value of C_P can be determined as follows:

For a normal working wind turbine,

$$0 \le \lambda_i \le \tfrac{1}{2}$$

and at maximum power coefficient,

$$C_P = \tfrac{2}{3}\,C_T$$

We thus have the following approximate relationship for rotor mean lift coefficient related to power:

$$\bar{C}_l \simeq 18\left(\frac{C_P}{\sigma}\right)\left(\frac{1}{TSR^2}\right) \qquad (11.31)$$

This approximation shows, as did the thrust equation (Eq. 11.29) earlier, the sensitivity of the mean lift coefficient to tip-speed ratio. In other words, blade angle of attack is very sensitive to tip-speed ratio changes and only linearly dependent on power coefficient, or, alternatively, on pitch-angle (θ) change. One consequence of this is the rapid variation of $\bar{C}_l$ for a constant rpm wind turbine as a result of wind gusts. The *variable* rpm wind turbine, on the other hand, operating at approximately constant *tip-speed ratio*, has much less $\bar{C}_l$ variation caused by wind turbulence.

This equation also gives an approximate amplitude to the blade angle-of-attack range resulting from wind turbulence. This will give a good direct approximation to the stochastic wind input to the blade-root moments, and hence, to the fatigue-life input spectrum of the blades.

Another aspect of this is useful in testing wind turbines: scale modeling tip-speed ratio to reproduce stall. One of the difficulties in wind-turbine field testing is accumulating sufficient test points in the higher wind speeds to make an analysis statistically significant. The most usual example is in determining a power curve for a fixed-pitch turbine.

For fixed-pitch rotors, stall attenuates the output at rated and higher wind speeds, and the aims of proper rotor design are (1) to provide relatively constant power output, (2) to control thrust, and (3) to decrease power coefficient steadily as wind speed increases. All this is basically just providing a smooth transition in an orderly planned way between behaving like a *lift* device (below rated wind speed) and like a *drag* device (above rated wind speed). For this transition, stall must occur in a controlled manner and be fully tested both above and below rated speed. The higher wind-speed performance can be simulated by scaling on *tip-speed ratio*, that is, simply decreasing the rotor rpm simulates the higher wind speeds by achieving the same physical aerodynamic conditions on the blades. Keeping the tip-speed ratio the same preserves the mean angle of attack, the stall condition, the same rotor wake states, and the same power coefficients that would be achieved in actual high-wind, full rpm condition. The dimensional power curve can then be simply recaptured from the (nondimensional) power coefficient vs. tip-speed ratio curve of the scaled part. This approach also illustrates the great power of using nondimensional variables in testing and analysis.

The Test Center for Small Wind Turbines at Riso in Denmark uses this scaling technique to determine the post-stall power curves of fixed-pitch wind turbines (see Figs. 11.7 and 11.8). It can be seen that this simple scaling of

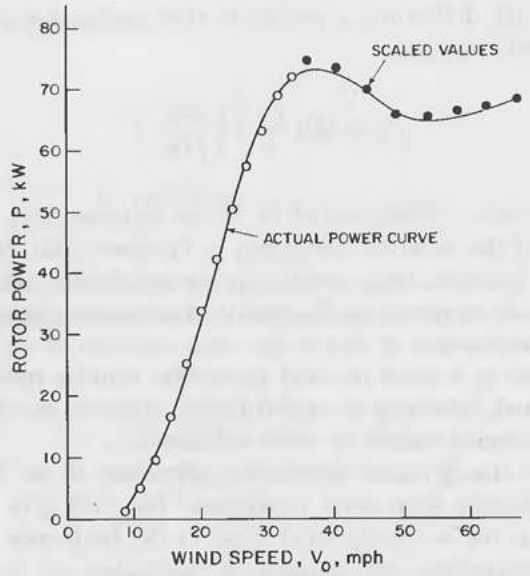

Figure 11.7. Measured and calculated power curves. (From Ref. 21.)

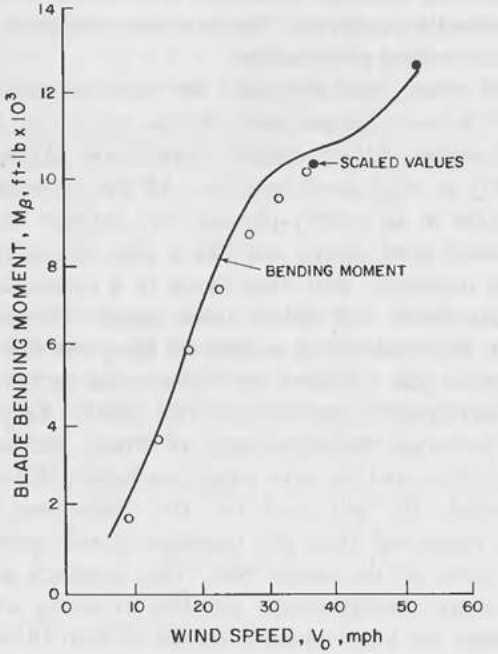

Figure 11.8. Measured and calculated bending moments. (From Ref. 21.)

tip-speed ratio reproduces very closely the physical rotor behavior in high wind speeds, in power (in-plane moments), and in thrust (root flapping moments). The Reynolds number has not been held constant in this scaling, and its effects might become important if the scaled range is too large.

The preceding discussion all pertained to axisymmetric flow, where angle of attack varies more or less uniformly over the entire rotor disk. Another region of stall in helicopters occurs in forward flight on the retreating blade. In fact, the loss of lift on the retreating blade resulting from stall is the limiting factor in high-speed helicopter flight. The angles of attack on the retreating side are high because of the reduction in the local blade element velocity caused by forward speed. The opposite, that is, an addition, occurs on the advancing side. Physically, the crossflow on a wind-turbine rotor acts in the same way—the crossflow velocity adding to the relative wind on the advancing side and diminishing it on the retreating side (see Fig. 11.9).

Actual wind-turbine blades stall at the root first, with the stall progressing

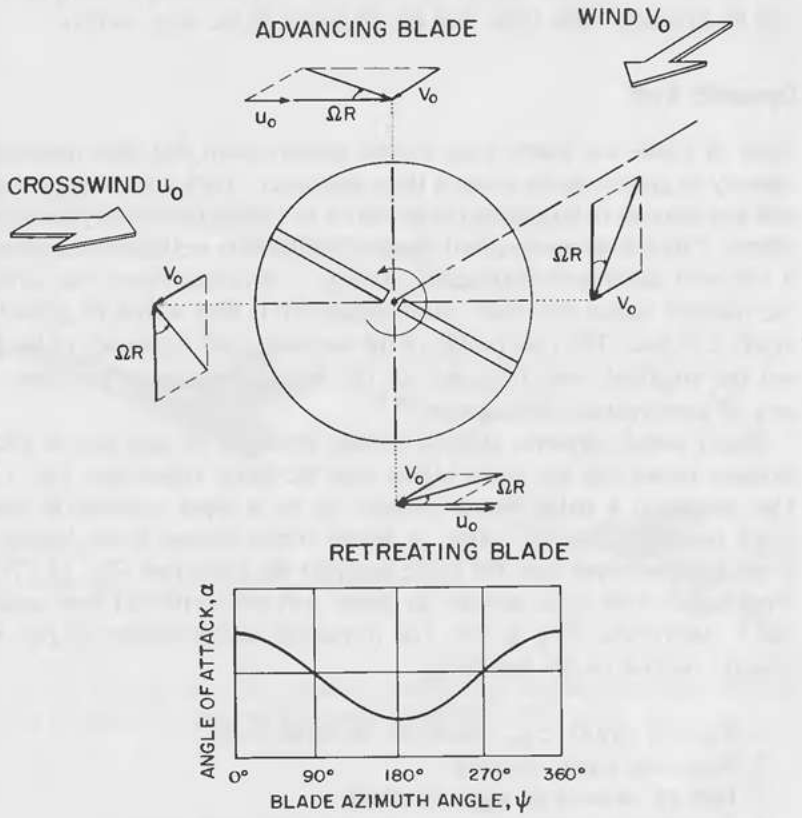

Figure 11.9. Advancing and retreating blades in a crosswind.

outboard as C_T, C_P, and C_l are increased, finally stalling at the tip. The inboard stall can be lessened by using large twist in the blade and large inboard chords at the expense of a lower tip-speed ratio. Crossflow aggravates the inboard stall on the retreating blade, as seen by the blade element diagrams in Fig. 11.9. For a stall-controlled machine, proper design will take the transition from unstalled to stalled blades into account, making it as smooth as possible.

For pitch-controlled blades, the same effects apply during the pitching lulls. It is clear that blade twist and planform, and to a lesser extent, airfoil selection, completely determine the stalling behavior of the rotor. It is advantageous to have *higher* pitch-angle sensitivity in a pitch-controlled rotor and *lower* sensitivity in a stall-controlled machine. This fact is reflected at present in the wind-turbine industry in high tip-speed ratio, low-solidity designs for pitch control, and high-solidity, slower designs for stall control. For wind turbines, moreover, it is clear that any flow event having high thrust or thrust excursions will be limited by stall, and if the excursion is fast enough, the type of stall will be dynamic. This topic will be discussed in the next section.

Dynamic Stall

Pilots of fixed- and rotary-wing aircraft quickly learn that their transient-load capacity is greater while doing a tight maneuver. They experience a delay of stall and increase in lift during the maneuver as a result of unsteady aerodynamic effects. This is commonly called *dynamic stall* and is well described physically if not well developed analytically. During a dynamic event, the airfoil lift and moment values can reach much higher levels than would be predicted by steady 2-D data. The relationship of the amplitude and frequency of the event, and the amplitude and frequency of the airfoil response is a current major area of aerodynamic investigation.[20,22]

Simply stated, dynamic stall on a blade produces lift and section pitching-moment values that are much higher than the static values (see Fig. 11.10). This occurs in a pulse that is brought on by a rapid increase in angle of attack past the static stall value. A strong vortex formed at the leading edge is quickly convected over the blade and into the wake (see Fig. 11.11). This event begins with rapid increase in forces and ends with full flow separation and a catastrophic drop in lift. The formation and movement of this vortex strongly depend on the following:

1. Type of airfoil, e.g., cambered or uncambered
2. Beginning angle of attack
3. Rate of increase of angle of attack
4. Excursion of angle of attack past the static stall value

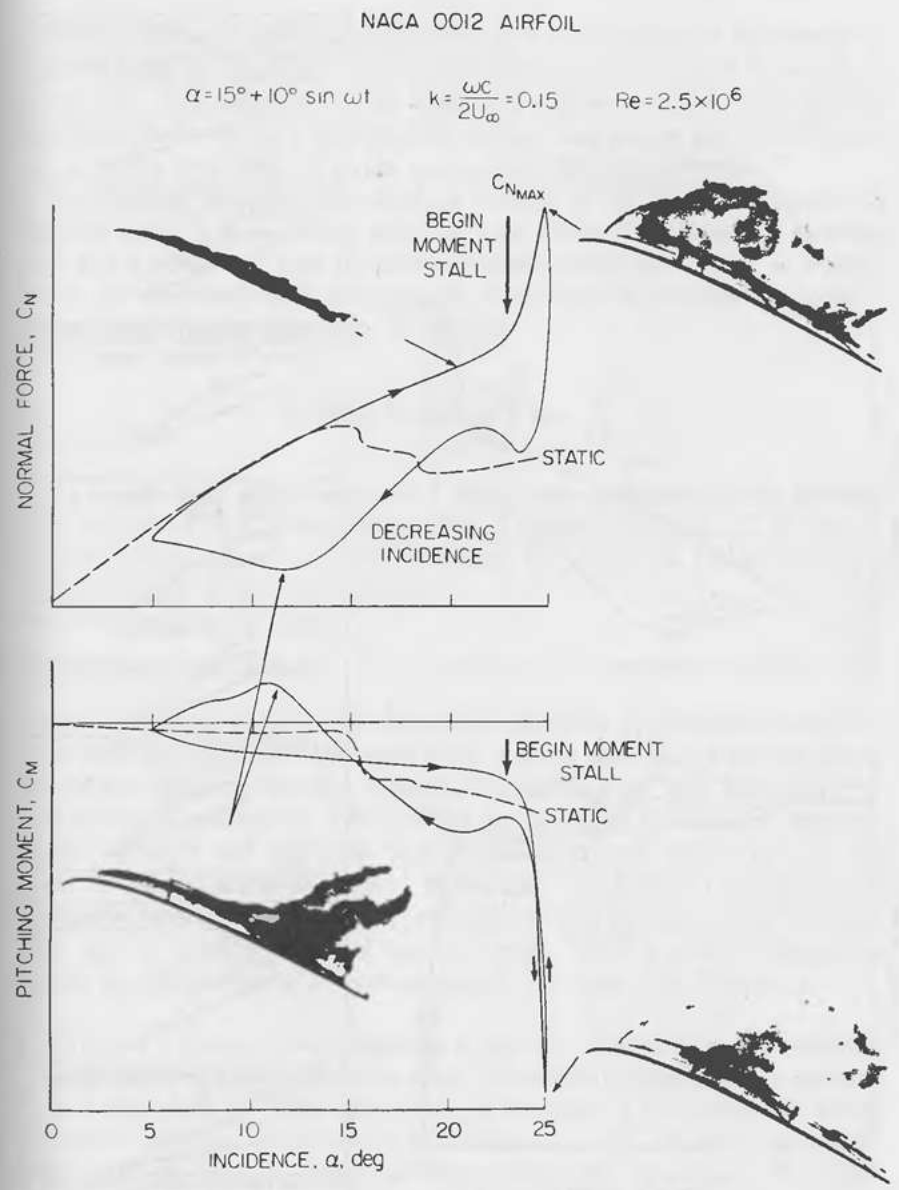

Figure 11.10. Typical static and dynamic variation of normal force and pitching moment as a function of angle-of-incidence. (From Ref. 20.)

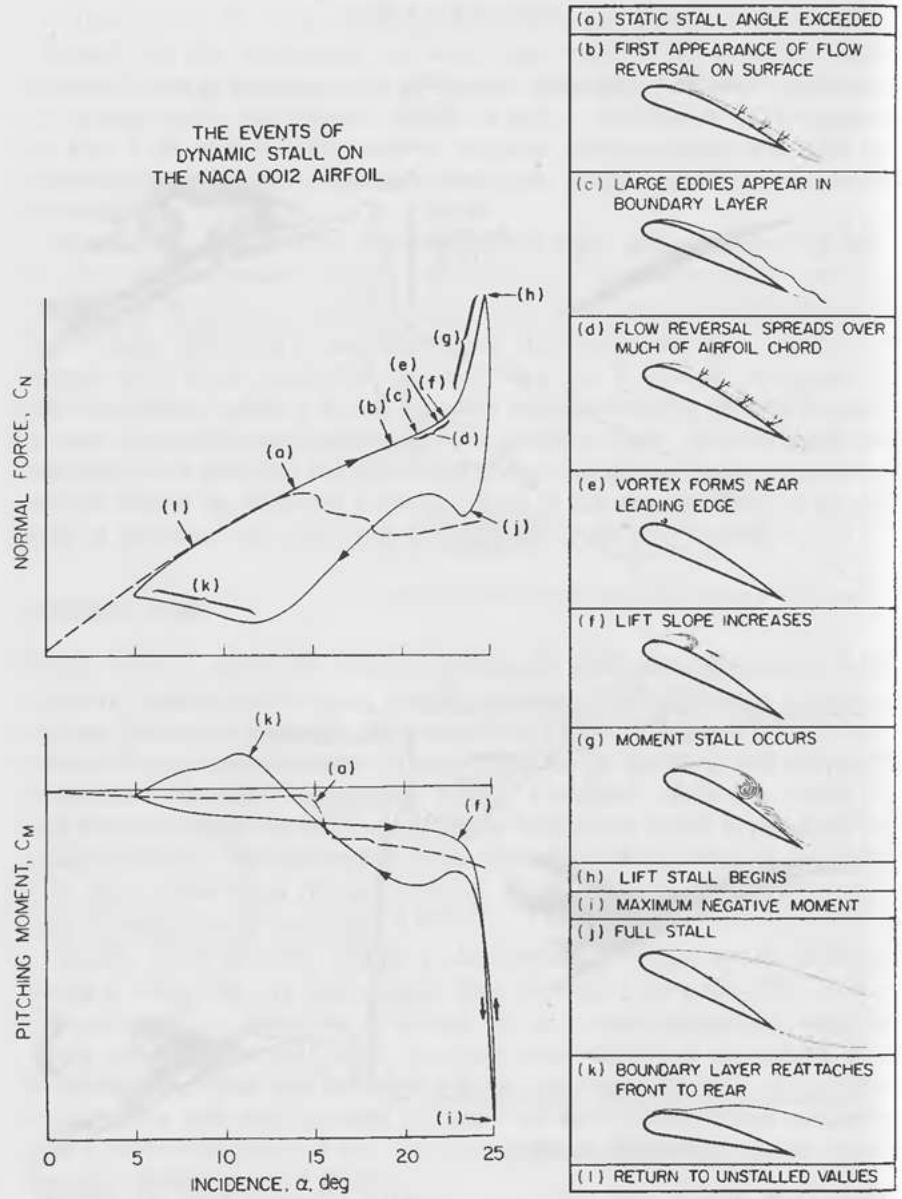

Figure 11.11. Dynamic stall events on a NACA 0012 airfoil. (From Ref. 20.)

It is clear that the event depends both on the amplitude and the history of angle of attack on the blade. There is also a hysteresis or delay of reattachment of the flow and a recovery of the blade forces after the event. The physical mechanism is not strongly dependent on surface roughness or Reynolds number but is mildly dependent on airfoil camber and leading-edge radius.[20]

The reduced frequency discussed in relation to the complex Theodorsen function (Sec. 11.5) is thought to be the most significant indicator of dynamic stall and is commonly used to correlate dynamic stall data. It can be thought of as the nondimensional time needed to convect the disturbance (vortex) across the airfoil into the wake, as follows:

$$\text{Reduced frequency} = k = \frac{\omega c}{2V_o}$$

An experimental plot of an airfoil's normal force coefficient during dynamic stall vs. values of k from 0.02 to 0.25 is shown in Fig. 11.12. It can be seen that slight effects are seen at reduced frequencies as low as 0.02 and increase rapidly as frequency increases.

Stall-Induced Vibrations

Since a helicopter blade can be thought of as having a "dynamic maneuver" each rotation, especially in forward flight with its associated harmonic angle-of-attack variations, unsteady aerodynamic effects have long been observed and studied on helicopters. These effects are frequently seen at high operating angles of attack and appear as high control loads that place limits on the speed and thrust of the helicopter. In hover, "stall flutter" is really a stall-induced vibration that is caused by dynamic stalling at some part of the rotor disk and its associated control moment peaks.[10,11,12] For this vibration to occur, the blade must be flexible in torsion. To quote from Johnson:

> Consider a hovering rotor operating at high lift. A gust or other disturbance may trigger dynamic stall of the blade. The resulting large transient moment will then twist the blade nose-down. If the blade is sufficiently flexible in torsion, this nose-down motion will reduce the angle of attack enough for the flow to reattach. With the return of attached flow loads, the blade rebounds up in pitch, overshooting the static stall level because of the small damping of the torsional motions. The overshoot in pitch increases the angle of attack so that the blade stalls, and the cycle begins again. An oscillation of the blade in and out of stall is thus established. The energy to sustain the oscillation comes from the hysteresis of the moment coefficient as a function of angle of attack during dynamic stall; the loops represent

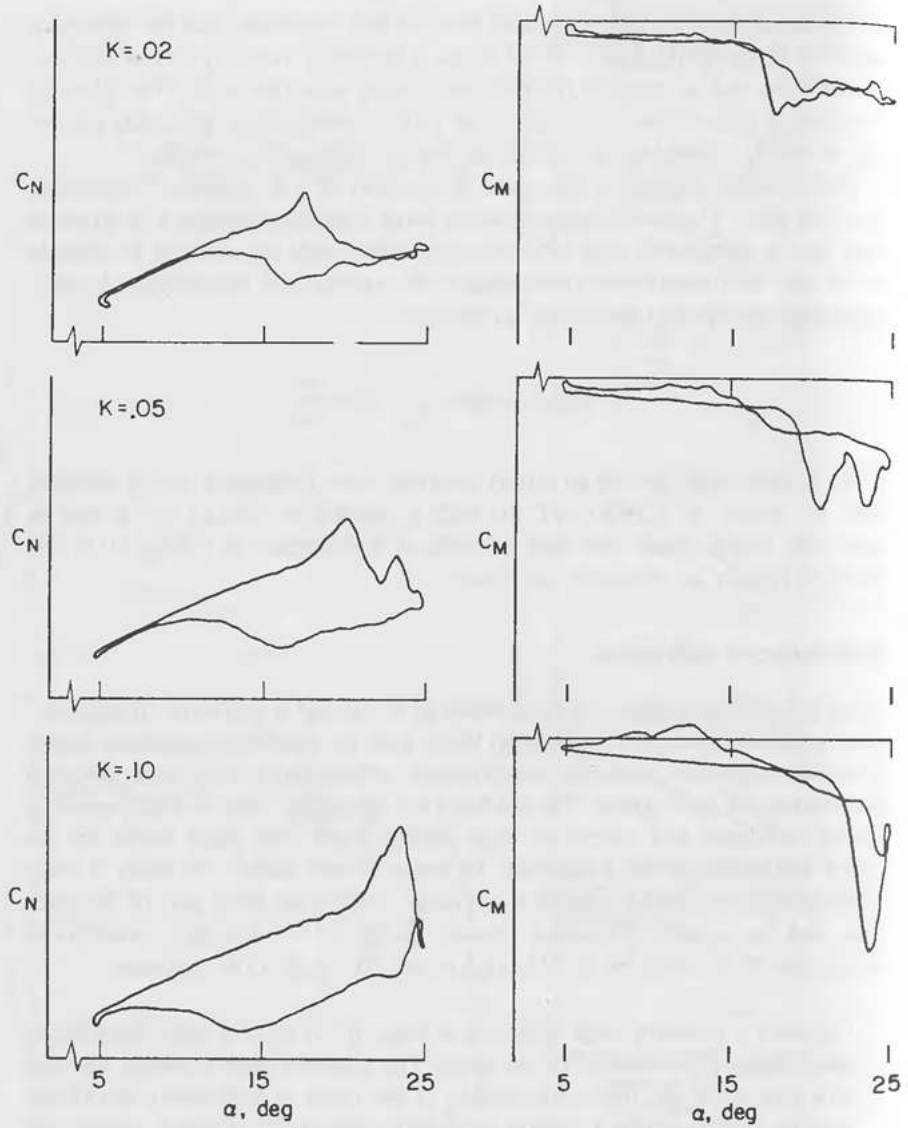

(a) k = 0.02, 0.05, 0.10

Figure 11.12. Normal force and pitching moment on a NACA 0012 airfoil. (From Ref. 20.)

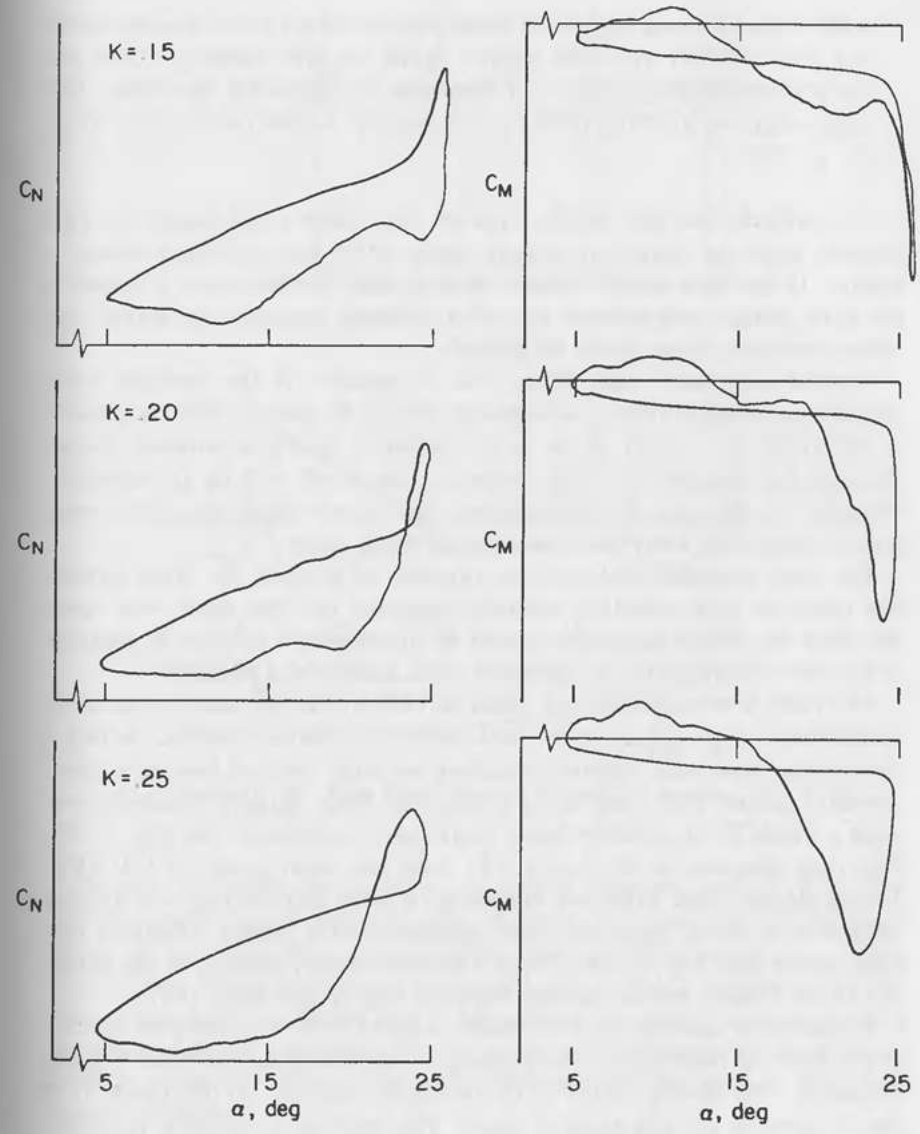

(b) k = 0.15, 0.20, 0.25

Figure 11.12. (*Continued*)

a net amount of work performed on the blade during a cycle. The oscillation is a limit cycle in which the balance of the negative damping in stall and the positive damping below stall determine the oscillation amplitude. This single-degree-of-freedom limit cycle instability is called stall flutter. (Ref. 15, p. 882).

It is unlikely that this specific type of stall flutter could happen in wind turbines since the blades are usually much stiffer than helicopter blades in torsion. If the pitch control system were flexible or there were a failure in the pitch linkage that reduced the pitch stiffness, however, the elastic stall flutter described above would be possible.

Another aeroelastic stall flutter case is possible if the torsional blade frequency coalesces with an aerodynamic forcing frequency. This could occur in helicopters as a result of the wake vorticity's having a harmonic forcing function that matches the pitch frequency; the result will be an aeroelastic vibration. In the case of wind turbines, this is not likely since the vortex wake is convected away from the actuator much faster.

The most important stall-induced vibration to consider for wind turbines can occur on stall-controlled machines operating near the rated wind speed and does not require the blade to twist at all, simply to oscillate in flapping. It has been described for an operating wind turbine by Lundsager.[18,19]

The Nibe A wind turbine was tested in 1980 by the national electric utility in Denmark. It is a fixed-pitch, stall-controlled, upwind machine, having a three-bladed rotor with flapwise and chordwise stay diagonal bracing at about one-third radius. This brace acted to raise the blade flapping frequency over what a simple 20-m cantilever blade would have experienced (see Fig. 11.13). The rotor diameter is 40 meters (131 feet) and rated power is 630 kVA. During testing, large amplitude vibrations in blade flap bending root moment were seen to occur when the rotor approached fully stalled conditions near rated power (see Fig. 11.14). These vibrations greatly influenced the fatigue life of the blades, and the turbine has been largely idle since 1981.

A qualitative description of the flutter is given here. The vibration consists of the blade tip oscillating in the flapping direction at its natural blade flapping frequency. The driving energy of the oscillation comes from the hysteresis of the lift curve at the stall angle of attack. This oscillation can occur regardless of dynamic stall, although it is aggravated by dynamic stall effects and requires that only the following conditions be met:

1. The entire blade is stalled, except for the tip
2. Tip angle of attack is near stall, or section C_l is near $C_{l_{max}}$
3. Blade frequency of vibration in flapping is high relative to rotor speed, i.e., $p = \omega_\beta/\Omega \cong 3$ or above
4. Lift-curve slope has a precipitous drop in C_l at stall (see Fig. 11.15)

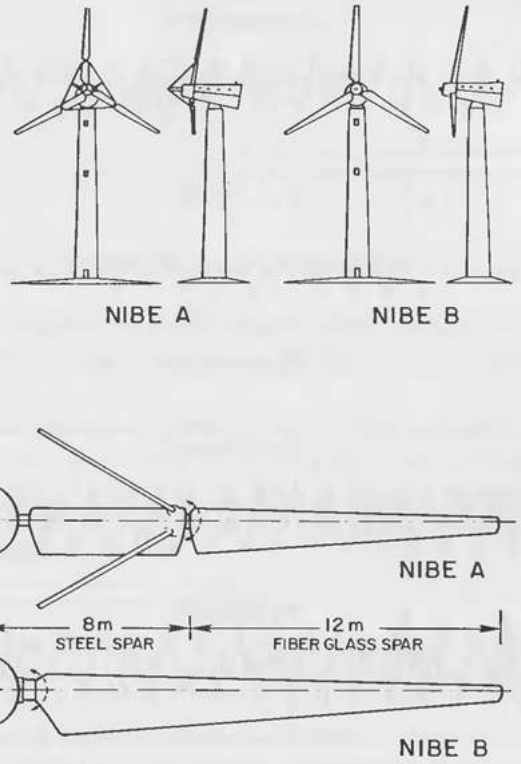

Figure 11.13. Nibe A and B wind turbines. (From Ref. 18.)

Consider the blade element at the tip section as shown in Fig. 11.16. The airfoil is operating with its local angle of attack, α_o, near stall, and the blade forces are high enough to cause a steady flapping deflection, β_o (i.e., steady blade coning flexure). Now consider what happens with a sudden loss of lift, such as that which might be caused by a relatively minor wind gust pushing the angle of attack past stall. The tip would rebound towards a zero coning position under the influence of the centrifugal restoring moment and blade flexural stiffness.

During the downwind motion, the angle of attack will increase because of the flapping velocity of the tip $R_{\dot{\beta}}$, but when the limit is reached, the angle of attack drops back below the stall value, flow is reattached, lift again builds up on the blade, and aerodynamic force drives the blade tip up again towards the original β_o deflected position. If there is overshoot, the blade can again stall, initiating the cycle all over again.

The oscillation thus established is a *limit cycle* (limited by the stalling point), a cycle that occurs at the flapping frequency of the blade and exhibits

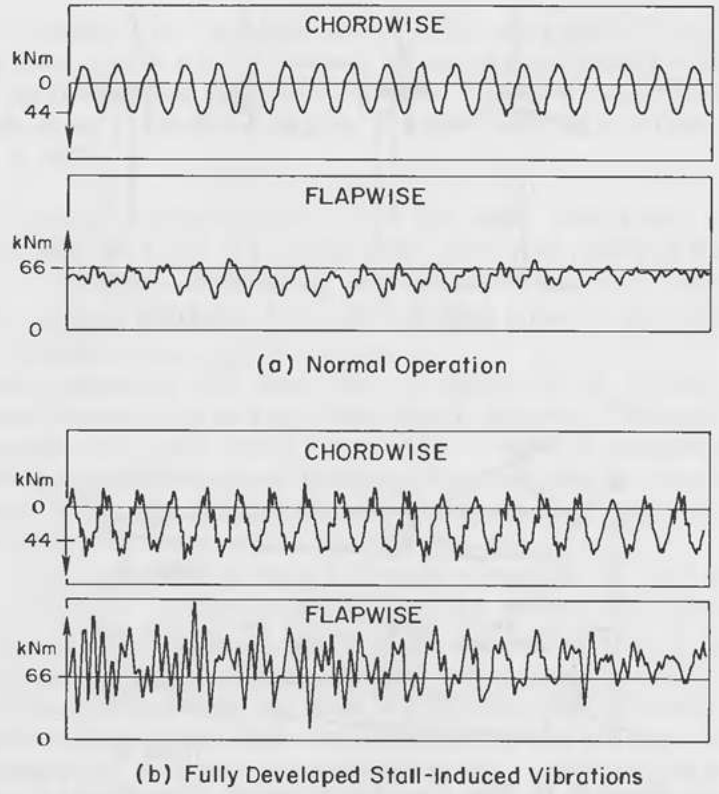

Figure 11.14. Chordwise and flapwise blade moments. (From Ref. 18.)

an amplitude excursion above and below the stall point; it also has a mean or starting point near, but just below, stall.

The frequency of the angle-of-attack oscillation is the natural frequency in flapping, ω_β, and the amplitude depends on the hysteresis in the lift-curve slope and the maximum tip flapping velocity, $R_{\dot{\beta}}$. The resulting blade-tip motion has the same frequency, and its amplitude is a function of the starting

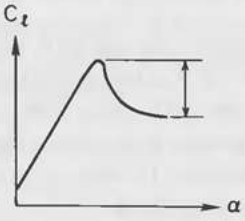

Figure 11.15. Lift curve slope.

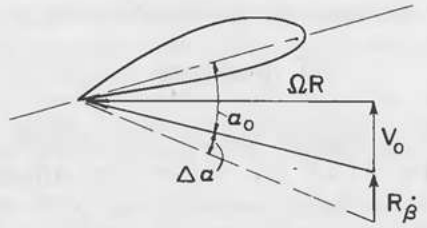

Figure 11.16. Tip blade element.

deflected flexural position, β_o, the amount of angle-of-attack overshoot, and the mitigating normal blade aerodynamic damping in flap (which is low since the rest of the blade is stalled).

It is clear that this stall-induced vibration can be greatly aggravated by dynamic stall, which can drastically increase the hysteresis and overshoot in α near stall (see Fig. 11.10). For the Nibe A turbine, dynamic stall plays a major role, which can be verified by calculating the reduced frequency for that case, as follows:

$$k = \frac{\omega c}{2V_o}$$

where:

ω = frequency of angle of attack oscillation
c = chord
V_o = local free stream = tip speed ΩR

For the Nibe A turbine:

$$\omega = \omega_\beta = 2 \text{ Hz} = 12.57 \text{ rad/sec}$$

$$c = c_{\text{TIP}} = 600 \text{ mm} = 1.97 \text{ ft}$$

$$\Omega = 33.4 \text{ rpm} = 3.5 \text{ rad/sec}$$

$$R = 20 \text{ m} = 65.6 \text{ ft}$$

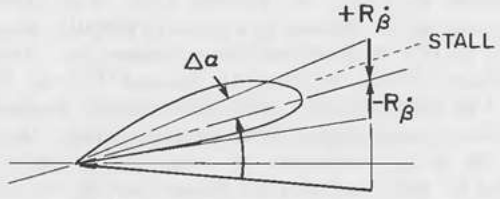

Figure 11.17. Oscillation in angle of attack.

Then the reduced frequency for the Nibe A turbine is

$$k = 0.054$$

This value will give a moderate dynamic-stall response, as shown in Fig. 11.12 and also in Fig. 11.17. It is clear that the dynamic-stall aggravating effect will increase if the natural frequency, ω_β, or tip chord is larger, or if the tip speed is reduced.

REFERENCES

1. Loewy, R. G. Review of rotary-wing V/STOL dynamic and aeroelastic problems. American Institute of Aeronautics and Astronautics, Paper No. 69-202, Feb. 19, 1969.
2. Miller, R. H., and Ellis, C. W. Helicopter blade vibration and flutter. *Journal of the American Helicopter Society*, Alexandria, VA (July 1956).
3. Friedmann, P., and Tong, D. Dynamic nonlinear elastic stability of helicopter rotor blades in hover and in forward flight. NASA CR-114485, MIT ASRL TR-166-3, Cambridge, MA, May 1972.
4. Lemnios, A. Z. The aeroelastic behavior of rotary wings in forward flight. Ph.D. dissertation, University of Connecticut, Storrs, CT, June 1967.
5. Houbolt, J. C., and Brooks, G. W. Differential equations of motion for combined flapwise bending, chordwise bending, and torsion of twisted non-uniform rotor blades. NACA Report 1346, 1958.
6. Ormiston, R. A., and Hodges, D. H. Linear flap-lag dynamics of hingeless helicopter rotor blades in hover, *Journal of the American Helicopter Society* 17:2, Alexandria, VA (Apr. 1972).
7. Hohenemser, K. H. Hingeless rotorcraft flight dynamics. AGARD-Ograph 197, 1974.
8. Hansford, R. E., and Simons, I. A. Torsion-flap-lag coupling on helicopter rotor blades. *Journal of the American Helicopter Society*, Alexandria, VA (Oct. 1973).
9. Pei, C. C. Pitch-lag instability of helicopter rotor blades. *Journal of the American Helicopter Society*, Alexandria, VA (July 1985).
10. Miller, R. H. Unsteady airloads on helicopter rotor blades. *Journal of the Royal Aeronautical Society* 68:640 (Apr. 1964).
11. Carta, F. O. An analysis of the stall flutter instability of helicopter rotor blades. *Journal of the American Helicopter Society*, Alexandria, VA (Oct. 1967).
12. Ham, N. D., and Young, M. I. Torsional oscillations of rotor blades due to stall. *Journal of Aircraft* (May 1966).
13. Gohard, J. C. Free wake analysis of wind turbine aerodynamics, vol. VIII, *Wind Energy Conversion*. MIT ASRL TR-184-14, Cambridge, MA, Sept. 1978.
14. Mayer, D.; Coleman, C.; Currin, H.; Stoddard, F. S.; et al. Development of a 4KW SWECS-critical design review. Prepared for Contract BPFO8501C, Rocky Flats Plant, Wind Systems Program, US DOE, by NorthWind Power Company, Inc., Warren, VT, Sept. 1980.
15. Johnson, W. *Helicopter Theory*. Princeton, NJ: Princeton University Press, 1980.
16. Stoddard, F. S. Wind turbine dynamics: Field testing examples. Presented at Energy Sources Technology Conference and Exhibition, ASME Petroleum Division, Houston, TX, Jan. 1983.
17. Chilcott, R. E. The design, development and testing of a low-cost 10 hp windmill prime mover. Publication No. MT 7, 2nd ed., Brace Research Institute, McGill University, Quebec, Canada, June 1970.

18. Lundsager, P.; Petersen, H.; and Frandsen, S. The dynamic behavior of the stall-regulated Nibe A wind turbine: Measurements and a model for stall-induced vibrations. Riso Report M-2253, Riso National Laboratory, Denmark, Nov. 1981.
19. Lundsager, P. On the power regulation of small wind turbines based on experience with small Danish wind turbines. Test Plant for Small Windmills, Riso National Laboratory, Denmark. Presented at Fifth Biennial Wind Energy Conference & Workshop, U.S. Department of Energy, Washington, D.C., Oct. 1981.
20. Carr, L. W.; McAlister, K. W.; and McCroskey, W. J. Analysis of the development of dynamic stall based on oscillating airfoil experiments. NASA TN-D-8382, NASA Ames Research Center, Moffett Field, CA, Jan. 1977.
21. Rasmussen, F. Blade and rotor loads for Vestas 15. Riso-M-2402, Test Plant for Small Windmills, Riso National Laboratory, Denmark, June 1983.
22. Noll, R. B., and Ham, N. D. Dynamic stall of small wind systems. Contract No. DE-ACO4-76DPO3533. Prepared for Wind Energy Research Center, Rockey Flats Energy Systems Group, Golden, CO, Feb. 1983.

12

WIND TURBINE LOAD SPECIFICATION

12.1 INTRODUCTION

For the wind-turbine designer, the most crucial task is the blade design since the principal loads on the turbine originate in the rotor. That is the reason so much effort is placed on the statics and dynamics of wind-turbine blades. It is enough to note that if the loading regime of a wind-turbine rotor can be properly specified, accomplishing an adequate design will be no more than a routine task. This chapter describes the specification of loading for a wind-turbine rotor. It should be kept in mind, however, that the wind-turbine environment, when compared to aircraft environment, for instance, is very complex and is not yet well understood.[1] Since turbulence and other extreme conditions of wind cannot yet be adequately described mathematically, wind-turbine loading specifications, at present, remain partly guesswork.

The load specification serves as the judge and jury on the array of design concepts thought up by an inventive designer. To be considered properly, each concept must be evaluated against the others by means of calculations and analysis. The winning concept will emerge from this design process very easily, provided that the following common sense rules apply:

1. Specification of loads are drawn up to the same degree of sophistication for each competing concept
2. Critical points in the structural load paths are identified
3. Structural adequacy is determined by stress level
4. Preferable attributes of the design (i.e., cost of energy) can be quantified.

The rotor design process can be stated simply. After a preliminary design has been chosen, the blade structure is estimated and arbitrarily specified so that the loads can be calculated for its assumed weight, stiffness, type of material, and dimensions. The control system—that is, the method by which extreme loads are avoided—is also planned at this point. The first loading specification is then calculated for a "straw man" rotor. This load spec,

which is probably a simple table of values as developed in Sec. 12.6, is judged against the assumed blade and hub structure, and the stresses are calculated. It is then a simple matter to judge whether the "straw man" is adequate or not.

The preceding process must be repeated many times in the design of an adequate wind turbine. It should be obvious that if this process could be carried out entirely by computer or on paper, a successful rotor design might be achieved without any construction or testing being involved. Unfortunately, since the available theories are not yet good enough and knowledge of the wind inflow not complete enough for that, test data must be relied on for many design guides, as will be seen later in this chapter.

Despite these caveats, the present analysis methods are completely adequate for preliminary design, for the process of weeding out unsuitable inventions or designs, and for bringing the few best prototypes to the testing field for verification. The wind-turbine industry has unfortunately often been characterized by builders who have not prepared a preliminary design at all but have merely relied on trial-and-error field results to expose deficiencies. That approach is simply pursuing development the hard way: building the actual "straw man" concept in full-scale each time a change is made, and then doing a full scale "field test" to identify critical structural defects.

As the concept rotor is refined and changes are made to strengthen or "beefup" deficiencies in the load path, the load spec also changes, becoming more and more complex. A curious fact is that, no matter how complex it may be, a load spec can never represent the "truth, the whole truth, and nothing but the truth"; that is, the load spec can never indicate on paper the entire loading regime that will occur in practice. It is a model only, a stratagem invented by logic that allows a design idea to be judged, and by use of which a smart organization can save resources, time, and effort. Invariably, when the turbine in question is finally built and put into service, the unknown will happen. Some wind turbine designers call this the "Hammer of God." At some point, a combination of events—partly weather, partly structural oversight, partly unknown happenings—will transpire, and a failure will result. As a designer, you can only hope that these unattributable failures will be rare and random—in the Danish expression, that they will be "lonely swallows." If, however, they repeat with regularity, an engineering oversight is indicated, and that requires study, testing, and a fresh solution so that it may be avoided in the future.

12.2 TYPES OF LOADS AND SPECIFICATIONS

Recalling the aeroelastic triangle of Chap. 7, the loads in any of the members of a wind turbine fall into one of the following three categories but are also

related to the other two:

1. Inertial forces
2. Aerodynamic forces
3. Structural forces

The *aerodynamic forces* are the most difficult to visualize and to test. Unsteady and nonlinear, they are further complicated by the random processes of the atmosphere. In studying them, "stochastic" or statistical testing must be relied on rather than more direct "deterministic" testing like that provided by a wind tunnel. Part I of this text provides a broad and practical look at the origin and characteristics of aerodynamic forces. It is obvious that much remains to be learned about the aerodynamics of wind turbines, particularly the unsteady aerodynamic behavior caused by wind turbulence.[1,2,3,4]

The *inertial forces* originate simply as a result of introducing mass, motion, and gravity to the static forces. The *structural forces* are the elastic restraints that relate deflections to the applied forces. Calculation of the structural and inertial forces would be routine and straightforward were it not for the complication of the changes in aerodynamic forces when motions and deflections occur, and which are difficult to predict.

When the "straw man" preliminary design concept has been defined, a layout or sketch is prepared to show the arrangement of items in the turbine and their rough dimensions. To concentate on the rotor: the rotor blades, their root attachments, the hub structure, and the hub attachment to the drive train are all specified. Also, the control system is chosen, and its effects sketched in the rotor drawing. The static structural load path is determined simply by the logical flow of forces through the system. The major aerodynamic and structural forces and their reactions in the bedplate are shown in Table 12.1 for a normal rotor load path.

Statically speaking, this is the simple load path for applied aerodynamic loading on a wind turbine blade. The load path is the same for varying wind loading, as for instance, that caused by wind turbulence. When dynamics

Table 12.1. Rotor Load Path: Static Forces.

Type of Force:	Due to:	Resisted at:
Aerodynamic	Airfoil pressure distribution	Airfoil chordwise
Aerodynamic	Section forces	Blade root
Structural	Blade-root forces	Blade root/hub attachment
Structural	Combined blades	Hub structure
Structural	Hub forces	Windshaft attachment
Structural	Shaft forces	Bedplate attachment

Table 12.2. Blade-Root Forces and Bending Moments by Duration.

Duration	Source	Type	Explanation
Steady	Average wind	Aerodynamic	From power production
	Centrifugal	Inertial	Due to rotation
	Pitch imbalance	Aerodynamic	Pitch misalignment
	Axis offline	Inertial	Blade-axis misalignment
Transient	Wind gust	Aerodynamic	Nature of wind
	Crosswind	Aerodynamic	Nature of wind
	Pitching	Aerodynamic	Pitch control turbines only
	Actuation	Inertial/Aerodynamic	Control system operation
	Erection	Inertial	Construction by-product
	Impact	Inertial	Foreign object strike
Alternating	Gravity	Inertial	Blade weight
	Gyroscopic	Inertial	Due to yawing
	Crosswind	Aerodynamic	Due to steady yaw error
	Tower wake	Aerodynamic	Downwind turbines
	Tower dam	Aerodynamic	Upwind turbines
	Coriolis	Inertial	Flap/lead-lag coupling
	Mass imbalance	Inertial	Blade out of balance
	Resonance	Structural	Instability
	Flutter	Aeroelastic	Instability

(mass, motion, and gravity) are introduced into the structure of the blade, however, the motions and deflections of the structure must be considered. Now *all* the structural items in the rotor—including the pieces that are physically connected to, but not a part of, the primary load path as described—must be considered since they have mass and stiffness. Vibration, instabilities, and fatigue then become possible.

Loads in the loading specification can be characterized by their duration—as steady, transient, or alternating; their source—as aerodynamic, inertial, or structural; their frequency of occurrence; and their most likely failure mode—simple overstress, repeated overstress, or fatigue. Table 12.2 separates blade root bending moments into duration categories.

These loads, and others peculiar to each "straw man," must find their way into various stages of the loading specification and the design process. It is straightforward to construct increasingly more complex levels of sophistication into the rotor loading specifications as calculations are improved in each of these areas and as the design edges closer and closer to practicality.

12.3 FIRST LEVEL: STATICS

The blade has a specified geometry and structure, which are defined by the following:

Blade radius = R
Twist distribution = $\theta_o(r)$
Taper or chord distribution = $c(r)$
Airfoil type and distribution = NACA 4412-18
Coning angle = β_{PRECONE}
Blade weight = M_b
Blade mass distribution = $m(r)$
Section stiffness distribution = $EI(r)$
Blade-root extreme fiber distance = C
Root section moment of inertia = I_{R_o}
Blade mass moment of inertia = I_b

The first three values allow simulation of the aerodynamic performance, including power output, productivity, and drivetrain torque matching. The structural and mass properties of the blade allow for a first cut at the inertial loads and stresses and the blade deflections for any set of imposed conditions. The blade has a specified operating condition, as follows:

Rotational speed = Ω
Pitch angle = θ_P
Wind speed = V_o

These values—the result of the desired power output of the design given the blade aerodynamic starting point previously described also define the equilibrium, or steady operating point, of the turbine.

Static equilibrium loads are calculated next, as follows:

Thrust = T
Torque = τ
Blade centrifugal force = $F_{\text{CENTRIFUGAL}}$

It is also useful to have some nondimensional parameters:

Thrust coefficient = $C_T = T/\frac{1}{2}\rho A V_o^2$
Power coefficient = $C_P = D/\frac{1}{2}\rho A V_o^3$
Solidity = σ = blade area$/\pi R^2$
Disc loading = C_T/σ
Tip speed ratio = $TSR = \Omega R/V_o$
Lock number = ratio of aerodynamic to inertial forces = γ
Reynolds number = ratio of aerodynamic to viscous forces = R_e

The static adequacy of the "straw man" can now be evaluated by calculating the root bending moments and resulting stresses:

M_β = Root flap moment
M_ζ = Root lead-lag moment = Output torque/Number of blades

If no computer integration of flap moment is available, momentum theory can be used as a preliminary value:

$$M_\beta = \text{Flap moment} \simeq \tfrac{2}{3} R[\text{Thrust of one blade}] \qquad (12.1)$$

This calculation uses the assumed aerodynamic loading distribution of a uniform inflow actuator, namely a triangular distribution, which has an equipollent single-force system at 2/3 blade radius. This simple approximation has been found to be surprisingly close to complicated strip theory integrations, at least as close as 90 percent when the windmill power coefficient is high.[3]

Next, the root bending stress is calculated from the classical flexure formula:

$$\sigma_B = \text{Stress due to bending} = \frac{MC}{I_{R_o}} = \sigma_{R_1} \qquad (12.2)$$

Next the stress caused by centrifugal force can be added, where the bending moment due to centrifugal force is caused by the coning angle, if there is one (see Fig. 12.1).

Root stresses are as follows:

Axial stress = Centrifugal force/Root area = σ_{R_2}
Stress due to bending = $MC/I_{R_o} = \sigma_{R_3}$

The total root stress is then:

$$\sigma_R = \sigma_{R_1} + \sigma_{R_2} + \sigma_{R_3} \qquad (12.3)$$

This is the root stress in the flapping direction, or orthogonal to the plane of rotation. To this must be added the stress in the lead-lag direction that is

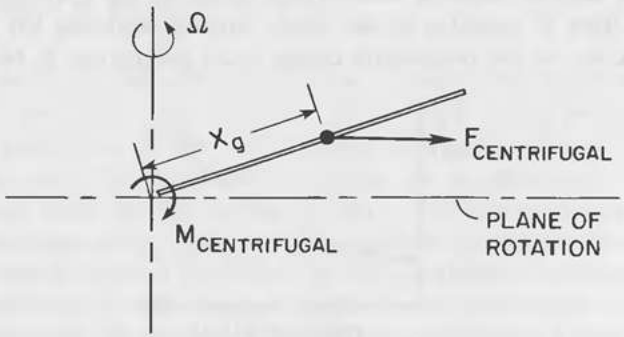

Figure 12.1. Bending Moment Due to Centrifugal Force.

caused by the blade driving torque. Usually it is small and has roughly the ratio of the airfoil section L/D at stall to the flapping moment. In this simplified way, the blade is thought of as an "aerodynamic amplifier" that amplifies the natural wind drag forces, in the flap direction, through a more or less efficient airfoil amplifier to about tenfold. The driving torque is simply a very small forward inplane component of this large "amplified" flapping moment. It overcomes the airfoil drag and provides a little more torque to pull the blade forward and produce power. In this idealized way, it is easily seen why it takes so much blade length to produce a relatively small amount of driving torque, and why wind turbine thrust is so very high at the zero slip condition, which is simply the point at which the small driving vector component is only large enough to overcome the blade drag.

The lead-lag root moment is added vectorially to the flap moment, as follows:

$$\text{Total moment} = \text{Square root of the sum of the squares}$$

$$M_{\text{Total}} = [M_\beta^2 + M_\zeta^2]^{1/2} \tag{12.4}$$

At this point, the static load specification can be applied to the structure and the static adequacy judged. The results are usually calculated in the form of a graph of root stress vs. wind speed and vs. power output (see Figs. 12.2 and 12.3). The centrifugal stress shows up as a constant value and the thrust stress increases as the square of the wind speed.

These two curves provide the road map for all the work to follow. They represent the least root stress the turbine will ever see, since they depict the ideal, steady equilibrium conditions. Any additions of other conditions will always aggravate the loads and increase the stresses. At this point in the design process, many alternative concepts can often be eliminated on the basis of simple root overstress alone.

Plots can also be made of other critical points in the rotor primary load path when there is suspicion of the steady stresses becoming too high. It is usual, however, for the preliminary design stress calculations to be limited to

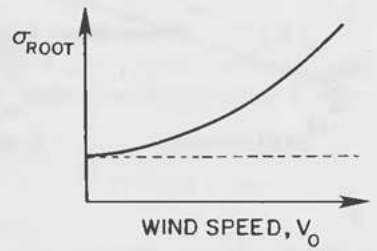

Figure 12.2. Root Total Stress vs. Steady Wind Speed.

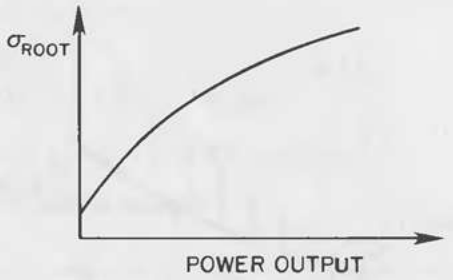

Figure 12.3. Root Total Stress vs. Power Output.

the blade roots as they are in helicopter preliminary design, since the roots offer a convenient place for calculation from the following aspects:

1. Blade-root moments can be calculated readily from first principles, as seen here.
2. Blade-root moments can be related to blade stresses without having to know the detailed structural arrangement of the entire blade—just the blade-root portion.
3. The blade root is a convenient junction point of the primary load path from the airfoil sections to the hub; the latter functions to sum the individual blade-root contributions.
4. If the blade is to be pitch-regulated or controlled, the pitching moment of the blade, which must be resisted by the pitch control linkages, is reacted at the blade-root attachment.
5. The root-attachment method is usually common to the competing blade designs in a preliminary design.
6. The calculation of centrifugal forces and moments is simple at the blade root; only the blade mass moment of inertia, I_b, or the blade weight and center of gravity are necessary.

A first-cut design tradeoff on deflections, coning angle, blade weight, root attachment, and steady root stress can also be made at this point by solving the static equilibrium of the blade flapping angle for a variety of expected operational cases. The two steady forces that are in opposition are the thrust force on the blade and the centrifugal force. Each gives rise to a flapping bending moment at the blade root, in opposite directions: Flapping wind moment tends to increase flap angle, β, and centrifugal "restoring" moment tends to decrease β. The moment balance where centrifugal moment just balances the wind flap moment will yield zero root flapping-bending moment, as shown in Fig. 12.4.

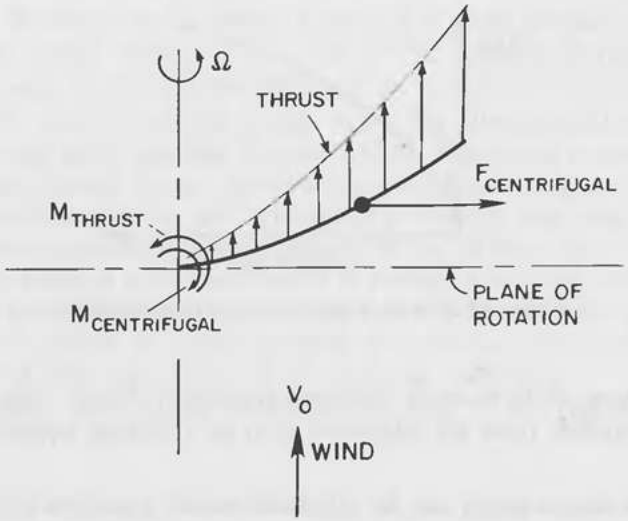

Figure 12.4. Flapping Free Body Diagram.

12.4 SECOND LEVEL: TRANSIENTS

At this point in the design, the rotor has an equilibrium or steady operating range of values, one for each steady wind speed for the power curve. To this set of baseline conditions are superimposed now a set of transient loading conditions, or load cases, to judge the next level of structural adequacy. These categories are still manifestations of statics, or events that would cause simple overstress events for the wind turbine; no manifestation of dynamics has yet entered the spec development.

Wind Gust: Rotor Stopped

It is common practice to specify an extreme gust condition for the specific site of interest and for the rotor in either the stopped or running configuration. At this point in the design process, the control system bounds on cut-out wind speed can be determined.

For the stopped rotor the extreme gust will act on the exposed surface of the blades and on the rest of the system. Only the blade will be considered since that extreme load condition is the most significant one. For a fixed-pitch turbine, the blade will be at the same pitch setting as it is in the running condition—that is, flatwise to the wind—and thus exposed at its maximum force coefficient (vulnerability) to the gust. For a typical extreme gust the

calculation proceeds as follows:

$V_{\text{gust}} = 125$ mph
Dynamic pressure $= \frac{1}{2}\rho A V_o^2$
Solidity $= \sigma$
Drag coefficient $= C_D = 1.3$ at 90° incidence[5]

Then the wind force of the blade is

$$\text{Force} = \frac{C_D[\frac{1}{2}\rho A V_o^2]\sigma\pi R^2}{(\text{number of blades})}$$

The root moment can be approximated by assuming that the planform-area centroid of the blade is at half span, and the stress is found in the usual way:

$$\text{Root stress} = \sigma_R = \frac{MC}{I_{R_o}}$$

This root stress will always be a large number for the extreme gust case. A 125-mph hurricane loading is the driving-load condition, static or dynamic, for almost all the fixed pitch turbines now operating.

For the blade that is feathered in the extreme wind condition, the conditions are the same, except that the drag coefficient is now reduced to about 0.10, or roughly one-thirteenth that of the 90-degree (feathered) drag coefficient. For this turbine, the hurricane loading on the rest of the turbine (i.e., nacelle and tower) is the significant value.

Wind Gust: Rotor Operating

For a uniform axial wind gust with the rotor operating, the conditions are complex. The rotor is exposed to a wind gust that is superimposed on the existing wind and on the airfoil flow, pressure forces, and moments. The analytical mechanism necessary for wind gusts to cause transient blade loads can be viewed as having two parts—the effect on relative velocity and the effect on angle of attack, as follows:

$$\begin{array}{ccc} \text{Lift} = C_l[\frac{1}{2}\rho V_{\text{rel}}^2]\, c & & \alpha \\ \| & & \| \\ (V + \Delta v) & & (\alpha + \Delta\alpha) \end{array} \qquad (12.6)$$

The major gust effect occurs in the angle of attack term. It is pointed out in Ref. 19 of Chap. 11 that a stall-controlled rotor reacts very differently to wind gusts than a pitch-controlled rotor does. Simply stated, it boils down to this: The stall-controlled rotor is not vulnerable to wind gusts in high winds because it is already acting like a "drag device" (i.e., Savonius rotor). Since its lift coefficient curve is already far past the stall point and exhibits low slope, it has low sensitivity to small changes in angle of attack. This can also be viewed as a region where the "aerodynamic amplifier" gain of the stall-controlled rotor has been drastically "turned down" by stall. At lower wind speeds, the stall-controlled rotor is sensitive to wind gusts. Fortunately, the gust amplitudes tend to be lower at lower average wind speeds.[6] The pitch-controlled rotor has the ability to relieve the gust loading by reducing angle of attack mechanically.[7] However, as pointed out in Ref. 19 of Chap. 11, there will always be a range of frequencies that is too fast for the pitching control system to handle, and within which the pitch-controlled machine will be sensitive to gusts. Also, the pitch-controlled rotor is further vulnerable in this frequency range since it is usually operating at a point on the lift-curve slope far enough below stall for wind gusts to cause a large overshoot and hysteresis in lift coefficient and blade thrust due to dynamic stall.

At this stage in preliminary design, it is useful to take a deterministic view of wind-gust loading. A complicating factor is the unsteady behavior of airfoils when operating near stall. That is, the behavior near stall cannot be predicted by the convenient two-dimensional wind-tunnel test curves, since the conditions are not steady and uniform (see Section 11.6). The major effects of dynamic stall are to produce a force hysteresis and a much higher momentary lift coefficient than the steady data would indicate. For example, a NACA 4415 maximum lift coefficient, under steady conditions vs. dynamic stall, is 1.4 vs. more than 2.2. This means that the actual gust load on the dynamically stalled blade is over 50 percent higher than would be predicted by simple steady-state theory. Therefore, it is practical and judicious to use a *gust safety factor*—based on empirical observations—for calculations of gust loading (see Table 12.3).

There is no scientific justification for the preceding "fudge factor" other than that field-test data on wind gusts tend to justify these numbers (see Ref. 16 in Chap. 11). The task remains for a good empirical gust-sensitivity prediction method to be found, as has been for the stalled lift and drag coefficients for NACA 44XX series airfoils (Ref. 21 in Chap. 11).

To proceed, using this simple gust safety-factor approach, a number of gust cases can be identified in the preliminary design for the site of interest. Each gust will have an assumed starting speed, ending speed, and rise time. The blade response will show more or less dynamic stall response, depending on the starting wind speed, the angle of attack, the reduced frequency, and the

Table 12.3. Arbitrary Safety Factor on Wind-Gust Loading Due to Dynamic Stall.

Wind speed	For pitch-controlled rotor	For stall-controlled rotor
10 MPH	1.2	1.2
15	1.3	1.3
20	1.4	1.5
25	1.5	1.6
30	1.6	1.8
35	1.8	1.6
40	1.8	1.5
45	1.6	1.3
50	1.5	1.1
55	1.3	1.0
60	1.0	1.0

airfoil. The disturbance and the assumed blade response are shown in Figs. 12.5 and 12.6.

The response shown in Fig. 12.6 is based on field-test data. Figure 12.7 gives a strip-chart recording of an incident gust and rotor response—in this case, total rotor thrust. The "overshoot" part of the response can be clearly seen; it is not predicted by the steady-state aerodynamic theory. The gust safety-factor "fudge factor" (Table 12.3) is based on recordings like this one from operating wind-turbine rotors.

As can be seen from the figures, the peak dynamic blade load due to the gust is the peak of the response. This is the load that should appear in the load specification for the blade.

If a computer strip theory is being used to calculate aerodynamic blade-root moments, the gust load can be estimated, as before, by calculating the normal quasi-steady moments for points 1, 2, and 3 on the graph, and then arbitrarily multiplying the safety factor from the table times value 2 at the response peak. If momentum theory is being used, the safety factor is

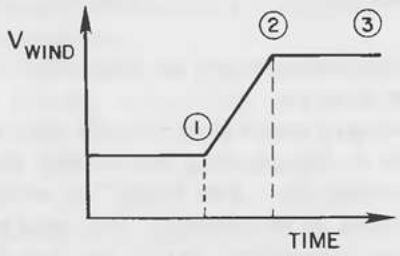

Figure 12.5. Assumed Gust Profile: Gust vs. time.

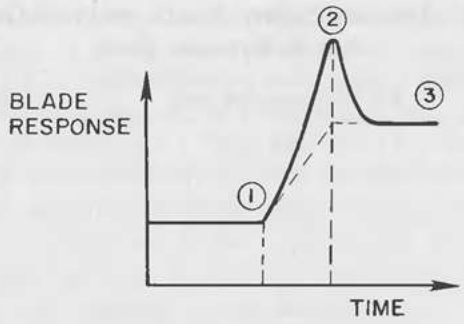

Figure 12.6. Assumed Blade Response: Blade load vs. time.

multiplied times the quasi-steady thrust coefficient at point 2. Then the root bending moment is found in the normal way from the thrust on one blade in its equipollent load system. For example, consider the following gust case:

Initial wind speed = 25 mph
Gust amplitude = 10 mph
Final wind speed = 35 mph
Initial rotor thrust = steady-state value
Final rotor thrust = steady-state value
Transient thrust at gust peak response = (Gust factor) (Steady-state value)

Blade-root bending moments are found by converting the rotor thrust to flapping moments at the blade roots, as in Sec. 12.3. For this example, the moments are

$$\text{Initial flap moment} = \frac{1}{b}\left[\frac{4}{9}\rho A\left(25 \times \frac{88}{60}\right)^2\right]\left[\frac{2}{3}R\right]$$

$$\text{Final flap moment} = \frac{1}{b}\left[\frac{4}{9}\rho A\left(35 \times \frac{88}{60}\right)^2\right]\left[\frac{2}{3}R\right]$$

$$\text{Gust moment} = 1.6 \times [\text{Final flap moment}]$$

Likewise, the transient deflection can be found by using the "overshoot" response curve in the same way.

A *stochastic* (statistical) view of gusts uses the gust-power spectral density as shown in Fig. 12.8. The abscissa is the gust frequency that can be visualized as corresponding to a "gust length" as would be measured by an anemometer superimposed on the "normal" axial-wind velocity. The ordinate is the gust-power density spectrum, that is, the variance of the fluctuating wind vs. frequency for the particular site depicted. The spectrum can be

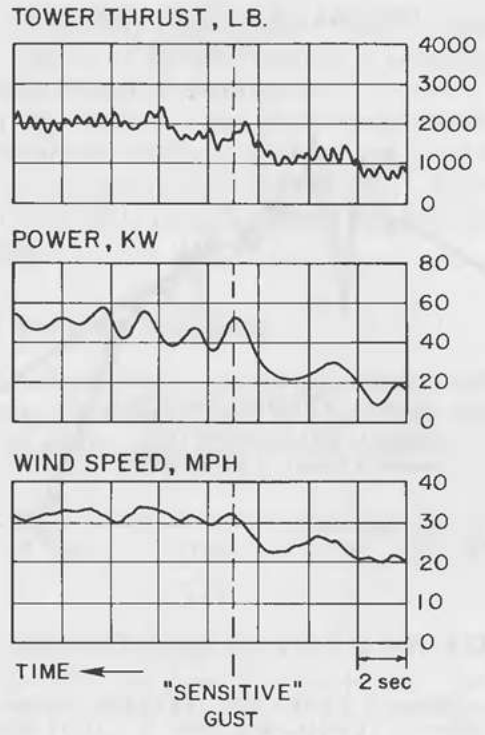

Figure 12.7. Typical Gust Response Data (see Ref. 16 in Chap. 11).

thought of as the probability distribution for the gust frequency range of the abscissa, or the likelihood of having a gust of a particular length and frequency. This spectrum can be constructed analytically by assuming homogeneous, isotropic turbulence and specifying an integral-length scale and turbulent energy for the wind.[8.9] The classical spectrum described in this way has been well verified with test data; it is shown in Fig. 12.8. This graph represents the gust spectrum that would be imposed on a building or bridge structure given the same atmospheric conditions.

Recent research has shown that the gust spectral density is different if the measurement point is rotating, as would be the case for an airfoil section on a wind-turbine blade (see Figure 12.9). This graph was constructed by assuming the preceding factors, plus a rotor diameter and speed. As can be seen, harmonic "spikes" now appear in the spectrum at integer multiples of the rotor speed, Ω. These are the simple multiples of incoming wind perturbation on the rotating blade, and correspond to the harmonics in the Fourier-series representation of aerodynamic loading. The first spike is the one-per-rev cyclic

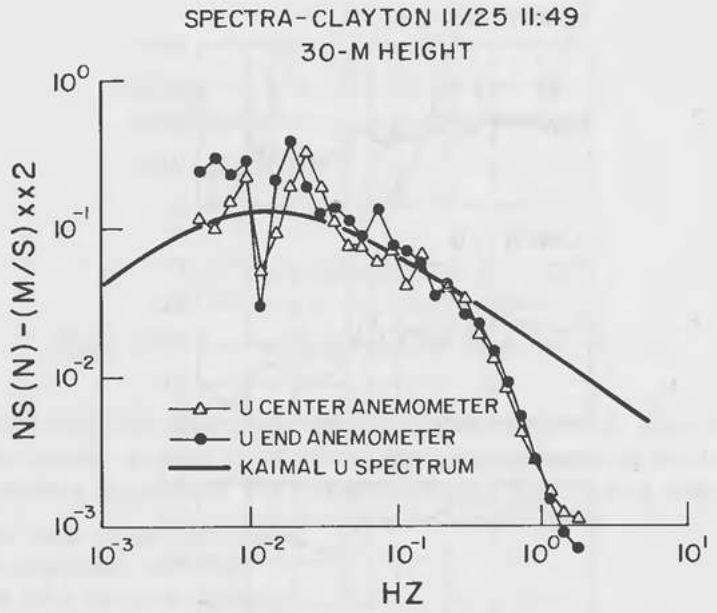

Figure 12.8. Normal Gust-Power Spectral Density (Ref. 12.9).

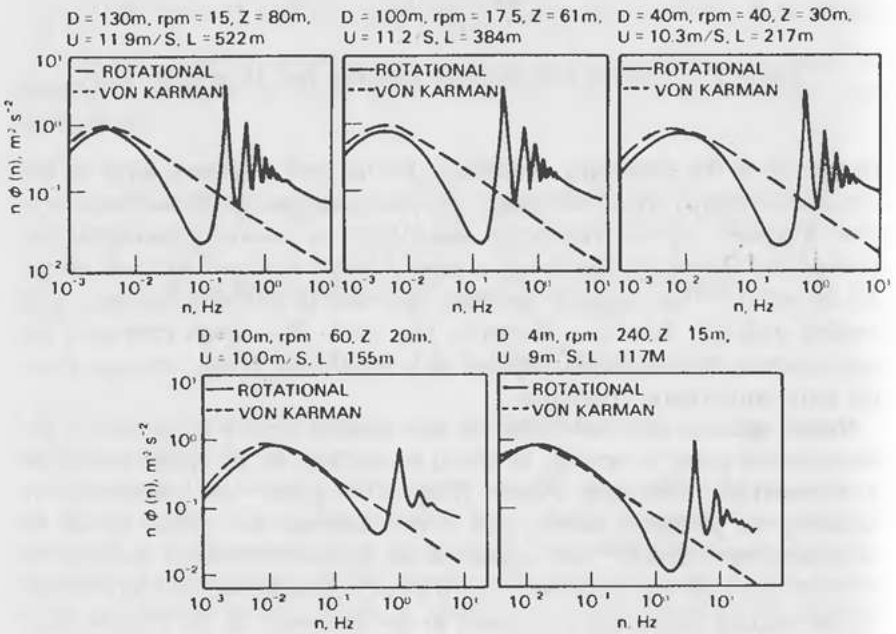

Figure 12.9. Rotating-Blade-Gust Spectral Density (Ref. 12.8).

perturbation that is caused by a linear-inflow "front" crossing the rotor plane (see Fig. 12.10). The higher harmonics are due to increasingly more complex inflow fronts passing through the rotating disc.

It is clear that Fig. 12.10 is a first step towards describing stochastically the array of atmospheric turbulence occurring on a wind-turbine blade. It remains for this to be translated into a useful array of blade loading in order to assess the effect on blade design. A useful and promising start has been provided by Garrad.[18]

Crosswind and Yaw-Rate Transients

Crosswind is defined in Chap. 7 as a superimposed wind component that appears in the plane of the rotor. It can be viewed as a gust in the wind that causes a change in relative wind direction and magnitude.

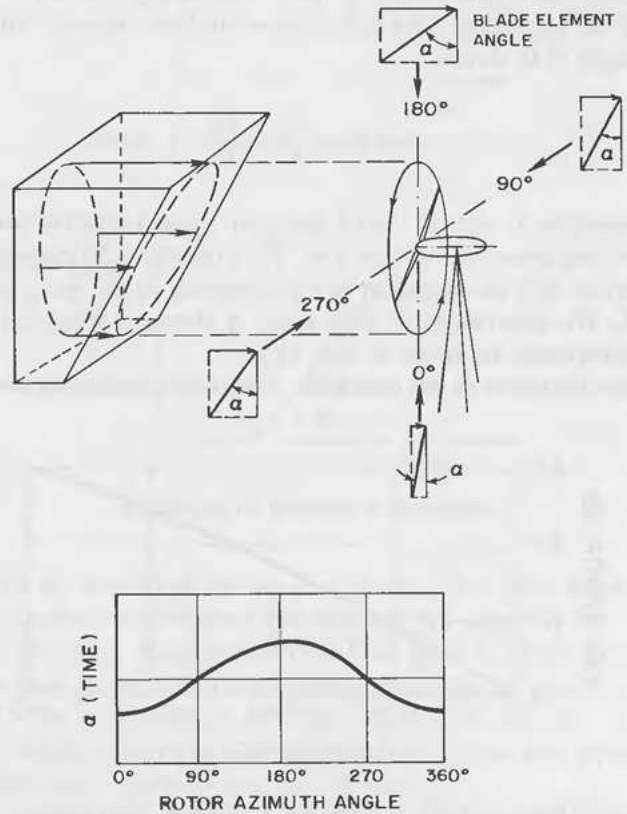

Figure 12.10. One-Per-Rev Linear-Shear Inflow Front.

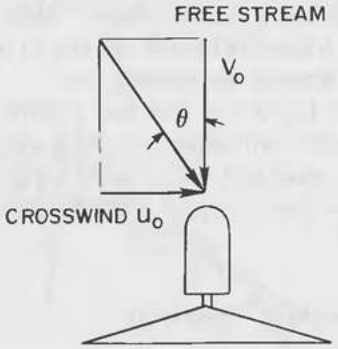

Figure 12.11. Crosswind on the Rotor.

Since the angle Θ represents the instantaneous relative wind direction, it is also the instantaneous yaw angle. It has a time-history equivalent to the gust risetime of the analogous wind gust. The equivalence between crosswind U_o and yaw angle Θ is simply:

$$\tan \Theta = \frac{U_o}{V_o} = \frac{\overline{U}_o}{\overline{V}_o} \tag{12.7}$$

It is convenient to view a "wind direction" gust as having two parts: an *increase in wind speed* and a *rotor yaw*. For example, a 50-percent crosswind with a risetime of 2 sec results in two disturbances to the rotor, as shown in Fig. 12.13. The disturbance in wind speed is shown in Fig. 12.14, and the yaw gust component is shown in Fig. 12.15.

Both these disturbances are transients. The speed component can be readily

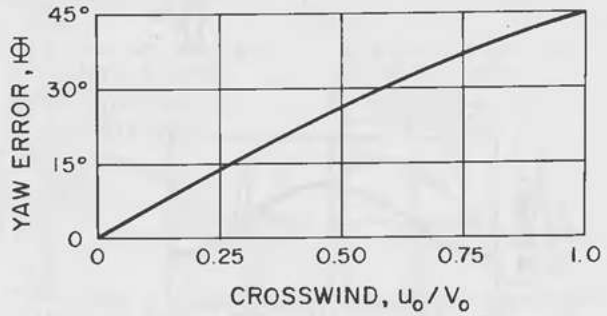

Figure 12.12. Crosswind and Yaw-Angle Equivalence.

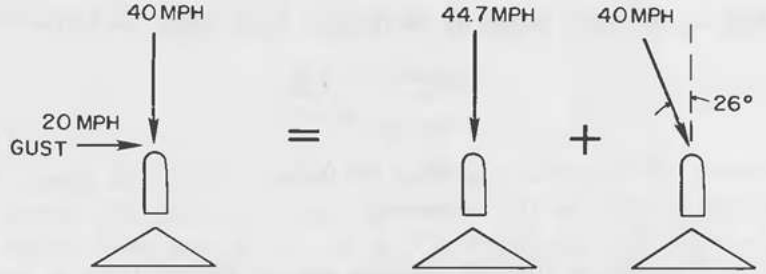

Figure 12.13. 50-percent Crosswind Example.

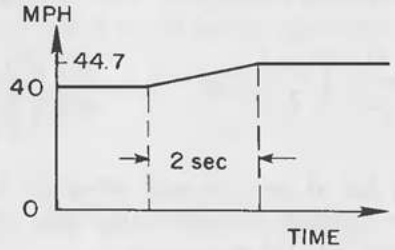

Figure 12.14. Wind-Speed Gust Component.

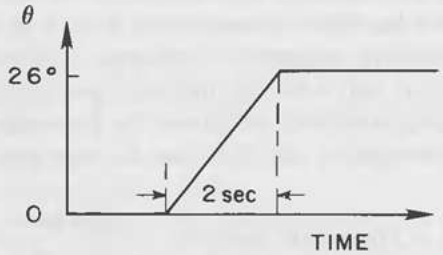

Figure 12.15. Yaw-Gust Component.

calculated by the method of the previous section. The yaw component is not so simple. As discussed in Sec. 12.5, a steady yaw angle on the rotor causes alternating, or cyclic, blade loads. Therefore, the rotor in this example will have cyclic load in response to the crosswind as long as steady yaw error is maintained. The wind turbine will then track back into the wind, either through its natural positive yaw stability derivative (free yaw systems) or via external mechanical means (forced yaw systems).

Cyclic moments due to crosswind are calculated in the usual way by

multiplying the cyclic angles by the flapping hinge spring, as follows:

$$\begin{aligned} M_{\beta_{1s}}\big|_{\text{Crosswind}} &= K_\beta \beta_{1s} \\ M_{\beta_{1c}}\big|_{\text{Crosswind}} &= K_\beta \beta_{1c} \end{aligned} \tag{12.8}$$

The cyclic angles are from the summary chart in Figure 12.22:

$$\begin{aligned} \Delta\beta_{1s}\big|_{\text{Crosswind}} &= -\frac{\bar{U}_o}{\Delta}\left\{\left(\frac{\gamma}{8}\right)^2\left(\frac{16}{3}\right)A(K-1)+\left(\frac{\gamma}{8}\right)^2 4A_3K\right\} \\ \Delta\beta_{1c}\big|_{\text{Crosswind}} &= -\frac{\bar{U}_o}{\Delta}\left\{\left(\frac{\gamma A_3}{2}\right)K(K-1)-\left(\frac{\gamma}{8}\right)^2\left(\frac{\gamma}{2}\right)\left(\frac{4}{3}\right)A\right\} \end{aligned} \tag{12.9}$$

The cyclic moments due to the yaw-angle offset are found from Eqs. 12.8 and 12.9. These are transient moments since they will die out when the turbine has yawed back into the wind again.

During the yawing-back motion, the rotor will experience a yaw rate, q, which can also cause dynamic load on these blades. If the turbine is free in yaw and has strong yaw stability, this restoring q can be very large—on the order of 35 deg/sec has been observed (see Ref. 3 in Chap. 9)—causing large transient gyroscopic moments. Gyroscopic, alternating root-flapping bending moment occurs only when the turbine is yawing; gyroscopic moment requires two orthogonal rotational velocities. The gyroscopic flapping moment appears in the cosine equation (Eq. 9.33) as the only purely inertial term:

$$\Delta M_{\beta_{1c}}\big|_{\text{Inertial}} = \text{Gyroscopic moment} = -\frac{2\bar{q}K(K-1)}{\Delta}K_\beta \tag{12.10}$$

where:

q = Yaw rate
Δ = Denominator
K = Nondimensional flap frequency $= \left(\dfrac{\omega_\beta}{\Omega}\right)^2$
K_β = Flapping hinge spring

Rewriting, using the identities, neglecting hinge offset, and using algebraic manipulation, the above reduces to the familiar gyroscopic form from classical dynamics:

$$M\big|_{\text{Gyroscopic}} = 2I_b q\Omega \tag{12.11}$$

This inertial alternating moment will be present whenever the turbine is being yawed. The moment is large and can be reduced only by reducing blade weight, blade rpm, or yaw rate q. The normal approach for reducing this load in practical wind turbines is to restrict yaw rate by using a yaw damper. In larger turbines, where blade weight is correspondingly higher, this alternating load is one of the chief design drivers of the blade structure.

There are also aerodynamic terms that produce blade-root bending moments as a result of yaw rate, as well as the inertial gyroscopic term:

$$\begin{aligned} \Delta\beta_{1s}\big|_{\text{Yaw rate}} &= -\frac{\bar{q}}{\Delta}\left\{\left(\frac{\gamma}{8}\right)K(K-1)+\left(\frac{\gamma}{8}\right)2K+\left(\frac{\gamma}{8}\right)^2 4A_3K\bar{l}\right\} \\ \Delta\beta_{1c}\big|_{\text{Yaw rate}} &= -\frac{\bar{q}}{\Delta}\left\{\left(\frac{\gamma}{2}\right)A_3K(K-1)\,\bar{l}-\left(\frac{\gamma}{8}\right)^2 K\right\} \end{aligned} \tag{12.12}$$

The gyroscopic term usually dominates the moment unless the blade is very light (as would be the case for the flexible fiberglass blade such as that used in Sec. 10.6). It is prudent in the design process to calculate all the terms in the yaw transient and then drop the aero terms only if they are found to be much smaller than the gyroscopic term.

Yaw stability is discussed in Sec. 10.5. Steady yaw tracking error can be caused by blade design (gravity) and wind shear, which will lead to alternating loads; these are discussed in Sec. 12.5.

Another moment occurs during the yawing motion of a two-bladed turbine in the nonrotating tower coordinate system. The tower moment for a two-bladed rotor is taken from Eq. 10.11:

Yawing:

$$M_{X'}\big|_{\text{2 blades}} = K_\beta\beta_{1s} + K_\beta\beta_{1c}\sin 2\psi - K_\beta\beta_{1s}\cos 2\psi$$

Pitching: (12.13)

$$M_{Y'}\big|_{\text{2 blades}} = -K_\beta\beta_{1c} - K_\beta\beta_{1s}\sin 2\psi - K_\beta\beta_{1c}\cos 2\psi$$

The two two-per-rev terms in Eq. 12.13 cause tower-top vibrations that may be substantial design loads. For a teetering rotor, $K_\beta = 0$, and thus these tower moments will not appear (the dynamics appearing instead as teetering motion of the rotor).

For a 3- or b-bladed turbine, the tower moments are taken from Eq. 10.13:

Yawing:

$$M_{X'} = \frac{b}{2} K_\beta \beta_{1s}$$

Pitching: (12.14)

$$M_{Y'} = -\frac{b}{2} K_\beta \beta_{1c}$$

The yawing moment on the tower top due to steady yaw angle (steady crosswind) is therefore found by substituting the sine cyclic due to crosswind (Eq. 12.9) into Eq. 12.14. The same is true for the tower pitching moment. The nacelle pitching moment, $M_{Y'}$, must be resisted by the tower top bearing and mounting. The yaw restoring moment, $M_{X'}$, must be resisted by the yaw drive gears or the yaw damper system, unless it is a completely free-yawing rotor.

Figure 12.16 presents the calculated tower yawing and pitching moments for the example rotor of Chap. 10 (Sec. 10.6). The cyclic values used in Eq. 12.14 are the perturbations due to crosswind (Eq. 12.9), with an added term to account for rotor preconing, β_{PC} (see Eq. 9.36), and a substitution for yaw angle Θ has been made:

$$\Delta\beta_{1c} = \frac{1}{\Delta}\left\{\left[\left(\frac{\gamma}{8}\right)^2\left(\frac{\gamma}{2}\right)\left(\frac{4}{3}\right)A - \left(\frac{\gamma}{2}\right)A_3K(K-1)\right]\overline{V}_o \sin\Theta + \left[\left(\frac{\gamma}{8}\right)^2\left(\frac{4}{3}\right)K\right]\overline{V}_o \sin\Theta\,\beta_{PC}\right\}$$

$$\Delta\beta_{1s} = -\frac{1}{\Delta}\left\{\left[\left(\frac{\gamma}{8}\right)^2\left(\frac{16}{3}\right)A(K-1) + \left(\frac{\gamma}{8}\right)^2 4A_3K\right]\overline{V}_o \sin\Theta + \left[\left(\frac{\gamma}{8}\right)^2\left(\frac{4}{3}\right)K(K-1)\right]\overline{V}_o \sin\Theta\,\beta_{PC}\right\}$$

As can be seen from the figure, the yaw moment is always stabilizing, and preconing increases it appreciably. The pitching moment, on the other hand, is reduced by preconing. Recalling that this is a light ($\gamma = 14.07$), high-

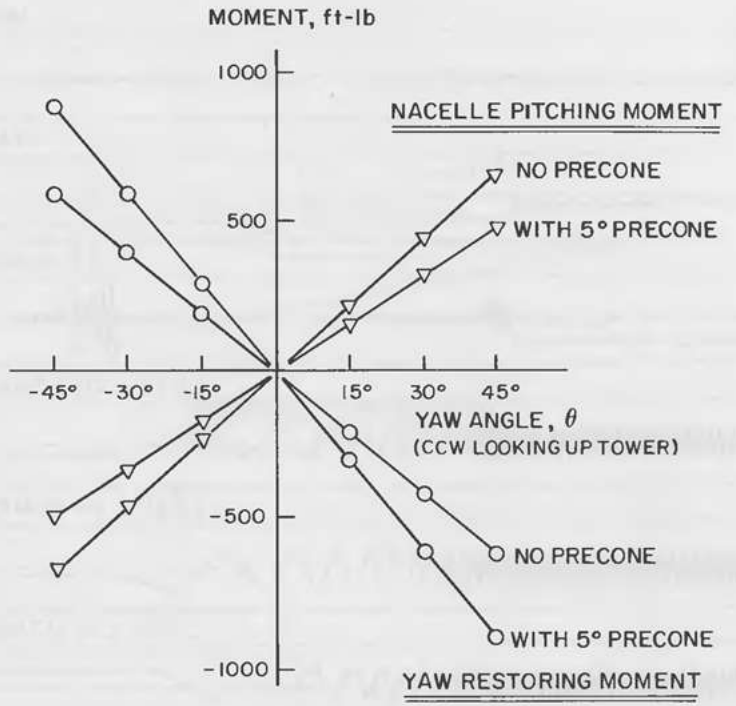

Figure 12.16. Calculated Rotor Yawing and Pitching Moments (Example of Ch. 10).

speed (TSR = 7.0) rotor, the conclusion can be made that, for this type of rotor, preconing is a design advantage.

Pitching Transients

For a rotor with pitch control, the blade will experience transient loads due to pitch change and independent of wind gusts. The most significant transient load occurs when pitch change is being used to stop the rotor at high power. There are two conceivable ways to "dump load" at high power levels: either by increasing the angle of attack to cause stall or decreasing the angle of attack to reduce lift coefficient. Both methods potentially can result in high transient lift coefficients due to unsteady aerodynamics effects.

Very little data are available on these control loads. Some tests on the Danish Nibe A and Nibe B turbines are reported in Ref. 18 of Chap. 11 and Nielsen et al.[10] Both turbines are shown in Fig. 11.13. Nibe A is a stall-controlled rotor that uses pitch change in the stalling direction to brake the rotor. Its normal operation pitching range is from +1 to −4 degrees. To stop the rotor, the pitch is changed to −20 degrees (nose-up, thereby increasing

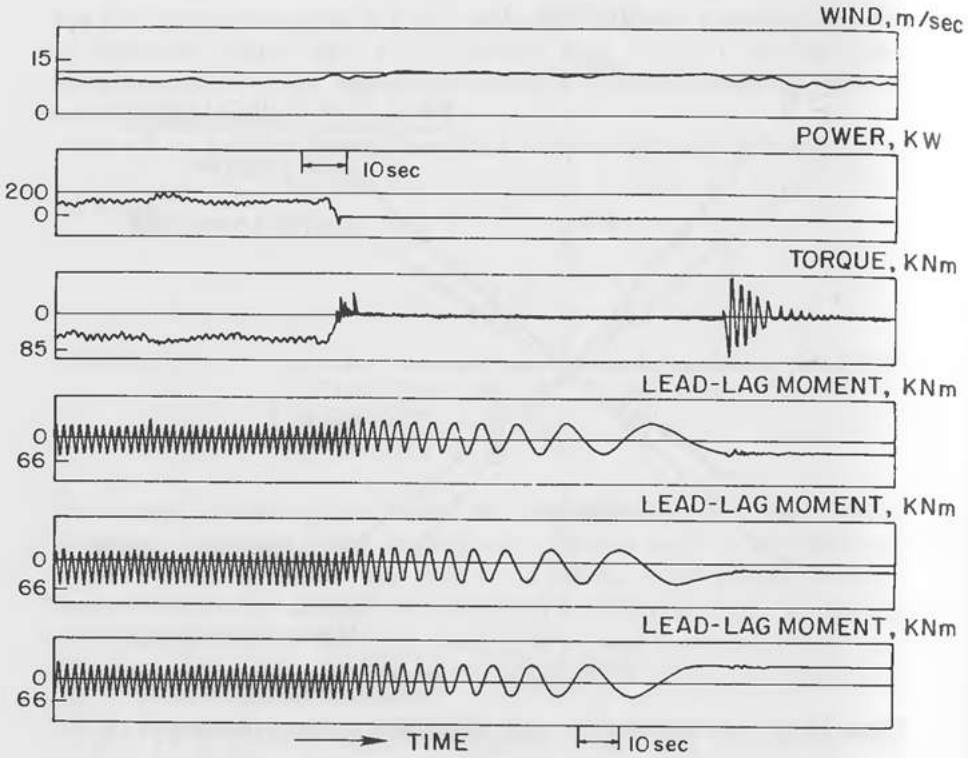

Figure 12.17. Nibe A Standard Brake Trace (Ref. 12-10).

angle of attack). Figure 12.17 shows a strip chart recording of the lead-lag blade bending moments, shaft torque, and power during a normal stop.

Surprisingly, as can be seen in the traces, there were no load transients of consequence, and the bending moments were largely unaffected by the braking, contrary to what might be expected since the blade is rapidly going through stall. However, as discovered in the test program, the mechanism for stopping the rotor was simply to increase the drag sufficiently to change the positive driving torque to negative driving torque. This simply slowed the rotor down smoothly and safely, as shown in Fig. 12.18, which gives the blade-element diagrams in normal operation and in normal braking.

The Nibe B turbine is a pitch-regulated turbine and exactly the same size as the Nibe A turbine. To stop the Nibe B, the pitch change is from operating pitch to full feather, +90 degrees. A typical chart recording is given in Fig. 12.19. The chart clearly shows the large flapwise and chordwise transient moments experienced by the blades. These transients were so high that the

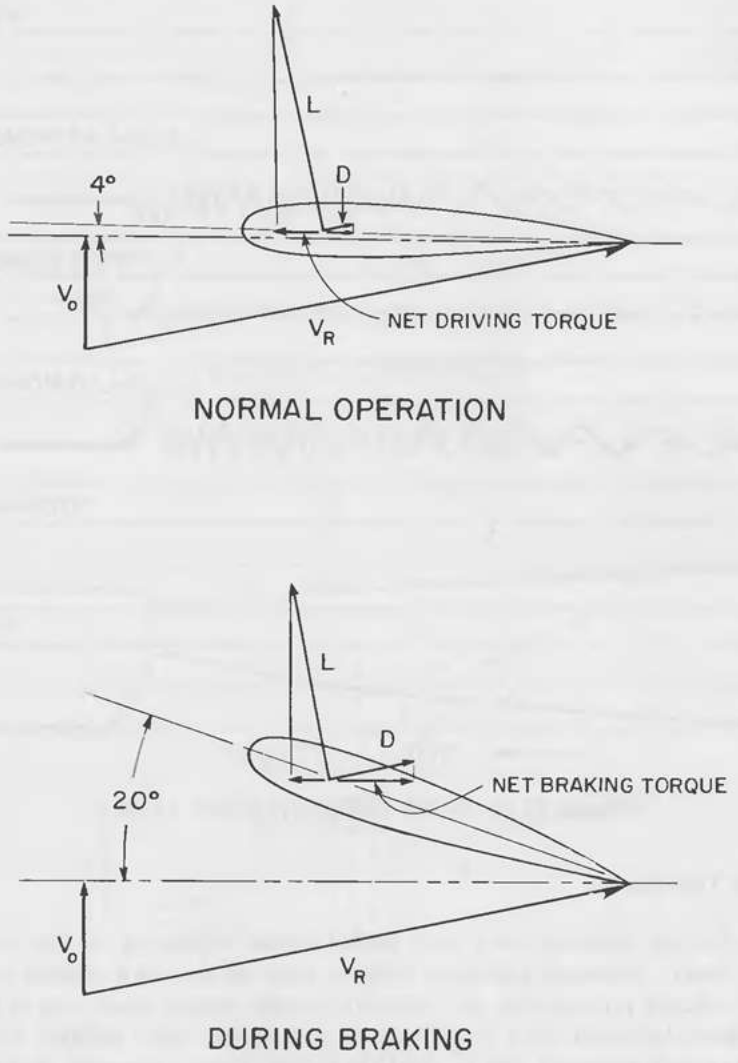

Figure 12.18. Nibe A Blade Element Diagrams (Ref. 12-10).

braking procedure for the turbine was modified, thus making this feathering procedure suitable only for emergencies. The mechanism for these high transients was not the obvious one of passing through the power or lift coefficient peak. Referring to the blade-element diagrams in Fig. 12.20, it can be clearly seen that the blade goes into a region of negative lift when the rapidly pitching airfoil meets and passes the relative wind angle.

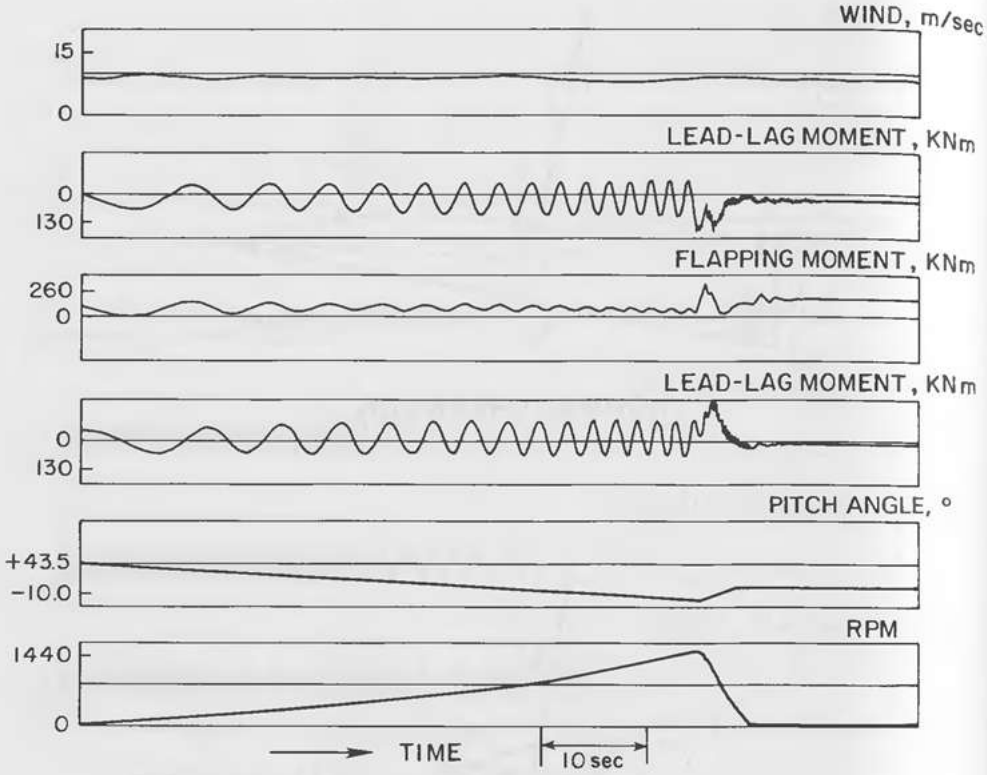

Figure 12.19. Nibe B Braking Trace (Ref. 12.10).

Other Transients

Other loading transients may need consideration, depending on the concept under study. *Actuation transients* refer to parts of the rotor control system with sufficient proximity to the blade to transfer control loads. An example is a blade flyweight on a centrifugal force-actuated blade pitching system. The flyweight moments will be constant during normal operation, that is, at constant operating rpm. In overspeed, however, the centrifugal force builds as the square of the rpm, and so does the centrifugal control moment on the blades.

Other transients of possible interest are *erection transients*, e.g., gravity loads during erection, and *environmental transients*, e.g., blade-strike loads. Good "shopping lists" of environmental loads can be found in the American Wind Energy Association (AWEA) WECS Structural/Mechanical Design Criteria (Draft) Industry Consensus Standard[11] and the Canadian Standards Association (CSA) SWECS Safety, Design, and Operation Criteria Preliminary Standard.[12]

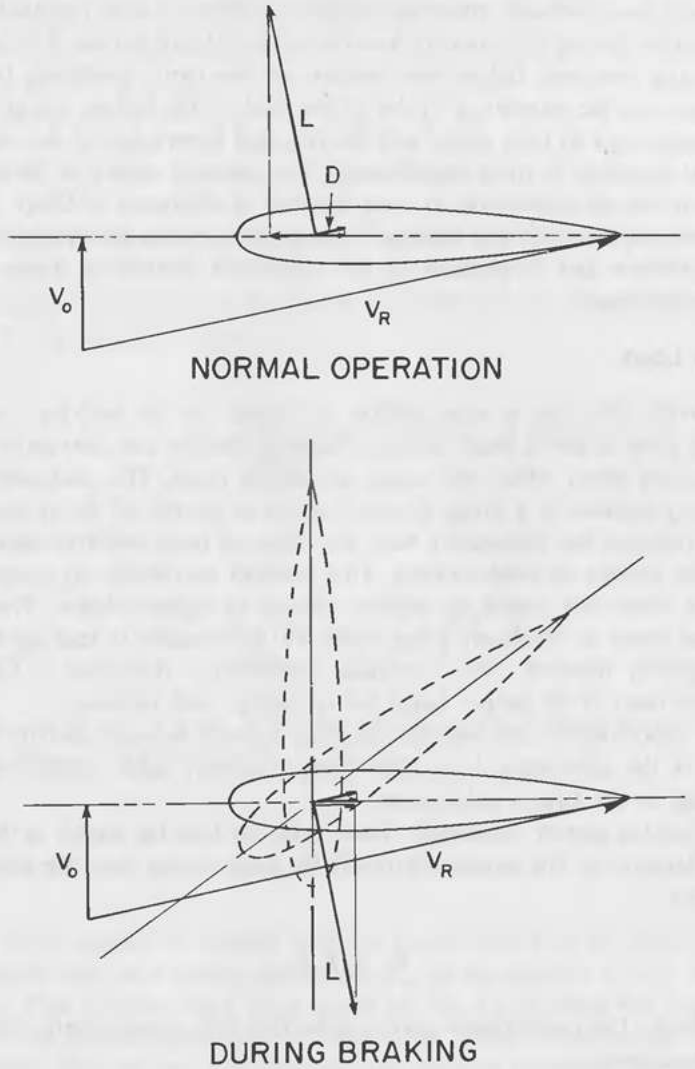

Figure 12.20. Nibe B Blade Element Diagrams (Ref. 12-10).

12.5 THIRD LEVEL: ALTERNATING LOADS

At this point in the design, the specification of loading has covered the steady and the transient loads to which the rotor will be exposed. Historically, the transients have caused the great majority of wind-turbine failures. The reason is simply that transient loads are much higher in magnitude than other types of loads, and the turbines were simply overstressed at critical points.

A much more difficult structural problem is failure due to repeated cycles of alternating loading substantially lower in magnitude, or *fatigue*. The problem of assessing imminent failure now consists of two parts, predicting both the *magnitude* and the *number of cycles* of the load. Wind-turbine design theory has shortcomings in both areas, and the required knowledge of the nature of structural materials is more complicated. The classical theory of fatigue and its state-of-the-art application to wind turbines is discussed in Chap. 13 and in Waldon and Hansen[13] and Murtha.[14] The present section attempts to estimate the magnitudes and frequencies of the significant alternating loads on the wind-turbine blade.

Gravity Load

The gravity effect on a wind turbine is mostly in the lead-lag direction, although there is also a small effect in flapping. Gravity can also cause steady yaw tracking error, which will cause alternating loads. The alternating lead-lag gravity moment is a strong dynamic driver to the rest of the system. This forcing function has historically been the cause of most tower resonance and instability failures of wind turbines. This moment also builds up cycles faster than any other and cannot be reduced except by lighter blades. There is a rotational speed at which any given blade will be unstable in lead-lag because of the gravity moment. This "pendular instability," discussed in Chap. 8, has never been in the proper range for operating wind turbines.

It is important to calculate the lead-lag gravity moment and to have it appear in the alternating load spec since it always adds cycles and load magnitude to the fatigue calculation.

The lead-lag gravity moment is found from the lead-lag angles in the same way as flapping is. The moment is merely the hinge spring times the deflection, as follows:

$$M_\zeta = K_\zeta \zeta_o$$

and so forth. The predominant gravity-deflection term appears only in the sine cyclic component:

$$\zeta_{1s} = -\frac{2B}{(K_2 - 1)} \tag{12.15}$$

Simply stated, the "horizontal scissoring" (lead-lag sine cyclic) of the rotor blade will be maximum when the blade is level, and the response will be primarily in the sine component. As seen in Sec. 9.5, there will also be a cosine component of gravity when there is a steady lead-lag angle, ζ_o. This latter is a very small disturbance, however, since lead-lag stiffness is usually large and ζ_o is very small. From Eqs. 9.46, 9.47, and 9.48, we have lead-lag general-motion solutions:

$$\underset{\text{Gravity}}{\zeta_{1c}|} = \tfrac{1}{2}[\zeta_o \times \underset{\text{Gravity}}{\zeta_{1s}}] \tag{12.16}$$

The physical mechanism for this cosine response is inertial coupling between ζ_o and ζ_{1s}.

The flapping response to the gravity moment is more complicated. From Eq. 9.18, we have the cosine cyclic,

$$\underset{\text{Gravity}}{\beta_{1c}|} = -\frac{1}{\Delta}\gamma B(K-1)A \tag{12.17}$$

and the sine cyclic,

$$\underset{\text{Gravity}}{\beta_{1s}|} = -\frac{1}{\Delta}\left(\frac{\gamma}{8}\right)^2 BA$$

As shown in Sec. 9.4 Eq. 9.19, the components are related by the familiar "cyclic sharing" relationship due to gravity:

$$\frac{\Delta\beta_{1c}}{\Delta\beta_{1s}} = \frac{K-1}{(\gamma/8)} \tag{12.18}$$

This cyclic sharing in flapping is due to gravity acting on the blade through the moment arm of a steady flap angle, β_o, at an azimuth ψ of 0 and 180 degrees. This "cosine input" is verified by Eq. 12.18 using the method of Sec. 9.4. In lead-lag, gravity is a "sine input" since it acts on the blade at an azimuth ψ of 90 and 270 degrees. The lead-lag degree of freedom does not have this "cyclic sharing" response.

The alternating blade lead-lag moments to calculate for the gravity effect are

$$M_{1s} = K_\zeta \zeta_{1s}$$

and (12.19)

$$M_{1c} = K_\zeta \zeta_{1c}$$

where:

$$\zeta_{1s}\Big|_{\text{Gravity}} = -\frac{2B}{(K_2 - 1)} \qquad (12.20)$$

$$\zeta_{1c}\Big|_{\text{Gravity}} = \tfrac{1}{2}[\zeta_o \times \zeta_{1s}]_{\text{Gravity}}$$

The alternating blade flapping root moments (see Fig. 12.21) are taken from

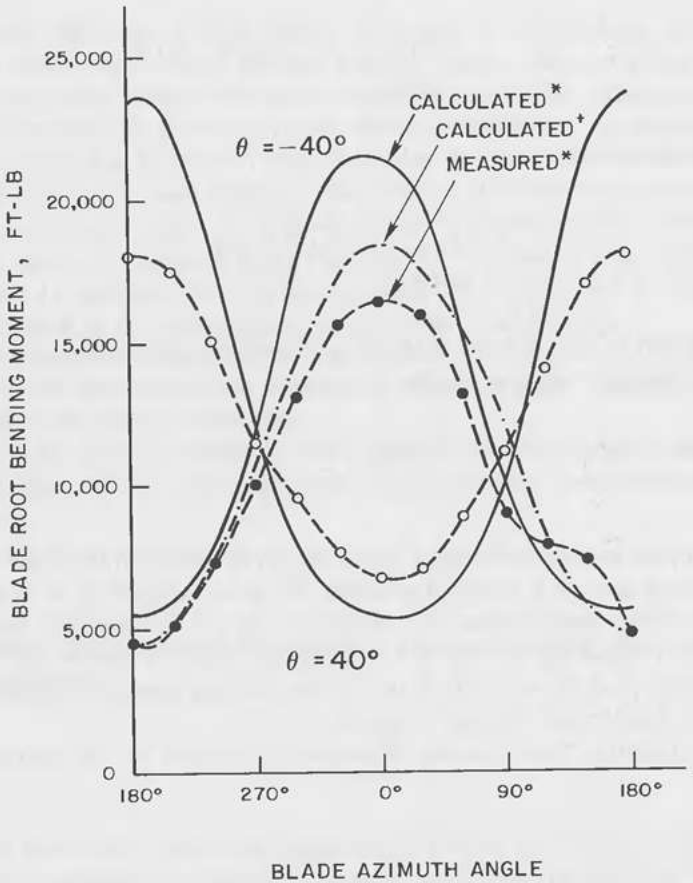

Figure 12.21. Flapwise Blade Root Moment During One Revolution at ±40° Steady Yaw Angle at 54.4 mph [*Calculated and Measured (Ref. 11.21); †Calculated by Present Theory].

Axisymmetric Flow + *Hinge Spring* + *Gravity*	*Crosswind*	*Yaw Rate*	*Wind Shear*
$\beta_o = \frac{1}{\Delta}\left\{\frac{\gamma A}{2}\left[(K-1)^2 + \left(\frac{\gamma}{8}\right)^2\right]\right.$	$-$	$-$	$-\Big\}$
$\beta_{1c} = \frac{1}{\Delta}\left\{\right.$	$+\left(\frac{\gamma}{8}\right)^2\left(\frac{\gamma}{2}\right)\frac{4}{3}A\bar{U}_o$	$-2\bar{q}K(K-1)$	$\Big\}$
	$-\frac{\gamma A_3}{2}K(K-1)\bar{U}_o$	$-\frac{\gamma A_3}{2}K(K-1)\bar{q}\bar{l}$	$-\frac{\gamma}{2}\left(\frac{K_1\bar{V}_o}{4}\right)K(K-1)$
$\left.-\gamma BA(K-1)\right\}$		$+K\bar{q}\left(\frac{\gamma}{8}\right)^2$	
$\beta_{1s} = \frac{1}{\Delta}\left\{\right.$	$-\left(\frac{\gamma}{8}\right)^2\frac{16}{3}A(K-1)\bar{U}_o$	$-\left(\frac{\gamma}{8}\right)^2 4A_3 K\bar{q}\bar{l}$	$\Big\}$
	$-\left(\frac{\gamma}{8}\right)^2 4A_3 K\bar{U}_o$	$-\frac{\gamma}{8}\bar{q}K(K-1)$	$-\left(\frac{\gamma}{8}\right)^2 K_1\bar{V}_o K$
$\left.-\frac{\gamma^2}{8}BA\right\}$		$-2\bar{q}K\left(\frac{\gamma}{8}\right)$	

where

$$\Delta = K\left[(K-1)^2 + \left(\frac{\gamma}{8}\right)^2\right]$$

Figure 12.22. Summary Chart: Rotor Flapping Dynamics.

the summary chart in Fig. 12.22, as follows:

$$M_{\beta_{1s}} = K_\beta \beta_{1s}$$
$$M_{\beta_{1c}} = K_\beta \beta_{1c} \tag{12.21}$$

where:

$$\beta_{1s}\Big|_{\text{Gravity}} = -\frac{1}{\Delta}\left(\frac{\gamma^2}{8}\right) BA$$
$$\beta_{1c}\Big|_{\text{Gravity}} = -\frac{1}{\Delta}\gamma BA(K-1) \tag{12.22}$$

In Sec. 10.5, the yaw stability due to gravity and wind shear was discussed. It was found that gravity and wind shear both cause destabilizing tower yaw moments, which are counteracted in a free yaw turbine by the crosswind term at a steady yaw tracking error, Θ. The approximate steady yaw tracking error due to gravity (Eq. 10.19) is

$$\Theta \simeq \frac{\Omega R}{V_o}\left[\frac{3B}{2(2K-1)}\right] \tag{12.23}$$

This yaw error term must be calculated to ascertain whether the candidate rotor will have appreciable steady yaw error as a result of gravity. If so, an alternating crosswind moment will be present. This must be calculated, as shown in the next section, and included in the blade spec.

Crosswind Load

The transient effects of crosswind, or steady yaw angle, were discussed in Sec. 12.4. The major effect of steady yaw angle is to produce large alternating blade-root moments due to asymmetric aerodynamics, which is the source of this alternating load. This section presents a calculation for the case of steady yaw angle.

From the summary chart in Fig. 12.22, crosswind terms appear in both the sine and cosine components of root flapping moment, as follows:

$$\Delta\beta_{1c}\Big|_{\text{Crosswind}} = -\frac{\overline{U}_o}{\Delta}\left\{\frac{\gamma}{2}A_3K(K-1) - \left(\frac{\gamma}{8}\right)^2\left(\frac{\gamma}{2}\right)\frac{4}{3}A\right\}$$
$$\Delta\beta_{1s}\Big|_{\text{Crosswind}} = -\frac{\overline{U}_o}{\Delta}\left\{\left(\frac{\gamma}{8}\right)^2\frac{16}{3}A(K-1) + \left(\frac{\gamma}{8}\right)^2 4A_3K\right\} \tag{12.24}$$

A calculation for the cyclic root bending moment due to a steady 40-degree yaw angle (83-percent crosswind) is presented in Fig. 12.21, which shows the measured root moment and also the calculation of this moment from Ref. 21 in Chap. 11. This rotor blade is quite stiff ($K = 13.8$) and has a fixed-pitch design with no preconing angle. It can be seen in Fig. 12.21 that the blade response is largely cosine, thus producing large nacelle pitching moments and rather small yaw stabilizing moments. The major reasons for this are the low speed (TSR = 1.75 and stalled) and the high blade weight ($\gamma = 5.07$).

Wind Shear

Wind shear is a pure cosine-input perturbation in flapping (see Fig. 11.9). For small rotor diameters, on the order of 50 feet in diameter and less, the crosswind perturbations are much larger than wind shear. However, frequent wind shear at a site will cause alternating cycles to build up at a rate almost equivalent to gravity loads. From the summary chart of Fig. 12.22, wind-shear terms appear in both the sine and cosine components of root flapping moment:

$$\Delta\beta_{1c}\Big|_{\text{Wind shear}} = -\frac{1}{\Delta}\left(\frac{\gamma}{2}\right)\frac{K_1\overline{V}_o}{4}K(K-1)$$
$$\Delta\beta_{1s}\Big|_{\text{Wind shear}} = -\frac{1}{\Delta}\left(\frac{\gamma}{8}\right)^2 K_1\overline{V}_oK \tag{12.25}$$

The blade-root moments are again found by multiplying the cyclic angles times the flapping spring, as follows:

$$M_{\beta_{1c}}\Big|_{\text{Wind shear}} = K_\beta\beta_{1c}\Big|_{\text{Wind shear}}$$
$$M_{\beta_{1s}}\Big|_{\text{Wind shear}} = K_\beta\beta_{1s}\Big|_{\text{Wind shear}} \tag{12.26}$$

In Sec. 10.5, the yaw stability due to gravity and wind shear was discussed. It was found that gravity and wind shear both cause destabilizing tower yaw moments, which are counteracted in a free-yaw turbine by the crosswind terms at a steady yaw tracking error, Θ. The approximate error due to wind shear (Eq. 10.21) is as follows:

$$\Theta \simeq \frac{3K}{16A + 12A_3} \tag{12.27}$$

Again, as in Sec. 12.5 on gravity, this yaw error may be substantial,

resulting in significant alternating load. The method of the last section is used to calculate this alternating moment.

Tower Wake and Tower Dam Loads

The tower wake impinging on a downwind rotor causes a one-per-rev aerodynamic perturbation in each blade's revolution. This appears as a one-per-rev pulse in the blade-root bending moment. For an upwind rotor, the blade passing in front of the tower is affected by the "reflection" from the tower, which is called *tower dam.*

Some work has been done towards estimating and measuring the tower wake (and dam) effect analytically[15,16,17] (see also Ref. 4 in Chap. 8), but the problem is complicated by the lack of knowledge of the unsteady aerodynamic response of the blade. In preliminary design, it is judicious to allow a tower wake (dam) alternating load in the blade bending-moment specification.

Other Alternating Loads

Other sources of alternating loads are Coriolis coupling, imbalance, resonance, and flutter. The latter two, both instabilities, are discussed in Chap. 11.

Imbalance on a rotor can be of two types: *mass imbalance* or *out-of-tracking*. Mass imbalance is the simple inertial effect of one blade's being out-of-balance and appears as a normal one-per-rev. It is calculated in the same way as the alternating gravity moment. Out-of-tracking is aerodynamic imbalance caused by blades being at different pitch angles, thereby experiencing different angles of attack and loading. Out-of-track blades are easily recognized in field testing as those that do not trace the same tip-path plane. For this reason, blade tips are often color-coded to differentiate the blade that needs adjustment.

Coriolis coupling, not usually a problem, is included here only for the sake of completeness. It is described by the $X_{\beta'}$ term derived in Eq. 9.40. This is very simply the effect of the flapping velocity, β', on lead-lag moments. As the blade vibrates up and down in flapping, a reaction moment is produced in the lead-lag direction as a result of the kinetics of the rotating coordinate frame ("Coriolis effect"). The lead-lag Coriolis moment is defined as follows:

$$M_{\zeta'|\text{Coriolis}} = I_b \Omega^2 \Bigg\{ \underbrace{2\beta}_{\text{I}} - \underbrace{\left(\frac{\gamma}{2}\right) A_4}_{\text{II}} + \underbrace{\left(\frac{\gamma}{2}\right) \cos\psi \left[\left(\frac{K_1 \bar{V}_o}{2} \right) + \frac{\theta_p}{3} (\bar{U}_o + \bar{q}\bar{l}) \right] + \left(\frac{\gamma}{2}\right) \sin\psi \left[\left(\frac{\bar{q}}{2} \right) + \frac{2}{3} \beta \bar{U}_o \right]}_{\text{III}} \Bigg\} \tag{12.28}$$

Table 12.4 Loading Specification: Blade-Root Flapping Moments.

Source	*Type*	*Calculated Moment, ft-lb*	*Frequency*	*Estimated Cycles/Year*	*Root Stress, psi*
Steady wind	Steady aerodynamic	6000	Continuous	—	15,720
Wind gust	Transient aerodynamic	13,000	12/hr	10^5	34,000
Gravity	Alternating inertial	140	1/rev	60×10^6	370
Gyroscopic	Alternating inertial	1800	1/rev	10^6	4700
Crosswind	Transient aerodynamic	400	1/rev	5×10^6	1050
Aerodynamic imbalance	Steady aerodynamic	2100	Continuous	—	5500
Mass imbalance	Alternating inertial	300	1/rev	60×10^6	790
Centrifugal	Steady inertial	3650 (lb)	Continuous	—	365 (tension)

Table 12.5. Loading Specification: Blade-Root Lead-Lag Moments.

Source	Type	Calculated Moment ft-lb	Frequency	Estimated Cycles/Year	Root Stress, psi
Steady wind	Steady aerodynamic	1000	Continuous	—	2220
Wind gust	Transient aerodynamic	1700	12/hr	10^5	3800
Gravity	Alternating inertial	1800	1/rev	60×10^6	4000
Gyroscopic	Alternating inertial	Nil	—	—	Nil
Crosswind	Transient aerodynamic	Nil	—	—	Nil
Aerodynamic imbalance	Steady aerodynamic	420	Continuous	—	930
Mass imbalance	Alternating inertial	400	1/rev	60×10^6	900
Coriolis coupling	Alternating inertial	500	1.7/rev	10^6	1100
Centrifugal	Steady inertial	Nil	—	—	Nil

The physical interpretation of this moment is simply

Lead-lag Coriolis moment = Centrifugal force × Flapping velocity

As discussed in Sec. 10.6, the flapping velocity consists of three parts: (1) the *inertial moment* due to flapping angle, β (Coriolis moment), (II) the *aerodynamic damping*, and (III) the *cyclic perturbations*. The flapping velocity is not likely to be large unless there is a loss of aerodynamic damping (unlikely, that is, unless the rotor is completely stalled) or there is substantial cyclic load as a result of strong wind shear or large yaw error. These effects can be estimated in the design process by arbitrarily choosing a maximum/minimum value of flap angle, $\pm\beta$, and by assuming that the blade will vibrate for a number of cycles at those limits and superimpose a set of perturbations (see Sec. 10.6). If it is seen at all, this moment shows up in strip-chart recordings of lead-lag blade moment as a vibration at the natural frequency of the flapping motion. It thus appears as a periodic, alternating load only when the blade is being forced at its natural frequency in flapping by some other perturbation, such as tower wake or drivetrain frequency. This Coriolis lead-lag moment is not more significant than it is simply because the blade, in its flapping vibration, is almost always critically damped and cannot develop a destructive resonance.

12.6 SUMMARY CHART AND LOAD SPECIFICATION

The flapping dynamics of the rotor are summarized in the Summary Chart of Fig. 12.22, which reproduces Fig. 10.3. Tables 12.4 and 12.5 give a sample loading specification for a hypothetical "straw man" rotor. This example is for a 10-m (32.5-ft) diameter, three-bladed, fixed-pitch rotor that operates at 100 rpm. Table 12.4 gives the flapwise blade-root dynamic moments and Table 12.5, the lead-lag. Root stress was calculated by assuming a flap root-section modulus (I/C) of 4.580 in.^{3}, a lead-lag root-section modulus of 5.400 in.^{3}, and a cross-sectional area of 10 in.^{2}. All that remains to judge the "straw man" blade adequate is to multiply appropriate safety factors times the respective moments and add the root stresses for the expected combined load cases.

REFERENCES

1. Stoddard, F. S. (principal investigator), et al. Wind turbine aerodynamics research needs assessment. DOE/ER/30075-H1, NTIS DE 86009189, Washington Consulting Group, Washington, D. C. Prepared for U.S. Department of Energy, Office of Energy Research, Washington. D. C., Jan. 1986.
2. Harper, C. W.; Ashley, H.; Bisplinghoff, R. L.; and Eggers, A. J., Jr. On uncertainties in

the aerodynamics and structural dynamics of upwind rotors on large HAWT's in relation to their reliable and long life operation. Prepared by RANN, Inc., Palo Alto, CA, DOE Contract No. DE-ACO4-82AL21362. Wind Energy Systems Program Office, U.S. Department of Energy, Washington, D. C., Apr. 1983.

3. De Vries, O. Fluid dynamic aspects of wind energy conversion. AGARD-Ograph No. 243, National Aerospace Laboratory, the Netherlands, 1979.
4. Montgomerie, B. Unsteady aerodynamics applied to the horizontal axis wind turbine disc. FFA Internal Memorandum, National Aeronautical Laboratory, Sweden, Nov. 1984.
5. Hoerner, S. F. *Fluid Dynamics Drag*. Published by the author, 1958.
6. Cliff, W. C., and Fichtl, G. H. Wind velocity change criteria (gust rise) for wind turbine design. PNL-2526, Battelle Pacific Northwest Laboratory, Richland, Washington, July 1978.
7. Bowes, M. A.; Howes, H. E.; and Perley, R. Development of a 40 kw horizontal axis wind turbine generator. Kaman Aerospace Corp., Bloomfield, CT. Presented at Small Wind Turbine Systems 1976 Workshop on R & D Requirements, Rocky Flats Plant, Boulder, CO, Feb. 1979.
8. Connell, J. R., and George, R. L. Scaling wind characteristics for designing small and large wind turbines. Battelle Pacific Northwest Laboratory. Presented at Sixth Biennial Wind Energy Conference and Workshop, U.S. Department of Energy and American Solar Energy Society, Minneapolis, MN, June 1983.
9. Powell, D. C.; Connell, J. R.; and George, R. L. Verificaton of theoretically computed spectra for a point rotating in a vertical plane. PNL-5440, Battelle Pacific Northwest Laboratory, Richland, WA, Mar. 1985.
10. Nielsen, P., et al. Measurements on the Nibe wind turbines: Jan. 1980 to Mar. 1981. Research Association of the Danish Electricity Supply Undertakings, DEFU Report No. EEV 81-04, May 1981.
11. Wind energy conversion systems structural/mechanical design criteria. Draft Consensus Standard, American Wind Energy Association, Alexandria. VA, Oct. 1985.
12. ——. Small wind energy conversion systems (SWECS)—Safety, design, and operation criteria. CSA Preliminary Standard F416-M1985, Canadian Standards Association, Rexdale (Ontario), Canada, May 1985.
13. Waldon, C. A., and Hansen, A. C. Fatigue modeling for small wind systems: Basic theory. RFP-3564, UC-60, Wind Energy Research Center, Energy Systems Group, Rocky Flats Plant, Boulder, CO, June 1983.
14. Murtha, S. J. Loads and fatigue evaluation of the Hamilton Standard WTS-4 wind turbine. United Technologies Corp. Hamilton Standard Div. Presented at WindPower '85, American Wind Energy Association and U.S. Department of Energy, Conference and Exhibition, San Francisco, CA, Aug. 1985.
15. Glasgow, J. C.; Miller, D. R.; and Corrigan, R. D. Comparison of upwind and downwind rotor operations of the DOE/NASA 100-KW wind turbine. NASA CP-2185, DOE Publication CONF-810226. Presented at Wind Turbine Dynamics Workshop, NASA Lewis Research Center, Cleveland, OH, Feb. 1981.
16. Snyder, M. H. Further investigations of near-field wakes of circular and 12-sided cylinders and effects of shrouds and strakes. Wichita State University, NASA CR-168169. Prepared for NASA Lewis Research Center, Cleveland, OH, Feb. 1983.
17. Chung, S. Y. Aerodynamics of wind turbine with tower disturbance. MIT ASRL TR-184-15, Massachusetts Institute of Technology, Cambridge, MA, Sept. 1978.
18. Garrad, A., and Hassan, U. Taking the guesswork out of wind turbine design. Presented at American Wind Energy Conference, Cambridge, MA, Sept. 1986.

PART III

SYSTEM ENGINEERING

13

FATIGUE

13.1 INTRODUCTION

Designing for the fatigue loads that a wind system will have to survive over its design life is a difficult task at best. Many good designers know they must keep load levels low and avoid stress concentrations caused by holes, burrs, sharp corners, etc. As if this were not enough to worry about, there are considerations of corrosion and galvanic action that can precipitate or aggravate crack formation. A windmill can be exposed to many of the natural elements (water, salt spray, cold, heat, sand, etc.) depending on its location. Obviously, an extensive amount of information must be considered to avoid fatigue problems.

Like all rotating machines, windmills are *generators of fatigue*. Every revolution of its components (i.e., rotor, transmission, generator, yaw column, etc.) produces a load cycle, known as a *fatigue cycle*. Each of these cycles causes a finite amount of damage, resulting in a reduction in the component fatigue life. When enough cycles are experienced, a fatigue crack may develop. Continued loadings will cause propagation of the crack until failure results. To estimate fatigue life, designers have relied on techniques ranging from safety factors on material yield strength to load and cycle estimates used in conjunction with linear damage rules (Palmgren/Miners') and material fatigue data.

Ultimately, fatigue designing is based on knowing the magnitudes of the loadings and the number of times they are applied. In order to arrive at such values, however, an understanding of their causes should be achieved. The loads can be calculated (estimated) from the equations and theories in this book, but a completed design may experience unexpected system responses that produce loadings sufficient to cause failure. The following will explain some of the design considerations and a technique to determine a fatigue design stress. Chapter 7 of *Mechanical Engineering Design* by Shigley and Mitchell provides a brief, general introduction to design for fatigue. Reference 22 by Garrad & Hassan reports a promising new approach to fatigue design for wind turbines.

13.2 LIFE PREDICTION

A fatigue cycle is usually thought of as a loading and an unloading. This actually represents only one-half a fatigue cycle. A full cycle can be thought of as a sine wave. The loading starts at point 1 in Fig. 13.1 and increases to a maximum (point 2). The loading then decreases, passing through the starting load level (point 3) until a minimum load is obtained (point 4). The load level then increases until the starting level is again attained (point 5). This type of cyclic loading, when repeated with the same maximum and minimum loads, is called *constant amplitude loading*. Much fatigue data is obtained on high-speed rotating-beam machines in which the applied stress is completely reversed bending and the mean stress is zero. Material response to fatigue may differ substantially, depending upon whether the loading is in bending, torsion, or in axial loading.

Fatigue loads can be a combination of mean and cyclic loadings. The mean load can be zero, positive (tension), or negative (compression); it is defined as the mean of the load over the cycle. Such cyclic loads are referred to as *alternating loads* (see Fig. 13.2). The alternating part is defined as the difference between the maximum and the mean for the cycle.

Rotating machinery may experience either a single mean-load level and a number of alternating load levels, or a number of different mean-load levels and a single alternating load level. There can also be a number of mean and alternating load levels. When any of these occur, they are referred to as *spectrum loading* (in some cases, *block loading*). Spectrum loading is caused by varying operating conditions, and these either repeat themselves (*block loading*) or can be so disparate as to seldom recur in any recognizable order. The latter is sometimes referred to as *random loading*. Examples of each in Fig. 13.3 show the primary differences.

The loadings in these examples are the same in number and magnitude (mean and alternating stress). The primary differences are that the order of loading is different and block loading usually repeats whereas random seldom, if ever, does. The effect of the loading order on the fatigue life can be either beneficial (increase life) or detrimental (cause an early failure). Since this phenomenon is complex and specific information on each material is difficult to obtain, it is recommended that the order of loading be ignored.

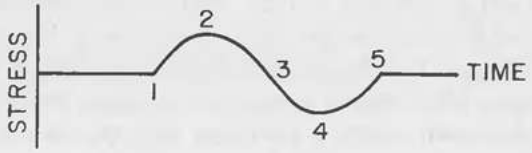

Figure 13.1. Fatigue load cycle.

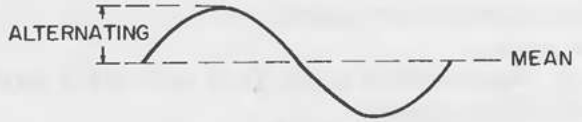

Figure 13.2. Alternating and mean loads.

Random loads are often arranged in groupings that correspond to an associated cause. For aircraft, these usually involve stages of a flight (mission),[1,2] including taxi, take off, climb, cruise, descent, landing, and taxi again. The aircraft industry also recognizes the possibility of unusual loadings, called *100th flight loads*. In addition, applications and removal of half cycles of the mean are also accounted for in the life calculations. These are referred to as a *spectrum of loads*.

The same technique is very suitable for windmill fatigue design and analysis. Each distinct operating condition has loadings that can be calculated, however random in nature. Experience has shown that statistical methods provide good representations of mean and alternating load levels.[2]

The different operating conditions might include the following:

1. Nonoperation (wind velocity too low)
2. Start-up (below cut-in)
3. Cut-in (connection of generator to power source)
4. Power production
   (a) with no pitch or yaw changes

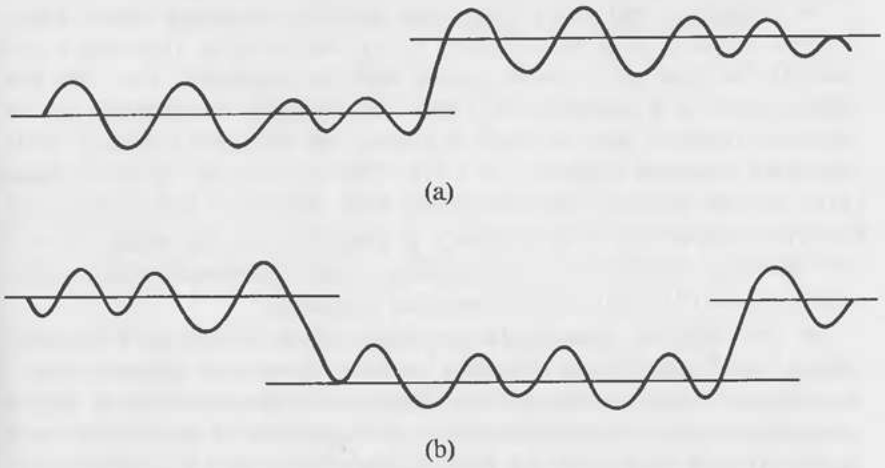

Figure 13.3. (a) Block loading, and (b) random loading.

(b) with blade-pitch control active
(c) with yawing
5. Shutdown (disconnect from power; blade pitch and/or brake active)
6. High wind-velocity survival

Item 4 may encompass conditions that cannot be treated separately, depending on the control system and the algorithm used.

In addition, special conditions might include the following:

7. Emergency shutdown (during 2 through 5 above)
8. Loss of public utility (during 4 above)
9. Maintenance (nonoperating) (during all wind conditions)

Once the operating conditions have been established and the load levels calculated, the next step is to estimate the number of cycles. These can be obtained by using information such as rotational speed (revolutions per minute) and the fundamental vibrational frequencies of the component/system. A rotor that turns at 60 rpm, or 1 revolution per second, has a rotational frequency of 1 Hz. If the rotor has two blades, there may be two cycles of loading for each revolution. With three blades, the loading is more complex, and system damping becomes a major factor in determining which cyclic frequency dominates. There may also be stress amplifications due to the coincidence of rotating and fundamental component/system frequencies (i.e., the rotor-blade fundamental frequency is equal to, or near, a multiple of the rotational frequency). The calculation of these values will provide the information needed to construct a Campbell diagram, such as that shown in Fig. 13.4.[2,21]

This diagram is used to avoid operating conditions that cause trouble where the lines intersect. It is not sufficient to say that the same frequencies will occur all the time. An example occurs with the two-bladed rotor that has loading cycles at a frequency of 2 Hz. The frequency is dependent on the operating condition, and, in cases of yawing, the dominant frequency tends toward the rotational frequency, or 1 HZ. This is in part due to the fact that as the yaw rate increases, the aerodynamic loads dominate.[3] After determining the cyclic frequencies, it is necessary to determine the percentage of time each operating condition is experienced by using a combination of a wind-velocity curve (Weibull) and the operating conditions.[4]

The most familiar damage rules available include the Linear (Palmgren-Miner),[5] the Double Linear (Manson),[6] and the Power Law (Corten-Dolan).[7] A component design engineer should insist upon fatigue testing of critical components if any substantial number of machines is to be built, since errors in prediction of fatigue life by these damage rules can be as great as 60 percent either over or under.[8,9,10,11] Reports indicate that as the number of

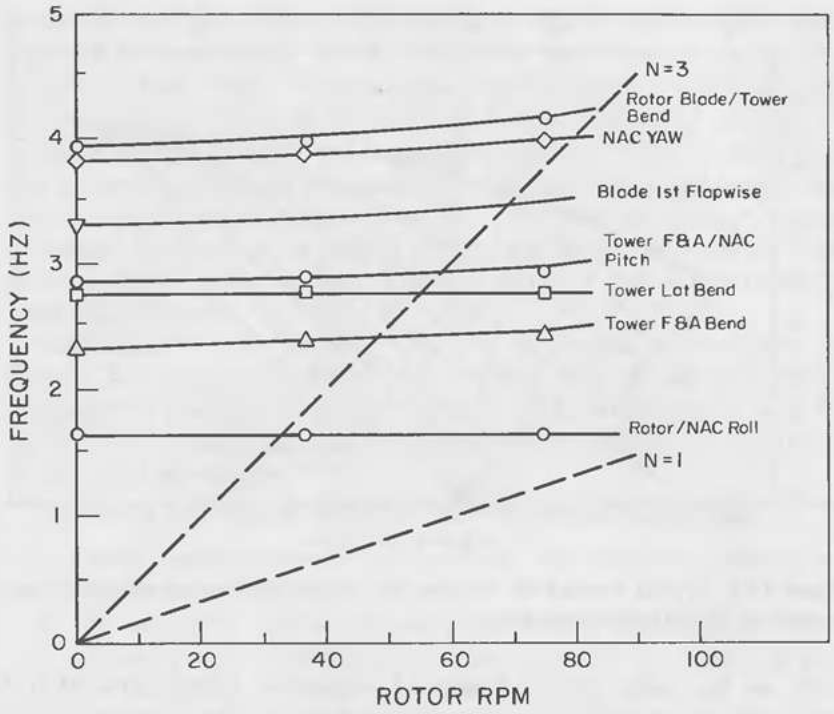

Figure 13.4. Campbell diagram (three-bladed rotor).

cycles increases, so does the accuracy of the life prediction. With the above in mind, the Linear rule (Palmgren-Miner) is the best choice. The rule briefly states that all damage has a linear relationship to failure, as follows:

$$\frac{n_1}{N_1} + \frac{n_2}{N_2} + \ldots + \frac{n_i}{N_i} = C \cong 1 \tag{13.1}$$

where

n_i = number of cycles of stress σ_i
N_i = total life corresponding to stress σ_i

When this sum is equal to or greater than 1, failure is predicted.

The allowable number of cycles to failure (N_i) is obtained from material fatigue data. Curves come in a variety of formats from S/N (log of the constant stress amplitude versus log of the number of cycles) to Constant-Life diagrams. Goodman diagrams are also a source of information but are not very common. Figure 13.5 is an example of a Constant-Life diagram.[12,13]

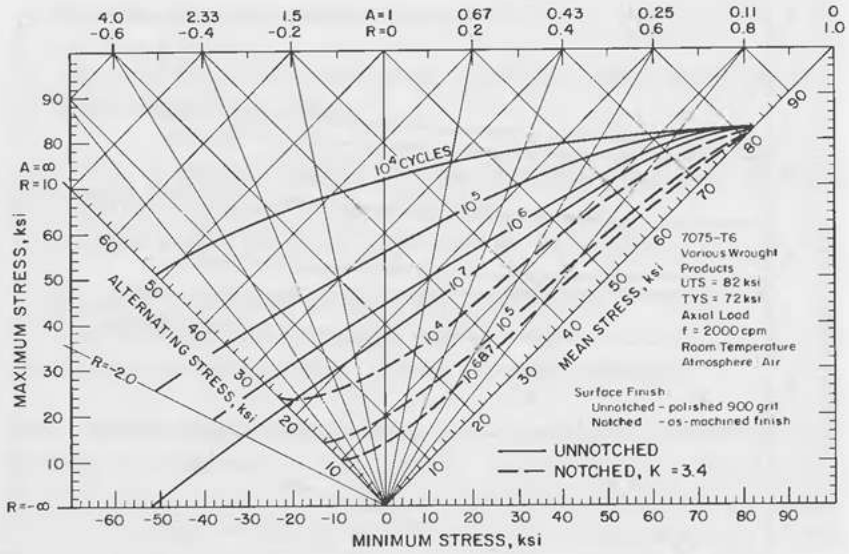

Figure 13.5. Typical constant-life diagram for fatigue behavior of various wrought products of 7075-T6 aluminum alloy.

As can be readily seen, a Constant-Life diagram offers a great deal of information, being composed of a good many S/N type curves. Since windmill loads vary significantly, a Linear Constant Life curve may be required. It is recognized that S/N curves are more readily available, but books are available that contain Constant-Life curves.[13]

If you were to try Miners' rule to estimate the fatigue life for a free-yaw windmill, you would find some important information missing. The prediction of yaw characteristics has not been formulated at the present time, and thus the percentage of time a windmill will yaw at a particular yaw rate cannot be calculated. Yaw-induced gyroscopic loads are very important as they can be 6 to 10 times as high as the loads when a windmill is not yawing.[14] Insights into the importance of yaw loadings and the number of cycles experienced are presented in the following sections, along with methods to estimate the percentage of time at various yaw rates.

13.3 CAUSES AND CURES

Statistics of windmill failures indicate that rotor blades have the highest percentage of failures of all the components, at more than 50 percent.[15] Three factors are primarily responsible. First, many components are "off-the-shelf" (i.e., generators, transmissions, etc.), and design practices in the industries

producing these items tends to be conservative. Second, wind loads are directly imparted to rotor blades, which are already susceptible to induced (i.e., gyroscopic) loads. Third, vibrations from rotor imbalance or system frequency interaction can also cause loadings that are unexpected and can cause failures.

Studies of vertical-axis[16] and large horizontal-axis[17] windmills have shown that primary fatigue loads are caused by centrifugal forces and gravity. Since the rotor speeds are relatively constant, the cyclic loads are relatively constant. In smaller systems, those of roughly 100 kW and below, this is not necessarily the case. Rotor speeds of these windmills can vary over a wider range, as much as 1000 rpm.

Describing the exact reaction of a rotor to changes in wind speed and direction has been attempted, but to date these theories are still not completely validated.[17,18] Research on a horizontal axis, downwind windmill, with three rigidly attached rotor blades, has given many basic insights into the complexities of the wind/load transfer.[14,19]

Preliminary conclusions from this research include the following:

1. During steady operation, with no yaw, the rotor loads increase with increased wind speed.
2. The mean loads may be adequately described by a Rayleigh distribution, whereas a normal distribution provides a good fit for alternating loads.
3. The causes of windmill yaw motion are complex and not totally understood. The current thinking tends toward the following conclusions:
   (a) Short-duration changes in wind direction often have little to no effect on the yawing of a windmill.
   (b) Velocity changes, in the form of horizontal (and even vertical) wind shear across the rotor disk, appear to be partially responsible for yaw motion. (See Fig. 13.6 for an example.)
   (c) The gyroscopic loads induced by yaw motion appear to be higher than any of the other loads measured and are thus considered to be a critical loading condition for free-yaw windmills.
4. During periods of high wind-velocity survival, fundamental loading frequencies tend to dominate, since little to no rotor yawing occurs during this condition. Stress reversals are possible if the rotor is parked edgewise to the wind or if the rotor is caught upwind (for downwind windmills). Tower contact by the blades is also possible under these circumstances.
5. Emergency shutdowns and similar stoppages normally do not occur in sufficient numbers to be a design consideration. This is especially true if blade pitch control and/or brakes are normally used. Only in cases where unusually high pitch rates and/or oversized brakes are used to react quickly can damage occur in a few cycles. This possibility should be avoided.

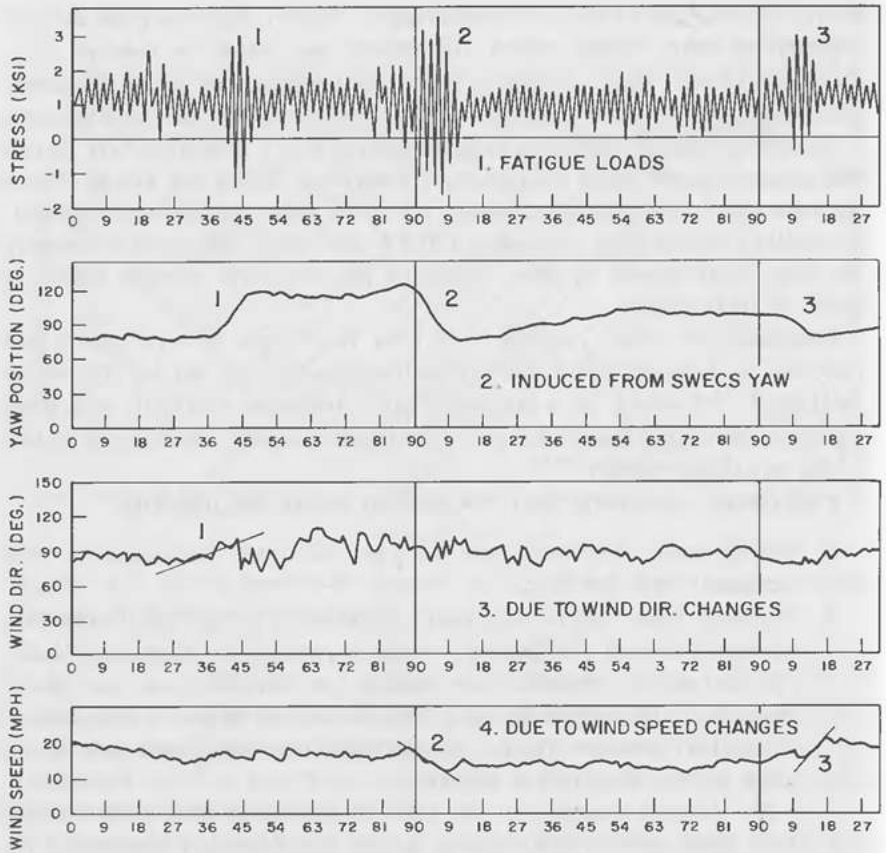

Figure 13.6. Fatigue loads during yaw.

Items 1, 2, 4, and 5 of this list can be dealt with through conventional calculations and designs. Item 3, on the other hand, presents some unknowns. These include the effects of differences in design shapes for the nacelles, differences in rotors, whether the rotor is upwind or downwind of the tower, etc. In addition, there appears to be a need to know statistics on wind shears and how they relate to the yawing motion. Without this information, the number of yaw-induced loads may not be calculated. If the yaw contribution to fatigue damage cannot be determined, a critical fatigue loading may be underestimated and result in a premature failure. The gathering of wind-shear statistics is time-consuming, however, and the related effect on a rotor is difficult to determine.

Research has given an insight into the yaw phenomenon and may in fact eventually lead to techniques that do not need the wind-shear data.[14] Load

data has been accumulated for two different horizontal-axis windmill-rotor configurations: (1) A three-bladed, downwind rigid rotor; and (2) a two-bladed, upwind, passive-cyclic-pitch (PCP) rotor. The preliminary findings indicate that for each windmill the characteristics that depend upon yaw rate remain the same, even though the mean wind velocity changes, as noted in Fig. 13.7.

The corresponding wind-speed distributions tended to be Rayleigh, thus indicating that the Weibull distribution can also be used. It is recommended that local distributions be checked as recent reports indicate some may be different. Some areas have recorded bipolar distributions, but since the data is limited, this may not represent a mean of the yearly distributions. The load magnification curves of Fig. 13.7 were derived from bending moment vs yaw rate curves, similar to the one in Figure 13.8 for a three-bladed rotor. Figure 13.8 also compares calculations[3] to actual data[14] and MOSTAB computer calculations.[20] The quasi-steady, or "base," level in which the windmill is not yawing, the blades are not changing pitch angle, and wind conditions are relatively steady is defined as normal operation.

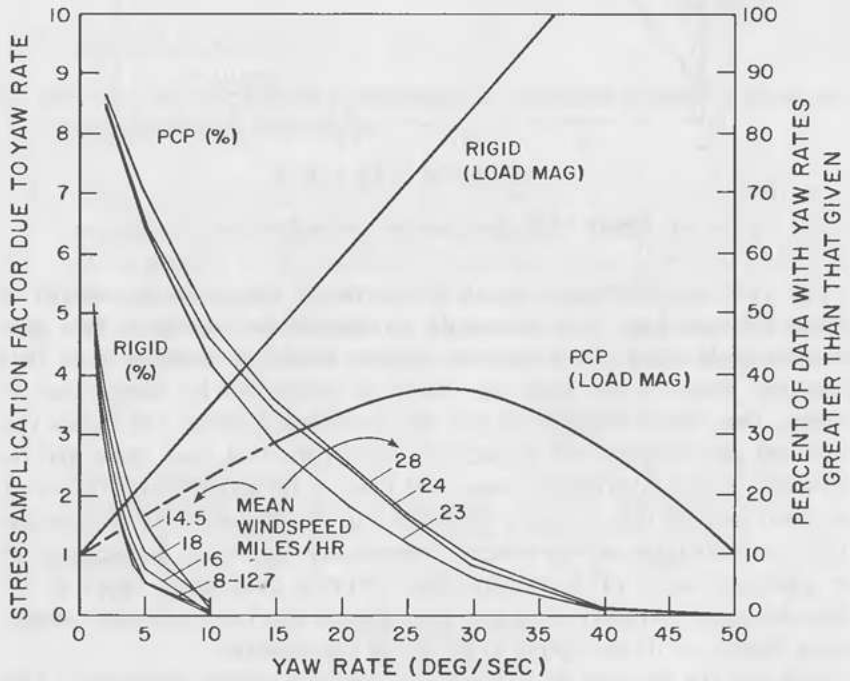

Figure 13.7. Test data showing effect of yaw rate on fatigue stresses for a rigid and a passive cyclic pitch rotor.

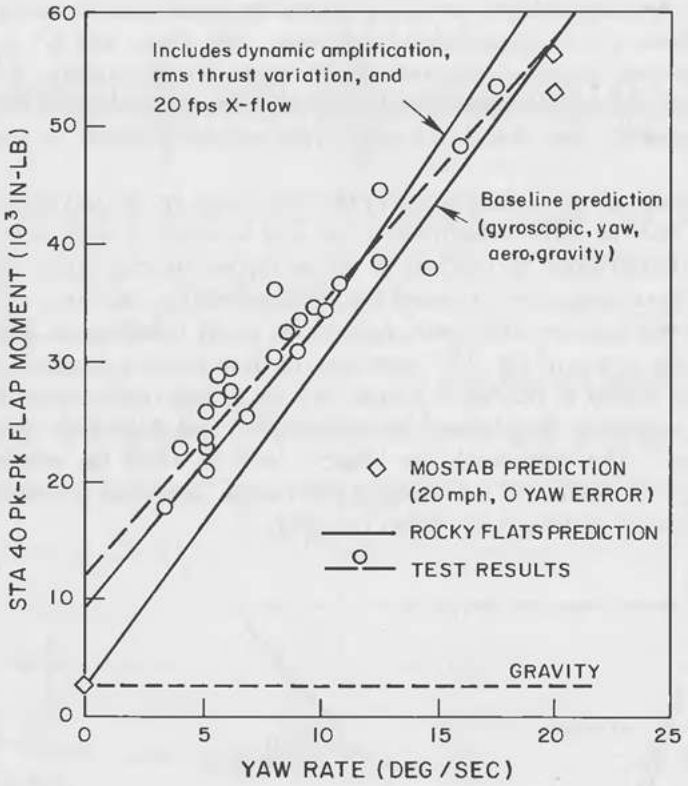

Figure 13.8. Flap moment versus yaw rate.

The yaw-rate information allows a designer to determine the number of cycles for each load level during the yawing of the windmill. This data, however preliminary, does indicate definite trends. A designer need only determine where in the graph the family of curves for his design may be located. One choice might be to pick the conservative curves (the higher yaw rates and percentages), but fatigue-life calculations will soon show that the allowable design (alternating) stress will have to be approximately one-tenth the yield strength (i.e., a safety factor of 10). This figure is for areas where stress concentrations are not present. Some safety factors can be increased by an additional factor of 3 or more, thus giving a total safety factor of 30. Most designers—certainly those who must address cost factors—would consider safety factors of 10 and above to be out of the question.

How can this situation be avoided? By designing around the problem. First set a maximum allowable yaw rate as a design criterion. Even though the number of cycles may be higher, the loads are not, and, in fatigue, loads

and cycles have a log relationship. Reducing the loads to half will more than double the allowable cycles. This can be easily seen in the Constant-Life diagram. Developing a curve similar to that for the three-bladed rotor will be helpful in determining the stress magnification you feel is allowable.[3] In this case, a recommended value is between 1.5 and 2, which translates into 2 to 4 degrees per second.[14]

Setting these criteria requires that the design include a device to restrict/control the yaw rate (i.e., a damper). Many of the large windmills use yaw drives. This does not provide a complete solution, as any freedom in the drive system may allow short-duration yaw rates in excess of those arising from driven motion. Gyroscopic loads magnify quickly, and significant damage may thus be incurred unexpectedly.

The rotor system is complex to design and costly as well. The remaining components—drive shafts, yaw columns, etc.—will not be discussed here since their overdesign does not have the same cost impact. Conventional design practices are recommended for these areas and should be sufficient. Similar cycle estimate techniques should be used for all areas of design to assure that all loading conditions are accounted for.

13.4 CALCULATIONS

The following may be applied to determine an allowable alternating stress for a component such as a rotor blade:

1. Insofar as possible, partition the operation of your windmill into operational modes identified by one variable. These operating modes will be peculiar to the machine. The sample modes shown in Fig. 13.9 follow those for the Grumman WS-33 discussed in Chap. 15.
2. Use the Weibull distribution of wind velocity to determine the yearly hours of operation in each mode. Use a mean wind velocity representative

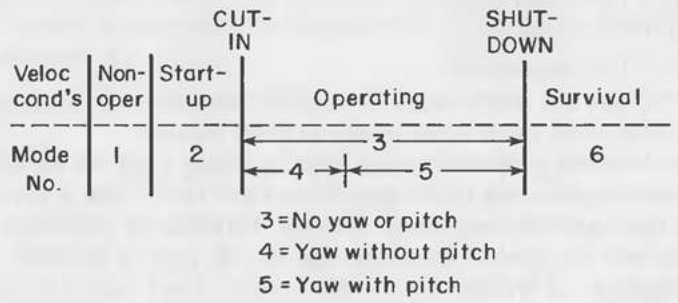

Figure 13.9. Operating conditions.

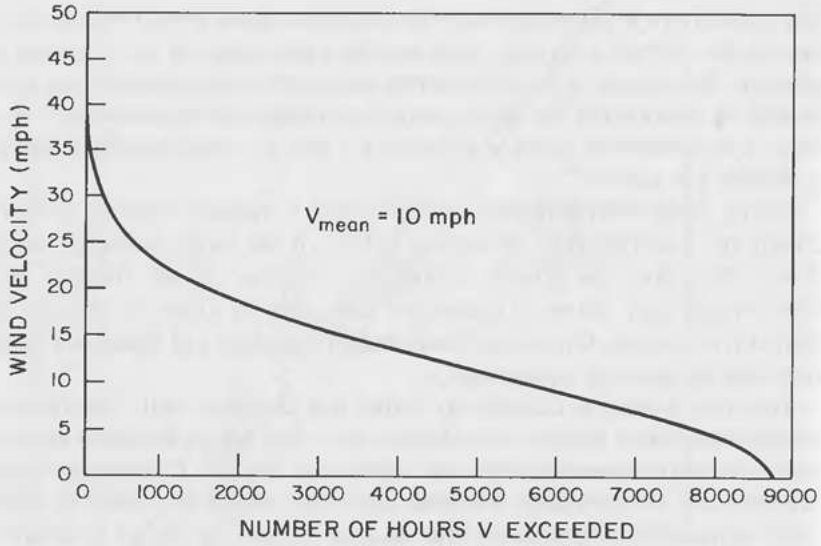

Figure 13.10. Wind velocity distribution.

of your intended location and the hub height of your windmill to develop the curve shown in Fig. 13.10. Tabulate the hours the machine will spend in winds above a given velocity as shown in Fig. 13.11. From this information and the definition of the operating modes, determine the incremental number of hours the machine will spend in each of the modes identified in Fig. 13.9.

3. Determine the cyclic frequency for each operating mode. This data is again peculiar to the machine. Data shown below is for the WS-33:
   (a) 7 Hz—fundamental
   (b) 3 Hz—rotational
   (c) 3 Hz—rotational
   (d) 1 Hz—aerodynamic
   (e) 1 Hz—aerodynamic
   (f) 7 Hz—fundamental
4. Determine the alternating and mean stresses for each mode (see Fig. 13.12), using calculations shown in other chapters.
5. As discussed previously, establishing a design value for the maximum allowable yaw rate under gyroscopic loads means that a yaw damper or other such device must be included. Estimate the percentage of time that will be spent at each yaw rate for the type of windmill you are designing. At first this will be just a guess, but a rule of thumb would be to start slightly high.

Vel. (mph)	8	12	25	40
# Hrs > V	5700	5000	700	50

Figure 13.11. Time above a given velocity.

6. From calculations of flap moment (p-p) vs yaw rate, overlay the relation on the percent of data versus yaw rate (see Sec. 13.3). Determine the time spent (hr/yr) at the various yaw rates.
7. For each mode of operation, determine the total number of cycles using the following:

$$\text{Cycles}_{\text{total}} = \frac{\text{Hours}}{\text{Year}} \times \frac{3600 \text{ Sec}}{\text{Hour}} \times \text{Frequency} \qquad (13.2)$$

For example, using a normal distribution for each mode, calculate the number of cycles for a distribution of alternating stresses using minimum increments of 1000 psi (corresponding to fatigue-life curves), as shown in Fig. 13.13.

$$J_{\text{stress}}(i) = (\text{Total cycles}) \times \text{Coefficient} \qquad (13.3)$$

For purposes of design, the distribution of mean stress in each mode is not considered unless the level is high. As can be seen in the Constant-Life diagram, changes in mean stress have little effect at lower levels.

8. Obtain a fatigue-life curve for the material (Constant-Life curve if possible). Remember the fatigue data must reflect the stress concentration and corrosion factors, if these are present.
9. Apply Miner's Rule in conjunction with the Constant-Life fatigue data for each mean-stress and alternating-stress increment in each mode, as given by Eq. 13.1.

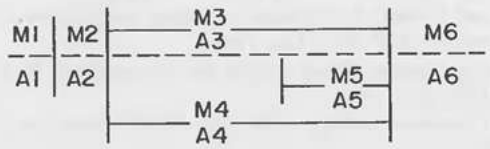

Figure 13.12. Design mean and alternating stresses.

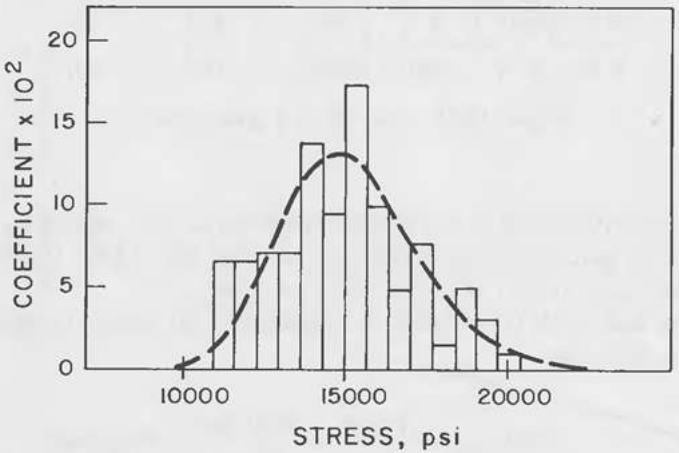

Figure 13.13. Typical distribution for flapwise bending stress.

10. If the preceding sum is equal to or greater than 1, the alternating stress is high enough for the rotor to fail in one year or less.
11. If the sum is less than 1, divide it into 1 in order to obtain the predicted number of years to failure:

$$\text{Years} = \frac{1}{\sum_{j=1}^{k} \frac{n_j}{N_j}} \tag{13.4}$$

12. To arrive at a design alternating stress, repeat the process until the number of years to failure meets your design criteria (i.e., 10, 20, or 30 years).

REFERENCES

1. Cruse, T. A.; Meyer, T. G. Structural life predictions and analysis technology. Pratt and Whitney Aircraft, 1978.
2. Och, F. Fatigue life estimation methods for helicopter structural parts. NATO Review of Current Requirements and Substantiation Procedures, 1978.
3. Waldon, C. A., and Hansen, A. C. Fatigue modelling for small wind systems. Rocky Flats Wind Systems Program, RFP-3564, June 1983.
4. Waldon, C. A. Wind machine fatigue analysis and life prediction. Rocky Flats Wind System Program, RFP-3135, Apr., 1980.
5. Miner, M. A. Cumulative damage in fatigue. ASME Transactions, *Journal of Applied Mechanics* (1945).
6. Manson, S. S. Applications of a double linear damage rule to cumulative fatigue. Fatigue Crack Propagation, STP-415, ASTM, 1967.

7. Corten, H. T., and Dolan, T. J. Cumulative fatigue damage. Proceedings of the International Conference on Fatigue of Metals. ASME Transactions, IME, 1956.
8. Hashin, Z. A reinterpretation of the Palmgren-Miner Rule for fatigue life prediction. University of Pennsylvania, 1979.
9. Jarkoski, B. Z.; Aslam, M.; and Jeelani, S. Prediction of cumulative fatigue damage. TI-NAVY-1, 1978.
10. Manson, S. S. Fatigue life prediction in bending from axial fatigue information. Case Western University, Cleveland, OH, 1982.
11. Ohgi, F.; Miller, W. R.; and Martin, J. Cumulative damage and effects of mean strain in low cycle fatigue of a 2024-T351 aluminum alloy. ASME Journal of Basic Engineering, 1966.
12. Haugen, E. B. Modern statistical materials selection. *Materials Engineering* (July 1982).
13. Dept. of the Navy, Metallic materials and elements for flight vehicle structures. MIL-5-Handbook.
14. Waldon, C. A. Effects of yaw rate on the fatigue life of horizontal axis WECS. Proceedings of Wind Workshop VI, Minneapolis, MN, 1983.
15. Waldon, C. A. An overview of fatigue failures at the Rocky Flats Wind Systems Test Center. *Wind Turbine Dynamics*, NASA Conference Publication 2185, CONF-810266, Feb. 1981.
16. Veers, P. S. Blade fatigue life assessment with applications to VAWTS. Sandia National Laboratory, NM, 1981.
17. Spera, D. A. Comparison of computer codes for calculating dynamic loads in wind turbines. NASA TM-73773, 1977.
18. Dowling, N. E. Fatigue failure prediction for complicated stress-strain histories. *Journal of Materials* 7:71–87 (Mar. 1972).
19. Eckerman, G. J.; Wright, A. S.; and Hodgkin, J. P. High wind loading of parked SWECS rotors: Preliminary data. National Conference, American Wind Energy Association, Oct. 1982.
20. Hoffman, J. A. Coupled dynamic analysis of wind energy systems. NASA CR-135152, 1977.
21. Adler, F. M., et al. Development of an 8 kilowatt wind turbine generator for residential type applications, Phase 1. RFP-3007/71787/3533/79-15-2, 1980.
22. Garrad, A. D., and Hassan, U. The dynamic response of wind turbines for fatigue life and extreme load prediction. Presented at the EWEC Wind Energy Conference, Rome, Italy, Oct. 1986.

14

ELECTRICAL GENERATORS

14.1 INTRODUCTION

Of the many good references on the theory of electrical machines, only a few will be referred to here. Although much of the development of this theory occurred during the 1930s, older references may still be useful. Of the newer works, an elementary introduction oriented toward wind turbine analysis is given by G. L. Johnson (see Chap. 5 of Ref. 3). Electrical machine expertise may be only as far away as your local university, provided it has an electrical engineering program with an electrical machinery lab. Detailed dynamic modelling of electrical machines for control and transient analysis requires a somewhat different treatment than that given in straight electrical machine theory.

General Requirements

In developing a wind turbine, one option is to predicate the design around an existing generator. Alternatively, the generator may be taken as an integral part of the design process. We begin with a general overview that should be of benefit to the designer pursuing either option and then continue with some specific comments based upon recent wind farm experience.

Most wind-driven generators are connected to an existing utility grid that can supply electric power when wind velocities are low and can absorb wind power when the velocities are high. The utility regulates the voltage within reasonable limits.

The generator should be able to deliver the power developed by the turbine over a wide range of wind velocity. It is not practical to design a generator to cover the highest possible wind velocities. In general, the higher the peak power to be developed, the higher the cost. Since the highest wind velocities usually come in gusts, it is desirable to take advantage of the short-time overload capacity of a generator. Any pull-out limit of the generator must be taken into account, however, as will be explained later.

There are two general types of generators that should be considered: constant speed and variable speed. The simplest are the constant-speed generators,

either the induction generator with a squirrel-cage rotor (similar in construction to the simplest induction motor) or the synchronous generator (similar in construction to a synchronous motor). These generators run at, or near, a synchronous speed that is determined by the number of poles. For a 60-Hz power system, this synchronous speed in rpm is 7200 divided by the number of poles. If the synchronous speed is chosen to match some lower wind velocity, it would then generate power only whenever the wind velocity increased above this value.

With adjustable-pitch blades, the full advantage of the constant-speed generator can, in theory, be realized over a wide range of wind velocities. Even with fixed blades and constant speed, power can be developed over a considerable range of wind velocities, but with reduced efficiency except for a limited range. For smaller units, the low cost and simplicity of the constant-speed generator may make it the best choice, even for a fixed-pitch blade. The choice is a matter of evaluating cost versus extra power generated.

Two general types of variable-speed generators are available: the wound-rotor induction generator and a synchronous generator with a frequency converter. Each of these generator types will be discussed in sufficient detail for a choice to be made, with due consideration given to turbine characteristics and other factors.

14.2 SYNCHRONOUS GENERATORS

Synchronous generators can be the salient-pole type with field windings or permanent-magnet machines. When connected to a public utility of fixed frequency, they have to run at constant speed. When they are directly connected to the turbine, their low rpm dictates a very short pole pitch since the number of poles is equal to 7200 divided by the rpm.

Although a permanent-magnet machine with many small poles can be used for such low speeds, it has the major disadvantage that the field cannot be removed in case of a fault to ground. Nevertheless, if the machine is grounded by a high resistance, it is possible to avoid serious burning if braking is provided to stop it quickly.

To synchronize the speed and the angle, both must be very close to correct values. This may be difficult to attain with the turbine torque changing rapidly with wind gusts. Typically, the speed should be matched within 1 percent and the angle within 30 electrical degrees. To do so will require some form of brake to hold the speed nearly steady. With sudden torque changes of 50 percent, as might well occur with high wind gusts, the speed might change 1.0 percent in a little over 1 second, and the chance of catching the angle within the required limits is low. Some time might be required to match speed and angle correctly, and one might even have to wait for the wind to steady.

Thus an incentive exists for either using an automatic synchronizer or building this capability into a programmable controller.

A salient-pole synchronous motor with field coils on the poles is identical to a synchronous generator except that the power is reversed. Typical synchronous motors have an 80-percent power factor and a 150- to 250-percent pull-out torque. The rating chosen should thermally match the maximum rms load over a 10-min period. The pull-out power should at least match the maximum load we expect to carry without tripping off the line.

14.3 SQUIRREL-CAGE INDUCTION GENERATORS

The squirrel-cage induction generator (SCIG) is the simplest and usually the cheapest form of generator. It has a limited range of speed. When it runs at synchronous speed, the fact that the magnetic flux developed by the stator winding is traveling at the rotor speed means that no current is induced in the rotor and no torque is produced. At a higher wind velocity, the turbine tries to run at a higher speed. This increase represents a "slip speed" that causes the flux to cut through the rotor bars, thereby inducing a voltage that circulates a current, producing power and a countertorque.

Over a limited range, the power and torque are proportional to the slip, but the current produces a reactive voltage (and flux) drop that is initially out of phase and has little effect. At larger values, the drop rapidly reduces the flux, requiring more current for a given torque until a "pull-out slip" is reached. Beyond this point, the torque and power decrease.

It is not practical to operate in the range beyond "pull-out slip" not only because the torque is dropping and speed may increase excessively, but also because the power loss in the stator windings, rotor bars, and end rings is excessive and might overheat these parts very rapidly. The most limiting part of this rotor heating is usually the end ring, which expands radially and tends to bend and fatigue the rotor bars or the brazed connections. Extra rotor heat also causes a higher air temperature, which raises stator-coil temperatures. Stator windings roast out at these high loadings.

The curves of Fig. 14.1 show the slip and rotor winding loss for a typical generator as a function of the torque. The percent rotor loss that can be tolerated depends on the ventilation and the construction. Typically, any rotor loss greater than 25 percent of rating that exists for more than 10 minutes at a time would give excessive temperature and stress. Short-time overloads in excess of this value can be judged by assuming the heat to go up with the product of slip and torque and using a thermal time constant of 10 minutes. If the details of a design are known, more accurate limits can be established by careful thermal transient calculations.

The slip for a given torque can be increased by increasing the rotor bar

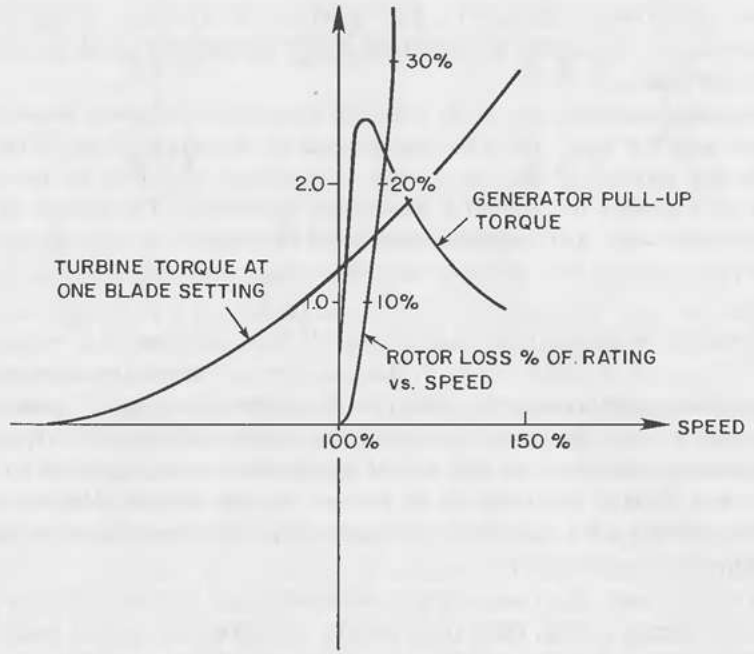

Figure 14.1. Induction generator torque-speed matching.

resistance, but the product of torque and increased slip represents more rotor loss and a temperature increase.

Generators have a continuous rating at which certain temperature limits are not exceeded (typically, for a generator with class B insulation, the limit is 120°C, or 80°C above an assumed 40°C maximum air temperature).

The other most important characteristic is the percent pull-out torque. The cost of a generator is nearly proportional to the continuous rating and about proportional to the square root of the pull-out torque.

The problem of picking the most economical generator to do the job requires knowing the turbine power needed over the range of wind velocities and the power-speed characteristics of the chosen generator.

Since there will be rare cases of excessive wind velocity with turbine torque that exceeds the pull-out value of the generator, it is necessary to establish this pull-out value and provide for tripping the generator off the line if the pull-out speed or power is exceeded for more than about 10 seconds. The generator can be restored to the line at any time the turbine speed falls below the pull-out speed of the generator.

At low wind velocities, the turbine speed will drop below the synchronous speed, and the generator torque will reverse and drive the turbine at just

below synchronous speed. The only problem in this range is the loss of power, and if this persists for appreciable time, the machine should be removed from the line.

One other characteristic of the induction generator is its power factor, which varies with the load. The kW load divided by the power factor is the total kVA (the product of the line voltage and current multiplied by the square root of 3 divided by 1000) for three-phase generators. The current has two components—real and reactive—which add as vectors at right angles. The reactive current is out of phase with the voltage and represents no average power.

Excessive reactive current is objectionable because it causes a voltage drop in the line and in transformers. A fixed portion of the reactive current is the magnetizing current required to force the flux across the air gap. The minimum practical air gap is used, as limited by mechanical considerations. The magnetizing current in per unit of full load* varies from 20 percent for large four- and six-pole generators to 40 percent or more for ten poles and up.

The reactive kVA caused by the stator and rotor reactance is another 15 to 20 percent at full load.

For small users of power, since the utility does not normally measure power factor or reactive kVA, there is no penalty. For larger connected loads, there is often a demand charge based on the maximum kVA for any 15-min period. In these cases, a bank of shunt capacitors can be used to compensate for the reactive current at some load. This bank, however, should have its own switch and a voltage relay set to trip it off for any voltage more than 115 percent of normal. This breaker should open in 15 cycles or less, since the capacitor current may exceed the magnetizing current if the main breaker opens and the voltage may rise to excessive values.

14.4 VARIABLE-SPEED GENERATORS

Variable-speed generators can be used to take best advantage of turbine characteristics and generate the maximum power available at any wind speed up to some peak limit set by the rating of the generator and the frequency converter.

Two general types of variable-speed generators are practical, but both are more expensive than constant-speed generators. The additional cost must be evaluated against the additional power generated. The simplest, and usually the cheapest, variable-speed generator uses a synchronous machine with a solid-state dc-link frequency changer, as shown in Fig. 14.2. The thyristor bridge connected to the machine terminals is a controlled rectifier, and the

*In the "per unit" system, currents, voltages, and power increments are expressed as a fraction of, or a percentage of, a base value that must be defined.

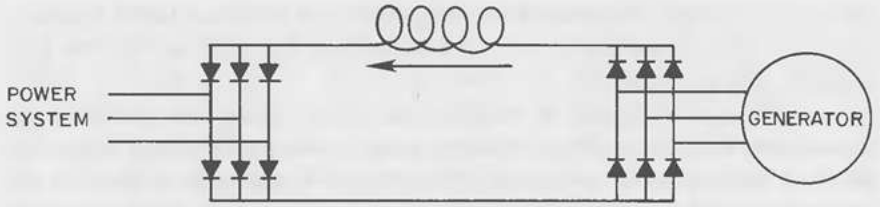

Figure 14.2. Generator system.

dc-current loop feeds a second thyristor bridge that functions as a inverter to feed power back into the power system. (See the subsequent section on frequency converters.)

The rating of the generator and the solid-state converters should be chosen to match, not the highest possible wind speed, but rather some value that will be reached a sufficient percentage of the time to justify the incremental expense of the increased rating.

Since generators have fairly long thermal time constants—about 20 minutes—they can be overloaded for a number of minutes. Thyristors have two limits: a short-circuit rating that cannot be exceeded for more than a few cycles and a short time rating that is limited by the heat sinks, which usually have a thermal time constant of only about 2 minutes. Hence, it is desirable to rate the converter at the maximum load beyond which the unit is tripped off the line.

The ac generator voltage at the top operating speed can be well above the line voltage and the dc voltage held down to match the dc voltage of the inverter at lower speeds by delaying the gate control angle on the rectifier. However, this results in a lower power factor on the generator. The lowest power factor rating (PF) of typical synchronous generators and motors is 80 percent.

For this PF at peak load, the generator voltage can be 40 percent above the line voltage. With fixed excitation on the generator, the ac voltage drops somewhat as the speed goes down, but as the load drops, the flux in the generator rises, thus limiting the voltage drop. At some speed lower than 60 percent of top operating speed, the rectifier dc voltage, even with no delay, would be so low as to require a gate phase advance in the inverter, thereby lowering the output power factor. At 60-percent speed, however, we have about 22-percent load; hence, a lower power factor at lower speeds and loads will cause no big increase in reactive power.

If a 90-percent power factor generator is chosen, the ac voltage at top operating speed should be about 25 percent above the line voltage. As we decrease speed, the flux will rise, but at about 70 percent of top speed and below it will be necessary to advance the firing to match the dc voltage with

the ac line voltage. Since the kW at 70-percent speed will be about 35 percent of peak, the reduced line power factor resulting from the advance in gate angle is still not serious.

A more exact analysis of voltage and power factor can be made by considering the internal voltage of the generator as the source voltage equivalent to E_o in the section on converters. This internal voltage may be taken as the voltage back of subtransient reactance in the generator, E''. Physically, it is the voltage caused by the flux linking the damper winding, which is constant for the commutating period. However, E'' will change with speed and with current and power factor. The vector diagram can be constructed using the synchronous reactance to represent the armature reaction, as shown in Fig. 14.3. If such a diagram is constructed for the peak load, the excitation required can be determined. Holding this excitation constant, and assuming voltage E'' to be proportional to flux and speed, we can determine (E''/s) for any given speed and torque. Torque is proportional to (E''/s) times the inphase component of current. To keep the output power factor high, the dc voltage can be kept proportional to the ac line voltage over the upper part of the speed range, and the rectifier can control its dc voltage by controlling the gate-angle delay. More ideal control would regulate the inverter gate angle as a function of current to keep the margin angle adequate but not excessive. Doing so will give a slightly rising voltage with current. The rectifier control can match this voltage with the ac line voltage by providing a suitable compensation for current.

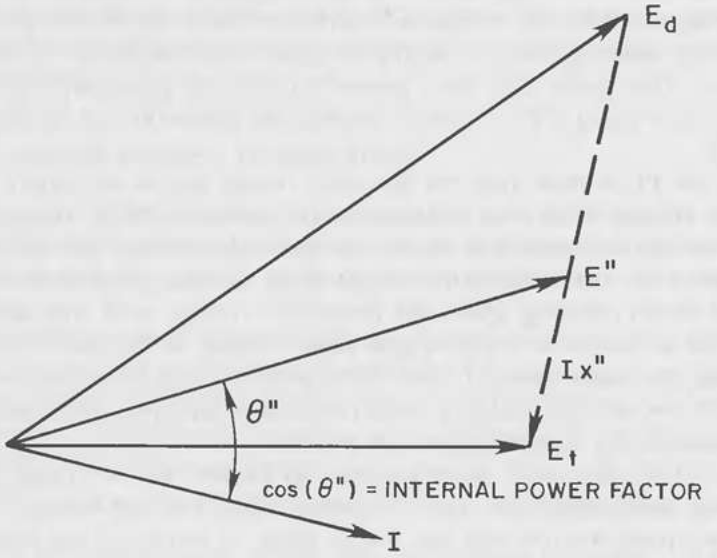

Figure 14.3. Vector diagram for armature reaction.

In an effort to match the ac line voltage below some lower speed where the rectifier is at zero delay, it is necessary to phase-advance the inverter gate angle to match the lower dc voltage output of the rectifier. This could be programmed as a function of speed or voltage of the generator. Another type of control would be to regulate for a given current, which would be programmed as a function of speed. The current would be set a little higher than that required at unity power factor for the load required. Doing so has the advantage of preventing a sudden dip in highline voltage from resulting in an inverter fault.

14.5 WOUND-ROTOR INDUCTION GENERATOR

The wound-rotor induction machine is most commonly used as a variable-speed motor, and a review of its operation as a motor may help explain the induction generator. The flux poles in this machine rotate at a synchronous speed determined by line frequency and the number of poles. At no load, the machine runs at the synchronous speed but is slowed down by load on the shaft. The difference from the synchronous speed, called the *slip*, induces in the secondary (usually the rotor) a voltage producing a current that supplies the torque. Up to about rated torque, the rotor current and torque are proportional to slip, but as the torque and current increase, the flux is reduced by the leakage flux until a peak torque is reached, known as the *pull-out torque*.

Below rated torque, the slip for a given torque is proportional to the resistance of the rotor circuit. Figure 14.4 shows typical torque characteristics for different resistance values. The torque characteristics can be changed in steps by switching resistors or changed continuously by using a variable liquid rheostat. Adjustable rotor resistance is often taken advantage of to control the speed of motors.

Running above synchronous speed, a slip frequency voltage is induced in the secondary and power flows out of it, but the torque is reversed and power then flows out of the primary. The turbine power output, P_t, divides between primary and secondary. If s is taken as the fraction of rated speed, the secondary rotor power is $P_t(s)/(1 - s)$ and the stator power is $P_t/(1 - s)$. With a resistor in the secondary, this power is wasted, and the efficiency is $1/(1 - s)$, neglecting the loss in the machine.

14.6 INDUCTION GENERATOR WITH RESISTANCE CONTROL

With a continuously variable resistance, the turbine torque can be matched right up to the pull-out point. Such matching can be accomplished with a liquid rheostat in which either the spacing or the area of the electrodes are varied. Sodium carbonate is most often used as the electrolyte. A heat

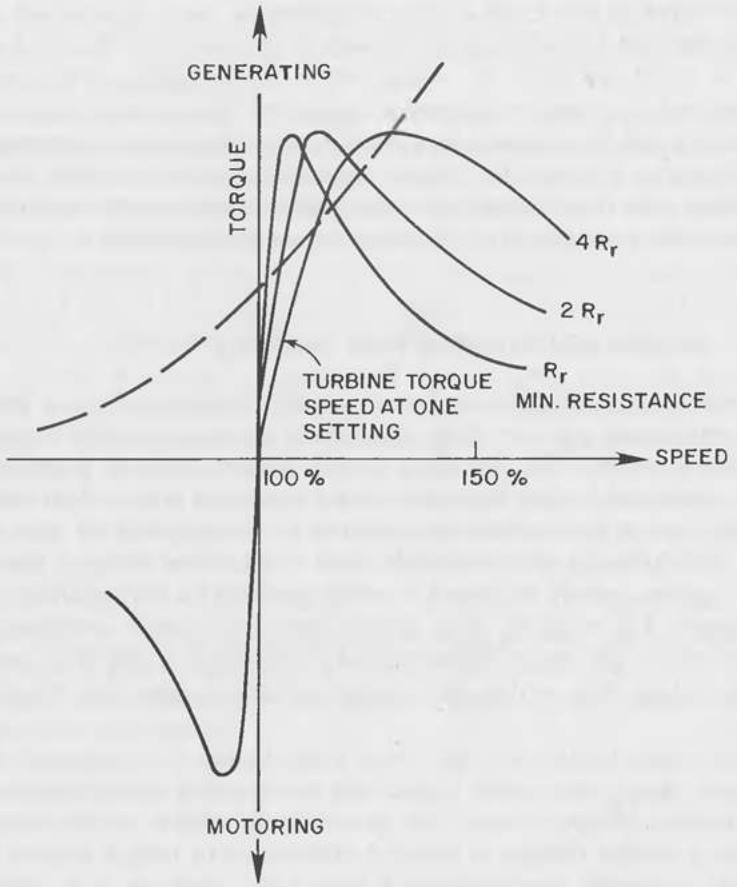

Figure 14.4. Torque-speed curves for a resistance-controlled induction generator.

exchanger is required, and sufficient velocity and area between electrodes must be allowed to avoid boiling.

A slip higher than the value at pull-out should be avoided because it may cause self-excited oscillations—as follows. A momentary increase in speed can cause a decrease in generator torque equivalent to a negative damping effect. From the torque curves of Fig. 14.4, it will be seen that one can stay below the pull-out slip by increasing the secondary resistance as the load and speed increase. Increased slip represents increased generation loss, which would indicate the desirability of keeping the slip low. The turbine characteristic, however requires increased generator speed as the wind velocity and torque increase. A study of the turbine loss combined with the generator loss

as functions of speed would allow one to program the ideal torque for a given speed.

As the pull-out torque or rotor current is reached on a high wind gust, the machine should trip off the line.

14.7 INDUCTION GENERATOR WITH A CYCLO-CONVERTER

As explained in the section on converters, the cyclo-converter is capable of chopping out sine waves of lower frequency than line frequency, and one can control the frequency magnitude and phase angle. Such a converter can be applied to the slip rings of a wound-rotor induction machine, using it to generate a sine wave of current whose magnitude and phase angle are controllable. Such control in turn provides control of torque or power at a given speed. Power as a function of speed may then be programmed to take full advantage of the power available at a given speed. The power that flows in or out of the slip rings is the per-unit slip times the stator power, or $s(1 - s) \times$ (total power), where s is defined as synchronous speed minus operating speed in per-unit terms. The total power required is the output power plus machine and converter losses, which amount to only a few percent.

If we choose a synchronous speed of 80 percent of the top permissible operating speed, we can operate as low as 60 percent of top speed without exceeding 25-percent slip frequency. Below this level, the current is low and operation can remain satisfactory even though the wave shape may have some distortion. Since the cost of the cyclo-converter is proportional to its peak current and voltage, limiting the slip limits the cost.

To avoid harmonics of current, it is necessary to get good sine waves of voltage with accurate phase angles of relative phases. Otherwise, such harmonics will cause harmonics of torque. If the latter harmonics happen to coincide with some torsional natural frequency, excessive stress in shafts or blades may result. A large number of control elements are needed to generate the sine wave that will avoid all such harmonics.

When the slip frequency exceeds 25 percent (15 Hz on a 60-Hz line), possible distortions of the wave shape may give low-frequency harmonics that may coincide, in turn, with low-frequency torsional modes. Hence, it is desirable to stay within 25 percent of synchronous speed unless considerable damping is provided, such as that provided by rubber-block couplings (the Holeset coupling is one commercial type).

In fact, the damping provided by rubber-block couplings can hold down the amplification, even in resonance, to 10 times or less so that harmonics of current may be permitted up to 5 percent. A sine wave made up of square waves might need only 12 steps to keep the harmonics within this limit.

14.8 FREQUENCY CHANGERS USED WITH WIND-TURBINE GENERATORS

As explained previously, there are two types of generators. A dc-link frequency changer as shown in Fig. 14.2 can be used to tie the variable-speed salient-pole generator to a fixed-frequency system. To understand this type of converter, we view the second bridge as a controlled rectifier in which the relation betwen dc voltage and current is given by the typical rectifier regulation curves (Fig. 14.5) for different loads and angles of delay. Here, the slope of the dc regulation curve for a fixed angle of delay, in per-unit terms, is just $x/2$, where x is the generator subtransient reactance on a rated kW base. We can make this essentially a controlled current source by a control that rapidly increases the delay angle as the load current increases.

The first bridge is an inverter feeding into the power system; it is essentially a controlled rectifier in which the delay angle is more than 90 deg and the dc voltage and power flow are reversed from the rectifier. Here, for a fixed firing angle, the voltage has a rising regulation curve, $x/2$, where x is the percent transformer and system reactance on a rated kW base.

The natural dc regulation curves for rectifier and inverter are shown in Fig. 14.5. The natural regulation curves of the rectifier have about a 10-percent droop ($x/2$) for a fixed angle of delay, but, with this angle controlled to give a very steep incremental droop, we approach a constant-current output. The power can then be controlled by changing the angle of advance on the inverter, as shown for 30- and 40-deg advance curves.

There is a limit in voltage for a given current that cannot be exceeded without running out of margin angle. The margin angle is the angle at which commutation must be completed ahead of the point at which the anode again goes more positive and there is risk of the inverter's going into a short-circuit condition. This limit is shown for a 20-deg margin angle in Fig. 14.5. For the inverter, the source voltage, E_o, is fixed proportional to system voltage. For the rectifier, it is proportional to E'' of the generator—the internal voltage back of the subtransient reactance that may be regarded as the voltage back of the commutating reactance. E'' can change in a few cycles with the load or with excitation, and this changing value can be kept track of by drawing a vector diagram, as in Fig. 14.3.

Cyclo-Converter

Another form of solid-state converter is the cyclo-converter (Fig. 14.6), which can chop out lower frequency waves from a line frequency. For each phase, we have a pair of bridges back-to-back that will take current in either direction and swing the voltage plus or minus.

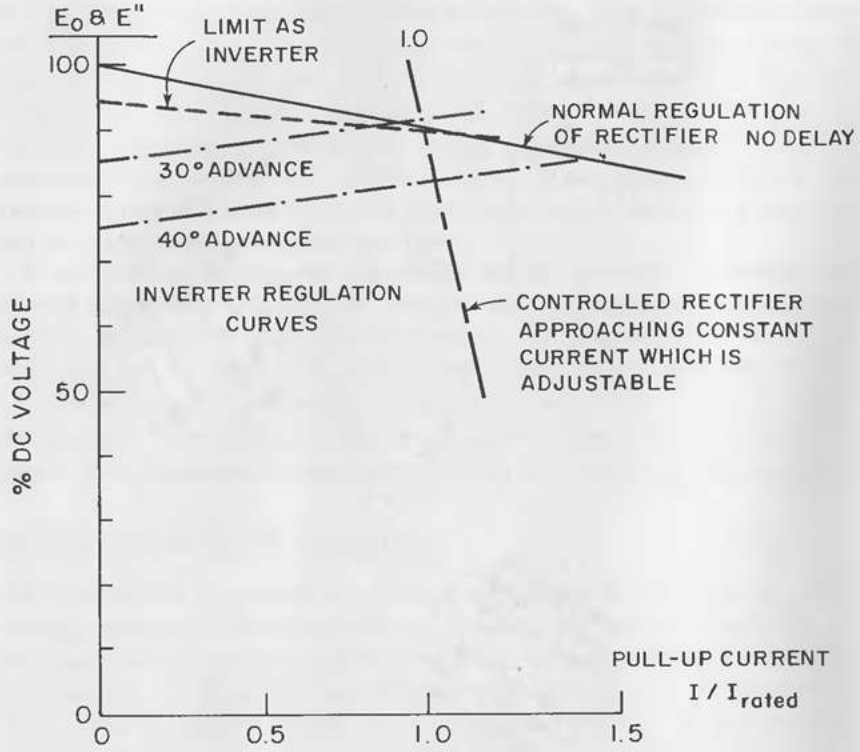

Figure 14.5. Inverter-rectifier regulation curves.

Good sine waves may be had for output frequencies below one-quarter of the line frequency. Above this ratio, wave distortion resulting in torque pulsations may occur. The stator of a low-frequency salient-pole generator could be connected through the system to provide a variable-speed generator. The arrangement would be expensive because we would be handling full power through a complicated converter with a poor inherent power factor.

A more common application is to supply the slip rings of a wound-rotor induction machine with a slip frequency as high as 20 to 25 percent of line frequency.

14.9 PRACTICAL ASPECTS OF USING SQUIRREL-CAGE INDUCTION GENERATORS IN WIND TURBINES

This section describes problems that may arise in using squirrel-cage induction generators (SCIG) in wind turbines. It is assumed that the designer is familiar with the general theory of their connection to power systems.

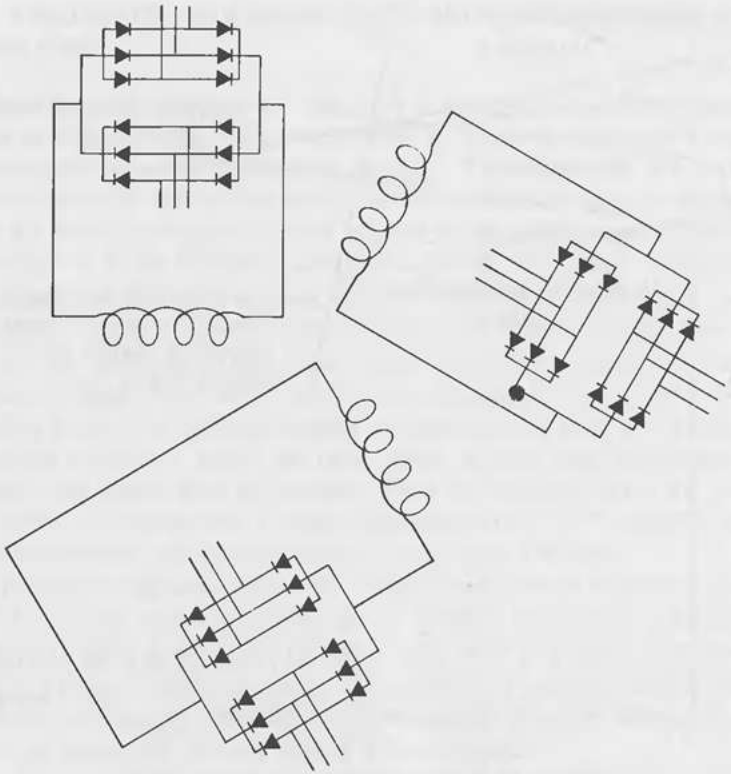

Figure 14.6. Cycloconverter.

Starting Procedures

A SCIG can be used to motor a wind turbine up to operating speed by applying the generator locked-rotor torque, typically 0.8 to 2.75 times the full-load torque, to the drive train. Transient pulsating torques of twice the locked-rotor torque, or 1.6 to 5.5 times the full-load rating, will result. The generator will develop the full locked-rotor average torque in a very short time (perhaps 100 milliseconds for a 75-kW machine) after voltage is applied. This time constant is usually much faster than the period of the first vibration mode of the drive train, causing the latter to "see" a step function in torque. If the drive train is underdamped in this operating region, it will experience large torque oscillations.

During the motor-up time, the generator will draw 6 to 8 times the full-load current from the utility line. The effect of this transient has different implications, depending upon whether the machine is a single unit connected

to a grid or part of a wind farm. If it is a single unit on a grid and the utility line has limited capacity, a full-voltage start will cause the line voltage to drop and lights to flicker. Each utility company has specifications on allowable voltage drops, including their frequency and length of occurrence. In general, the utility will permit across-the-line starting of induction generators if other customers along the line will not be bothered by the voltage flicker. If the machine is part of a wind farm, this policy may limit the number of machines that are allowed to start at the same time.

If the wind turbine rotor is self-starting and the generator is connected to the line at synchronous speed, the voltage drop will only last long enough to build up the magnetic fields in the generator. The magnitude of the current surge will still be equal to the locked-rotor current of the generator, but for a 75-kW machine, it will last for approximately only 100 milliseconds. Since the generator will experience high acceleration during start-up, many users specify 4 to 6-percent full-load slip to control the duration of the transient.

Starting Effects on the Generator

The longevity of a generator is primarily determined by the longevity of the winding insulation. Insulation life is shortened by excessive heat (to be discussed later) and mechanical abrasion. Whenever large currents flow through the windings, the windings will flex, causing wear on the insulation. If a wind turbine is allowed to free-spin in marginal winds, and if the controller energizes the generator at synchronous speed, the system may connect and disconnect hundreds or thousands of times per day. The insulation of a generator can be designed for this type of abuse, but an "off-the-shelf" generator will typically not be built for such conditions. Properly designed programmable control systems do not permit more starts per hour than standard windings can tolerate. Temperatures and wind velocities are also factors in the control algorithm.

Impulse Torques Due to Generator Residual Voltage

Large impulse torques can occur when a generator is disconnected and reconnected to the utility line, as in the following scenario.

A wind turbine producing power is disconnected from its utility line. (This may occur due to a temporary line fault.) The generator is then reconnected to the line before its residual voltage has decayed, and the residual voltage is 180 degrees out of phase with the line voltage. Under these conditions, instantaneous values of 10 to 20 times full-load current and torque may occur, and this torque spike will be applied to the drive train. Earl Babbitts recommends that SCIGs subject to such repeated overcurrents be ordered with

special windings having short end turns, tight lacing, surge cords or end caps, multiple dips and bakes of varnish, and sufficient impedance to limit torque spikes.[6] If a programmable controller is used, a time interval sufficient to allow for complete collapse of the magnetic field of the generator before restart can be enforced. In this case, the special windings may not be necessary.

If enough parallel capacitance is connected to the generator, it may self-excite when disconnected from the utility line. This could cause its terminal voltage to increase above the line voltage, thus causing a larger torque spike when the generator is reconnected to the utility line. This is another problem that can be prevented by appropriate use of a programmable controller. Its undesirable effect can be turned to advantage and provide capacitor braking by inserting a resistor bank load on the generator output lines at the time of disconnect, thereby allowing losses in the resistors to supplement the mechanical brake.

This electrical-braking approach is discussed in detail by Scheda and Helmick.[6] They point out that the capacitance bank needed is about the same size as that required to provide 100-percent power-factor compensation to the induction generator. Thus, this capacitor bank is desirable for both dynamic braking and for power-factor compensation. If the full short-term overload capacity of the generator is utilized, twice the rated torque can be absorbed by using a resistor bank sufficient to absorb twice the rated output of the machine. Capacitive braking is all the more effective during generator overspeed and remains effective down to about 80-percent rated speed. For further details, see Reference 6. Although the extra braking capability from capacitive braking is good, the designer must realize that it will vanish should the generator burn out or be unconnectable due to some other fault. Other primary or secondary overspeed control methods must be provided.

Generator Heat Rise

A generator's steady-state, full-load rating is a function of the heat rise of the generator. The limiting factor is the temperature-withstanding capability of the winding insulation. The life of this insulation deteriorates quickly when the winding temperature exceeds the rating of the insulation.

The generator manufacturer determines the full-load rating of a generator on the basis of the heat rise of the generator at *rated* line voltage. If a generator is operated at a voltage lower than rated voltage, the generator current will be larger than the current at rated voltage and will thus reduce the full-load capability of the generator.

Almost all wind-farm generators are sold with RTDs (Resistive Temperature Detectors) installed to detect winding temperature rise. When used in conjunction with programmable controllers, RTDs, which are extremely reliable, can positively prevent operational overheating.

If the generator line voltage exceeds rated voltage, magnetic saturation may result. When this happens, the line current will increase, causing increased heating in the generator. Once again, these consequences will decrease the full-load rating of the generator.

Line-to-line voltage imbalance causes negative sequence currents in induction generators. Negative-sequence currents generate a torque in the opposite direction of normal rotation. The negative-sequence torque is subtracted from the normal (positive-sequence) torque, causing a reduction of generator efficiency and increasing the heat rise of the generator windings. This, in turn, reduces the full-load power rating of the generator. Programmable controllers can handle line imbalance and eliminate this problem.

If the generator is used to motor-up a wind turbine from standstill, the large starting currents will quickly heat up the generator. The control system designer must make sure that the generator has time to cool down between motor-ups. Again, the programmable controller can easily be programmed to prevent too-frequent starting.

REFERENCES

1. Nasar, Syed A. *Electric Energy Conversion and Transmission*. New York: Macmillan, 1985.
2. IEEE recommended practice for industrial and commercial power system analysis. ANSI/IEEE Standard 399-1980 (distributed in cooperation with Wiley Interscience), 1980.
3. Johnson, Gary L. *Wind Energy Systems*. New York: Prentice-Hall, 1985.
4. Curtice, D., and Patton, J. Operation of small wind turbines on a distribution system. Final Report, RFP-3177-2, Rockwell International. Energy Systems Group, Rocky Flats, March 1981. Work done by Systems Control, Inc., Palo Alto, CA.
5. Andersen, T. S., and Kirschbaum, H. S. Multi-speed electrical generator application to wind turbines. AIAA/SERI Wind Energy Conference, Boulder, CO, Apr. 1980.
6. Scheda, F. A., and Helmick, C. G. Harnessing self-excitation for wind turbine induction generators. Procedings, Fourth ASME Wind Energy Symposium, Dallas, TX, Feb. 17-21, 1985.
7. Babbitts, Earl. Application and performance advantages of an optimally designed induction generator. Application Notes. Marathon Electric, Wausau, WI, Sept. 1984.
8. *Electrical Transmission and Distribution Reference Book*, 4th ed. E. Pittsburgh, PA: Central Station Engineers of the Westinghouse Electric Corp., 1964.
9. Electric Utility Reference Book, vol. 3. *Distribution Systems*. E. Pittsburgh, PA: Electric Utility Engineers of the Westinghouse Electric Corp., 1959 (Rev. 1965).

15

Control Systems

15.1 INTRODUCTION

An otherwise well-designed wind turbine can perform poorly for all that or even self-destruct if it is not properly controlled. Controls are used for the following functions: (1) to enable automatic operation, (2) to keep the turbine aligned with the wind, (3) to engage and disengage the generator, (4) to govern the rotor speed, (5) to protect the turbine from overspeed or damage caused by very strong winds, and (6) to sense malfunctions and warn operators of the need to perform maintenance or repair, etc. Controls for an individual machine may be integrated into a data-gathering system for a wind farm, and a master computer can act as a supervisory control and diagnostic tool for the entire farm.

To maximize the power generated per dollar of investment, there will be a trend to use control technology to increase the quality of performance, reduce costs of operation, and increase reliability. Control may also be used to extend fatigue life by minimizing and smoothing effects of suddenly-applied loads.

There is a vast literature on the theory of control, but only a few works specifically oriented toward the special control problems of wind turbines. No attempt can be made to introduce the basic theory here, but a wind-turbine designer should have at least a basic background in servo theory—i.e., control of continuous systems—before attempting to design a wind-turbine control system.

A comprehensive global survey of modeling and control of large horizontal-axis wind turbines was presented in the doctoral thesis of Sven E. Mattsson.[1] A brief survey of mechanical and electromechanical controls for small wind turbines is given in Ref. 3 (pp. 60–72).

For a small machine, the controls must be simple and passive. For a large machine, on the other hand, the cost of controls represents but a small percentage of the total cost, and very elegant and precise controls can often be justified.

Although passive controls do their own sensing and use natural forces for their actuation, active controls may use electrical, mechanical, hydraulic,

pneumatic, or other means in any combination to suit the desired purpose. This allows a great deal more flexibility in control strategies for the larger machines.

Active control systems depend upon transducers to sense the many variables—rotation speed, power produced, generator temperature, voltage, current, windspeed, pitch angle, etc.—that will determine the control action needed. Transducers used for control must be of high quality—rugged and extremely reliable. They must not only accurately measure the variable they are supposed to sense but refrain from responding to erroneous inputs. This capacity is critical, since extraneous signals wandering around a control loop can result in unreliable operation, instabilities, and other problems. A problem for small machines is that good control sensors tend to be expensive. They are thus subject to a definite economic limit on the sophistication of such instrumentation if they are to be sold at a reasonable cost. Another important point is that the machine not be encumbered with so many interacting protective controls that it is hardly ever allowed to run.

A difficulty with complex active-control systems is their sensitivity to lightning. Lightning strikes are very common in certain places and extremely uncommon in others. Although very careful design and testing of electronics packages and cabling are necessary to protect control circuits from lightning, the necessary technology is available. Even the fuel control systems on the newer turbofan engines of aircraft are now electronic, and these are critical to aircraft safety.

There are about as many different approaches to wind-turbine control systems as there are machines, and each designer will have individual preferences. We will illustrate here some typical control systems to aid the discussion.

15.2 RPM CONTROL (MECHANICAL)

Few wind systems have controls that constantly change the rotor-blade angle of attack (pitch angle) to match the instantaneous wind velocity. Even though this feature might produce more power, it has not been considered practical. Most rotors can be considered fixed pitch over most of the operating range of wind velocities. Nevertheless, many designers have found it necessary to control the blade pitch angle to accomplish the following;

1. Start the rotor turning.
2. Set the pitch angle to a "run" position
3. Control rpm to prevent the rotor from overpowering the generator
4. Protect the rotor and system from high wind-velocity damage

The preceding goals can be accomplished through either mechanical or electronic means.

One passive mechanical method is centrifugal stalling. For instance, some machines, both dc and ac, use flyweights attached to the blades so that the blades will have a high pitch angle for starting ($\theta \cong 10$ deg). As the rpm increases, the flyweights produce a moment that moves the pitch angle toward a run position ($\theta \cong 2$ deg). If the rpm becomes greater than the generator or alternator is designed for, the flyweights continue to rotate the blade pitch until they stall and the increased drag reduces the rpm.

The UTRC and the Dunlite machines are good examples of the centrifugal-stall technique. Both are designed to remain rotating during high wind velocities (see Figs. 15.1 and 15.2).

Another passive control technique that has been successfully used is centrifugal feathering. The original Jacobs turbine used the centrifugal force on the blades themselves to cause the blades to feather, i.e., go to progressively higher pitch angles (and negative angle of attack, α) as the windspeed and rpm increase. This control motion, exactly opposite to the centrifugal stalling method, enables passive reduction of the power input and thrust loads on the rotor, thus allowing the system to continue to generate rated power even at very high wind velocities.

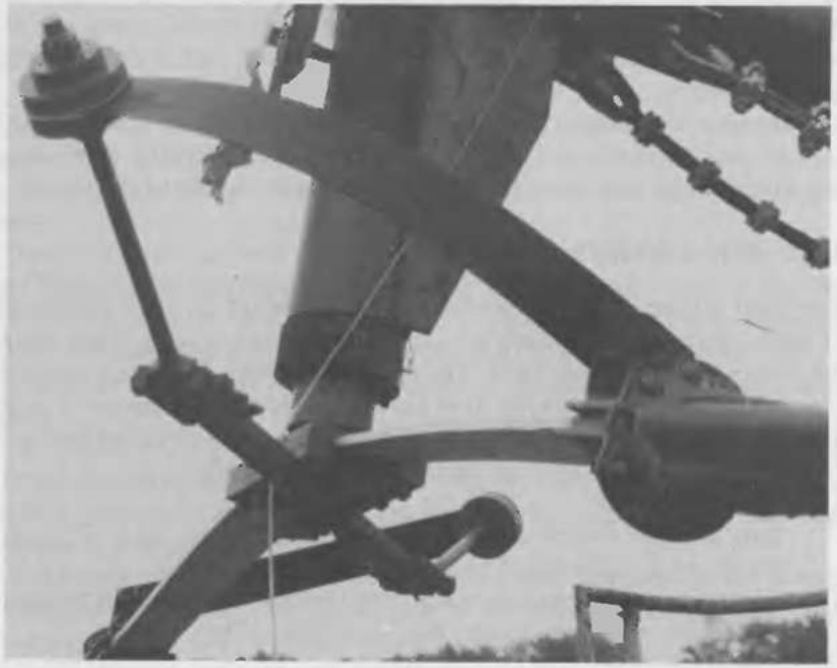

Figure 15.1. UTRC pendulum and flexbeam assembly.

Figure 15.2. Dunlite 2.0-kW wind turbine.

It should be noted that in the centrifugal-stall-controlled systems mentioned the generators are disconnected during high wind velocities; consequently, the rotor rpm *must* be controlled to prevent destruction. There are two philosophies concerning this problem.

The first approach is based on the belief that it is preferable to keep the rotor turning and use centrifugal stiffening to reduce blade bending stresses and help prevent tower strikes. The second approach is to stop the rotor, assuming that the dynamic stresses from gyroscopic induced loads will be more severe than the direct wind loadings.

The behavior of many different wind turbines in high winds has been observed at the Rocky Flats, CO, test site. A number of two-bladed downwind rotor machines whose rotors are stopped in a normal operating-pitch regime

Figure 15.3. Grumman WS 33 wind turbine.

during storms have tended to orient themselves upwind of the tower. This makes their blades susceptible to striking the tower. Such has not been the case, however, for machines whose blades are set to a pitch angle of 90 degrees (i.e., feathered) for their storm survival mode, as is the case of the Grumman WS 33 shown in Fig. 15.3. In the WS 33, the stresses remain low, and a tendency for the rotor to move upwind of the tower has not been apparent. This capability must be weighed against the added cost and complexity of building such sophistication into the machine. The Grumman system uses a computer to control servo actuators that rotate the blade pitch to the desired position.

This level of sophistication has yet to be seen in purely mechanical systems. The most successful flyweight-driven mechanical systems have been those with the simplest designs. The flyweight system of the Millville 10-kW machine used a series of detents and was less successful.

The centrifugal-stalling or flyweight system has been proven to work, but it must be adjusted accurately so as not to incur overspeed damage to the transmission or generator. It should be noted that the aforementioned systems also have a brake on the rotor shaft to stop the rotor when conditions warrant. This would include overspeed, vibration, and maintenance.

15.3 ELECTRONIC CONTROLS

The system shown in Figure 15.3—the 8-kW Grumman WS-33 machine—is a good example of an electronically controlled system. A small computer determines the system's operational status and commands the appropriate actions. It receives input from sensors monitoring wind speed, rpm, vibration, power, and blade-pitch angle. From this input, the desired blade-pitch angle can be obtained by a command to the pitch actuators. This technique controls rotor rpm throughout the entire range of operation. If any problems are detected, such as exceeding the preset operational limits, the system commands the blade-pitch servos to put the rotor in a nonoperational position (pitch angle of 90 deg), and an operator is required to reset the system prior to restarting. Although an operators' time is required to resolve the problem, it ultimately helps prevent serious damage to the system and avoids potentially costly repairs.

The level of control sophistication is an important design tradeoff. For larger machines, the cost of control hardware and software is likely to be a small part of the manufacturing cost of the unit. For small machines, this is not the case, and a much less complex control system is needed. The designer of small wind turbines should adhere to the old adage, "Keep It Simple" (KIS), and attempt to build in passive, reliable controls that will still manage to keep the energy-gathering performance as high as possible. The designer of medium to large wind turbines can utilize more complex controls to relieve loads and maximize performance and machine life.

If the primary control system should fail, for any reason, it is important to have a back-up system that can prevent machine damage. A backup overspeed control system can take many forms including tip brakes or spoilers, blade pitch changes to cause stall, and others. It is important to note that a brake located on the rotor shaft won't necessarily stop the rotor in very high winds, as was discussed in Chap. 1. If the blade pitch is fixed or set near the run condition—i.e., with a tip pitch of near zero degrees—the rotor will try to maintain a fixed tip-speed ratio. If the wind speed then increases drastically and the generator is unable to absorb the added torque, even full application of a brake may do nothing more than burn out the brake. It might also result in damaging one of the shafts, the gearbox, or the rotor, however, from overly large static or dynamic loads. Thus reliance on a brake as a backup device is unsatisfactory.

Since power is obtained largely by the outer third of the blade, this is also the most effective place to destroy it. Very small control surfaces that ruin the smooth flow of air over the airfoil near the tips or greatly increase the blade profile drag will have a very large effect on output power. Likewise, a small change in angle that results in stall of this section of the blade will reduce rotor power output considerably.

Many of the upwind and downwind rotors of dc power-generating systems are fixed pitch. Among additional rpm control techniques these systems use are the following:

1. A tail vane to rotate the rotor edgewise to the wind direction (see Fig. 15.4).

Figure 15.4. Millville 10 kW wind turbine.

Figure 15.5. Grumman Windstream 25-kW wind turbine.

2. Blade tip plates that extend to cause braking of the rotor when overspeed is experienced (see Fig. 15.5).
3. Side wheels that are small rotors connected by shafts to gears that rotate the nacelle and rotor to be either perpendicular or parallel to the wind direction (see Fig. 1.1).
4. A VARCS (Vertical Axis Rotational Control System) spring that assists the rotation of the rotor and generator vertically. The effect is similar to that produced by a tail vane except that the rotor moves from in front of the generator to a position above it and the tail remains oriented in line with the wind direction (see Fig. 15.6).

Figure 15.6. NorthWind 2-kW high-reliability prototype (1980).

Methods 1, 3, and 4 all experience gyroscopic loads during the motion described. Since it occurs during severe wind conditions, it may represent a critical design-load condition. Many of these systems try not to shut down completely but maintain some power production during these high wind-velocity conditions. This allows them to return to operation without operator assistance or the use of a sophisticated electronic control system. Such wind systems were designed for a particular mode of operation, and this may or may not be applicable to all systems.

15.4 POWER CONTROL (MECHANICAL)

In regard to power, the controls are two-fold. One is the connection of the generator to the utility when the rpm at the generator is at synchronous speed. This is defined in Chap. 14 as the condition where there is no excess torque and no power either in or out of the generator. The other is the control of

rotor rpm so as not to overpower the generator (exceed the slip, torque, or other ratings) and cause damage to the power-generating system. Rotor rpm control was discussed in the previous section, and the only reminder here is that if you electrically disconnect the generator, you *must* use some means to control rotor rpm.

Mechanical methods have been tried, unsuccessfully, to initiate the electrical connection of ac generators to the utility. The Millville machine tried a governor-type device that closed a microswitch, which in turn caused the electrical contactor to connect with the generator. This type of device was found to be inaccurate (i.e., off-synch), unreliable (different cut-in rpm's), and hard to adjust. It thus created severe loadings on the drive train and rotor. The immediate consequence was a rotor-shaft coupling failure that indicated the severity of the loadings. High currents were also experienced across the power slip rings, as evidenced by their burning.

Several devices presently on the market are economical, reliable, measure rpm accurately, and provide the signal to close the electrical contactors. All are preferable to any direct mechanical method.

15.5 ELECTRICAL CUT-IN

The electronic sensor to connect the generator correctly will differ for ac and dc systems.

DC generators have a very low power output at low rpm. For them, the correct connection is made when the rotor rpm is adequate to generate some power but remains low enough for it not to cause a sudden jolt to the rotor system when electrical connection is made. The sensitivity of this cut-in point to speed is much lower for dc than for ac systems, not only because of the nature of the former but the lack of any frequency control on the generated power. These control systems are usually generator current or voltage activated. They are very common, economical, and no further sophistication is required.

AC generators, on the other hand, represent a design condition that is more difficult to meet. First of all, the connection to the utility must be made as close to synchronous frequency as possible to help eliminate rotor-shaft and generator torque spikes.

The rpm sensing devices are usually accurate to some small percent of the synchronous rpm (for example, $\pm$ 4% of 1800 = $\pm$ 72 rpm). If the torque curve for the generator in the synchronized mode indicates that the torque at 1728 or 1872 rpm is high, the sensing device is not the proper one, and a more accurate device must be found.

As explained in Chap. 14, each generator has a maximum amount of slip it can experience without harmful effects. With this in mind, the rpm-sensing

device must also be able to detect this rpm and provide a contactor disconnect signal. Both the connect and disconnect signals go to the switching devices, which in turn close or open the contactor. For those machines with mechanical rotor control, the rpm sensor signal can be sent directly to the contactor actuating circuitry. For machines with electronic rotor control (computers and servo actuators), the rpm sensor signal is input to the computer, and the program logic initiates the appropriate action (closing or opening the contactor). This step is taken because other control actions (e.g., blade pitch) must be coordinated with the electrical contactor activation. The rotor pitch must be adjusted for the no-electrical-load conditions. Most systems sense either high rpm or high power and adjust the blade pitch angle before opening the contactor at or near the zero power output condition. This precaution avoids the sudden jolt experienced by the abrupt loss of torque. Here again the designer who opts for computer control has the design freedom to make the cut-in almost perfectly smooth, thus extending the life of the gears, shafts, and rotor. This goal can be met, however, only if careful design and testing are undertaken to assure the reliability of the more complex system specified.

One final consideration that should be discussed is the loss of utility power on the line. This has the same net effect as the sudden opening of the contactor. In some cases, where large capacitors are connected to the utility line, the line does not go completely down. As a result, the generator is still excited and produces some power. The big change is the loss of frequency control. The power, no longer regulated to a frequency of 60 Hz, is controlled only by whatever is on the line. The wind system is usually then free to change frequency, to increase rotor and generator rpm, etc. A mechanical rotor control system will handle this automatically, as it does for any increased rpm. The electronic control system must be able to differentiate between the various conditions and shut down when the change in frequency is detected.

Total loss of power is an additional problem for an electronically controlled system. In this case, when the power to the computer is gone (unless there is a battery backup), the power to operate the blade-pitch servo actuators is also gone. This is potentially a very dangerous situation, for the rotor will probably remain at fixed pitch and we are back to the old rotor-run-away situation again.

One solution to this problem, as exemplified in the Grumman WS-33, is to connect a small dc generator to the high-speed shaft. When ac power is lost, a relay connects the dc generator to the servo actuator, and the latter drives the blade pitch to a protective position (90 degrees). Any rotor rotation continues this action until the rpm is essentially zero. Micro-switches prevent any further movement of blade-pitch control. Once the power has been restored, the computer controls can be reset and operation resumed.

REFERENCES

1. Mattsson, Sven Erik. Modelling and control of large horizontal axis wind power plants. Doctoral thesis, Department of Automatic Control, Lund Institute of Technology, Lund, Sweden, Dec. 1984.
2. Martinez-Sanchez, M., and Labuszewski, T. *Drive System Dynamics*. Wind Energy Conversion, vol. 4. U.S. DOE COO-4131-T1, Sept. 1978.
3. Le Gourieres, D. *Wind Power Plants, Theory and Design*. Permagon Press, 1982.
4. Harner, Kermit. High Power Wind Energy Conversion Systems—A Control Challenge. Slides presented at the American Wind Energy Association Conference, Warren, VT, Oct. 1976.
5. Hirschbein, M. S., and Young, M. I. Stability of large horizontal-axis axisymmetric wind turbines. NASA TM 81623, Dec., 1980.
6. Miller, D. R., and Putoff, R. L. Aileron controls for wind turbine applications. DOE/NASA/20320-60, NASA TM-86867, Aug., 1984.
7. Cao, H. V., and Wentz, W. H. Jr. Performance and aerodynamic braking of a horizontal-axis wind turbine from small-scale wind tunnel tests. WER-37, Center for Energy Studies, Wichita State University, July, 1985.

Index